Mathematical Modeling of Free-radical Six-component Bulk and Solution Polymerization

by

Woosung Jung

A thesis
presented to the University of Waterloo
in fulfillment of the
thesis requirement for the degree of
Master of Applied Science
in
Chemical Engineering

Waterloo, Ontario, Canada, 2008

AUTHOR'S DECLARATION

I hereby declare that I am the sole author of this thesis. This is a true copy of the thesis, including any required final revisions, as accepted by my examiners.

I understand that my thesis may be made electronically available to the public.

Woosung Jung

Abstract

The purpose of this project is to reexamine established free-radical polymerization theories and build a mechanistic reactor model for multi-component (up to six monomers) bulk and solution polymerizations under batch/semi-batch reactor configurations. The six-monomer system of interest is: Styrene (Sty), n-Butyl acrylate (BA), Butyl methacrylate (BMA), Hydroxyethyl acrylate (HEA), Hydroxybutyl acrylate (HBA), and Acrylic acid (AA). In order to develop a flexible, comprehensive, and user-friendly model, not only a physical/kinetic database of individual monomers and ingredients such as solvents, initiators, and chain transfer agents, but also a *co*-polymer database of reactivity ratios, and glass transition temperatures were built and combined with the modeling steps. Through an extensive literature search for polymerization models and kinetics, the simulation model was developed in a general way to cover the range from *homo*- to *hexa*-polymerization at both regular and elevated temperature levels, and explain various polymerization kinetics and characteristics.

Model testing was conducted with experimental data as much as possible to check the model's reliability. Due to limited experimental data for higher multi-component polymerizations, the simulation model was tested with *homo*-polymerizations and other available cases of combinations of two to four monomers. Very reasonable agreement was found between model predictions and experimental data on rate of polymerization, molecular weight, polymer composition, sequence length, etc. through the entire conversion.

This multi-component modeling study continuously requires experimental checkups and parameter fine-tuning for better predictions. Further literature search or experimental studies still remain necessary for the hydroxyalkyl acrylate kinetic database and model testing of the depropagation feature. Sensitivity analysis also could be performed to locate critical parameters. This model should find use in industry for analyzing and optimizing reactor conditions as well as in the academic field as a research and educational tool.

Acknowledgements

I have reached another milestone in my life. The last two years will be remembered as one of the most important moments to me: full of tough, exciting, and precious experiences… Thank God!

Space is too limited to thank all the people in my mind. First of all, I gratefully express deep appreciation to my gentle supervisors, professors Duever and Penlidis, who have shown their kind and invaluable interaction, support, and advice for my academic success and personal life as well. I also acknowledge IPR and PSE members for their help, and BASF SE for funding and constant interest in my project.

Many thanks to my dearest guys, Heon Park, Jurngu Song, Sangman Hwang, Sejin Kim, Jinsung Choi, and Hwangyong Shim. I will never forget our great time of friendship.

I would like to thank my brilliant lab mate, Ian D. Washington for sharing hard times to overcome the difficulties.

Finally, I most deeply acknowledge my mother and father, and families-in-law for their unceasing encouragement, support, patience, and prayers. Without them, everything would have been impossible and meaningless.

Dedication

To my wife Jungeun and my son Joonho… I love you.

Table of Contents

List of Figures

List of Tables

Chapter 1

Introduction

1.1 Objectives

Multi-component free-radical polymerization is composed of highly competitive reactions between the same or different radical/monomer species. As the number of monomer species increases, the number of possible reactions also significantly increases and therefore the polymerization mechanism becomes complicated. Notwithstanding this, both the mathematical modeling and the study of multi-component recipes have attracted considerable industrial and academic interest for several decades due to the added economical benefits of enhanced polymer properties and expanded applications via various combinations of monomers.

The objectives of this project are to reexamine the established free-radical polymerization theories and build a mechanistic reactor model for multi-component (up to six monomers) bulk and solution polymerizations under batch/semi-batch reactor configurations. Figure 1.1 shows the project objectives and scope. A lot of effort was put on searching the literature for physical/kinetic parameters, types of models, and experimental data. Using the parameter database of monomers and ingredients (initiators, solvents, chain transfer agents, and impurities), along with a *co*-polymer database (reactivity ratios and polymer glass transition temperatures), the simulation model was gradually developed into a generalized and comprehensive one, which covers the range from *homo*- to *hexa*-polymerization, and can provide quick and reliable predictions of productivity (reaction rate) and quality behaviour

(molecular weight, polymer composition, sequence length, and branching) of multi-component polymers over a wide range of reaction conditions. After that, the model predictions were compared with available experimental data and results from this stage are discussed on a case by case basis.

This modeling work includes several features: terminal model, pseudo rate constant method, diffusion-controlled kinetics at high conversion, thermal initiation, depropagation at elevated temperatures, molecular weight calculations of linear/branched polymers, and macroscopic (composition) and microscopic (sequence length distribution) characteristics. These features are going to be discussed in detail in Chapter 4.

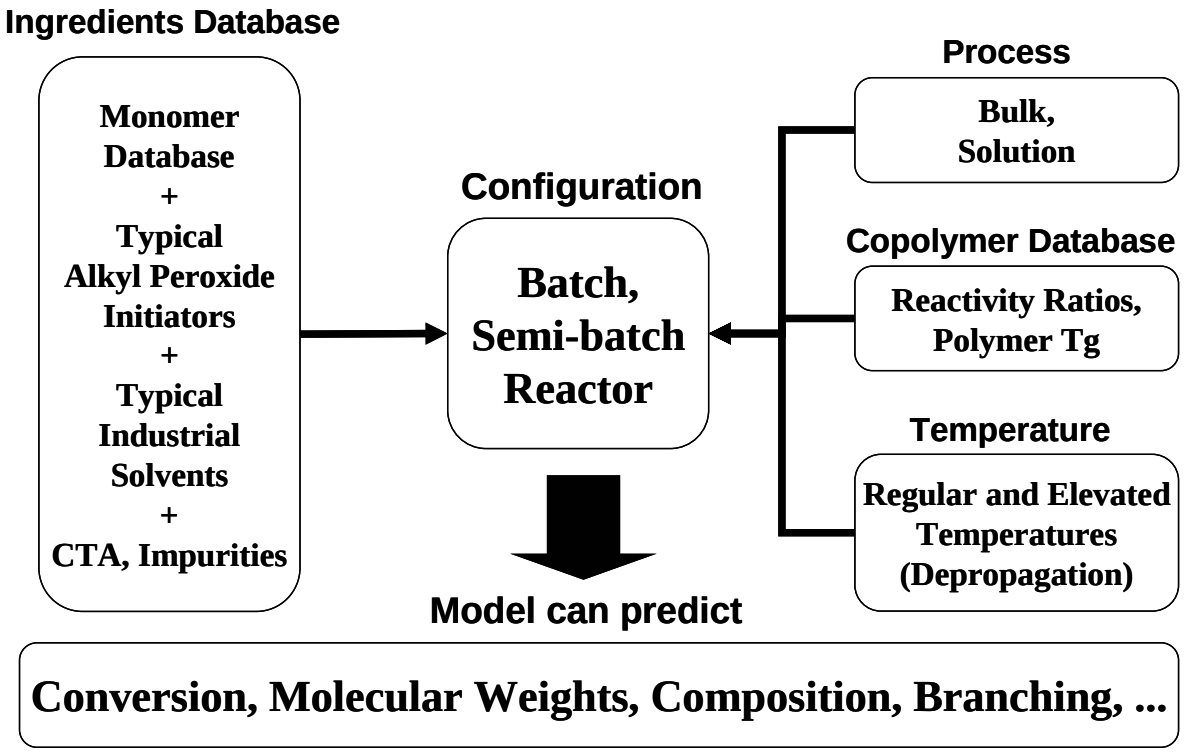

Figure 1.1. Project objectives diagram

1.2 Outline

Chapter 1 presents the objectives of this project and an outline of the thesis. It also gives a brief explanation of model features.

Chapter 2 introduces free-radical multi-component polymerization kinetics. Starting with the three basic reactions, namely initiation, propagation, and termination, several other transfer/side reactions will be discussed briefly. Assumptions for simulation modeling and an extensive literature review will follow.

Chapter 3 contains batch/semi-batch reactor model development. All the balance equations and the calculated quantities for multi-component polymerization modeling are presented. Chapter 3 also introduces diffusion-control kinetics, sequence length distribution calculations, and depropagation modeling.

Model and simulation features are summarized in Chapter 4. The polymerization recipe for a six-monomer system is introduced here. Successful model predictions for this recipe are the final target of this thesis.

Chapter 5 has nine sections of model testing and troubleshooting results with discussion. Various experimental data (conversion, molecular weight, polymer composition, sequence length, etc.) were compared with model predictions. Depropagation features are also discussed herein.

Chapter 6 is composed of eleven sections about model testing of monomer systems related with the specific recipe discussed in Chapter 4. Due to lack of literature experimental data sources, the model could be compared with *homo*- to *tetra*-polymerization experimental data.

Hexa-polymerization model prediction trends related to the specific recipe are shown in Chapter 7. Although they may not be accurate since many kinetic parameters are unknown, they will be helpful in furthering our understanding of polymerization behaviour in multi-component systems.

Chapter 8 is the final chapter dealing with concluding remarks and recommendations for futural model development.

Appendix A compares several multi-component polymer composition calculation options tested and used in the model.

Appendix B is dealing with a comparison of several versions of molecular weight moment equations and related calculation options tested and used in the model.

Appendix C cites the physical/kinetic database of monomers used in the model.

Finally, Appendix D discusses a case study of Sty thermal polymerization. Model prediction results for average molecular weights are compared with experimental data at elevated temperature levels.

Chapter 2

Brief Polymerization Background & Literature Review

2.1 Kinetics of free-radical multi-component polymerization

Free-radical polymerization happens when an unsaturated vinyl monomer's π bond is attacked by a radical and turns into a new active radical center for successive addition of another monomer (repeating unit). The reaction mechanism is quite different from step polymerization. Any two molecules, such as monomer-monomer, monomer-dimer, or dimer-trimer, can react with each other, and high molecular weight polymer is formed only at high conversion levels in step polymerization (Figure 2.1b, Odian, 1970). On the other hand, in free-radical polymerization, a monomer can only react with propagating radicals, which grow very quickly to a high molecular weight (typically 10^4-10^6 g/mol for industrial use) and eventually become unreactive (dead) polymer molecules (Figre 2.1a, Odian, 1970).

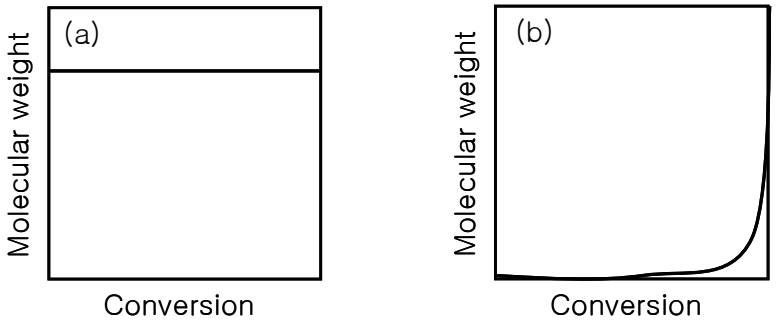

Figure 2.1. Typical molecular weight vs conversion
(a) Free-radical polymerization; (b) Step polymerization

In multi-component free-radical polymerization, more than two monomers are participating in chain growth and this leads to a "combination" of properties of the individual polymers. Due to reactivity differences and comonomer composition, polymer properties will be significantly affected. The reactions considered in the model development are discussed in the following subsections (r and s denote chain length, and i and j represent monomer species).

2.1.1 Initiation

$$I \xrightarrow{k_d} 2R_{in}^{\bullet} \tag{2-1}$$

$$R_{in}^{\bullet} + M_i \xrightarrow{k_{p,0i}} R_{1,i}^{\bullet} \tag{2-2}$$

The initiation step involves two reactions. First, commercially important azo or peroxide initiators usually yield a pair of primary radicals by thermal homolytic cleavage. Not all primary radicals can participate in further reactions. After decomposing, the radicals are trapped by the reaction mixture due to the cage effect. Within the cage, some radicals may recombine, react with each other or with monomer, or diffuse out to initiate polymerization. Upon exiting, some radicals lose their reactivity and become stable. This is described by the initiator efficiency (usually in the range of 0.3 to 0.8), which is essentially the fraction of radicals that successfully lead to growing chains.

2.1.2 Thermal initiation by monomer (Diels-Alder mechanism)

$$nM_i \xrightarrow{k_{th}} mR_{1,i}^{\bullet} + \text{byproducts} \tag{2-3}$$

Styrenics can undergo initiation without necessarily the presence of an added chemical initiator. This initiation rate is negligible compared to the contribution via chemical initiator decomposition, however, it becomes significant at elevated temperatures (higher than 120℃).

This purely (auto)thermal or self-initiation follows a Diels-Alder mechanism, as described in Hui and Hamielec (1972).

2.1.3 Propagation

$$R^{\bullet}_{r,i} + M_j \xrightarrow{k_{pij}} R^{\bullet}_{r+1,j} \tag{2-4}$$

In this step, radicals grow by addition of successive monomer species (typically, hundreds or thousands). It should be noted that the higher reactivity a monomer species has, the more it can incorporate into a polymer chain. This is an important feature of multi-component polymerization that allows the synthesis of an almost unlimited number of different products by variations in the nature and relative amounts of the monomer species in the product.

According to the terminal model based on the first order Markov process, the reactivity of a propagating radical depends only on the monomer unit at the growing radical end and is independent of chain composition. The propagation step is important in a multi-component polymerization because the monomer composition and arrangements eventually encountered in a polymer are mostly dependent on reactivity differences between radical species *i* and monomer species *j*. At elevated temperatures where thermodynamic equilibrium is in effect, chains may undergo reversible reaction (depropagation), and this is discussed later in Chapter 3.

2.1.4 Termination

$$R^{\bullet}_{r,i} + R^{\bullet}_{s,j} \xrightarrow{k_{tc}} P_{r+s} \text{ (combination)} \tag{2-5}$$

$$R^{\bullet}_{r,i} + R^{\bullet}_{s,j} \xrightarrow{k_{td}} P_r + P_s \text{ (disproportionation)} \tag{2-6}$$

Chain growth stops and (an) unreactive polymer molecule(s) is (are) obtained at some point from the reaction of two radicals, either by combination or disproportionation. While

termination by combination (coupling) makes two radicals into one dead polymer, the other does not. In disproportionation, a hydrogen atom in the *beta* position of one of the radical centers is transferred to another and a terminal double bond is formed.

2.1.5 Transfer to monomer

$$R^{\bullet}_{r,i} + M_j \xrightarrow{k_{fmij}} P_r + R^{\bullet}_{1,j} \tag{2-7}$$

Radical transfer is a chain-breaking reaction. A radical can be moved from a growing chain to any existing or added substance, such as monomer, initiator, solvent, chain transfer agent (CTA), and impurity. This (side) reaction effectively stops the growth of the original chain. As a result, a polymer's chain length and hence its molecular weight will be decreased.

Transfer to monomer is unavoidable in polymerization. The other transfer reactions to a small molecule follow a similar mechanism (monomer is replaced by other components). Among them, transfer to initiator was considered negligible in the model due to the fairly low content of initiator compared to other ingredients in the mixture, and the fact that initiator molecules are as of lately designed to be stable, so they do not participate in transfer reactions, which would effectively waste valuable and expensive initiator species.

2.1.6 Transfer to solvent

$$R^{\bullet}_{r,i} + S \xrightarrow{k_{fsi}} P_r + R^{\bullet}_1 \tag{2-8}$$

Solvent transfer reaction is important in solution polymerization. For the purpose of lowering the viscosity of a polymerizing mixture and moderating diffusion-control kinetics, the added amount of solvent is sufficiently large to participate in this reaction and influence molecular weight. Organic solvents, such as toluene or xylene, are typical solvents. In multi-component polymerization, reactivities of the different radical species and solvent concentration will affect the rate of this transfer reaction.

2.1.7 Transfer to chain transfer agent (CTA)

$$R_{r,i}^{\bullet} + CTA \xrightarrow{k_{fCTAi}} P_r + R_1^{\bullet} \tag{2-9}$$

CTA is an intentionally added compound in the mixture in order to reduce and control the molecular weight. The typical range of the ratio k_{fCTA}/k_p is 10^{-3}-10^{1}, higher than the other ratios, such as k_{fS}/k_p (10^{-6}-10^{-3}) or k_{fm}/k_p (10^{-6}-10^{-4}). Therefore, even a small addition of CTA readily affects the molecular weight of a polymer. If CTA concentration increases considerably, very short chain length will be obtained by telomerization.

2.1.8 Transfer to impurity (retarder/inhibitor)

$$R_{r,i}^{\bullet} + Z \xrightarrow{k_{fZi}} P_r - Z^{\bullet} \text{ (unreactive)} \tag{2-10}$$

Impurity can be any compound which not only reduces chain length, but also suppresses the polymerization rate. It converts all kinds of radicals to unreactive or less reactive species, and the polymerization stops completely (inhibitor) or slows down (retarder) until the impurities are consumed.

2.1.9 Transfer to polymer (long chain branching)

$$R_{r,i}^{\bullet} + P_{s,j} \xrightarrow{k_{fpij}} P_{r,i} + R_{s,j}^{\bullet} \tag{2-11}$$

As conversion increases, transfer reaction to polymer becomes significant. This results in the abstraction of a hydrogen atom from the dead polymer by the growing radical and a new radical site forms somewhere on the polymer backbone instead. Thus, if any monomer species is added to the revived chain, branched polymer will be produced (tri-functional branching). Transfer to polymer broadens the molecular weight distribution (increase of polydispersity) and increases the weight average molecular weight considerably, but does not influence the number average molecular weight. Unlike other rate constants, measuring the

transfer to polymer rate constant is inherently difficult. Because of this, there are relatively few reliable parameter values/sources available in the literature.

2.1.10 Terminal double bond polymerization (long chain branching)

$$R^{\bullet}_{r,i} + P_{s,j} \xrightarrow{k^{*}_{pij}} R^{\bullet}_{r+s} \tag{2-12}$$

This is another mechanism for forming long chain branching (LCB). Terminal double bonds on a dead polymer molecule are obtained by either termination via disproportionation reactions or especially transfer to monomer reactions. Another radical can attack this double bond and one large branched macroradical is created. Eventually, this increases both the number and weight average molecular weights and broadens the molecular weight distribution considerably.

2.1.11 Internal double bond polymerization (crosslinking)

$$R^{\bullet}_{r,i} + P_{s,j} \xrightarrow{k^{**}_{pij}} R^{\bullet}_{r+s} \tag{2-13}$$

Crosslinking or network polymer formation is due to the presence of a *di*-functional monomer, such as 1,3-butadiene, an important monomer widely used in the rubber industry. Addition of a radical to this monomer yields an allylic radical with two possible reasonance structures. This radical reaction proceeds via propagation at either the 1,2 carbon or 1,4 carbon sites. Both polymers have an unsaturated (pendant or residual) double bond internally and this will react with another radical to cause crosslinking (or *tetra*-functional long chain branching).

$$R^{\bullet} + CH_2 = CH - CH = CH_2 \begin{cases} \nearrow\ R - CH_2 - \dot{C}H - CH = CH_2 \ \text{(1,2-polymer)} \\ \searrow\ R - CH_2 - CH = CH - \dot{C}H_2 \ \text{(1,4-polymer)} \end{cases}$$

2.2 Assumptions used in the simulation model

The following typical assumptions used in polymer reactor modeling, have been extended in the multi-component case.

1. **Perfect mixing**
   There are no concentration or thermal gradients in the polymerizing mixture.

2. **Kinetic behaviour follows terminal model.**
   The reactivity of a radical center is independent of chain length and depends only on the monomer at the end of the radical chain.

3. **Steady-State Hypothesis (SSH) is valid for radicals.**
   Rates of initiation and termination readily become equal to each other.

4. **Long Chain Approximation (LCA-I) is valid.**
   Strictly speaking, the rate of monomer disappearance (polymerization) is due to initiation and propagation. But monomer consumption is largely due to propagation steps for producing long chains and consumption by initiation is disregarded.

5. **Long Chain Approximation (LCA-II) is valid.**
   In order to satisfy the steady state of radical species in the multi-component case, the *cross*-propagation rates are assumed equal.

2.3 Literature review

The collected references are classified based on the number of monomers and these are organized again in chronological order. References are cited by usefulness for kinetics, modeling, and experimental/kinetic data. Unfortunately, polymerization references for more than four monomers could not be found anywhere. Therefore, it will be better to divide reference subsections according to the number of monomers, starting from *tetra*-polymerization.

2.3.1 *Tetra*-polymerization

Sahloul (2004) reported experimental data regarding Sty, EA, HEA, and MAA *tetra*-polymerization. She not only measured conversion, polymer composition, and molecular weights, but also estimated *co*-polymer reactivity ratios at elevated temperatures. Significant experimental errors were identified due to gel formation from the hydroxyalkyl monomer.

2.3.2 *Ter*-polymerization

Alfrey and Goldfinger (1944, 1946) were the first who derived the polymer composition equation containing three components using the steady state assumption. Walling and Briggs (1945) extended this to the general case of *n* monomers and verified that predicted and observed polymer compositions agree well for three and four component systems of Sty, MMA, AN, and vinylidene chloride. More simplified *ter*-polymer equations were proposed by Valvassori and Sartori (1967) and later modified by Hocking and Klimchuk (1996). In this thesis, their equations are extended to a six-component system and compared with one another.

Galbraith *et al*. (1987) calculated the *ter*-polymer molecular weight distribution (MWD) and composition of Sty/BA/HEA (or HEMA) using Monte Carlo simulation and investigated the influence of initiation and termination reactions on the molecular weight distribution (MWD) and composition. A practical reactor simulation modeling of solution and emulsion systems was developed by Hamielec *et al.* (1987b). Using pseudo rate constants and free volume theory, the model provided a common framework for multi-component free-radical polymerization. This work was extended by Dubé *et al*. (1997) to a more comprehensive version with additional mechanisms.

Dubé and Penlidis (1995b) suggested a systematic approach to a multi-component polymerization kinetic study. In order to conduct *ter*-polymerization, they started from *homo*-polymerization of each monomer and estimated *co*-polymer reactivity ratios of BA/MMA, BA/VAc, and MMA/VAc. After that, full conversion *ter*-polymerization experiments were performed and data collected for polymerization rate, molecular weight, and composition,

which were verified by Gao and Penlidis (2000) and Keramopoulos and Kiparissides (2003) through their own modeling work. Dubé and Penlidis (1996) also conducted a hierarchical data analysis of replicate experimental work in emulsion *ter*-polymerization for better accuracy of measured data.

Experimental studies on Sty/HEA *co*- and Sty/HEA/EA *ter*-polymerization were conducted by McManus *et al*. (1998). The reactivity ratios of Sty and HEA showed dependence on the initial monomer feed ratios and the possible conclusion was a polarity change of HEA. Also a limited investigation took place over the full conversion range for reaction rates and composition of Sty/HEA *co*-polymerization along with reaction rates of Sty/HEA/EA *ter*-polymerization.

Another systematic study of the multi-component polymerization of BA, MMA, and alpha-methyl styrene (AMS) was implemented by McManus *et al.* (2004) and Leamen *et al*. (2006). While the latter ones concentrated on parameter estimation and modeling work, the former ones focused on full conversion range studies of *ter*-polymerization at 115 and 140℃ and examined depropagation effects on reaction rates, composition, and molecular weights.

Finally, Li and Hutchinson (2007) calculated the propagation rate constant of Sty/BA/BMA *ter*-polymerization at 60 to 120℃ using the implicit penultimate model. The references for *tetra*- and *ter*-polymerization mentioned above are summarized in Table 2.1.

No. of monomers	Reference	Reference type
Tetra-	Sahloul (2004)	Sty/EA/HEA/MAA
Ter-	Alfrey, Goldfinger (1944, 1946)	Polymer composition
	Walling, Briggs (1945)	Polymer composition
	Valvassori, Sartori (1967)	Polymer composition
	Galbraith *et al*. (1987)	Reactivity ratios
	Hamielec *et al*. (1987)	Comprehensive

Ter- (continued)	Dubé, Penlidis (1995)	Model testing
	Hocking, Klimchuk (1996)	Polymer composition
	Dubé, Penlidis (1996)	Emulsion exp. data
	Dubé *et al*. (1997)	Comprehensive
	McManus *et al*. (1998)	Model testing
	Gao, Penlidis (2000)	Model testing
	Keramopoulos, Kiparissides (2003)	Model testing
	McManus *et al*. (2004)	Depropagation
	Leamen *et al*. (2006)	Depropagation
	Li, Hutchinson (2007)	Penultimate kinetics

Table 2.1. Reference list for *tetra*- and *ter*-polymerization studies

2.3.3 *Co*-polymerization

There are many more references in *co*-polymerization, which will be discussed by topic and chronological order. The pioneering work for the *co*-polymer composition equation was developed independently by three groups, namely Alfrey and Goldfinger (1944), Mayo and Lewis (1944), and Wall (1944). Thereafter, Merz *et al*. (1946) attempted to generalize for sequence length distribution and to consider the penultimate monomer unit effect on the *co*-polymer composition equation.

Polymer heterogeneity studies were conducted by several researchers. Harwood and Ritchey (1964) proposed the run number, a parameter for characterizing sequence length distribution (SLD) in *co*-polymers. Stockmayer (1945) used the Gaussian model for the bivariate distribution of *co*-polymer chain length and composition. His modeling work was extended and developed further so that it can include the effect of the molar masses of

different monomer types on the final distribution by Tacx *et al*. (1988), and that both instantaneous and cumulative composition distributions (CCD) can be calculated for the whole polymerization process by Engelmann and Schmidt-Naake (1993). Meanwhile, Scholtens *et al*. (2001) investigated control strategies for CCD in the Sty/MA continuous emulsion process.

On the other hand, Meyer and Lowry (1965) introduced an analytical solution of the integral form of the *co*-polymer composition equation as a function of conversion, based on earlier work by Skeist (1946). This analytical solution was used for Sty/MMA *co*-polymer composition calculations by Chan and Meyer (1968).

2.3.3.1 Kinetic studies: *co*-polymer reactivity ratios

Reactivity ratios play a major role in multi-component polymerization. Several research groups have studied the correlation between reactivity ratios and the polar/steric effect of vinyl monomers. Otsu *et al*. (1965) investigated reactivity ratios between Sty and alkyl methacrylates (CH2=CCH3-COO-**R**), such as methyl (MMA), ethyl (EMA), propyl, butyl (BMA), dodecyl (DMA), phenyl methacrylate, etc. Measured *co*-polymer compositions were used to estimate reactivity ratios according to the Fineman-Ross (1950) linearization method at low conversion level. Plotting the ratios with a polar substituent constant in the Hammet-Taft equation, they concluded that reactivities depend on the polar character more so than on the structure of the alkyl groups. Cameron and Kerr (1967) conducted a similar study of Sty and alpha-substituted methyl acrylate (CH2=C**R**-COO-CH3) *co*-polymerizations and verified that both the steric and polar nature of substituents directly attached on the reacting vinyl site affect the reactivity ratios. A more comprehensive correlation study was performed by Borchardt (1982). He used the Alfrey-Price equation for *co*-polymer reactivity ratios for combinations of Sty, acrylates, methacrylates, and carboxylic acids. After that, he calculated correlation coefficients between the ratios and the several constants regarding polar and steric factors. As a result, it was revealed that the two factors do not always affect the two reactivity ratios together with the same degree.

Chow (1975) did elemental analysis for *co*-polymer composition of Sty with HEA, hydroxypropyl acrylate (HPA), and 2-(1-aziridinyl) ethyl methacrylate (AEM), and estimated reactivity ratios. He also recalculated *Q-e* values which are more reasonable than the ones found in the literature. Borchardt (1982) used ^{13}C-NMR absorption frequencies of the polymerizing double bond carbon atoms for *Q-e* values. He calculated reactivity ratios and compared them with literature values from 54 *co*-polymerizations. Utilizing the ratios with a computer program made by Harwood (1968), the dyad/triad sequence fractions were determined. This computer program was used later to compare with measured dyad/triad/tetrad fractions in MA/MMA system by Kim and Harwood (2002).

Catala *et al*. (1986) determined reactivity ratios between HEA with MA, EA, and BA using the Fineman-Ross method. They indicated that HEA/MA showed a completely random (Bernoullian) behaviour, i.e., both of the reactivity ratios were one. On the other hand, increasing bulkiness of the alkyl ester group (ethyl- and butyl-) led to favored reaction between HEA radicals with these monomers. However, according to the phase separation experiments regarding the hydrophilic-hydrophobic balance which is dependent on the reaction conditions (temperature/pH) by Mun *et al*. (2007), the water soluble HEA/BA *co*-polymer also exhibited Bernoullian behaviour in aqueous solvents and less than 30 mol % of BA content.

In the early days when computers were not readily available, two approaches widely used were the Fineman-Ross or Kelen-Tüdos techniques, linear least-squares methods which are incorrect from a statistical point of view, unfortunately still used nowadays. For instance, Jianying *et al*. (2006) obtained reactivity ratios of Sty with other monomers such as MMA, EMA, BMA, HEA, etc. with the extended Kelen-Tüdos method at 125℃.

An advanced reactivity ratios estimation approach, Error-in-Variables Model (EVM), was proposed by Patino-Leal *et al*. (1980). Considering uncertainties in all measured variables, it differs from nonlinear least-squares in which error is only present in the dependent variables. Reilly and Patino-Leal (1981) developed a Bayesian point estimator in order to find parameters' point and interval estimates using EVM, which was turned into an efficient computation algorithm by Reilly *et al*. (1993). Duever *et al*. (1983) extended this

method from binary to ternary systems and proved that it was more reliable than using the least-squares method. Rossignoli and Duever (1995) compared reactivity ratios obtained from both methods and confirmed the usefulness of EVM. This statistically powerful estimation method was developed into a computer program (RREVM) by Dubé *et al*. (1991) and later upgraded by Polic *et al*. (1998). The latter authors also gave an extensive literature review on the estimation of reactivity ratios.

Co-polymer reactivity ratio estimations at high temperature were performed by several workers. McManus *et al*. (1999) used EVM to estimate reactivity ratios of bulk BA/MMA *co*-polymerization at an elevated temperature range (60 to 140℃) and derived Arrhenius expressions to describe how the ratios vary with temperature. Deviation from the Mayo-Lewis model due to depropagation was not observed in this system. Chambard *et al*. (1999) also investigated the temperature dependence of the reactivity ratios of Sty/BA with the nonlinear least-squares method. Sahloul and Penlidis (2004, 2005) calculated Sty/EA, Sty/MAA, EA/HEA, and HEA/MAA reactivity ratios in bulk and solution up to 130℃, and developed Arrhenius expressions as well.

2.3.3.2 Modeling studies

Branson and Simha (1943), Simha and Branson (1944), and Walling (1949) studied *co*-polymerization modeling in early efforts. Taking the *co*-polymer sequence distribution into consideration, Johnston (1973) developed the glass transition temperature equation from the Fox equation, which was essential for free volume calculation. A dependence of the glass transition temperature of the *co*-polymers on the dyad sequence distribution was found by Switata-Zeliazkow (1993).

Johnson *et al*. (1978) conducted Sty/MMA *co*-polymerization up to high conversion and observed deviations of the measured data from the Skeist equation at the onset of autoacceleration. Dionisio and O'Driscoll (1979) confirmed this and discussed the possible diffusion-control of propagation reaction at high conversion. Teramachi *et al*. (1984) used the same experimental results and calculated the CCD. Revisiting this monomer system,

O'Driscoll and Huang (1989, 1990) measured reaction rates, polymer compositions, and molecular weights and concluded that terminal model is acceptable for composition even to high conversion but penultimate model is better to explain the rate data at low conversion. This penultimate effect was also considered in the Sty/BA *co*-polymerization concerning the variation of reaction rates as a function of monomer feed composition and the presence of solvents (benzene) by Fernández-García *et al*. (2003).

Lord (1984) and Garcia-Rubio *et al*. (1985) reported on the kinetic modeling of bulk Sty/AN *co*-polymerization to predict conversion, number/weight average molecular weights, and number average sequence length during the entire conversion. Free volume theory was adopted in their model for explaining diffusion-controlled kinetics. This monomer system was investigated again and the influence of gel effect on the kinetics, MWD, CCD, and SLD was examined by Balaraman *et al*. (1986).

Sty/BA *co*-polymerization kinetic and modeling studies were investigated by Dubé (1989) and Dubé *et al*. (1990). The reactivity ratios, rate of polymerization, polymer composition, and number/weight average molecular weights were measured through the full conversion range. With the same methodology, Dubé and Penlidis (1995) conducted systematic *co*-polymerization studies of BA/MMA, BA/VAc, and MMA/VAc and extended them further to *ter*-polymerization. It was reported that the largely different reactivity ratios in MMA/VAc *co*-polymerization caused the double-rate phenomenon. Another full conversion experimental study of Sty/EA and Sty/HEA systems was done by McManus and Penlidis (1996) and Kim (1994), respectively.

Based on the terminal model and pseudo-kinetic rate constant method, Xie and Hamielec (1993) introduced the moments calculation for molecular weights of linear, long chain branched, and crosslinked *co*-polymers. Using these equations, Vivaldo-Lima *et al*. (1994) extended the model to the Sty/divinylbenzene system which forms network polymers.

Gao and Penlidis (1998) published a comprehensive *co*-polymerization simulator and database package. Reviewing and model-testing 15 styrenic/acrylate systems, their predictions proved reliable and satisfactory. The model was extended to MMA/BA/VAc *ter*-polymerization and the results were successful (Gao and Penlidis, 2000). Using the

simulation package, Fujisawa and Penlidis (2008) introduced modeling work regarding three classes of *co*-polymer composition control strategies in a semi-batch reactor, and discussed the influence of the policies on polymerization rate, composition, molecular weight, branching, and sequence length distribution.

Another important topic, depropagation, has been developed in parallel since McCormick (1957) discovered experimentally that AMS does not polymerize above 61℃ and verified the relation between thermodynamic equilibrium concentration and the ceiling temperature. Lowry (1960) assumed three cases in which one of the two monomers undergoes reversible propagation and suggested the corresponding *co*-polymer composition equations. Later on, several efforts to develop a more general equation took place. Howell *et al*. (1970) and Izu and O'Driscoll (1970) tried to describe both the SLD and composition by considering conditional probability and Monte Carlo methods, respectively. Wittmer (1971) added some correction factors which compensate for radical effects with different terminal sequence distributions, into the Mayo-Lewis equation.

The depropagation model for *co*-polymer composition by Krüger *et al*. (1987) was considered more general and stable with better convergence properties than the ones by Lowry (1960) and Wittmer (1971), and this was discussed by Palmer *et al*. (2000, 2001) via AMS/MMA bulk and solution (toluene) batch *co*-polymerizations at 60 to 140℃. They estimated the equilibrium constants and *cross*-depropagation ratios as well as reactivity ratios, and obtained experimental data regarding conversion, composition, and molecular weights through the full conversion range. Using the data, Cheong and Penlidis (2004) showed reasonable model predictions, and Leamen *et al*. (2005a, 2005b) reinvestigated this monomer system for more acceptable parameters and expanded to AMS/BA/MMA *ter*-polymerization.

All depropagating models mentioned above were based on terminal model kinetics. On the other hand, combined works of depropagating effects with the penultimate model were considered by Grady *et al*. (2002) and Li *et al*. (2005, 2006). BMA/BA *co*-polymerization kinetic and modeling studies were performed at temperatures above 120℃. They used a semi-batch starved-feed policy which is popular in industry for the purpose of controlling polymer composition and molecular weight. They extended the equilibrium monomer

concentration equation by Bywater (1955) for the depropagating BMA monomer in a semi-batch reactor. Another important aspect was the intramolecular chain transfer and scission of BA polymerization. They combined this with the implicit penultimate unit effect model and showed good fitting results. Furthermore, Li *et al*. (2006) and Wang and Hutchinson (2008) investigated the kinetics of Sty/BMA and Sty/dodecyl methacrylate (DMA), respectively, and explained the depropagating behaviour with the penultimate model. Table 2.2 cites references for *co*-polymerization kinetic and modeling studies.

Reference	Reference type
Branson, Simha (1943)	Modeling
Alfrey, Goldfinger (1944)	Polymer composition
Mayo, Lewis (1944)	Polymer composition
Simha, Branson (1944)	Modeling
Wall (1944)	Polymer composition
Stockmayer (1945)	CCD
Merz *et al*. (1946)	Polymer composition
Skeist (1946)	Polymer composition
Walling (1949)	Modeling
Fineman, Ross (1950)	Reactivity ratio
Lowry (1960)	Depropagation
Harwood, Ritchey (1964)	SLD
Meyer, Lowry (1965)	Polymer composition
Otsu *et al*. (1965)	Reactivity ratios

Cameron, Kerr (1967)	Reactivity ratios
Chan, Meyer (1968)	Polymer composition
Harwood (1968)	SLD
Howell *et al*. (1970)	Depropagation
Izu, O'Driscoll (1970)	Depropagation
Wittmer (1971)	Depropagation
Johnston (1973)	Modeling
Chow (1975)	Reactivity ratios
Johnson *et al*. (1978)	Modeling
Dionisio, O'Driscoll (1979)	Modeling
Patino-Leal *et al*. (1980)	Reactivity ratios
Reilly, Patino-Leal (1981)	Reactivity ratios
Borchardt (1982)	Reactivity ratios
Hill *et al*. (1982)	SLD
Duever *et al*. (1983)	Reactivity ratios
Lord (1984)	Model testing
Teramachi *et al*. (1984)	CCD
Borchardt (1985)	Reactivity ratios
Garcia-Rubio *et al*. (1985)	Reactivity ratios Model testing
Balaraman *et al*. (1986)	CCD, SLD
Catala *et al*. (1986)	Reactivity ratios

Krüger *et al*. (1987)	Depropagation
O'Driscoll, Reilly (1987)	Reactivity ratios
Tacx *et al*. (1988)	CCD
Dubé (1989)	Model testing Reactivity ratios
O'Driscoll, Huang (1989, 1990)	Modeling
Dubé *et al*. (1990)	Model testing Reactivity ratios
Dubé *et al*. (1991)	Reactivity ratios
Engelmann, Schmidt-Naake (1993)	CCD
Reilly et al. (1993)	Reactivity ratios
Switata-Zeliazkow (1993)	Modeling
Xie, Hamielec (1993)	Modeling
Kim (1994)	Model testing, Reactivity ratios
Vivaldo-Lima *et al*. (1994)	Modeling
Dubé, Penlidis (1995)	Model testing, Reactivity ratios
Rossignoli, Duever (1995)	Reactivity ratios
McManus, Penlidis (1996)	Model testing, Reactivity ratios
Gao, Penlidis (1998)	Model testing
Polic *et al*. (1998)	Reactivity ratios
Chambard *et al*. (1999)	Reactivity ratios
Martinet, Guillot (1999)	Depropagation

McManus *et al*. (1999)	Reactivity ratios
Palmer *et al*. (2000, 2001)	Depropagation
Scholtens *et al*. (2001)	CCD
Grady *et al*. (2002)	Depropagation
Kim, Harwood (2002)	SLD
Fernandez-Garcia *et al*. (2003)	Modeling
Cheong, Penlidis (2004)	Depropagation
Sahloul, Penlidis (2004, 2005)	Reactivity ratios
Leamen *et al*. (2005)	Depropagation
Li *et al*. (2005)	Depropagation
Jianying *et al*. (2006)	Reactivity ratios
Li *et al*. (2006)	Depropagation
Mun *et al*. (2007)	Reactivity ratios
Fujisawa, Penlidis (2008)	Modeling
Wang, Hutchinson (2008)	Depropagation

Table 2.2. Reference list for *co*-polymerization studies

2.3.4 *Homo*-polymerization

Most of the references for *homo*-polymerization cited below are related with kinetic studies in search of better parameters for multi-component polymerization and experimental data for model testing. Similarly to the *co*-polymerization subsection, this brief *homo*-polymerization literature review is also organized in kinetic and modeling study parts and summarized in Table 2.3.

2.3.4.1 Kinetic studies

Nair and Muthana (1961) studied kinetics of *n*-BMA and *i*-BMA bulk/solution *homo*-polymerizations. They measured the rate of polymerization and intrinsic viscosity for molecular weight calculations. EA polymerization was conducted by Raghuram and Nandi (1967, 1970). They observed severe autoacceleration in the bulk case and determined propagation and solvent-transfer rate constants in benzene.

Buback *et al*. (1989) observed the ratio of termination and propagation rate constants is dependent on conversion (10-60%) using laser-induced experiments on BA bulk polymerization. They expected its conversion dependence would also be applicable in the region where diffusion-control of propagation occurs, which was verified with measuring termination and propagation rate constants separately from ethylene, BA, and MMA polymerizations by Buback (1990).

Dubé *et al*. (1991) performed an experimental design for temperature and initiator effects on BA polymerization over the full conversion range and tested conversion data with a simulation model. The reproducibility of the data was ensured by replicate runs. This experimental and simulation study was continued on EA polymerization by Gao *et al*. (1997).

Pulsed-laser polymerization (PLP) in accordance with MWD measurements by gel permeation chromatography (GPC) greatly improved our estimates of propagation rate constants. For example, Buback *et al*. (1995) used this method for Sty, and further extended it to other monomers: EMA, *n*-BMA, and *i*-BMA by Hutchinson *et al*. (1995), BA measured by Lyons *et al*. (1996) and Asua *et al*. (2004), MAA by Beuermann *et al*. (1997), *n*-BMA and *n*-DMA by Hutchinson *et al*. (1997), and finally, BMA and *tert*-BMA by Buback and Junkers (2006). Because the accuracy of this technique is dependent on that of GPC, proper calibration is of great importance.

McKenna *et al*. (1999) conducted BA solution polymerization studies for the lumped rate constant ($k_p/k_t^{0.5}$) and reported that it decreased as the monomer concentration increased. They suggested a possible conclusion that the termination rate constant is chain-length dependent.

HEA bulk/solution *homo*-polymerization and atom transfer radical polymerization (ATRP) was carried out by Vargün and Usanmaz (2005). The reaction exhibited a distinctive gel effect without limiting conversion, high molecular weights (insoluble in common solvents), and strong intermolecular hydrogen bonding of the polymer (absorbed more than 30 wt% of water). This monomer was recently studied by Chen *et al*. (2007) via frontal polymerization, a localized reaction which is taking place directionally through the vessel and helpful for rapid synthesis of many polymers with spatially controlled microstructures and morphologies.

The mechanism for BA polymerization was investigated further by Peck and Hutchinson (2004). The BA monomer concentration in xylene was kept low by semi-batch starved-feed high temperature reactor operation and significant intramolecular transfer rates were observed resulting in a tertiary radical center which can proceed to termination, propagation, or β-scission. Further, they estimated the relevant parameters and formulated a mechanistic model. Quan *et al.* (2005) conducted NMR analysis on EA and BA polymerizations at high temperatures (140-180℃) up to high conversion. The obtained polymer structures were explained by chain transfer to solvent and the additional cyclization mechanism in acrylate polymerization, such as β-scission of the tertiary radical due to intramolecular chain transfer. Rantow *et al*. (2006) not only estimated the reaction constants through their BA experiments, but also presented microstructural quantities such as number-average terminal double bonds per chain (TDBC) and terminal solvent groups per chain (TSGC). Furthermore, they suggested a possible BA self-initiation by decomposition of impurities at high temperature, including modeling for the mechanism mentioned above.

2.3.4.2 Modeling studies

Numerous modeling studies on *homo*-polymerization have taken place over the last 30 years or so, and citing them all here is beyond the scope of this section. Gao and Penlidis (1996) reviewed sources of literature with useful experimental data for several monomer systems in their extensive paper, along with a summary of modeling efforts. They also

showed model predictions over a very wide range of monomer systems and conditions, using a comprehensive database of physico-chemical monomer characteristics (WATPOLY). Confirmations and additional extensions were given in Dhib *et al*. (2000), Gao *et al*. (1998, 2000) and Gao *et al*. (2004). Table 2.3 cites some of these most useful references for the present thesis.

Reference	Reference type
Bywater (1955)	Depropagation
McCormick (1957)	Depropagation
Nair, Muthana (1961)	Kinetics
Raghuram, Nandi (1967, 1970)	Kinetics
Hui, Hamielec (1972)	Kinetics Modeling
Friis, Nyhagen (1973)	Kinetics
Arai, Saito (1976)	Modeling
Husain, Hamielec (1978)	Modeling
Marten, Hamielec (1982)	Modeling
Stickler (1983), Stickler *et al*. (1984)	Modeling
Buback *et al*. (1989)	Kinetics
Buback (1990)	Kinetics Modeling
Dubé *et al*. (1991)	Kinetics Modeling
Kumar, Gupta (1991)	Kinetics
Kuindersma (1992)	Model testing

Gao (1992)	Model testing
Buback *et al*. (1995)	Kinetics
Hutchinson *et al*. (1995)	Kinetics
Gao, Penlidis (1996)	Model testing
Lyons *et al*. (1996)	Kinetics
Gao *et al*. (1997)	Model testing
Beuermann *et al*. (1997)	Kinetics
Hutchinson *et al*. (1997)	Kinetics
McKenna *et al*. (1999)	Kinetics
Dhib *et al*. (2000)	Model testing
Asua *et al*. (2004)	Kinetics
Peck, Hutchinson (2004)	Kinetics Modeling
Gao *et al*. (2004)	Modeling
Quan *et al*. (2005)	Kinetics
Vargün, Usanmaz (2005)	Kinetics
Buback, Junkers (2006)	Kinetics
Rantow *et al*. (2006)	Modeling
Matthews *et al*. (2007): Sty	Molecular weights
Chen *et al*. (2007)	Kinetics

Table 2.3. References for *homo*-polymerization studies

Chapter 3

Model Development

3.1 Model development in a batch/semi-batch reactor

3.1.1 Monomer and Radical balances

Assuming LCA-I, monomer balances are as follows.

$$\frac{dN_i}{dt} = F_{i,in} - R_{pi}V \tag{3-1}$$

where N_i, $F_{i,in}$, and R_{pi} stand for the moles, the molar inflow rate, and the rate of consumption of monomer species i, respectively, and V is the volume of the reaction mixtures. If the model is designed for six monomers, then i changes from 1 to 6 and there are 36 propagation reactions (30 *cross*-propagations and 6 *homo*-propagations), assuming, of course, no depropagation steps. In a batch reactor, $F_{i,in}$ becomes zero. R_{pi} is expressed in terms of rate constants, radical and monomer concentrations.

$$R_{pi} = \sum_{j=1}^{6} R_{ji} = R_{1i} + R_{2i} + \cdots R_{6i} = \left(k_{p1i}[R_1^\bullet] + k_{p2i}[R_2^\bullet] + \cdots k_{p6i}[R_6^\bullet]\right)[M_i] \tag{3-2}$$

$$[M] = \sum_{i=1}^{6}[M_i],\ \ [R^\bullet] = \sum_{i=1}^{6}[R_i^\bullet],\ \ f_i = \frac{[M_i]}{[M]},\ \ \Phi_j^\bullet = \frac{[R_j^\bullet]}{[R^\bullet]}$$

where [M], $[R^\bullet]$, f_i and $\Phi_j^\bullet$ are the total monomer and radical concentration, and the mole fraction of monomer species i and radical species j, respectively.

Now let us build the radical balances. In order to calculate the radical fraction $\Phi_j^\bullet$, radical balances are governed by LCA-II. Thirty *cross*-propagation reaction constants should be considered.

$$\begin{aligned}\frac{d[R_i^\bullet]}{dt} &= (R_{1i} + R_{2i} + \cdots + R_{6i}) - (R_{i1} + R_{i2} + \cdots + R_{i6}) \\ &= \left(k_{p1i}[R_1^\bullet] + k_{p2i}[R_2^\bullet] + \cdots + k_{p6i}[R_6^\bullet]\right)[M_i] \\ &\quad - \left(k_{pi1}[M_1] + k_{pi2}[M_2] + \cdots + k_{pi6}[M_6]\right)[R_i^\bullet] = \sum_{\substack{j=1 \\ (j\neq i)}}^{6} R_{ji} - \sum_{\substack{j=1 \\ (j\neq i)}}^{6} R_{ij} \approx 0\end{aligned} \tag{3-3}$$

Individual radical concentrations can be obtained from multiplying the total radical concentration by each radical fraction. The total radical concentration is calculated using the Steady-State Hypothesis (SSH), which will be introduced later.

Radical fractions can be solved for from a generalized system (set) of equations. Rearranging equation (3-3) into a matrix form,

$$\mathbf{M} \cdot \mathbf{r} = \mathbf{b} \tag{3-4}$$

where

$$\mathbf{M} = \begin{bmatrix} -\sum_{j=2}^{6}\left(k_{p1j}f_j\right) & k_{p21}f_1 & k_{p31}f_1 & k_{p41}f_1 & k_{p51}f_1 & k_{p61}f_1 \\ k_{p12}f_2 & -\sum_{\substack{j=1 \\ (j\neq 2)}}^{6}\left(k_{p2j}f_j\right) & k_{p32}f_2 & k_{p42}f_2 & k_{p52}f_2 & k_{p62}f_2 \\ k_{p13}f_3 & k_{p23}f_3 & -\sum_{\substack{j=1 \\ (j\neq 3)}}^{6}\left(k_{p3j}f_j\right) & k_{p43}f_3 & k_{p53}f_3 & k_{p63}f_3 \\ k_{p14}f_4 & k_{p24}f_4 & k_{p34}f_4 & -\sum_{\substack{j=1 \\ (j\neq 4)}}^{6}\left(k_{p4j}f_j\right) & k_{p54}f_4 & k_{p64}f_4 \\ k_{p15}f_5 & k_{p25}f_5 & k_{p35}f_5 & k_{p45}f_5 & -\sum_{\substack{j=1 \\ (j\neq 5)}}^{6}\left(k_{p5j}f_j\right) & k_{p65}f_5 \\ k_{p16}f_6 & k_{p26}f_6 & k_{p36}f_6 & k_{p46}f_6 & k_{p56}f_6 & -\sum_{j=1}^{5}\left(k_{p6j}f_j\right) \end{bmatrix}$$

$$\mathbf{r} = \begin{bmatrix}\Phi_1^\bullet & \Phi_2^\bullet & \Phi_3^\bullet & \Phi_4^\bullet & \Phi_5^\bullet & \Phi_6^\bullet\end{bmatrix}', \quad \mathbf{b} = \begin{bmatrix}0 & 0 & 0 & 0 & 0 & 0\end{bmatrix}'$$

Since $\sum_{i=1}^{6}\Phi_i^{\bullet}=1$, substituting $\Phi_6^{\bullet}=1-\Phi_1^{\bullet}-\Phi_2^{\bullet}-\Phi_3^{\bullet}-\Phi_4^{\bullet}-\Phi_5^{\bullet}$ and rearranging again, the following expression is obtained.

$$\mathbf{M}=\begin{bmatrix}
-\sum_{j=2}^{6}\left(k_{p1j}f_j\right)-k_{p61}f_1 & \left(k_{p21}-k_{p61}\right)f_1 & \left(k_{p31}-k_{p61}\right)f_1 & \left(k_{p41}-k_{p61}\right)f_1 & \left(k_{p51}-k_{p61}\right)f_1 \\
\left(k_{p12}-k_{p62}\right)f_2 & -\sum_{\substack{j=1\\(j\neq 2)}}^{6}\left(k_{p2j}f_j\right)-k_{p62}f_2 & \left(k_{p32}-k_{p62}\right)f_2 & \left(k_{p42}-k_{p62}\right)f_2 & \left(k_{p52}-k_{p62}\right)f_2 \\
\left(k_{p13}-k_{p63}\right)f_3 & \left(k_{p23}-k_{p63}\right)f_3 & -\sum_{\substack{j=1\\(j\neq 3)}}^{6}\left(k_{p3j}f_j\right)-k_{p63}f_3 & \left(k_{p43}-k_{p63}\right)f_3 & \left(k_{p53}-k_{p63}\right)f_3 \\
\left(k_{p14}-k_{p64}\right)f_4 & \left(k_{p24}-k_{p64}\right)f_4 & \left(k_{p34}-k_{p64}\right)f_4 & -\sum_{\substack{j=1\\(j\neq 4)}}^{6}\left(k_{p4j}f_j\right)-k_{p64}f_4 & \left(k_{p54}-k_{p64}\right)f_4 \\
\left(k_{p15}-k_{p65}\right)f_5 & \left(k_{p25}-k_{p65}\right)f_5 & \left(k_{p35}-k_{p65}\right)f_5 & \left(k_{p45}-k_{p65}\right)f_5 & -\sum_{\substack{j=1\\(j\neq 5)}}^{6}\left(k_{p5j}f_j\right)-k_{p65}f_5
\end{bmatrix}$$

$$\mathbf{r}=\begin{bmatrix}\Phi_1^{\bullet} & \Phi_2^{\bullet} & \Phi_3^{\bullet} & \Phi_4^{\bullet} & \Phi_5^{\bullet}\end{bmatrix}',\ \mathbf{b}=\begin{bmatrix}-k_{p61}f_1 & -k_{p62}f_2 & -k_{p63}f_3 & -k_{p64}f_4 & -k_{p65}f_5\end{bmatrix}'$$

Finally, radical fractions are calculated by $\mathbf{r}=\mathbf{M}^{-1}\cdot\mathbf{b}$.

3.1.2 Reaction volume

Due to the change in density from monomer to polymer, the volume of the polymerizing mixture will shrink during the reaction. This can be accounted for by the following equation.

$$\frac{dV}{dt}=\sum_{i=1}^{6}\left[\frac{F_{i,in}\,Mw_i}{\rho_{i,monomer}}-R_{pi}\,Mw_i\left(\frac{1}{\rho_{i,monomer}}-\frac{1}{\rho_{polymer}}\right)V\right] \tag{3-5}$$

where Mw_i, $\rho_{i,monomer}$, and $\rho_{polymer}$ are the molecular weight and the density of monomer species *i*, and the density of polymer, respectively.

3.1.3 Polymer balances

In a batch reactor, the amount of consumed monomers is equal to that of the generated polymer according to LCA-I. In a semi-batch reactor, additional balances are needed for the inflow of monomers that are incorporated in the polymer, according to Hamielec *et al*. (1987b):

$$\frac{dP_i}{dt} = F_{pi,in} + R_{pi}V \tag{3-6}$$

where P_i and $F_{pi,in}$ are the moles and molar inflow of monomer species i bound as polymer.

3.1.4 Additional ingredient balances

Initiator (N_I) and impurity (N_Z) balances are needed to build the full radical balance. Radicals are generally generated by initiator decomposition and consumed by termination, or by reaction with impurity acting as inhibitor/retarder.

$$\frac{dN_I}{dt} = F_{I,in} - k_d N_I \tag{3-7}$$

$$\frac{dN_Z}{dt} = F_{Z,in} - k_{fz} N_Z [R^\bullet] \tag{3-8}$$

where k_d and k_{fz} are the initiator decomposition rate constant and impurity reaction rate constant.

Now we are ready to calculate the total radical concentration using the following balance.

$$\frac{d\left(V[R^\bullet]\right)}{dt} = 2 f_{eff}\, k_d N_I - k_{fz} N_Z [R^\bullet] - k_t [R^\bullet]^2 V \tag{3-9}$$

where f_{eff} is initiator efficiency and k_t is the overall termination rate constant ($k_t = k_{tc} + k_{td}$).

Using the Steady State Hypothesis (SSH) for radicals, based on equation (3-9), the total radical concentration is

$$[R^\bullet] = \frac{1}{2}\left\{\left[\left(\frac{k_{fz}[Z]}{k_t}\right)^2 + 8\frac{f_{eff}\, k_d}{k_t}[I]\right]^{1/2} - \frac{k_{fz}[Z]}{k_t}\right\} \tag{3-10}$$

Multiplying this with the corresponding radical fractions gives the individual radical concentrations.

If a chain transfer agent (N_{CTA}) is added for molecular weight control or solvent (N_S) is present in the reactor, these balances should also be included.

$$\frac{dN_{CTA}}{dt} = F_{CTA,in} - k_{fCTA} N_{CTA}[R^{\bullet}] \tag{3-11}$$

$$\frac{dN_S}{dt} = F_{S,in} - k_{fS} N_S[R^{\bullet}] \tag{3-12}$$

where k_{fCTA} and k_{fS} represent chain transfer rate constant to CTA and solvent, respectively.

3.2 Calculated Outputs: Part A

3.2.1 Total/partial molar conversions

A number of important variables can be calculated from the above balances. The total molar conversion of monomers to multi-component polymer is given by

$$X = \frac{[M]_0 - [M]}{[M]_0} = \frac{\sum_{i=1}^{6} P_i}{\sum_{i=1}^{6} (N_i + P_i)} \tag{3-13}$$

Similarly, partial conversion of monomer species *i* is

$$X_i = \frac{P_i}{N_i + P_i} \tag{3-14}$$

Conversion versus time profiles directly show how fast polymerization proceeds.

3.2.2 Instantaneous/accumulated polymer composition

The instantaneous multi-component polymer composition, the overall mole fraction of monomer species *i* incorporated instantaneously in the polymer, is calculated as

$$F_i = \frac{dN_i}{\sum_{i=1}^{6}(dN_i)} = \frac{R_{pi}}{R_p} = \frac{\sum_{j=1}^{6} R_{ji}}{\sum_{i=1}^{6}\sum_{j=1}^{6} R_{ji}} = \frac{\sum_{j=1}^{6}\left(k_{pji}\Phi^{\bullet}_{j}\right)f_i}{\sum_{i=1}^{6}\sum_{j=1}^{6}\left(k_{pji}\Phi^{\bullet}_{j}\right)f_i} \tag{3-15}$$

Equation (3-15) is a generalized one and flexibly covers all kinds of multi-component cases (even *homo*-polymerization). When reduced to simpler cases, it becomes identical with the Mayo-Lewis (*co*-polymer), Alfrey-Goldfinger (*ter*-polymer), and Walling-Briggs equations (*ter*- and higher). Our simulation model can also compare with Valvassori-Sartori and Hocking-Klimchuck equations which are derived from a simplified LCA-II assumption (see Appendix A).

Instantaneous *co*-polymer composition normally changes in a batch reactor governed by reactivity ratios and this phenomenon is called 'composition drift'. It is one of the important indicators closely related with polymer's physical/chemical properties and should be controlled to produce a desired product. Estimation of reactivity ratios is the key factor to calculate the composition as well as the radical fraction mentioned above. The definition of a reactivity ratio under the terminal model is the ratio of a *homo*-propagation rate constant divided by a *cross*-propagation rate constant.

$$r_{ij} = \frac{k_{pii}}{k_{pij}} \quad (i \neq j) \tag{3-16}$$

where i stands for radical species and j for the monomer species.

In order to estimate these ratios, *co*-polymerizations should be conducted under various initial monomer fractions (f_{i0}) at conversion levels below 5%. The *co*-polymerization is stopped and the polymer samples are scanned through NMR (^{1}Proton or ^{13}Carbon) and initial *co*-polymer compositions (F_{i0}) are determined. Using initial monomer fraction and *co*-polymer composition data, reactivity ratios can be determined by either nonlinear least-squares or Error-in-Variables Model (EVM) techniques. The number of rate constants for propagation reactions and reactivity ratios in a multi-component polymerization are

$$No.\ of\ propagation\ reactions = \left(No.\ of\ monomer\ species\right)^2$$
$$No.\ of\ reactivity\ \ ratios = \left(No.\ of\ monomer\ species\right)\left(No.\ of\ monomer\ species - 1\right)$$

For example, *hexa*-polymerization involves 36 propagation reactions (assuming no depropagation) and we need 30 binary reactivity ratios for *cross*-propagations and 6 individual *homo*-propagation rate constants. Therefore, successful multi-component studies rely on the establishment of good *homo*- and *co*-polymerization kinetic data.

The accumulated polymer composition, the average mole fraction of monomer i incorporated into the polymer at a certain conversion level, is determined by

$$\overline{F_i} = \frac{P_i}{\sum_{i=1}^{6} P_i} \tag{3-17}$$

The accumulated composition is measured from full conversion range experiments and shows how the amount of monomer bound as polymer changes during the polymerization.

3.2.3 Multi-component pseudo rate constants for overall reaction rate calculations

The pseudo rate constant method enables a complicated multi-component polymerization system to be viewed as a virtual "*homo*-polymerization". The monomer/polymer compositions and radical fractions obtained above are used for the pseudo rate constant calculations in the multi-component case. The individual rate constants are put together into one overall pseudo rate constant by combining with radical fractions, monomer mole fractions, and (or) polymer compositions, depending on the specific reaction (step) mechanism.

3.2.3.1 Initiation

The rate of initiation in multi-component polymerization is the same as that used in *homo*-polymerization, such as

$$R_I = 2 f_{eff,pseudo} k_{d,pseudo} [I] \tag{3-18}$$

where [I] is the chemical initiator concentration, $f_{eff,\ pseudo}$ is the pseudo initiator efficiency, and $k_{d,\ pseudo}$ is the pseudo initiator decomposition rate constant. These pseudo values are calculated via superposition as follows:

$$f_{eff,pseudo} = \sum_{i=1}^{6} f_{eff,i} f_i \tag{3-19}$$

$$k_{d,pseudo} = \sum_{i=1}^{6} k_{d,i} f_i \tag{3-20}$$

Sty monomer undergoes thermal self-initiation without initiator. Its reaction, based on a Diels-Alder mechanism, is reported to follow a 3rd order model, hence the thermal initiation rate is calculated as follows.

$$R_{th} = 2 k_{th} [M]^3 \tag{3-21}$$

$$R_{I,total} = R_I + R_{th} \tag{3-22}$$

3.2.3.2 Propagation

The rate of multi-component polymerization is the rate of disappearance of monomer species in the system.

$$R_p = -\frac{d\left(\sum_{i=1}^{6} [M_i]\right)}{dt} = k_{p,pseudo} [M][R^\bullet] \tag{3-23}$$

The pseudo propagation rate constant can be expressed as

$$k_{p,pseudo} = \sum_{i=1}^{6} \sum_{j=1}^{6} k_{pij} \Phi_i^\bullet f_j \tag{3-24}$$

This can similarly be applied to pseudo termination and transfer rate constants.

3.2.3.3 Termination

It is important to note that there are two conventions (British and American) for termination rate parameters. The British convention is used in the model. The rate of termination is given by

$$R_t = k_{t,pseudo}[R^\bullet]^2 = \sum_{i=1}^{6}\sum_{j=1}^{6} k_{tij}[R_i^\bullet][R_j^\bullet]$$
$$= \sum_{i=1}^{6} k_{tii}[R_i^\bullet]^2 + \sum_{i=1}^{6}\sum_{\substack{j=2 \\ (i\neq j)}}^{6} 2k_{tij}[R_i^\bullet][R_j^\bullet] \tag{3-25}$$

where $i = j$, k_{tij} is the *homo*-termination rate constant.

$i \neq j$, k_{tij} is the *cross*-termination rate constant. And $k_{tij} = k_{tji}$

The pseudo termination rate constant is

$$k_{t,pseudo} = \sum_{i=1}^{6}\sum_{j=1}^{6} k_{tij}\Phi_{i_i}^\bullet\Phi_j^\bullet \tag{3-26}$$

It is common in the literature to redefine the *cross*-termination rate constants k_{tij} as

$$k_{tij} = \varphi\sqrt{k_{tii}k_{tjj}} \tag{3-27}$$

where φ is the *cross*-termination factor, or Walling's φ factor. It is reported as an adjustable parameter without any physical meaning by many research groups.

3.2.3.4 Transfer to monomer, polymer, CTA, solvent, and inhibitor

The pseudo rate constants for chain transfer reactions are as follows.

$$k_{fm,pseudo} = \sum_{i=1}^{6}\sum_{j=1}^{6} k_{fmij}\Phi_i^\bullet f_j \tag{3-28}$$

$$k_{fp,pseudo} = \sum_{i=1}^{6}\sum_{j=1}^{6} k_{fpij}\Phi_i^{\bullet}\,\overline{F_j} \tag{3-29}$$

$$k_{fCTA,pseudo} = \sum_{i=1}^{6} k_{fCTAi}\Phi_i^{\bullet} \tag{3-30}$$

$$k_{fS,pseudo} = \sum_{i=1}^{6} k_{fSi}\Phi_i^{\bullet} \tag{3-31}$$

$$k_{fZ,pseudo} = \sum_{i=1}^{6} k_{fZi}\Phi_i^{\bullet} \tag{3-32}$$

The transfer reactions ideally affect molecular weights but do not significantly affect the polymerization rates because they are relatively slower than propagation and termination reaction rates. In equations (3-28) and (3-29), theoretically we also need the *cross*-transfer reaction constants. However, these values have been scarcely reported, and they still remain unknown. Our model currently relies on reactivity ratios to estimate the *cross*-transfer rate constants to monomers. Hence, we defined some of the *cross*-transfer rate constants as

$$k_{fmij} = \frac{k_{fmii}}{r_{ij}} \tag{3-33}$$

$$k_{fpij} = k_{fpjj} \tag{3-34}$$

3.2.4 Number/weight average molecular weights and branching

The instantaneous number/weight average molecular weights of linear multi-component polymers can be calculated as

$$M_n = \frac{Mw_{eff}}{\tau + \frac{\beta}{2}} \tag{3-35}$$

$$M_w = \frac{Mw_{eff}\left(2\tau + 3\beta\right)}{\left(\tau + \beta\right)^2} \tag{3-36}$$

where M_n and M_w are number/weight average molecular weights, respectively.

$$Mw_{eff} = \sum_{i=1}^{6}\left[Mw_i \left(\frac{R_{pi}}{R_p} \right) \right] = \sum_{i=1}^{6} \left(Mw_i F_i \right) \tag{3-37}$$

$$\tau = \frac{k_{td}[R^{\bullet}] + k_{fCTA}[CTA] + k_{fS}[S] + k_{fZ}[Z]}{k_p[M]} + \frac{k_{fm}}{k_p}, \qquad \beta = \frac{k_{tc}[R^{\bullet}]}{k_p[M]} \tag{3-38}$$

Equations (3-35) and (3-36) are identical with the *homo*-polymerization case except for the pseudo effective molecular weight and rate constants. The instantaneous weight fraction of polymer of chain length r at some conversion level X and information about the instantaneous molecular weight distribution are given as follows.

$$w(r, X) = (\tau + \beta)\left[\tau + \frac{\beta}{2}(\tau + \beta)(r-1) \right] \frac{r}{(1 + \tau + \beta)^r} \tag{3-39}$$

The cumulative number/weight average molecular weights and weight fraction of polymer of chain length r are given by,

$$\overline{M_n} = \frac{X}{\int_0^X M_n^{-1} dX} \tag{3-40}$$

$$\overline{M_w} = \frac{1}{X}\int_0^X M_w dX \tag{3-41}$$

$$\overline{w(r, X)} = \frac{1}{X}\int_0^X w(r, X) dX \tag{3-42}$$

The equations described above are valid for linear (non-branched) systems. When additional reactions such as transfer reaction to polymer or terminal/internal double bond polymerization are significant, branched or crosslinked polymer molecules are obtained, and hence the method of moments should be applied for the radical and dead polymer distributions. The i^{th} moment of radical distribution Y_i and polymer distribution Q_i are defined as

$$Y_i = \sum_{r=1}^{\infty} r^i [R_r^{\bullet}] \tag{3-43}$$

$$Q_i = \sum_{r=1}^{\infty} r^i [P_r] \tag{3-44}$$

The zeroth, first, and second order moments of the radical distribution are as follows.

$$\frac{d(VY_0)}{dt} = \left(R_i - k_t Y_0^2 - k_{fZ} Y_0 [Z]\right) V \tag{3-45}$$

$$\frac{d(VY_1)}{dt} = \left\{ \begin{array}{l} R_i + k_p [M] Y_0 - k_t Y_0 Y_1 + \left(k_{fCTA}[CTA] + k_{fm}[M] + k_{fS}[S]\right)\left(Y_0 - Y_1\right) \\ + k_{fP}\left(Y_0 Q_2 - Y_1 Q_1\right) + k_p^*\left(Y_0 Q_1 - Y_1 Q_1 + Y_1 Q_0\right) + k_p^{**} Y_0 Q_2 - k_{fZ}[Z] Y_1 \end{array} \right\} V \tag{3-46}$$

$$\frac{d(VY_2)}{dt} = \left\{ \begin{array}{l} R_i + k_p [M]\left(Y_0 + 2Y_1\right) - k_t Y_0 Y_2 + \left(k_{fCTA}[CTA] + k_{fm}[M] + k_{fS}[S]\right)\left(Y_0 - Y_2\right) \\ + k_{fP}\left(Y_0 Q_3 - Y_2 Q_1\right) + k_p^*\left(Y_0 Q_2 + 2Y_1 Q_1 + Y_2 Q_0 - Y_2 Q_1\right) + k_p^{**}\left(Y_0 Q_3 + 2Y_1 Q_2\right) \\ - k_{fZ}[Z] Y_2 \end{array} \right\} V \tag{3-47}$$

Using again the Steady State Hypothesis of radicals, the above equations can be simplified.

$$Y_0 = \frac{1}{2}\left\{ \left[\left(\frac{k_{fz}[Z]}{k_t} \right)^2 + 8 \frac{f k_d}{k_t} [I] \right]^{1/2} - \frac{k_{fz}[Z]}{k_t} \right\} = [R^\bullet] \tag{3-48}$$

$$Y_1 = \frac{R_i + \left\{ k_p [M] + k_{fm}[M] + k_{fCTA}[CTA] + k_{fS}[S] + \left(k_{fp} + k_p^{**}\right) Q_2 + k_p^* Q_1 \right\} Y_0}{k_t Y_0 + k_{fm}[M] + k_{fCTA}[CTA] + k_{fS}[S] + k_{fZ}[Z] + k_{fp} Q_1 + k_p^*\left(Q_1 - Q_0\right)} \tag{3-49}$$

$$Y_2 = \frac{\left\{ \begin{array}{l} R_i + \left(\begin{array}{l} k_p [M] + k_{fm}[M] + k_{fCTA}[CTA] + k_{fS}[S] \\ + k_{fp} Q_3 + k_p^* Q_2 + k_p^{**} Q_3 \end{array} \right) Y_0 \\ + 2\left(k_p [M] + k_p^* Q_1 + k_p^{**} Q_2\right) Y_1 \end{array} \right\}}{k_t Y_0 + k_{fm}[M] + k_{fCTA}[CTA] + k_{fS}[S] + k_{fZ}[Z] + k_{fp} Q_1 + k_p^*\left(Q_1 - Q_0\right)} \tag{3-50}$$

In order to avoid open-ended equations, $Q_3 \approx \frac{Q_2}{Q_0 Q_1}\left(2Q_0 Q_2 - Q_2^2\right)$ is usually employed.

There are two approaches for the calculation of the moments of the polymer molecule distribution. Kuindersma (1992) and Gao (1992) used the zeroth, first, and second moments of the radical distributions while Hamielec *et al*. (1987b), Dubé *et al*., (1991) and Xie and Hamielec (1993) used the zeroth moment (radical concentration) only. After a comparative

evaluation of different approaches (see Appendix B), our model is currently using the Dubé *et al.* (1991) equations, as follows.

$$\frac{d(VQ_0)}{dt} = k_p[M]Y_0V\left(\tau + \frac{\beta}{2} - \frac{k_p^{**}Q_1 + k_p^{*}Q_0}{k_p[M]}\right) \tag{3-51}$$

$$\frac{d(VQ_1)}{dt} = k_p[M]Y_0V\left(1 + \tau - \frac{k_{td}Y_0}{k_p[M]}\right) = k_p[M]Y_0V\left(1 + \frac{k_{fm}}{k_p} + \frac{k_{fS}[S]}{k_p[M]} + \frac{k_{fCTA}[CTA]}{k_p[M]} + \frac{k_{fZ}[Z]}{k_p[M]}\right) \tag{3-52}$$

$$\frac{d(VQ_2)}{dt} = k_p[M]Y_0V\left\{\begin{array}{l}(1+\tau+\beta)+2\left(1+\dfrac{k_p^{*}Q_1+k_p^{**}Q_2}{k_p[M]}\right)\left(\dfrac{1+\tau+\beta+\dfrac{\left(k_p^{**}+k_{fp}\right)Q_2+k_p^{*}Q_1}{k_p[M]}}{\tau+\beta+\dfrac{k_{fp}Q_1}{k_p[M]}}\right)\\ +\beta\left(\dfrac{1+\tau+\beta+\dfrac{\left(k_p^{**}+k_{fp}\right)Q_2+k_p^{*}Q_1}{k_p[M]}}{\tau+\beta+\dfrac{k_{fp}Q_1}{k_p[M]}}\right)^2\end{array}\right\} \tag{3-53}$$

Finally, the cumulative average molecular weights are calculated as

$$\overline{M_n} = Mw_{eff}\frac{Q_1}{Q_0} \tag{3-54}$$

$$\overline{M_w} = Mw_{eff}\frac{Q_2}{Q_1} \tag{3-55}$$

The average number of *tri*/*tetra*-functional branches per molecule can be computed from the following equations (Dubé *et al*., 1991).

$$\frac{d(VQ_0\,\overline{B_{N3}})}{dt} = \left(k_{fp}Q_1 + k_p^{*}Q_0\right)Y_0V \tag{3-56}$$

$$\frac{d(VQ_0\,\overline{B_{N4}})}{dt} = k_p^{**}Q_2Y_0V \tag{3-57}$$

3.3 Diffusion-control kinetics

The termination, propagation, transfer reaction constants and the initiator efficiency can all be affected by the presence of diffusional limitations throughout the entire reaction and may show significant decreases. In bulk and concentrated solution polymerizations, reaction rate remarkably rises at middle or high conversion level and this leads to significant increases in polymer molecular weights. Furthermore, it has been frequently observed at high conversion that the reaction rate falls rapidly and a limiting conversion exists in spite of enough reaction time and initiator/monomer amount. The former is called the autoacceleration, Trommsdorff, Norrish-Smith, or simply gel effect and the latter is known as the glass-transition effect.

It is established that autoacceleration happens due to diffusional (mobility) limitations of radicals and macromolecules. As polymerization proceeds, the growing entangled polymer chains increase the reaction medium viscosity and the reduced radical mobility hinders termination further while initiator is continuously decomposed into small radicals and the chains are growing. As a result, the radical concentration increases and so does polymerization rate.

Several different approaches have been introduced to explain autoacceleration and glass-transition effect as a function of other process variables. We are going to invoke the free volume approach, which is a very powerful semi-empirical model and well tested in the past. The free volume equation is expressed as:

$$V_f = \sum_{i=1}^{n} [V_{f,i}^0 + \alpha_i (T - T_{g,i})] \frac{V_i}{V} \tag{3-58}$$

where:

i is component in the reaction mixture (monomer species, polymer, and solvent).

$V_{f,i}^0$ is free volume of component i at glass transition temperature.

α_i is thermal expansion coefficient above and below glass transition temperature.

T is reaction temperature.

T_{gi} is glass transition temperature for component i.

V_i, V are volume for component *i* and total reaction volume, respectively.

Free volume theory suggested the 'universal values' for $V_{f,i}^0$ and α_i are 0.025, 0.001 for monomers and solvent, and 0.00048 for polymers, respectively. Where appropriate data exist, these parameters may be estimated. The glass transition temperature of the polymer (T_{gpoly}) at some conversion level is calculated using Johnston's method.

$$\frac{1}{T_{gpoly}} = \sum_{i=1}^{6} \frac{w_i p_{ii}}{T_{gpi}} + \sum_{i=1}^{6} \sum_{\substack{j=2 \\ (j \neq i)}}^{6} \frac{w_i p_{ij} + w_j p_{ji}}{T_{gpij}} \tag{3-59}$$

where T_{gpi} is the glass transition temperature for the *homo*-polymer species *i*, T_{gpij} is that of an (ideal) alternating *co*-polymers coming from monomers *i* and *j*, w_i is the weight fraction of monomer *i* bound in the polymer chain, and p_{ij} is the probability of forming a dyad of monomers *i* and *j*. This probability will be discussed in the sequence length distribution section.

After the calculation of free volume, we are ready to investigate diffusion-control kinetics. A decrease for k_t will be observed first because termination is the (chemically) fastest step and high molecular weight macroradicals are involved during the reaction and are hence more vulnerable to restriction of mobility. The diffusion-control of the overall (pseudo) k_t is divided into three intervals: segmental, translational, and reaction-diffusion. When relatively high molecular weight polymers are being produced at low conversions, the termination rate may be controlled by segmental diffusion, which is described by Hamielec *et al*. (1987b) as follows.

$$k_{t,seg} = k_{t,pseudo}\left(1 + \delta_c\, c\right) \tag{3-60}$$

where:

$k_{t,pseudo}$ is a chemically controlled pseudo termination rate constant in equation (3-26).

δ_c is a parameter depending on the molecular weight and the solvent quality.

c is the mass concentration of accumulated polymer.

In this region, when the reaction medium is a thermodynamically "good solvent", the polymer coil size decreases and the termination rate constant may actually increase until the

onset of translational diffusion. To recap, in the first (segmental diffusion) interval, the overall termination rate constant is equal to the segmental diffusion termination rate constant ($k_{t,seg}$) plus the reaction-diffusion termination rate constant, as per equation (3-61). The reaction-diffusion termination rate constant is discussed later (see equation (3-69)).

$$k_{t,overall} = k_{t,seg} + k_{t,rd} \tag{3-61}$$

The second interval, translational diffusion or gel effect region, is determined by a gel effect parameter K_3 suggested by Marten and Hamielec (1982).

$$K_3 = \overline{M}_{w\,cr}^{\,m} \exp\left(\frac{A}{V_{f,cr1}}\right) \tag{3-62}$$

where:

$\overline{M}_{w\,cr}$ is the critical accumulated weight-average molecular weight of polymer.

$V_{f,cr1}$ is the critical free-volume.

A, m are gel effect model parameters for the specific monomer system found in the monomer database. Usually, $m = 0.5$

Stickler *et al*. (1984) performed experiments to determine K_3 values in MMA polymerization and built a temperature-dependent Arrhenius expression for K_3. In the multi-component case, we used the Arrhenius form and calculated a pseudo K_3, composed of the individual values of $K_{3,i}$ via superposition.

$$K_{3,i} = A_{K,i} \exp\left(\frac{E_{K,i}}{RT}\right) \tag{3-63}$$

$$K_{3,pseudo} = \exp\left[1/\sum_{i=1}^{6}\left(\frac{\overline{F_i}}{\log(K_{3,i})}\right)\right] \tag{3-64}$$

where $\overline{F_i}$ is the cumulative polymer composition of monomer species i.

$K_{3,pseudo}$ in equation (3-64) can be calculated for the polymer system in question based on the database characteristics of each monomer.

In the model, the calculated $K_{3,test}$ in equation (3-65) is compared with the predetermined $K_{3,pseudo}$ of equation (3-64) as conversion varies (increases).

$$K_{3,test} = \overline{M_w}^{\,m} \exp\left(\frac{A_{pseudo}}{V_f}\right) \tag{3-65}$$

$$\frac{1}{A_{pseudo}} = \sum_{i=1}^{6}\left(\frac{F_i}{A_i}\right) \tag{3-66}$$

where A_i and F_i are the gel effect model parameters and instantaneous polymer compositions for monomer species i, respectively. For A_i, see earlier the discussion around equation (3-62). These parameters are combined into a pseudo gel effect model parameter A_{pseudo} in the multi-component case, as per equation (3-66).

When $K_{3,test}$ becomes equal to or greater than $K_{3,pseudo}$, then the corresponding $\overline{M_w}$ and V_f (from equation (3-65)) at the specific time (conversion) step become $\overline{M_{w\,cr}}$ and $V_{f,cr1}$, respectively. This signifies the onset of the gel effect (translational diffusion region) and the translationally diffusion-controlled termination rate constant is now governed by equation (3-67).

$$k_{t,trans} = k_{t,cr}\left(\frac{\overline{M_{w\,cr}}}{\overline{M_w}}\right)^{n} \exp\left[-A_{pseudo}\left(\frac{1}{V_f} - \frac{1}{V_{f,cr1}}\right)\right] \tag{3-67}$$

where $k_{t,cr}$ is the overall termination constant at the critical point, and n is a parameter, usually equal to 1.75. This overall termination constant $k_{t,trans}$ will be observed to decrease significantly in this region.

To recap, in this second (translational diffusion) interval, the overall termination rate constant is equal to the translational diffusion termination rate constant ($k_{t,trans}$) plus the reaction-diffusion termination rate constant, as per equation (3-68).

$$k_{t,overall} = k_{t,trans} + k_{t,rd} \tag{3-68}$$

At very high conversion (usually, above 85%), it is expected that the chain mobility affected by translational diffusion will decrease so greatly that radical chains cannot move any more. However, two macroradicals may move toward each other by monomer addition. The final interval, reaction-diffusion or residual termination, is described as

$$k_{t,rd} = \frac{8\pi N_A \delta D}{1000} \tag{3-69}$$

$$\delta = \left(\frac{6V_m}{\pi N_A} \right)^{1/3} \tag{3-70}$$

$$D = \frac{n_s l_0^{\,2}}{6} k_p [M] \tag{3-71}$$

where:

N_A is the Avogadro's number.

D is a reaction diffusion coefficient.

δ is a reaction radius.

V_m is the molar volume of monomer.

n_s is the average number of monomer units in one polymer chain.

l_0 is the length of a monomer unit in the chain.

k_p is the propagation rate constant.

In this final interval, the overall termination rate constant is the same as in equation (3-68).

Stickler (1983) and Stickler *et al*. (1984) enhanced their kinetic model by adding $k_{t,rd}$ to $k_{t,trans}$ in equation (3-68), thus achieving a very good agreement between conversion data and model predictions in MMA polymerization.

Now let us discuss the glass-transition effect. Under viscous polymerizations where the reaction temperature is lower than the glass-transition temperature of the polymerizing mixture being synthesized, even the mobility of small monomer units is limited by diffusion in essentially a solid (glassy) polymer matrix. Thus, even propagation/transfer reactions become diffusion-controlled. The onset happens when the free volume of the polymerizing mixture becomes lower than an experimentally determined critical free volume, and this can be modeled similarly to the translational diffusion-controlled termination.

$$k_p = k_{p0} \exp\left[-B\left(\frac{1}{V_f} - \frac{1}{V_{f,cr2}} \right) \right] \tag{3-72}$$

$$k_{f,CTA/solvent/impurity} = k_{f0} \exp\left[-B\left(\frac{1}{V_f} - \frac{1}{V_{f,cr2}} \right) \right] \tag{3-73}$$

where:

k_{p0} and k_{f0} are chemically controlled propagation/transfer rate constants.

B is the glass-transition effect model parameter.

$V_{f,cr2}$ is the critical free volume for diffusion-control of propagation/transfer rate.

In addition, the initiator efficiency can also undergo diffusion-control and begins to decrease at high conversion, in a way similar to k_p. When the free volume of the reaction medium becomes less than an experimentally determined critical free volume, initiator efficiency is calculated using

$$f = f_0 \exp\left[-C\left(\frac{1}{V_f} - \frac{1}{V_{f,cr3}} \right) \right] \tag{3-74}$$

where:

f_0 is the initial initiator efficiency.

C is the efficiency-related model parameter.

$V_{f,cr3}$ is the critical free volume for diffusion-control of initiator efficiency.

3.4 Calculated Outputs: Part B

3.4.1 Number/weight average sequence lengths

Multi-component polymer composition, F_i (instantaneous) and $\overline{F}_i$ (cumulative), is able to describe the overall macroscopic instantaneous/accumulated mole ratio of monomer units in the polymer chain. In a batch reactor, composition drift happens and these composition values are not constant during polymerization because of different reactivities among

monomer species. However, F_i and $\overline{F}_i$ alone cannot describe the distribution of monomer sequences, for example, in block *co*-polymers such as -AA--A-BB--B-AA-, and purely alternating *co*-polymers such as -A-B-A-B-A-B-, having the same composition. This microstructural property, information about the average number of monomer units coming from how they are distributed along the polymer chain, can be revealed by the sequence length distribution. Because of reflecting intramolecular heterogeneity, average sequence length and sequence length distribution (SLD) can be important indicators of multi-component polymer behavior, especially when the individual *homo*-polymers incorporated have widely differing properties.

To illustrate this, a statistical approach (Koenig, 1980) will be introduced. Assuming the polymerization behaviour follows the terminal model, let us define the probability that a growing radical with unit *i* in its end adds monomer *j*, p_{ij}. This is the same definition used for the glass-transition temperature equation (3-59) earlier.

$$p_{ij} = \frac{k_{pij}[R_i^\bullet][M_j]}{\sum_{j=1}^{6} k_{pij}[R_i^\bullet][M_j]} = \frac{k_{pij}[M_j]}{\sum_{j=1}^{6} k_{pij}[M_j]} = \frac{k_{pij} f_j}{\sum_{j=1}^{6} k_{pij} f_j} \tag{3-75}$$

where

$$\sum_{j=1}^{6} p_{ij} = p_{ii} + \sum_{k=1}^{6} p_{ik} = 1 \qquad (k \neq i)$$

The probability of having *n* consecutive units of monomer *i*, that is a sequence of monomer *i* with length *n* in a growing chain, is,

$$N_{in} = p_{ii}^{n-1} \sum_{k=1}^{6} p_{ik} \qquad (k \neq i) \tag{3-76}$$

where

$$\sum_{n=1}^{\infty} N_{in} = \sum_{k=1}^{6} p_{ik} \left(\sum_{n=1}^{\infty} p_{ii}^{n-1} \right) \approx \sum_{k=1}^{6} p_{ik} \frac{1}{1-p_{ii}} = \frac{1-p_{ii}}{1-p_{ii}} = 1 \qquad (k \neq i)$$

Figure 3.1 gives an example. It is a simulation plot of Sty sequence length probability (N_{1n}) distribution in a Sty/AN *co*-polymer, where the initial Sty monomer feed composition ranges from 0.4 to 0.9. It is observed that increasing the chain (sequence) length leads to a decrease of the probabilities, and the tendencies are different according to feed compositions. As Sty content increases in the feed, Sty monomer becomes more likely to attach to the Sty radical than AN monomer does. As a result, the existence of longer sequences of Sty will make the probability distribution broader.

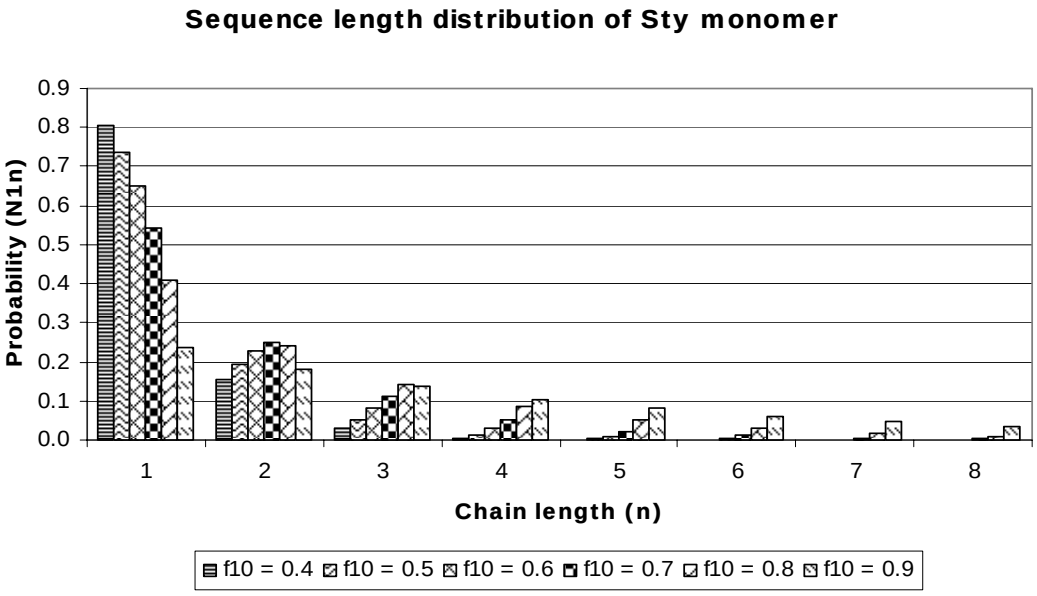

Figure 3.1. Sequence length distribution of Sty in Sty/AN *co*-polymer, T = 60℃

The instantaneous number-average sequence length of monomer *i* is calculated as

$$\overline{n_i} = \frac{\sum_{n=1}^{\infty} nN_{in}}{\sum_{n=1}^{\infty} N_{in}} = \sum_{n=1}^{\infty} nN_{in} = N_{i1} + 2N_{i2} + 3N_{i3} + \cdots = \sum_{n=1}^{\infty}\left(np_{ii}^{n-1}\sum_{k=1}^{6} p_{ik} \right) = \sum_{n=1}^{\infty}\left\{ np_{ii}^{n-1}\left(1-p_{ii}\right)\right\}$$
$$= \sum_{n=1}^{\infty} np_{ii}^{n-1} - \sum_{n=1}^{\infty} np_{ii}^{n} \approx \frac{1}{\left(1-p_{ii}\right)^2} - \frac{p_{ii}}{\left(1-p_{ii}\right)^2} = \frac{1}{1-p_{ii}} = \frac{1}{\sum_{k=1}^{6} p_{ik}} \quad (3\text{-}77)$$

The instantaneous weight-average sequence length of monomer *i* is given by

$$\bar{w}_i = \frac{\sum_{n=1}^{\infty} n^2 N_{in}}{\sum_{n=1}^{\infty} n N_{in}} = \frac{\sum_{n=1}^{\infty} n^2 N_{in}}{\bar{n}_i} = \sum_{k=1}^{6} p_{ik} \sum_{n=1}^{\infty} n^2 N_{in} = \sum_{k=1}^{6} p_{ik} \sum_{n=1}^{\infty} n^2 \left(p_{ii}^{n-1} \sum_{k=1}^{6} p_{ik} \right) = \left(\sum_{k=1}^{6} p_{ik} \right)^2 \sum_{n=1}^{\infty} n^2 p_{ii}^{n-1} \quad (3\text{-}78)$$

$$= (1 - p_{ii})^2 \sum_{n=1}^{\infty} n^2 p_{ii}^{n-1} \approx (1 - p_{ii})^2 \frac{1 + p_{ii}}{(1 - p_{ii})^3} = \frac{1 + p_{ii}}{1 - p_{ii}}$$

These equations are general. Considering the *co*-polymer case, for example, they can be expressed in terms of reactivity ratios and monomer feed compositions.

$$\bar{n}_1 = \frac{1}{1 - p_{11}} = \frac{1}{p_{12}} = \frac{k_{p11} f_1 + k_{p12} f_2}{k_{p12} f_2} = 1 + \frac{k_{p11} f_1}{k_{p12} f_2} = 1 + r_{12} \frac{f_1}{f_2} = 1 + \frac{f_1}{\frac{f_2}{r_{12}}} \quad (3\text{-}79)$$

$$\bar{n}_2 = \frac{1}{1 - p_{22}} = \frac{1}{p_{21}} = \frac{k_{p21} f_1 + k_{p22} f_2}{k_{p21} f_1} = 1 + \frac{k_{p22} f_2}{k_{p21} f_1} = 1 + r_{21} \frac{f_2}{f_1} = 1 + \frac{f_2}{\frac{f_1}{r_{21}}} \quad (3\text{-}80)$$

$$\bar{w}_1 = \frac{1 + p_{11}}{1 - p_{11}} = \frac{\frac{2k_{p11} f_1 + k_{p12} f_2}{k_{p11} f_1 + k_{p12} f_2}}{\frac{k_{p12} f_2}{k_{p11} f_1 + k_{p12} f_2}} = \frac{2k_{p11} f_1 + k_{p12} f_2}{k_{p12} f_2} = 1 + 2\frac{k_{p11} f_1}{k_{p12} f_2} = 1 + 2r_{12} \frac{f_1}{f_2} = 1 + \frac{2f_1}{\frac{f_2}{r_{12}}} \quad (3\text{-}81)$$

$$\bar{w}_2 = \frac{1 + p_{22}}{1 - p_{22}} = \frac{\frac{2k_{p22} f_2 + k_{p21} f_1}{k_{p21} f_1 + k_{p22} f_2}}{\frac{k_{p21} f_1}{k_{p21} f_1 + k_{p22} f_2}} = \frac{2k_{p22} f_2 + k_{p21} f_1}{k_{p21} f_1} = 1 + 2\frac{k_{p22} f_2}{k_{p21} f_1} = 1 + 2r_{21} \frac{f_2}{f_1} = 1 + \frac{2f_2}{\frac{f_1}{r_{21}}} \quad (3\text{-}82)$$

For the *ter*-polymer case,

$$\bar{n}_1 = \frac{1}{1 - p_{11}} = \frac{1}{p_{12} + p_{13}} = \frac{k_{p11} f_1 + k_{p12} f_2 + k_{p13} f_3}{k_{p12} f_2 + k_{p13} f_3} = 1 + \frac{k_{p11} f_1}{k_{p12} f_2 + k_{p13} f_3} = 1 + \frac{f_1}{\frac{f_2}{r_{12}} + \frac{f_3}{r_{13}}} \quad (3\text{-}83)$$

$$\bar{n}_2 = \frac{1}{1 - p_{22}} = \frac{1}{p_{21} + p_{23}} = \frac{k_{p21} f_1 + k_{p22} f_2 + k_{p23} f_3}{k_{p21} f_1 + k_{p23} f_3} = 1 + \frac{k_{p22} f_2}{k_{p21} f_1 + k_{p23} f_3} = 1 + \frac{f_2}{\frac{f_1}{r_{21}} + \frac{f_3}{r_{23}}} \quad (3\text{-}84)$$

$$\bar{n}_3 = \frac{1}{1 - p_{33}} = \frac{1}{p_{31} + p_{32}} = \frac{k_{p31} f_1 + k_{p32} f_2 + k_{p33} f_3}{k_{p31} f_1 + k_{p32} f_2} = 1 + \frac{k_{p33} f_3}{k_{p31} f_1 + k_{p32} f_2} = 1 + \frac{f_3}{\frac{f_1}{r_{31}} + \frac{f_2}{r_{32}}} \quad (3\text{-}85)$$

$$\bar{w}_1 = \frac{\dfrac{2k_{p11}f_1 + k_{p12}f_2 + k_{p13}f_3}{k_{p11}f_1 + k_{p12}f_2 + k_{p13}f_3}}{\dfrac{k_{p12}f_2 + k_{p13}f_3}{k_{p11}f_1 + k_{p12}f_2 + k_{p13}f_3}} = \frac{2k_{p11}f_1 + k_{p12}f_2 + k_{p13}f_3}{k_{p12}f_2 + k_{p13}f_3} = 1 + \frac{2k_{p11}f_1}{k_{p12}f_2 + k_{p13}f_3} = 1 + \frac{2f_1}{\dfrac{f_2}{r_{12}} + \dfrac{f_3}{r_{13}}} \quad (3\text{-}86)$$

$$\bar{w}_2 = \frac{\dfrac{2k_{p22}f_2 + k_{p21}f_1 + k_{p23}f_3}{k_{p21}f_1 + k_{p22}f_2 + k_{p23}f_3}}{\dfrac{k_{p21}f_1 + k_{p23}f_3}{k_{p21}f_1 + k_{p22}f_2 + k_{p23}f_3}} = \frac{2k_{p22}f_2 + k_{p21}f_1 + k_{p23}f_3}{k_{p21}f_1 + k_{p23}f_3} = 1 + \frac{2k_{p22}f_2}{k_{p21}f_1 + k_{p23}f_3} = 1 + \frac{2f_2}{\dfrac{f_1}{r_{21}} + \dfrac{f_3}{r_{23}}} \quad (3\text{-}87)$$

$$\bar{w}_3 = \frac{\dfrac{2k_{p33}f_3 + k_{p31}f_1 + k_{p32}f_2}{k_{p31}f_1 + k_{p32}f_2 + k_{p33}f_3}}{\dfrac{k_{p31}f_1 + k_{p32}f_2}{k_{p31}f_1 + k_{p32}f_2 + k_{p33}f_3}} = \frac{2k_{p33}f_3 + k_{p31}f_1 + k_{p32}f_2}{k_{p31}f_1 + k_{p32}f_2} = 1 + \frac{2k_{p33}f_3}{k_{p31}f_1 + k_{p32}f_2} = 1 + \frac{2f_3}{\dfrac{f_1}{r_{31}} + \dfrac{f_2}{r_{32}}} \quad (3\text{-}88)$$

These are easily extended to *tetra*-, *penta*-, and higher multi-component cases.

In order to determine the cumulative distribution as a weighted composite of the instantaneous values, we must perform an integration of the instantaneous values. Two basic approaches were found in the literature, the first one by Ray (1977) and the second one by Hamielec/MacGregor/Penlidis (HMP) (Hamielec *et al*., 1987a). The difference between the two is that HMP's equation is normalized in equation (3-91) while Ray's one is not. This leads to some differences in number/weight average sequence length calculations, which is going to be discussed later. The governing equations are expressed as follows.

$$\overline{N_{in,Ray}} = \int_0^{X_i} N_{in}\,dX_i = \int_0^{X} N_{in}F_i\,dX = \int_0^{X}\left(p_{ii}^{n-1}\sum_{k=1}^{6}p_{ik}\right)F_i\,dX = \int_0^{X}\left\{p_{ii}^{n-1}(1-p_{ii})\right\}F_i\,dX \quad (k \neq i) \quad (3\text{-}89)$$

$$\overline{N_{in,HMP}} = \frac{\displaystyle\int_0^{X_i}\left(\frac{N_{in}}{\bar{n}_i}\right)dX_i}{\displaystyle\int_0^{X_i}\frac{dX_i}{\bar{n}_i}} = \frac{\displaystyle\int_0^{X}\left(\frac{N_{in}}{\bar{n}_i}\right)F_i\,dX}{\displaystyle\int_0^{X}\frac{F_i\,dX}{\bar{n}_i}} = \frac{\displaystyle\int_0^{X}\left\{p_{ii}^{n-1}\left(\sum_{k=1}^{6}p_{ik}\right)^2\right\}F_i\,dX}{\displaystyle\int_0^{X}\left(\sum_{k=1}^{6}p_{ik}\right)F_i\,dX} = \frac{\displaystyle\int_0^{X}\left\{p_{ii}^{n-1}(1-p_{ii})^2\right\}F_i\,dX}{\displaystyle\int_0^{X}(1-p_{ii})F_i\,dX} \quad (3\text{-}90)$$

where

$$\sum_{n=1}^{\infty}\overline{N_{in,HMP}} = \frac{\displaystyle\int_0^{X}\left(\sum_{n=1}^{\infty}p_{ii}^{n-1}\right)(1-p_{ii})^2F_i\,dX}{\displaystyle\int_0^{X}(1-p_{ii})F_i\,dX} = \frac{\displaystyle\int_0^{X}\frac{1}{(1-p_{ii})}(1-p_{ii})^2F_i\,dX}{\displaystyle\int_0^{X}(1-p_{ii})F_i\,dX} = \frac{\displaystyle\int_0^{X}(1-p_{ii})F_i\,dX}{\displaystyle\int_0^{X}(1-p_{ii})F_i\,dX} = 1 \quad (3\text{-}91)$$

Ray's and HMP's cumulative number-average sequence lengths of monomer *i* are calculated as

$$\overline{N_{i,Ray}} = \frac{\sum_{n=1}^{\infty} n\,\overline{N_{in,Ray}}}{\sum_{n=1}^{\infty} \overline{N_{in,Ray}}} = \frac{\int_0^X \left(\sum_{n=1}^{\infty} n p_{ii}^{n-1}\right)(1-p_{ii})F_i dX}{\int_0^X \left(\sum_{n=1}^{\infty} p_{ii}^{n-1}\right)(1-p_{ii})F_i dX} \approx \frac{\int_0^X \frac{1}{(1-p_{ii})^2}(1-p_{ii})F_i dX}{\int_0^X \frac{1}{(1-p_{ii})}(1-p_{ii})F_i dX} = \frac{\int_0^X \frac{1}{(1-p_{ii})}F_i dX}{\int_0^X F_i dX} \tag{3-92}$$

$$\overline{N_{i,HMP}} = \frac{\sum_{n=1}^{\infty} n\,\overline{N_{in,HMP}}}{\sum_{n=1}^{\infty} \overline{N_{in,HMP}}} = \frac{\int_0^X \left(\sum_{n=1}^{\infty} n p_{ii}^{n-1}\right)(1-p_{ii})^2 F_i dX}{\int_0^X (1-p_{ii})F_i dX} \approx \frac{\int_0^X \frac{1}{(1-p_{ii})^2}(1-p_{ii})^2 F_i dX}{\int_0^X (1-p_{ii})F_i dX} = \frac{\int_0^X F_i dX}{\int_0^X (1-p_{ii})F_i dX} \tag{3-93}$$

Their cumulative weight-average sequence lengths of monomer *i* are given by,

$$\overline{W_{i,Ray}} = \frac{\sum_{n=1}^{\infty} n^2\,\overline{N_{in,Ray}}}{\sum_{n=1}^{\infty} n\,\overline{N_{in,Ray}}} = \frac{\int_0^X \left(\sum_{n=1}^{\infty} n^2 p_{ii}^{n-1}\right)(1-p_{ii})F_i dX}{\int_0^X \left(\sum_{n=1}^{\infty} n p_{ii}^{n-1}\right)(1-p_{ii})F_i dX} \approx \frac{\int_0^X \frac{1+p_{ii}}{(1-p_{ii})^3}(1-p_{ii})F_i dX}{\int_0^X \frac{1}{(1-p_{ii})^2}(1-p_{ii})F_i dX} = \frac{\int_0^X \frac{1+p_{ii}}{(1-p_{ii})^2}F_i dX}{\int_0^X \frac{1}{1-p_{ii}}F_i dX} \tag{3-94}$$

$$\begin{aligned}
\overline{W_{i,HMP}} &= \frac{\sum_{n=1}^{\infty} n^2\,\overline{N_{in,HMP}}}{\sum_{n=1}^{\infty} n\,\overline{N_{in,HMP}}} = \frac{\sum_{n=1}^{\infty} n^2\,\overline{N_{in,HMP}}}{\overline{N_{i,HMP}}} = \frac{\int_0^X \left(\sum_{n=1}^{\infty} n^2 p_{ii}^{n-1}\right)(1-p_{ii})^2 F_i dX}{\overline{N_{i,HMP}}\int_0^X (1-p_{ii})F_i dX} \\
&\approx \frac{\int_0^X \frac{1+p_{ii}}{(1-p_{ii})^3}(1-p_{ii})^2 F_i dX}{\overline{N_{i,HMP}}\int_0^X (1-p_{ii})F_i dX} = \frac{\int_0^X \frac{1+p_{ii}}{1-p_{ii}}F_i dX \Big/ \int_0^X (1-p_{ii})F_i dX}{\int_0^X F_i dX \Big/ \int_0^X (1-p_{ii})F_i dX} = \frac{\int_0^X \frac{1+p_{ii}}{1-p_{ii}}F_i dX}{\int_0^X F_i dX}
\end{aligned} \tag{3-95}$$

The cumulative distribution is in principle more useful, since it is closely related to triad or pentad data determined via NMR experiments. Figures 3.2 and 3.3 show the differences between Ray and HMP calculations for cumulative number/weight average sequence lengths in Sty/AN *co*-polymerization when $f_{Sty0} = 0.7$ and 0.9, respectively. The experimental number average sequence lengths obtained from Garcia-Rubio *et al*. (1985) are well-explained by the two equations. In Figure 3.2, the number/weight average sequence length prediction curves generated by Ray are consistent with the ones by HMP up to about 65% conversion.

However, as the conversion level goes higher, it is observed that Ray's number/weight average sequence length plots are higher than HMP's calculations. The discrepancies become distinct in Figure 3.3, when the initial feed content of Sty is 0.9. After a conversion level around 50%, the two models begin to digress from each other and Ray's weight average sequence length prediction shows an especially dramatic increase compared to HMP. The normalized HMP equation seems more acceptable since the sum of cumulative sequence probabilities becomes exactly one as per equation (3-91), whereas Ray's equations do not satisfy this. However, in the future, comparing with experimental data of weight average sequence length (if available), will be helpful to discriminate better between the two approaches.

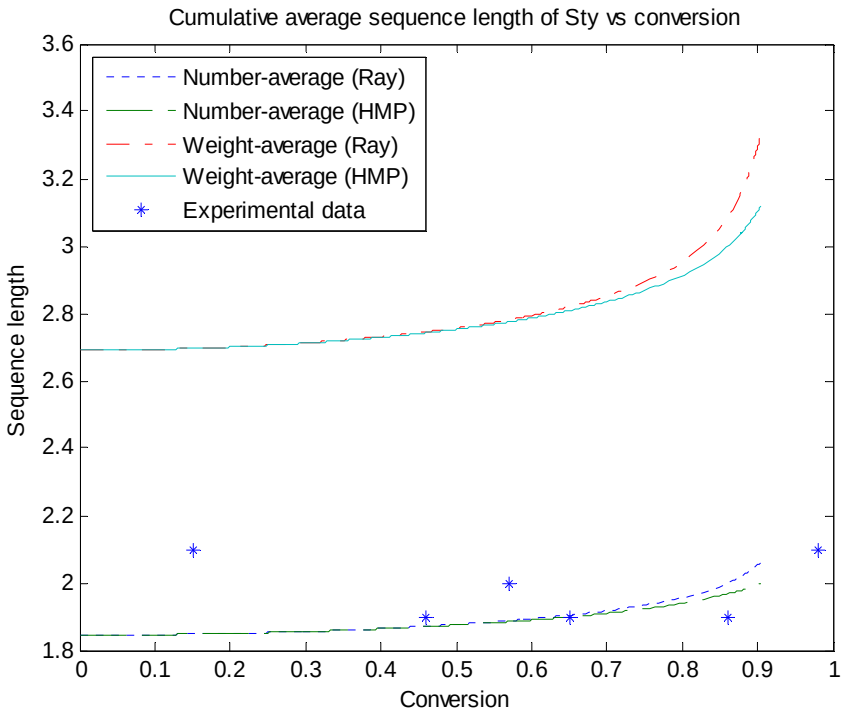

Figure 3.2. Sty cumulative average sequence lengths of Sty/AN *co*-polymer
T = 60℃, $[AIBN]_0$ = 0.05 M, and f_{Sty0} = 0.7

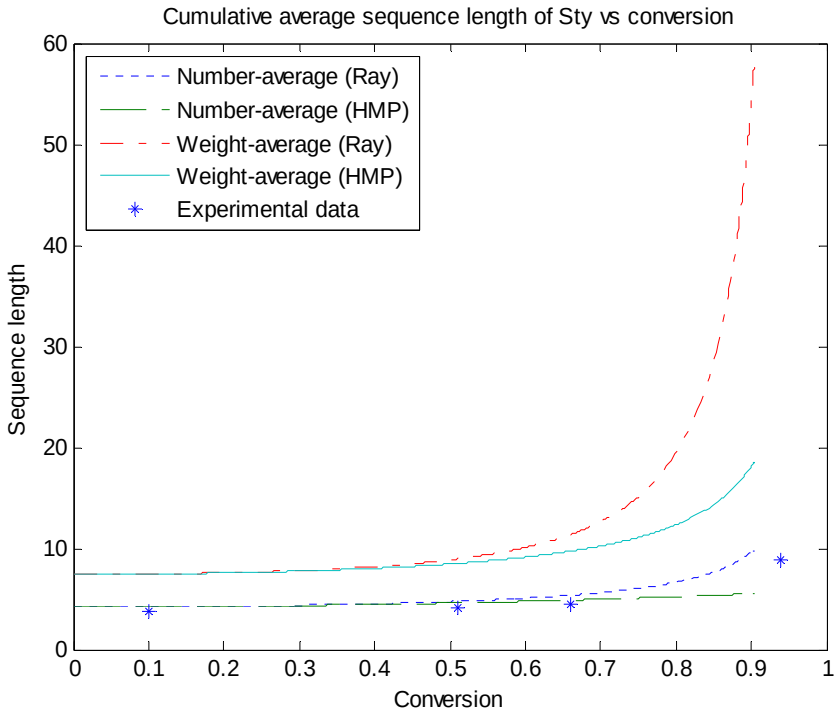

Figure 3.3. Sty cumulative average sequence lengths of Sty/AN *co*-polymer T = 60℃, $[AIBN]_0$ = 0.05 M, and f_{Sty0} = 0.9

3.4.2 Triad fraction calculation

Another method to investigate polymer microstructure is the calculation of dyad, triad, or pentad fractions. The model predictions can be compared with experimental measurements of the triad fractions having a given comonomer at the center. Let us investigate triad fraction calculations extended to multi-component polymers.

These triad fractions are related to combinations of dyad fractions, described by the probability functions p_{ij}.

$$A_{iii} = p_{ii}^2 = \left(\frac{r_{ij} f_i}{f_j + r_{ij} f_i} \right)^2 \tag{3-96}$$

$$A_{jij} = p_{ij}^2 = \left(\frac{f_j}{f_j + r_{ij} f_i} \right)^2 \neq p_{ji} p_{ij} \tag{3-97}$$

$$A_{iij} = A_{jii} = p_{ii}p_{ij} = p_{ii}(1 - p_{ii}) = \frac{r_{ij}f_i f_j}{(f_j + r_{ij}f_i)^2} \tag{3-98}$$

where $i, j = \{1, 2\}$

The reader should note here that the triad fraction A_{jij} is not equal to $p_{ji}p_{ij}$ in equation (3-97).

3.4.2.1 *Co*-polymer case

There are in total eight possible triads (2^3) in a *co*-polymer such as [111], [112], [121], [122], [211], [212], [221], and [222]. Six triads can be distinguishable among them: three patterns centered on monomer 1 such as [111], [112](=[211]), and [212], and another three patterns centered on monomer 2 such as [222], [221](=[122]), and [121]. Adding up the fractions for each centered monomer gives 1, such that

$$A_{111} + A_{112} + A_{211} + A_{212} = A_{111} + 2A_{112} + A_{212} = p_{11}^2 + 2p_{11}p_{12} + p_{12}^2 = (p_{11} + p_{12})^2 = 1^2 = 1 \tag{3-99}$$

$$A_{222} + A_{221} + A_{122} + A_{121} = A_{222} + 2A_{221} + A_{121} = p_{22}^2 + 2p_{22}p_{21} + p_{21}^2 = (p_{22} + p_{21})^2 = 1^2 = 1 \tag{3-100}$$

This calculation can be extended to multi-component cases.

3.4.2.2 *Ter*-polymer case

Among a total of 27(3^3) possible triads, 18 triads can be distinguished, which are

[111], [112](=[211]), [113](=[311]), [212], [213](=[312]), [313]

centered on monomer 1 (6 distinguishable triads out of 9),

[222], [221](=[122]), [223](=[322]), [121], [123](=[321]), [323]

centered on monomer 2 (6 distinguishable triads out of 9), and

[333], [331](=[133]), [332](=[233]), [131], [132](=[231]), [232]

centered on monomer 3 (6 distinguishable triads out of 9).

These fractions are calculated in the same way as in the *co*-polymer case. Only the fractions centered on monomer 1 will be considered from now on. The way is analogous for any monomer species *i*.

$$
\begin{aligned}
&A_{111} + A_{112} + A_{113} + A_{211} + A_{212} + A_{213} + A_{311} + A_{312} + A_{313} \\
&= A_{111} + 2A_{112} + A_{212} + 2A_{213} + A_{313} + 2A_{113} \\
&= p_{11}^2 + 2p_{11}p_{12} + p_{12}^2 + 2p_{12}p_{13} + p_{13}^2 + 2p_{11}p_{13} = (p_{11} + p_{12} + p_{13})^2 = 1^2 = 1
\end{aligned}
\tag{3-101}
$$

3.4.2.3 *Hexa*-polymer case

Among 216(6^3) possible triads, 126 triads can be distinguished, namely,

[111], [112](=[211]), [113](=[311]), [114](=[411]), [115](=[511]), [116](=[611]),
[212], [213](=[312]), [214](=[412]), [215](=[512]), [216](=[612]),
[313], [314](=[413]), [315](=[513]), [316](=[613]),
[414], [415](=[514]), [416](=[614]), [515], [516](=[615]), [616]

centered on monomer 1 (21 distinguishable triads out of 36),

[222], [221](=[122]), [223](=[322]), [224](=[422]), [225](=[522]), [226](=[622]),
[121], [123](=[312]), [124](=[421]), [125](=[521]), [126](=[621]),
[323], [324](=[423]), [325](=[523]), [326](=[623]),
[424], [425](=[524]), [426](=[624]), [525], [526](=[625]), [626]

centered on monomer 2 (21 distinguishable triads out of 36),

[333], [331](=[133]), [332](=[233]), [334](=[433]), [335](=[533]), [336](=[633]),
[131], [132](=[231]), [134](=[431]), [135](=[531]), [136](=[631]),
[232], [234](=[432]), [235](=[532]), [236](=[632]),
[434], [435](=[534]), [436](=[634]), [535], [536](=[635]), [636]

centered on monomer 3 (21 distinguishable triads out of 36),

[444], [441](=[144]), [442](=[244]), [443](=[344]), [445](=[544]), [446](=[644]),
[141], [142](=[241]), [143](=[341]), [145](=[541]), [146](=[641]),
[242], [243](=[342]), [245](=[542]), [246](=[642]),
[343], [345](=[543]), [346](=[643]), [545], [546](=[645]), [646]

centered on monomer 4 (21 distinguishable triads out of 36),

[555], [551](=[155]), [552](=[255]), [553](=[355]), [554](=[455]), [556](=[655]),
[151], [152](=[251]), [153](=[351]), [154](=[451]), [156](=[651]),
[252], [253](=[352]), [254](=[452]), [256](=[652]),

[353], [354](=[453]), [356](=[653]), [454], [456](=[654]), [656]

centered on monomer 5 (21 distinguishable triads out of 36), and

[666], [661](=[166]), [662](=[266]), [663](=[366]), [664](=[466]), [665](=[566]),

[161], [162](=[261]), [163](=[361]), [164](=[461]), [165](=[561]),

[262], [263](=[362]), [264](=[462]), [265](=[562]),

[363], [364](=[463]), [365](=[563]), [464], [465](=[564]), [565]

centered on monomer 6 (21 distinguishable triads out of 36).

Summation of the fractions centered on monomer 1 gives,

$$\begin{aligned}
&A_{111}+A_{112}+A_{113}+A_{114}+A_{115}+A_{116}+A_{211}+A_{212}+A_{213}+A_{214}+A_{215}+A_{216}\\
&+A_{311}+A_{312}+A_{313}+A_{314}+A_{315}+A_{316}+A_{411}+A_{412}+A_{413}+A_{414}+A_{415}+A_{416}\\
&+A_{511}+A_{512}+A_{513}+A_{514}+A_{515}+A_{516}+A_{611}+A_{612}+A_{613}+A_{614}+A_{615}+A_{616}\\
&=A_{111}+2A_{112}+2A_{113}+2A_{114}+2A_{115}+2A_{116}+A_{212}+2A_{213}+2A_{214}+2A_{215}+2A_{216}\\
&+A_{313}+2A_{314}+2A_{315}+2A_{316}+A_{414}+2A_{415}+2A_{416}+A_{515}+2A_{516}+A_{616}\\
&=p_{11}^2+2p_{11}p_{12}+2p_{11}p_{13}+2p_{11}p_{14}+2p_{11}p_{15}+2p_{11}p_{16}+p_{12}^2+2p_{12}p_{13}+2p_{12}p_{14}+2p_{12}p_{15}\\
&+2p_{12}p_{16}+p_{13}^2+2p_{13}p_{14}+2p_{13}p_{15}+2p_{13}p_{16}+p_{14}^2+2p_{14}p_{15}+2p_{14}p_{16}+p_{15}^2+2p_{15}p_{16}+p_{16}^2\\
&=\left(p_{11}+p_{12}+p_{13}+p_{14}+p_{15}+p_{16}\right)^2=1^2=1
\end{aligned} \tag{3-102}$$

It is estimated from Table 3.1 that if the number of monomers is *n,* there exist *n* centered monomers and $n\left(\frac{(n-1)^2+3(n-1)}{2}+1\right)$ distinguishable triads out of n^3 possible ones in the multi-component systems.

Sty/AN *co*-polymer triad fraction calculation plots are depicted in Figure 3.4 (Sty-centered) and Figure 3.5 (AN-centered). Experimental data are coming from Hill *et al*. (1982). Number one stands for Sty and two for AN monomer in the fraction. Basically, AN *homo*-propagation is faster than Sty and *cross*-propagation from AN radical with Sty monomer is more favoured than the reverse case. Therefore, as Sty monomer content increases, its sequence increases and Sty-rich fractions such as A111 and A121 become dominant in the *co*-polymer, while AN-rich fractions such as A222 and A212 are decreasing. On the other hand, A211+A112 and A122+A221 fractions are increasing up to some content level and decreasing later. This can be explained by the competition between two factors,

reactivity and monomer quantity. The same situation happens in another example, the MA-centered triad fraction plot in MMA/MA *co*-polymerization (Figure 3.6, MMA-centered fraction experimental data from Kim and Harwood (2002) were unavailable). The MA-rich fractions (A222 and A122+A221) are decreasing and the other MMA-rich fraction (A121) is increasing. These profiles are explained by model predictions satisfactorily.

No. of monomer species	Distinguishable triads	Total possible triads
1 (*homo*-)	1	1
2 (*co*-)	6	8
3 (*ter*-)	18	27
4 (*tetra*-)	40	64
5 (*penta*-)	75	125
6 (*hexa*-)	126	216
7	196	343
8	288	512
9	405	729
10	550	1000
11	726	1331
12	936	1728
…	…	…
19	3610	6859
20	4200	8000

Table 3.1. Number of distinguishable and possible triads in multi-component polymerization

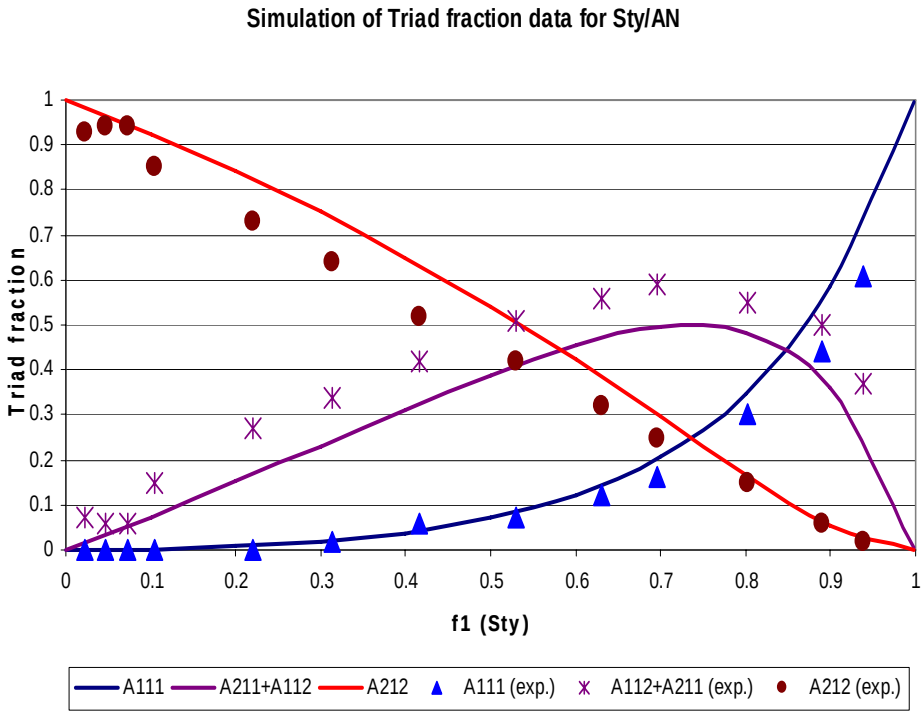

Figure 3.4. Sty-centered triad fraction calculation of Sty/AN *co*-polymer at T = 60℃

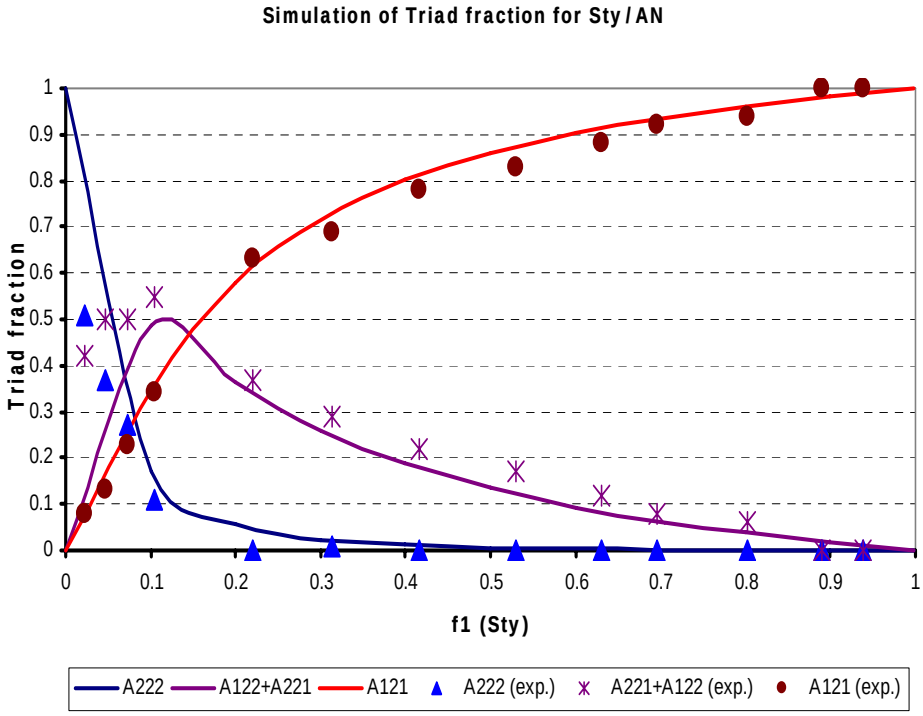

Figure 3.5. AN-centered triad fraction calculation of Sty/AN *co*-polymer at T = 60℃

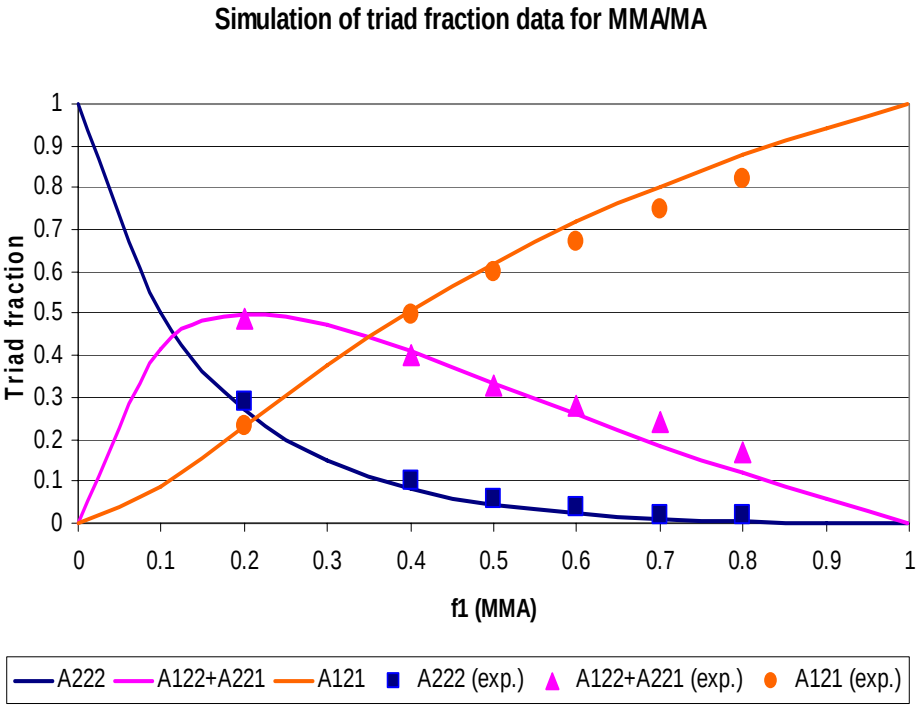

Figure 3.6. MA-centered triad fraction calculation of MMA/MA *co*-polymer at T = 50℃

3.5 Depropagation

The propagation steps can be reversible at elevated temperatures. The relative importance of the reverse reaction (depropagation) is governed by thermodynamic equilibrium, the Gibbs free energy ΔG_p.

$$\Delta G_p = \Delta H_p - T\Delta S_p \tag{3-103}$$

where ΔH_p and ΔS_p are the enthalpy and entropy change upon propagation, respectively. For spontaneous polymerization, ΔG_p must be negative. Depropagation is insignificant for many systems because the free energy is normally negative at typical reaction temperatures. Highly exothermic polymerization makes ΔH_p negative and the propagating polymer chain decreases the degrees of freedom in the system, resulting in negative ΔS_p also. However, as T

increases (usually over 120℃), equation (3-103) is becoming balanced and we call the temperature where this happens as the ceiling temperature T_c. The reversible propagation reaction between a radical of chain length r and a monomer unit M is expressed as

$$R_r^{\bullet} + M \underset{\bar{k}_p}{\overset{k_p}{\longleftrightarrow}} R_{r+1}^{\bullet} \tag{3-104}$$

Then the overall (net) polymerization rate becomes

$$\begin{aligned} R_p &= k_p[R^{\bullet}][M] - \bar{k}_p[R^{\bullet}] = k_p^{eff}[M][R^{\bullet}] \\ k_p^{eff} &= k_p - \frac{\bar{k}_p}{[M]} \end{aligned} \tag{3-105}$$

At extremely low monomer concentrations, the negative term significantly reduces the net rate. At equilibrium, the rate becomes zero and gives the following expression.

$$K_{eq} = \frac{k_p}{\bar{k}_p} = \frac{1}{[M]_{eq}} \tag{3-106}$$

The ceiling temperature is shown to be a function of monomer concentration.

$$\Delta G_p^0 = \Delta H_p^0 - T_c \Delta S_p^0 = -RT_c \ln(K_{eq}) = RT_c \ln([M]_{eq}) \tag{3-107}$$

$$T_c = \frac{\Delta H_p^0}{\Delta S_p^0 + R\ln([M]_{eq})} \tag{3-108}$$

In multi-component polymerization, depropagation affects not only the rate of polymerization but also polymer composition, sequence length distribution and molecular weights, therefore several equations should be modified. There are several different models that can be used to predict the composition of a reversible *co*-polymer system. In this thesis, Krüger's probabilistic approach (Krüger *et al*., 1987 and Leamen, 2005a) is used for the full depropagation model. Based on material balances and the general assumption that every component can depropagate, it is more powerful and robust than any other model (Lowry (1960) and Wittmer (1971)).

There are 72 reactions in total including 36 propagations and 36 depropagations which need to be considered for a 6-monomer system.

$$\begin{array}{lll} R_1^\bullet + M_1 \underset{\overline{k_{11}}}{\overset{k_{11}}{\longleftrightarrow}} R_{11}^\bullet & R_2^\bullet + M_1 \underset{\overline{k_{21}}}{\overset{k_{21}}{\longleftrightarrow}} R_{21}^\bullet & \cdots \quad R_6^\bullet + M_1 \underset{\overline{k_{61}}}{\overset{k_{61}}{\longleftrightarrow}} R_{61}^\bullet \\ R_1^\bullet + M_2 \underset{\overline{k_{12}}}{\overset{k_{12}}{\longleftrightarrow}} R_{12}^\bullet & R_2^\bullet + M_2 \underset{\overline{k_{22}}}{\overset{k_{22}}{\longleftrightarrow}} R_{22}^\bullet & \cdots \quad R_6^\bullet + M_2 \underset{\overline{k_{62}}}{\overset{k_{62}}{\longleftrightarrow}} R_{62}^\bullet \\ \vdots & \vdots & \vdots \\ R_1^\bullet + M_6 \underset{\overline{k_{16}}}{\overset{k_{16}}{\longleftrightarrow}} R_{16}^\bullet & R_2^\bullet + M_6 \underset{\overline{k_{26}}}{\overset{k_{26}}{\longleftrightarrow}} R_{26}^\bullet & \cdots \quad R_6^\bullet + M_6 \underset{\overline{k_{66}}}{\overset{k_{66}}{\longleftrightarrow}} R_{66}^\bullet \end{array} \tag{3-109}$$

Monomer and radical balances are expressed in equations (3-110) to (3-115) and (3-116) to (3-121), respectively.

$$R_{p1} = -\frac{d[M_1]}{dt} = \sum_{i=1}^{6} k_{pi1}[R_i^\bullet][M_1] - \sum_{i=1}^{6} \overline{k_{pi1}}[R_{i1}^\bullet] \tag{3-110}$$

$$R_{p2} = -\frac{d[M_2]}{dt} = \sum_{i=1}^{6} k_{pi2}[R_i^\bullet][M_2] - \sum_{i=1}^{6} \overline{k_{pi2}}[R_{i2}^\bullet] \tag{3-111}$$

$$R_{p3} = -\frac{d[M_3]}{dt} = \sum_{i=1}^{6} k_{pi3}[R_i^\bullet][M_3] - \sum_{i=1}^{6} \overline{k_{pi3}}[R_{i3}^\bullet] \tag{3-112}$$

$$R_{p4} = -\frac{d[M_4]}{dt} = \sum_{i=1}^{6} k_{pi4}[R_i^\bullet][M_4] - \sum_{i=1}^{6} \overline{k_{pi4}}[R_{i4}^\bullet] \tag{3-113}$$

$$R_{p5} = -\frac{d[M_5]}{dt} = \sum_{i=1}^{6} k_{pi5}[R_i^\bullet][M_5] - \sum_{i=1}^{6} \overline{k_{pi5}}[R_{i5}^\bullet] \tag{3-114}$$

$$R_{p6} = -\frac{d[M_6]}{dt} = \sum_{i=1}^{6} k_{pi6}[R_i^\bullet][M_6] - \sum_{i=1}^{6} \overline{k_{pi6}}[R_{i6}^\bullet] \tag{3-115}$$

$$\frac{d[R_1^\bullet]}{dt} = \sum_{i=2}^{6}\left(k_{pi1}[R_i^\bullet][M_1] + \overline{k_{p1i}}[R_{1i}^\bullet] \right) - \sum_{i=2}^{6}\left(k_{p1i}[R_1^\bullet][M_i] + \overline{k_{pi1}}[R_{i1}^\bullet] \right) \tag{3-116}$$

$$\frac{d[R_2^\bullet]}{dt} = \sum_{\substack{i=1 \\ (i\neq 2)}}^{6}\left(k_{pi2}[R_i^\bullet][M_2] + \overline{k_{p2i}}[R_{2i}^\bullet] \right) - \sum_{\substack{i=1 \\ (i\neq 2)}}^{6}\left(k_{p2i}[R_2^\bullet][M_i] + \overline{k_{pi2}}[R_{i2}^\bullet] \right) \tag{3-117}$$

$$\frac{d[R_3^\bullet]}{dt} = \sum_{\substack{i=1 \\ (i\neq 3)}}^{6}\left(k_{pi3}[R_i^\bullet][M_3] + \overline{k_{p3i}}[R_{3i}^\bullet] \right) - \sum_{\substack{i=1 \\ (i\neq 3)}}^{6}\left(k_{p3i}[R_3^\bullet][M_i] + \overline{k_{pi3}}[R_{i3}^\bullet] \right) \tag{3-118}$$

$$\frac{d[R_4^\bullet]}{dt} = \sum_{\substack{i=1 \\ (i\neq 4)}}^{6}\left(k_{pi4}[R_i^\bullet][M_4] + \overline{k_{p4i}}[R_{4i}^\bullet] \right) - \sum_{\substack{i=1 \\ (i\neq 4)}}^{6}\left(k_{p4i}[R_4^\bullet][M_i] + \overline{k_{pi4}}[R_{i4}^\bullet] \right) \tag{3-119}$$

$$\frac{d[R_5^\bullet]}{dt} = \sum_{\substack{i=1 \\ (i\neq 5)}}^{6}\left(k_{pi5}[R_i^\bullet][M_5] + \overline{k_{p5i}}[R_{5i}^\bullet] \right) - \sum_{\substack{i=1 \\ (i\neq 5)}}^{6}\left(k_{p5i}[R_5^\bullet][M_i] + \overline{k_{pi5}}[R_{i5}^\bullet] \right) \tag{3-120}$$

$$\frac{d[R_6^\bullet]}{dt} = \sum_{i=1}^{5}\left(k_{pi6}[R_i^\bullet][M_6] + \overline{k_{p6i}}[R_{6i}^\bullet] \right) - \sum_{i=1}^{5}\left(k_{p6i}[R_6^\bullet][M_i] + \overline{k_{pi6}}[R_{i6}^\bullet] \right) \tag{3-121}$$

Krüger calculated the penultimate radical concentration $[R_{ij}^\bullet]$ using the probability that a monomer of type *j* is attached to a penultimate radical ending in *i*, P_{ij} (upper-case letter). The reader should note that P_{ij} is different from the sequence length probability, p_{ij} (lower-case letter) which was defined earlier in equation (3-75) for the number/weight average sequence length calculations.

$$[R_j^\bullet] = \sum_{i=1}^{6}[R_{ij}^\bullet], \quad P_{ij} = \frac{[R_{ij}^\bullet]}{[R_j^\bullet]} \tag{3-122}$$

where $\sum_{i=1}^{6} P_{ij} = 1$

Equations (3-110) to (3-121) can be rewritten using equation (3-122) as follows.

$$R_{p1} = -\frac{d[M_1]}{dt} = \sum_{i=1}^{6} k_{pi1}[R_i^\bullet][M_1] - \sum_{i=1}^{6} \overline{k_{pi1}}\, P_{i1}[R_1^\bullet] \tag{3-123}$$

$$R_{p2} = -\frac{d[M_2]}{dt} = \sum_{i=1}^{6} k_{pi2}[R_i^\bullet][M_2] - \sum_{i=1}^{6} \overline{k_{pi2}}\, P_{i2}[R_2^\bullet] \tag{3-124}$$

$$R_{p3} = -\frac{d[M_3]}{dt} = \sum_{i=1}^{6} k_{pi3}[R_i^\bullet][M_3] - \sum_{i=1}^{6} \overline{k_{pi3}}\, P_{i3}[R_3^\bullet] \tag{3-125}$$

$$R_{p4} = -\frac{d[M_4]}{dt} = \sum_{i=1}^{6} k_{pi4}[R_i^\bullet][M_4] - \sum_{i=1}^{6} \overline{k_{pi4}}\, P_{i4}[R_4^\bullet] \tag{3-126}$$

$$R_{p5} = -\frac{d[M_5]}{dt} = \sum_{i=1}^{6} k_{pi5}[R_i^\bullet][M_5] - \sum_{i=1}^{6} \overline{k_{pi5}}\, P_{i5}[R_5^\bullet] \tag{3-127}$$

$$R_{p6} = -\frac{d[M_6]}{dt} = \sum_{i=1}^{6} k_{pi6}[R_i^\bullet][M_6] - \sum_{i=1}^{6} \overline{k_{pi6}}\, P_{i6}[R_6^\bullet] \tag{3-128}$$

$$\frac{d[R_1^\bullet]}{dt} = \sum_{i=2}^{6}\left(k_{pi1}[R_i^\bullet][M_1] + \overline{k_{p1i}}\, P_{1i}[R_i^\bullet] \right) - \sum_{i=2}^{6}\left(k_{p1i}[R_1^\bullet][M_i] + \overline{k_{pi1}}\, P_{i1}[R_1^\bullet] \right) \tag{3-129}$$

$$\frac{d[R_2^\bullet]}{dt} = \sum_{\substack{i=1 \\ (i\neq 2)}}^{6}\left(k_{pi2}[R_i^\bullet][M_2] + \overline{k_{p2i}}\, P_{2i}[R_i^\bullet] \right) - \sum_{\substack{i=1 \\ (i\neq 2)}}^{6}\left(k_{p2i}[R_2^\bullet][M_i] + \overline{k_{pi2}}\, P_{i2}[R_2^\bullet] \right) \tag{3-130}$$

$$\frac{d[R_3^\bullet]}{dt} = \sum_{\substack{i=1 \\ (i\neq 3)}}^{6}\left(k_{pi3}[R_i^\bullet][M_3] + \overline{k_{p3i}}\, P_{3i}[R_i^\bullet] \right) - \sum_{\substack{i=1 \\ (i\neq 3)}}^{6}\left(k_{p3i}[R_3^\bullet][M_i] + \overline{k_{pi3}}\, P_{i3}[R_3^\bullet] \right) \quad (3\text{-}131)$$

$$\frac{d[R_4^\bullet]}{dt} = \sum_{\substack{i=1 \\ (i\neq 4)}}^{6}\left(k_{pi4}[R_i^\bullet][M_4] + \overline{k_{p4i}}\, P_{4i}[R_i^\bullet] \right) - \sum_{\substack{i=1 \\ (i\neq 4)}}^{6}\left(k_{p4i}[R_4^\bullet][M_i] + \overline{k_{pi4}}\, P_{i4}[R_4^\bullet] \right) \quad (3\text{-}132)$$

$$\frac{d[R_5^\bullet]}{dt} = \sum_{\substack{i=1 \\ (i\neq 5)}}^{6}\left(k_{pi5}[R_i^\bullet][M_5] + \overline{k_{p5i}}\, P_{5i}[R_i^\bullet] \right) - \sum_{\substack{i=1 \\ (i\neq 5)}}^{6}\left(k_{p5i}[R_5^\bullet][M_i] + \overline{k_{pi5}}\, P_{i5}[R_5^\bullet] \right) \quad (3\text{-}133)$$

$$\frac{d[R_6^\bullet]}{dt} = \sum_{i=1}^{5}\left(k_{pi6}[R_i^\bullet][M_6] + \overline{k_{p6i}}\, P_{6i}[R_i^\bullet] \right) - \sum_{i=1}^{5}\left(k_{p6i}[R_6^\bullet][M_i] + \overline{k_{pi6}}\, P_{i6}[R_6^\bullet] \right) \quad (3\text{-}134)$$

Assuming the steady state hypothesis of radical concentrations, the left sides of equations (3-129) to (3-134) become zero. They are rewritten as,

$$\begin{aligned} &-[R_1^\bullet]\sum_{i=2}^{6}\left(k_{p1i}[M_i] + \overline{k_{pi1}}\, P_{i1} \right) + [R_2^\bullet]\left(k_{p21}[M_1] + \overline{k_{p12}}\, P_{12} \right) + [R_3^\bullet]\left(k_{p31}[M_1] + \overline{k_{p13}}\, P_{13} \right) \\ &+ [R_4^\bullet]\left(k_{p41}[M_1] + \overline{k_{p14}}\, P_{14} \right) + [R_5^\bullet]\left(k_{p51}[M_1] + \overline{k_{p15}}\, P_{15} \right) + [R_6^\bullet]\left(k_{p61}[M_1] + \overline{k_{p16}}\, P_{16} \right) = 0 \end{aligned} \quad (3\text{-}135)$$

$$\begin{aligned} &[R_1^\bullet]\left(k_{p12}[M_2] + \overline{k_{p21}}\, P_{21} \right) - [R_2^\bullet]\sum_{\substack{i=1 \\ (i\neq 2)}}^{6}\left(k_{p2i}[M_i] + \overline{k_{pi2}}\, P_{i2} \right) + [R_3^\bullet]\left(k_{p32}[M_2] + \overline{k_{p23}}\, P_{23} \right) \\ &+ [R_4^\bullet]\left(k_{p42}[M_2] + \overline{k_{p24}}\, P_{24} \right) + [R_5^\bullet]\left(k_{p52}[M_2] + \overline{k_{p25}}\, P_{25} \right) + [R_6^\bullet]\left(k_{p62}[M_2] + \overline{k_{p26}}\, P_{26} \right) = 0 \end{aligned} \quad (3\text{-}136)$$

$$\begin{aligned} &[R_1^\bullet]\left(k_{p13}[M_3] + \overline{k_{p31}}\, P_{31} \right) + [R_2^\bullet]\left(k_{p23}[M_3] + \overline{k_{p32}}\, P_{32} \right) - [R_3^\bullet]\sum_{\substack{i=1 \\ (i\neq 3)}}^{6}\left(k_{p3i}[M_i] + \overline{k_{pi3}}\, P_{i3} \right) \\ &+ [R_4^\bullet]\left(k_{p43}[M_3] + \overline{k_{p34}}\, P_{34} \right) + [R_5^\bullet]\left(k_{p53}[M_3] + \overline{k_{p35}}\, P_{35} \right) + [R_6^\bullet]\left(k_{p63}[M_3] + \overline{k_{p36}}\, P_{36} \right) = 0 \end{aligned} \quad (3\text{-}137)$$

$$\begin{aligned} &[R_1^\bullet]\left(k_{p14}[M_4] + \overline{k_{p41}}\, P_{41} \right) + [R_2^\bullet]\left(k_{p24}[M_4] + \overline{k_{p42}}\, P_{42} \right) + [R_3^\bullet]\left(k_{p34}[M_4] + \overline{k_{p43}}\, P_{43} \right) \\ &- [R_4^\bullet]\sum_{\substack{i=1 \\ (i\neq 4)}}^{6}\left(k_{p4i}[M_i] + \overline{k_{pi4}}\, P_{i4} \right) + [R_5^\bullet]\left(k_{p54}[M_4] + \overline{k_{p45}}\, P_{45} \right) + [R_6^\bullet]\left(k_{p64}[M_4] + \overline{k_{p46}}\, P_{46} \right) = 0 \end{aligned} \quad (3\text{-}138)$$

$$\begin{aligned} &[R_1^\bullet]\left(k_{p15}[M_5] + \overline{k_{p51}}\, P_{51} \right) + [R_2^\bullet]\left(k_{p25}[M_5] + \overline{k_{p52}}\, P_{52} \right) + [R_3^\bullet]\left(k_{p35}[M_5] + \overline{k_{p53}}\, P_{53} \right) \\ &+ [R_4^\bullet]\left(k_{p45}[M_5] + \overline{k_{p54}}\, P_{54} \right) - [R_5^\bullet]\sum_{\substack{i=1 \\ (i\neq 5)}}^{6}\left(k_{p5i}[M_i] + \overline{k_{pi5}}\, P_{i5} \right) + [R_6^\bullet]\left(k_{p65}[M_5] + \overline{k_{p56}}\, P_{56} \right) = 0 \end{aligned} \quad (3\text{-}139)$$

$$[R_1^\bullet]\left(k_{p16}[M_6]+\overline{k_{p61}}\,P_{61}\right)+[R_2^\bullet]\left(k_{p26}[M_6]+\overline{k_{p62}}\,P_{62}\right)+[R_3^\bullet]\left(k_{p36}[M_6]+\overline{k_{p63}}\,P_{63}\right)$$
$$+[R_4^\bullet]\left(k_{p46}[M_6]+\overline{k_{p64}}\,P_{64}\right)+[R_5^\bullet]\left(k_{p56}[M_6]+\overline{k_{p65}}\,P_{65}\right)-[R_6^\bullet]\sum_{i=1}^{5}\left(k_{p6i}[M_i]+\overline{k_{pi6}}\,P_{i6}\right)=0 \quad (3\text{-}140)$$

The probability P_{ij} is expressed in terms of rate constants and species concentrations as follows.

$$P_{ij}=\frac{k_{pij}[R_i^\bullet][M_j]-\overline{k_{pij}}[R_{ij}^\bullet]}{\sum_{l=1}^{6}k_{plj}[R_l^\bullet][M_j]-\sum_{l=1}^{6}\overline{k_{plj}}[R_{lj}^\bullet]}=\frac{k_{pij}[R_i^\bullet][M_j]-\overline{k_{pij}}\,P_{ij}[R_j^\bullet]}{\sum_{l=1}^{6}k_{plj}[R_l^\bullet][M_j]-\sum_{l=1}^{6}\overline{k_{plj}}\,P_{lj}[R_j^\bullet]} \quad (3\text{-}141)$$

In order to eliminate radical concentration terms in equation (3-141) via the steady state hypothesis, the depropagating radical fractions are arranged into an $\mathbf{M}\cdot\mathbf{r}=\mathbf{b}$ form again.

$$\mathbf{M}=\begin{bmatrix} a & \begin{pmatrix}k_{p21}[M_1]+\overline{k_{p12}}\,P_{12}\\ -k_{p61}[M_1]-\overline{k_{p16}}\,P_{16}\end{pmatrix} & \begin{pmatrix}k_{p31}[M_1]+\overline{k_{p13}}\,P_{13}\\ -k_{p61}[M_1]-\overline{k_{p16}}\,P_{16}\end{pmatrix} & \begin{pmatrix}k_{p41}[M_1]+\overline{k_{p14}}\,P_{14}\\ -k_{p61}[M_1]-\overline{k_{p16}}\,P_{16}\end{pmatrix} & \begin{pmatrix}k_{p51}[M_1]+\overline{k_{p15}}\,P_{15}\\ -k_{p61}[M_1]-\overline{k_{p16}}\,P_{16}\end{pmatrix} \\ \begin{pmatrix}k_{p12}[M_2]+\overline{k_{p21}}\,P_{21}\\ -k_{p62}[M_2]-\overline{k_{p26}}\,P_{26}\end{pmatrix} & b & \begin{pmatrix}k_{p32}[M_2]+\overline{k_{p23}}\,P_{23}\\ -k_{p62}[M_2]-\overline{k_{p26}}\,P_{26}\end{pmatrix} & \begin{pmatrix}k_{p42}[M_2]+\overline{k_{p24}}\,P_{24}\\ -k_{p62}[M_2]-\overline{k_{p26}}\,P_{26}\end{pmatrix} & \begin{pmatrix}k_{p52}[M_2]+\overline{k_{p25}}\,P_{25}\\ -k_{p62}[M_2]-\overline{k_{p26}}\,P_{26}\end{pmatrix} \\ \begin{pmatrix}k_{p13}[M_3]+\overline{k_{p31}}\,P_{31}\\ -k_{p63}[M_3]-\overline{k_{p36}}\,P_{36}\end{pmatrix} & \begin{pmatrix}k_{p23}[M_3]+\overline{k_{p32}}\,P_{32}\\ -k_{p63}[M_3]-\overline{k_{p36}}\,P_{36}\end{pmatrix} & c & \begin{pmatrix}k_{p43}[M_3]+\overline{k_{p34}}\,P_{34}\\ -k_{p63}[M_3]-\overline{k_{p36}}\,P_{36}\end{pmatrix} & \begin{pmatrix}k_{p53}[M_3]+\overline{k_{p35}}\,P_{35}\\ -k_{p63}[M_3]-\overline{k_{p36}}\,P_{36}\end{pmatrix} \\ \begin{pmatrix}k_{p14}[M_4]+\overline{k_{p41}}\,P_{41}\\ -k_{p64}[M_4]-\overline{k_{p46}}\,P_{46}\end{pmatrix} & \begin{pmatrix}k_{p24}[M_4]+\overline{k_{p42}}\,P_{42}\\ -k_{p64}[M_4]-\overline{k_{p46}}\,P_{46}\end{pmatrix} & \begin{pmatrix}k_{p34}[M_4]+\overline{k_{p43}}\,P_{43}\\ -k_{p64}[M_4]-\overline{k_{p46}}\,P_{46}\end{pmatrix} & d & \begin{pmatrix}k_{p54}[M_4]+\overline{k_{p45}}\,P_{45}\\ -k_{p64}[M_4]-\overline{k_{p46}}\,P_{46}\end{pmatrix} \\ \begin{pmatrix}k_{p15}[M_5]+\overline{k_{p51}}\,P_{51}\\ -k_{p65}[M_5]-\overline{k_{p56}}\,P_{56}\end{pmatrix} & \begin{pmatrix}k_{p25}[M_5]+\overline{k_{p52}}\,P_{52}\\ -k_{p65}[M_5]-\overline{k_{p56}}\,P_{56}\end{pmatrix} & \begin{pmatrix}k_{p35}[M_5]+\overline{k_{p53}}\,P_{53}\\ -k_{p65}[M_5]-\overline{k_{p56}}\,P_{56}\end{pmatrix} & \begin{pmatrix}k_{p45}[M_5]+\overline{k_{p54}}\,P_{54}\\ -k_{p65}[M_5]-\overline{k_{p56}}\,P_{56}\end{pmatrix} & e \end{bmatrix}$$

where

$$a=-\sum_{j=2}^{6}\left(k_{p1j}[M_j]+\overline{k_{pj1}}\,P_{j1}\right)-k_{p61}[M_1]-\overline{k_{p16}}\,P_{16},\quad b=-\sum_{\substack{j=1\\(j\neq 2)}}^{6}\left(k_{p2j}[M_j]+\overline{k_{pj2}}\,P_{j2}\right)-k_{p62}[M_2]-\overline{k_{p26}}\,P_{26}$$
$$c=-\sum_{\substack{j=1\\(j\neq 3)}}^{6}\left(k_{p3j}[M_j]+\overline{k_{pj3}}\,P_{j3}\right)-k_{p63}[M_3]-\overline{k_{p36}}\,P_{36},\quad d=-\sum_{\substack{j=1\\(j\neq 4)}}^{6}\left(k_{p4j}[M_j]+\overline{k_{pj4}}\,P_{j4}\right)-k_{p64}[M_4]-\overline{k_{p46}}\,P_{46}$$
$$e=-\sum_{\substack{j=1\\(j\neq 5)}}^{6}\left(k_{p5j}[M_j]+\overline{k_{pj5}}\,P_{j5}\right)-k_{p65}[M_5]-\overline{k_{p56}}\,P_{56}$$

and

$$\mathbf{r} = \begin{bmatrix} \Phi_1^\bullet & \Phi_2^\bullet & \Phi_3^\bullet & \Phi_4^\bullet & \Phi_5^\bullet \end{bmatrix}'$$

$$\mathbf{b} = \begin{bmatrix} -k_{p61}[M_1] - \overline{k_{p16}} P_{16} \\ -k_{p62}[M_2] - \overline{k_{p26}} P_{26} \\ -k_{p63}[M_3] - \overline{k_{p36}} P_{36} \\ -k_{p64}[M_4] - \overline{k_{p46}} P_{46} \\ -k_{p65}[M_5] - \overline{k_{p56}} P_{56} \end{bmatrix}$$

However, the probability terms are still in the equation $\mathbf{M} \cdot \mathbf{r} = \mathbf{b}$, with radical fractions and probabilities, and therefore the equation does not have an analytical solution. Hence, these nonlinear equations containing radical fractions and probabilities should be solved simultaneously by a numerical method. The number of variables in total is $n(n + 1)$ for an n-monomer system. In *hexa*-polymerization, for instance, 42 variables (36 probabilities and 6 radical fractions) are needed. The system of 42 nonlinear equations in P_{ij} and $\Phi_j^\bullet$ can be solved either by Newton's method or the trust region method from the radical balance equations (3-135) to (3-140) and probability equation (3-141). Subsequently, the monomer balance equations (3-123) to (3-128) can be solved and further calculations of conversion, polymer composition, etc. are possible.

Considering depropagation, the sequence length probability p_{ij} in equation (3-75) also needs to be redefined in equation (3-142). Again, the reader is cautioned so as the sequence length probability p_{ij} (lower-case letter) in the left side of equation (3-142) is not confused with the probability P_{ij} (upper-case letter) in the right side.

$$p_{ij} = \frac{k_{pij}[R_i^\bullet][M_j] - \overline{k_{pij}}[R_{ij}^\bullet]}{\sum_{l=1}^{6} k_{pil}[R_i^\bullet][M_l] - \sum_{l=1}^{6} \overline{k_{pil}}[R_{il}^\bullet]} = \frac{k_{pij}[R_i^\bullet][M_j] - \overline{k_{pij}} P_{ij}[R_j^\bullet]}{\sum_{l=1}^{6} k_{pil}[R_i^\bullet][M_l] - \sum_{l=1}^{6} \overline{k_{pil}} P_{il}[R_l^\bullet]} \qquad (3\text{-}142)$$

The next step is obtaining depropagation rate constants. In *hexa*-polymerization, 36 rate constants are necessary in total for a fully depropagating system. Krüger introduced the *cross*-depropagation ratios which can be estimated through experiment for a *co*-polymer model.

$$R_1^{'} = \frac{\overline{k_{p12}}}{k_{p21}} \qquad R_2^{'} = \frac{\overline{k_{p21}}}{k_{p12}} \qquad R_{11}^{'} = \frac{\overline{k_{p11}}}{k_{p12}} \qquad R_{22}^{'} = \frac{\overline{k_{p22}}}{k_{p21}} \tag{3-143}$$

Individual species equilibrium constants are expressed in terms of $R_{ii}^{'}$ and reactivity ratio r_{ij}.

$$K_{eq,i} = \frac{\overline{k_{pii}}}{k_{pii}} = \frac{R_{ii}^{'}}{r_{ij}} \tag{3-144}$$

From the above information, the extended *cross*-depropagation ratios for a six component system are as follows.

$$R_1^{'} = \frac{\overline{k_{12}}}{k_{21}} \quad R_2^{'} = \frac{\overline{k_{21}}}{k_{12}} \quad R_3^{'} = \frac{\overline{k_{13}}}{k_{31}} \quad R_4^{'} = \frac{\overline{k_{31}}}{k_{13}} \quad R_5^{'} = \frac{\overline{k_{14}}}{k_{41}} \quad R_6^{'} = \frac{\overline{k_{41}}}{k_{14}}$$

$$R_7^{'} = \frac{\overline{k_{15}}}{k_{51}} \quad R_8^{'} = \frac{\overline{k_{51}}}{k_{15}} \quad R_9^{'} = \frac{\overline{k_{16}}}{k_{61}} \quad R_{10}^{'} = \frac{\overline{k_{61}}}{k_{16}} \quad R_{11}^{'} = \frac{\overline{k_{23}}}{k_{32}} \quad R_{12}^{'} = \frac{\overline{k_{32}}}{k_{23}}$$

$$R_{13}^{'} = \frac{\overline{k_{24}}}{k_{42}} \quad R_{14}^{'} = \frac{\overline{k_{42}}}{k_{24}} \quad R_{15}^{'} = \frac{\overline{k_{25}}}{k_{52}} \quad R_{16}^{'} = \frac{\overline{k_{52}}}{k_{25}} \quad R_{17}^{'} = \frac{\overline{k_{26}}}{k_{62}} \quad R_{18}^{'} = \frac{\overline{k_{62}}}{k_{26}}$$

$$R_{19}^{'} = \frac{\overline{k_{34}}}{k_{43}} \quad R_{20}^{'} = \frac{\overline{k_{43}}}{k_{34}} \quad R_{21}^{'} = \frac{\overline{k_{35}}}{k_{53}} \quad R_{22}^{'} = \frac{\overline{k_{53}}}{k_{35}} \quad R_{23}^{'} = \frac{\overline{k_{36}}}{k_{63}} \quad R_{24}^{'} = \frac{\overline{k_{63}}}{k_{36}}$$

$$R_{25}^{'} = \frac{\overline{k_{45}}}{k_{54}} \quad R_{26}^{'} = \frac{\overline{k_{54}}}{k_{45}} \quad R_{27}^{'} = \frac{\overline{k_{46}}}{k_{64}} \quad R_{28}^{'} = \frac{\overline{k_{64}}}{k_{46}} \quad R_{29}^{'} = \frac{\overline{k_{56}}}{k_{65}} \quad R_{30}^{'} = \frac{\overline{k_{65}}}{k_{56}}$$

$$R_{101}^{'} = \frac{\overline{k_{11}}}{k_{12}} \quad R_{202}^{'} = \frac{\overline{k_{22}}}{k_{21}} \quad R_{303}^{'} = \frac{\overline{k_{33}}}{k_{31}} \quad R_{404}^{'} = \frac{\overline{k_{44}}}{k_{41}} \quad R_{505}^{'} = \frac{\overline{k_{55}}}{k_{51}} \quad R_{606}^{'} = \frac{\overline{k_{66}}}{k_{61}}$$

R'_{101}, R'_{202}, etc., are used to avoid overlapping with R'_{11} and R'_{22}.

Figures 3.7 and 3.8 show example simulation plots with depropagation. The Mayo-Lewis and Krüger model predictions are compared with experimental data from Martinet and Guillot (1999) for the instantaneous polymer composition drift of AMS in a AMS/MMA *co*-polymer at 60 and 80℃. Due to the low ceiling temperature of AMS (61℃), depropagation becomes dominant as the reaction temperature and the AMS feed ratio increase. When f_{AMS} is greater than 0.5, the Mayo-Lewis model assuming no depropagation does not hold any longer. Instead, the behaviour of polymer composition F_{AMS} is explained by Krüger's model very well at both temperature levels.

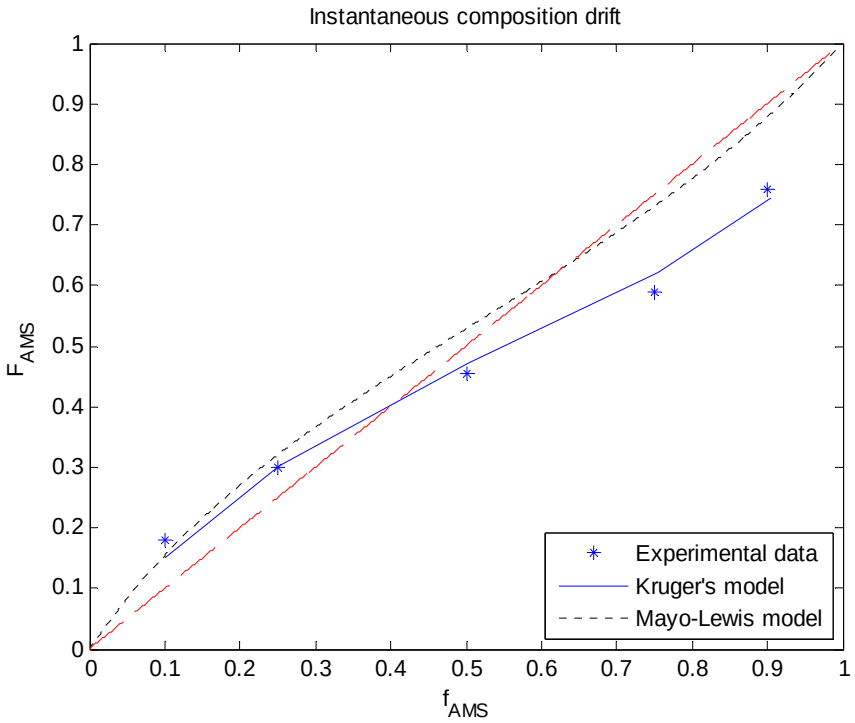

Figure 3.7. Simulation of composition drift of F_{AMS} in AMS/MMA *co*-polymerization T = 60℃, AIBN = 0.5 mol%

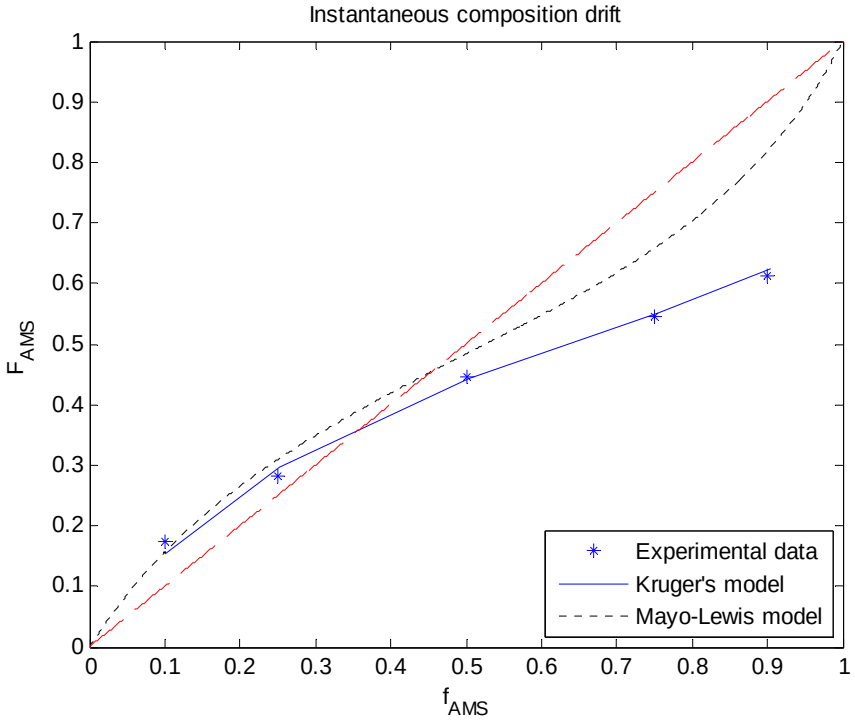

Figure 3.8. Simulation of composition drift of F_{AMS} in AMS/MMA *co*-polymerization T = 80℃, AIBN = 0.5 mol%

Chapter 4

Model and Simulation Features

4.1 Description

The multi-component polymerization simulation model was coded in MATLAB. Preliminary benchmarking was done versus predictions from WATPOLY, the comprehensive simulator and database package previously developed in the Department of Chemical Engineering, University of Waterloo, in Professor A. Penlidis' group (e. g., see Gao and Penlidis, 1996, 1998, 2000), which was coded in QuickBASIC under an MS-DOS environment. MATLAB offers powerful and convenient matrix calculations, various library functions for numerical computing, and easy graphical output presentations. Moreover, MATLAB is running under the Windows environment.

This modeling work started from *homo*-polymerization cases and extended to *co*-, *ter*-, and multi-component ones. Therefore, it can cover up to six monomers and is still further extendable via code generalization. The overall coded MATLAB program is composed of several functions: monomer and ingredients kinetic database functions, the subroutine model function containing the model differential equations, and the main function for calculating and plotting physical and chemical state variables of interest. The considered features in the model are as follows.

1. Bulk/solution polymerization
2. Batch/semi-batch reactor configuration
3. Isothermal/non-isothermal reaction by temperature profile
4. Pseudo rate constant method

5. Diffusion-controlled kinetics
6. Thermal initiation for styrenics
7. Branching/crosslinking (method of moments calculations)
8. Depropagation (Krüger's model extended to six monomers)

The model can predict the following output profiles.

1. Total/partial conversion
2. Overall/individual rate of polymerization
3. Total reaction volume (shrinkage)
4. Monomer/radical species concentrations
5. Other ingredients (e. g., initiator, solvent, CTA, inhibitor, etc.) concentrations
6. Residual monomer fraction and radical fraction
7. Instantaneous/accumulated polymer composition
8. Instantaneous/accumulated polymer composition distribution
9. Instantaneous/accumulated number and weight average molecular weights
10. Instantaneous/accumulated polydispersity index (PDI)
11. Instantaneous/accumulated full MWD (for linear chains)
12. Sequence length distribution
13. Instantaneous/accumulated number and weight average sequence lengths
14. Instantaneous/accumulated triad fractions
15. Average number of *tri*/*tetra*-functional branches per molecule
16. Polymer glass transition temperature and free volume characteristics
17. Pseudo termination/propagation/transfer reaction constants and initiator efficiency

4.2 Six-component polymerization recipe

The multi-component polymerization recipe (six monomer system) is described in Table 4.1. An extensive database of physico-chemical characteristics for each monomer is

summarized in Appendix C, containing Styrene (Sty), *n*-butyl acrylate (BA), *n*-butyl methacrylate (BMA), 2-hydroxyethyl acrylate (HEA), and acrylic acid (AA). No information was found in the literature for hydroxybutyl acrylate (HBA). Regular and elevated temperature ranges can be handled by the model, including thermal initiation (of styrenics) and depropagation scenarios. Since experimental data for *ter*-, *tetra*-, *penta*-, and *hexa*-polymerizations are very scarce (if non-existent), it was deemed better to test the model starting from known *homo*-polymerizations and extend to multi-component cases where literature data were available.

Ingredients	Reactor Configuration	Temperature
1. Monomers Styrene (10 wt%) n-Butyl acrylate (30 wt%) n-Butyl methacrylate (15 wt%) Hydroxyehtyl acrylate (20 wt%) Hydroxybutyl acrylate (20 wt%) Acrylic acid (5 wt%) 2. Solvent Xylene or Xylene/Ketones 3. Initiator *Di-tert*-butyl peroxide (DTBP, trigonox B)	Batch/semi-batch	50~180℃

Table 4.1. Typical multi-component polymerization recipe

Chapter 5

Model Testing/Troubleshooting

In this chapter, the multi-component polymerization model is tested with experimental data from various monomer systems: *homo*-polymerizations of Sty, MMA, EA, AN, and VAc, and *co*-polymerizations of Sty/EA, Sty/AN, BA/VAc, and MMA/VAc. Experimental results and model predictions are presented according to various recipes from literature sources. This exercise clearly shows that the multi-component model can successfully reduce to simpler cases, thus increasing one's confidence in the reliability of the model.

5.1 Sty *homo*-polymerization

Sty is one of the monomers that have been extensively studied. Figure 5.1 shows Sty bulk *homo*-polymerization model predictions and experimental data (Arai and Saito, 1976). We can see the autoacceleration and glass-transition effect in the plot. Predictions and data show good agreement over the entire conversion range.

The most distinctive characteristic of Sty is that it undergoes thermal self-polymerization without initiators at higher temperatures (over 100℃). Additionally, chain transfer to thermal initiation by-products can affect molecular weights (Hui and Hamielec, 1972), according to:

$$\tau_{total} = \tau - \left(1.013\times10^{-3}\right)\log_{10}\left(\frac{473.12-T}{202.5}\right)X \tag{5-1}$$

where $\tau = \dfrac{k_{td}[R^{\bullet}] + k_{fCTA}[CTA] + k_{fS}[S] + k_{fZ}[Z]}{k_p[M]} + \dfrac{k_{fm}}{k_p}$, T is the reaction temperature (K), and X is overall conversion.

Figures 5.2 and 5.3 are example plots of thermal initiation at 170℃ and the experimental data were obtained from Hui and Hamielec (1972). The model gives satisfactory predictions of both conversion and molecular weights.

In solution polymerization, an adequate amount of solvent helps maintain low viscosity of the reaction medium and moderates diffusion-controlled behaviour. This is observed in Figure 5.4, the example plot of solution polymerization. Experimental data are again from Hui and Hamielec (1972).

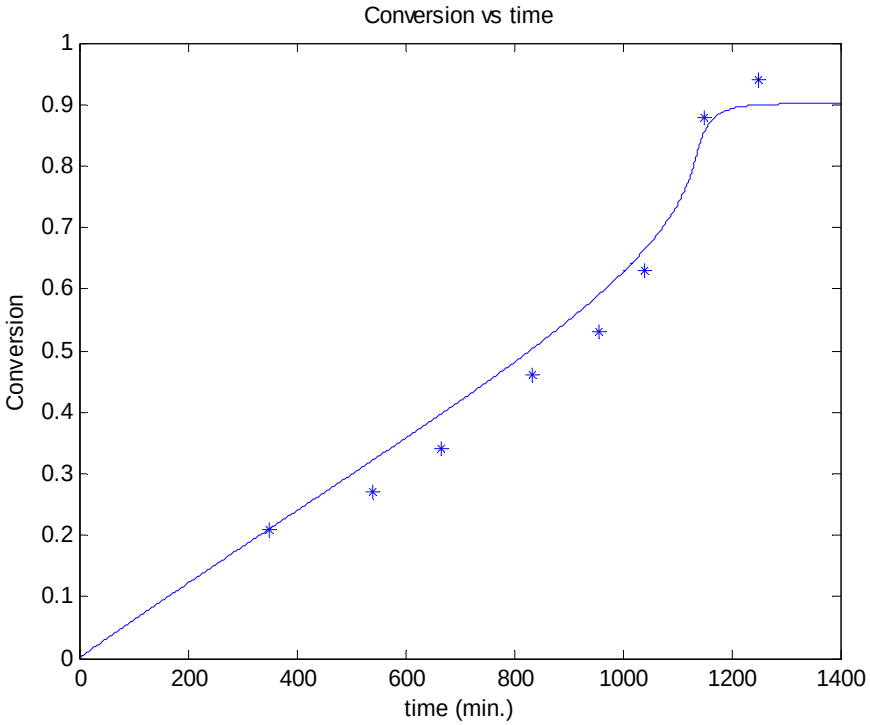

Figure 5.1. Simulation of bulk polymerization of Sty at 60℃, $[AIBN]_0$ = 0.0164 M

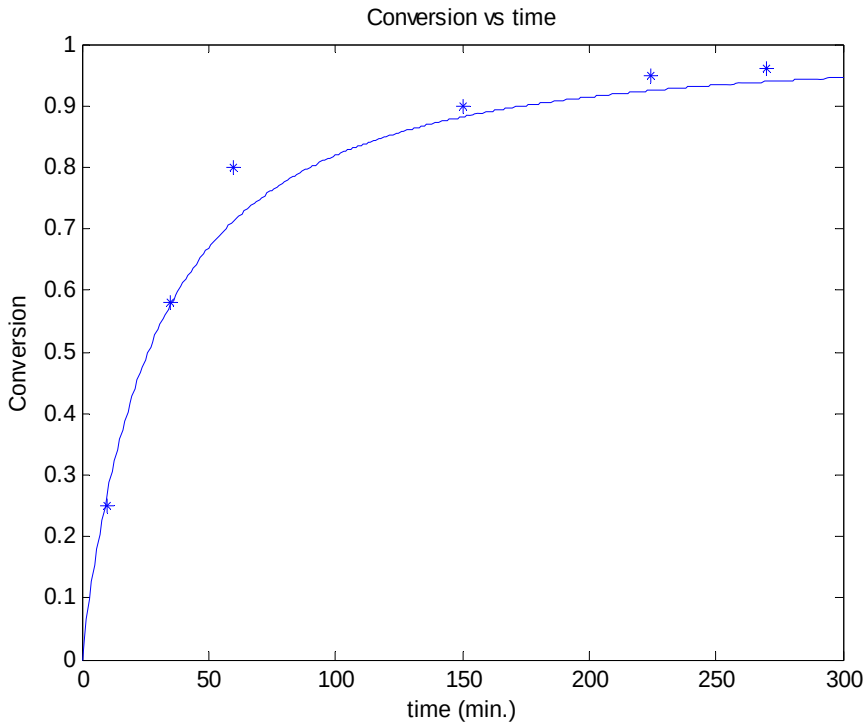

Figure 5.2. Simulation of bulk thermal polymerization of Sty at 170℃

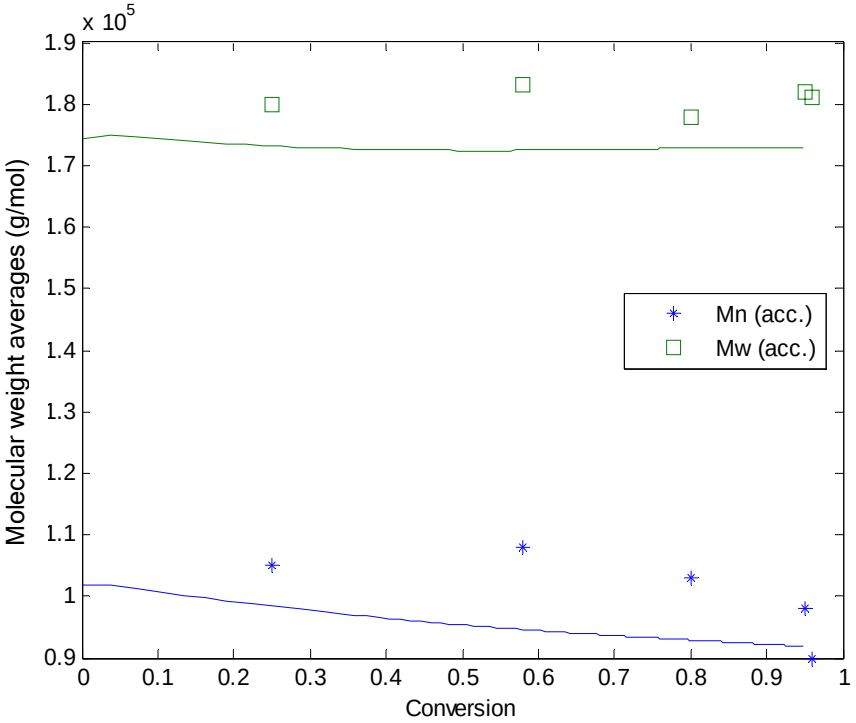

Figure 5.3. Simulation of molecular weights of Sty thermal polymerization at 170℃

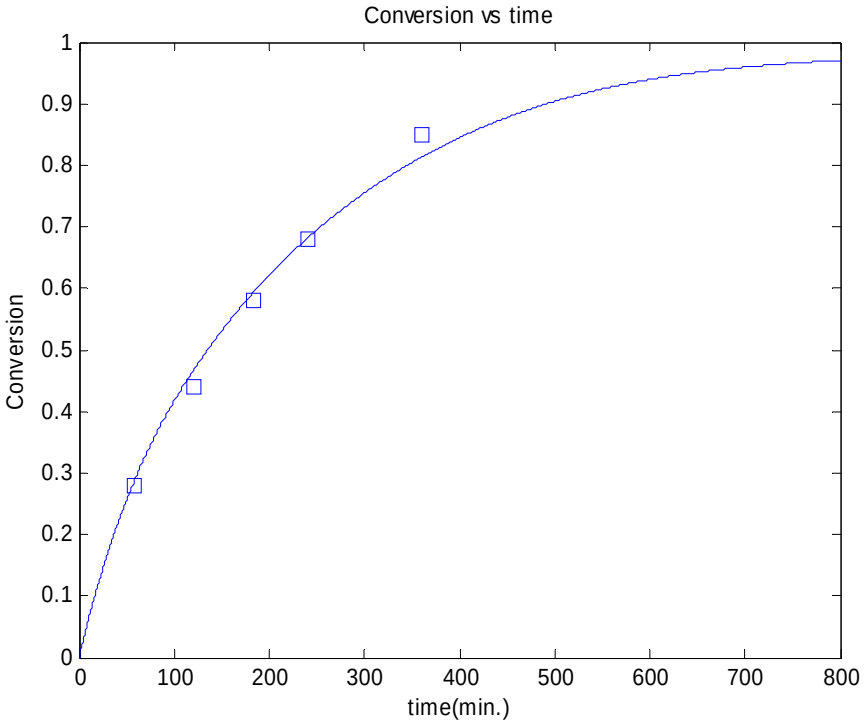

Figure 5.4. Simulation of solution polymerization of Sty
T = 80℃, $[AIBN]_0$ = 0.04 M and $[Toluene]_0$ = 1.8 M

5.2 MMA *homo*-polymerization

MMA is another widely studied monomer. The model is tested with the experimental data by Kumar and Gupta (1991). They conducted bulk polymerization experiments and measured conversion and molecular weights at 50, 70, and 90℃ using two AIBN initiator concentration levels of 0.0258 mol/L and 0.01548 mol/L. Figures 5.5 and 5.6 represent model predictions and experimental data of conversion, and Figures 5.7 to 5.10 show the number/weight average molecular weight calculations using the corresponding recipes. The model predictions again follow the experimental data well in this monomer system.

The previous figures also indicate that the model successfully explains free-radical polymerization trends. Comparing Figures 5.7 and 5.8, as well as Figures 5.9 and 5.10, it is observed that molecular weights decrease as reaction temperature is higher. Also, comparing Figures 5.7 and 5.9, as well as Figures 5.8 and 5.10, we can see that molecular weights increase as initiator concentration is lower.

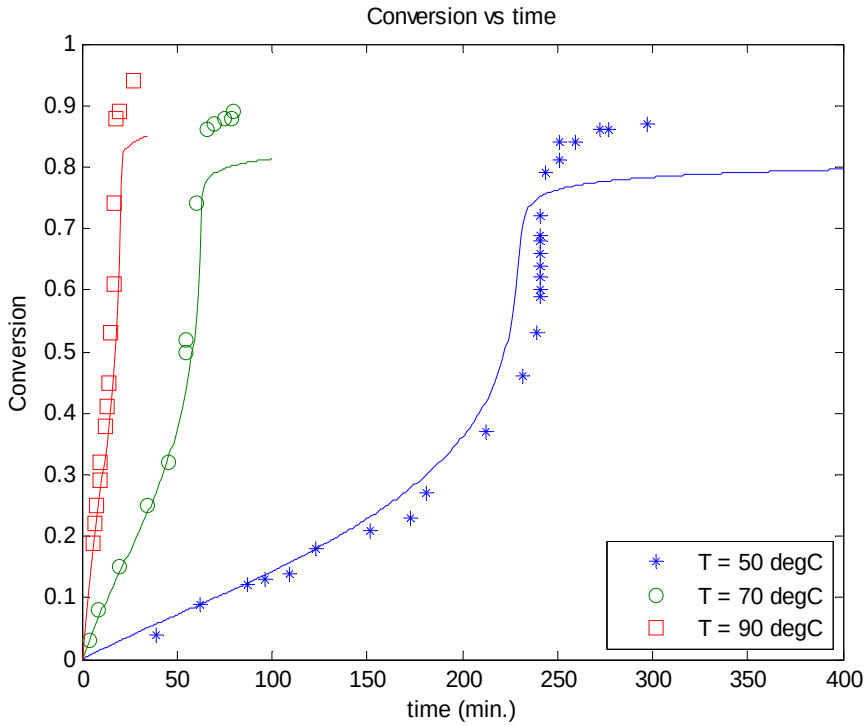

Figure 5.5. Simulation of bulk polymerizations of MMA at 50, 70, and 90℃, $[AIBN]_0$ = 0.0258 M

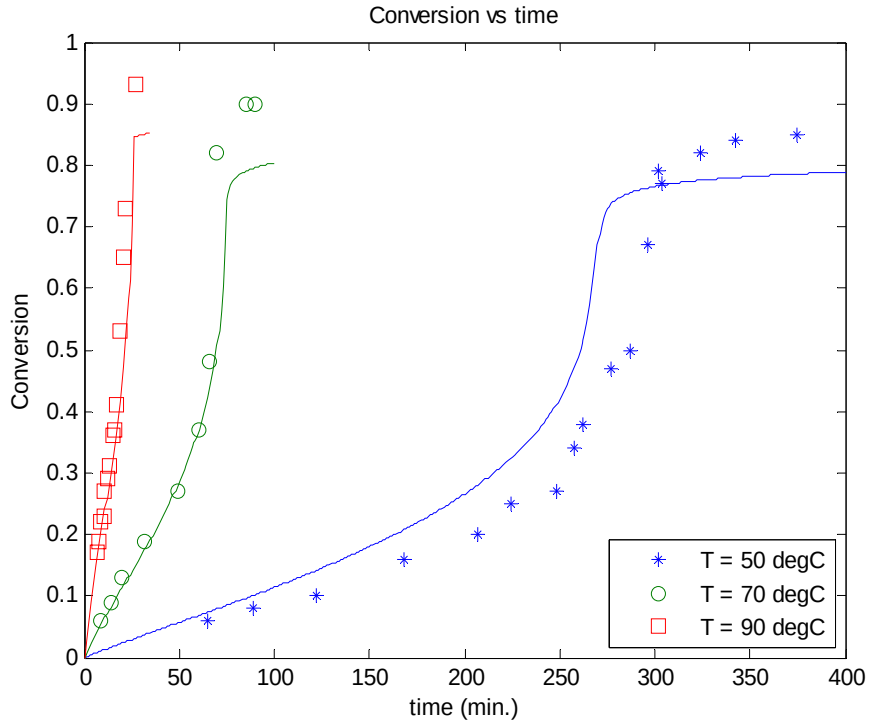

Figure 5.6. Simulation of bulk polymerizations of MMA at 50, 70, and 90℃, $[AIBN]_0$ = 0.01548 M

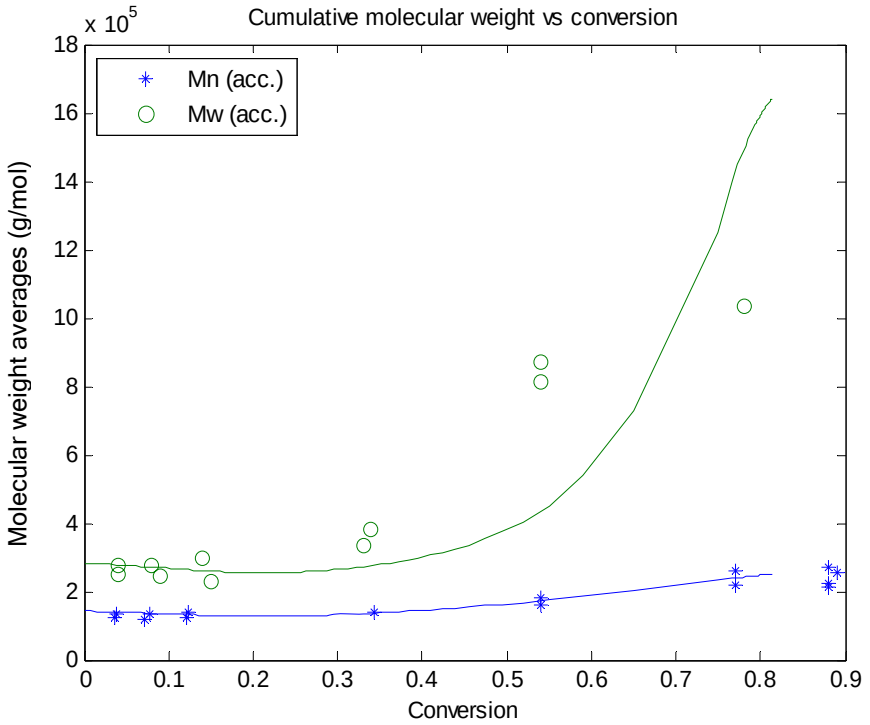

Figure 5.7. Molecular weight predictions for MMA polymerization at 70℃, $[AIBN]_0$ = 0.0258 M

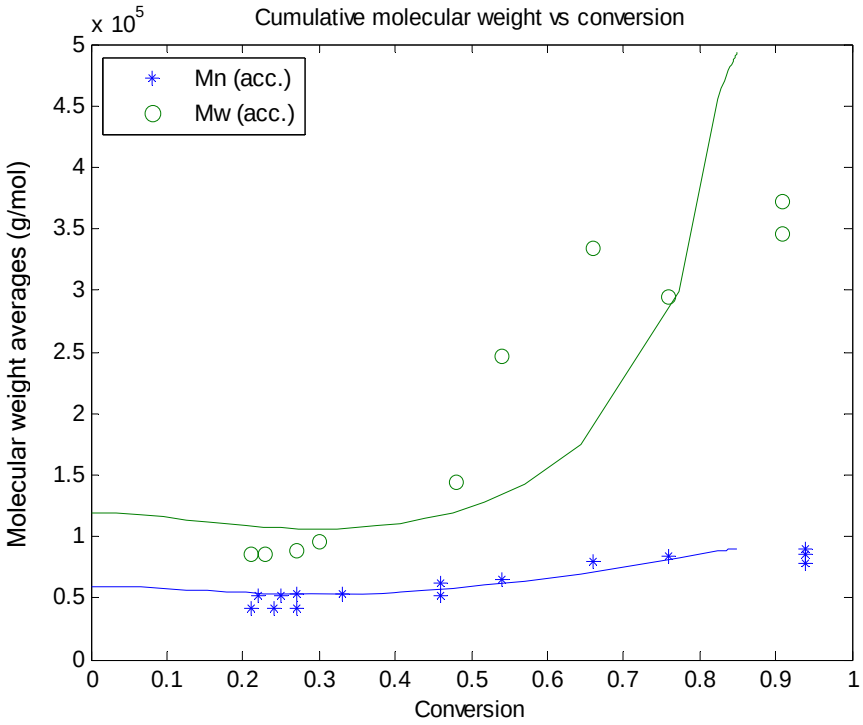

Figure 5.8. Molecular weight predictions for MMA polymerization at 90℃, $[AIBN]_0$ = 0.0258 M

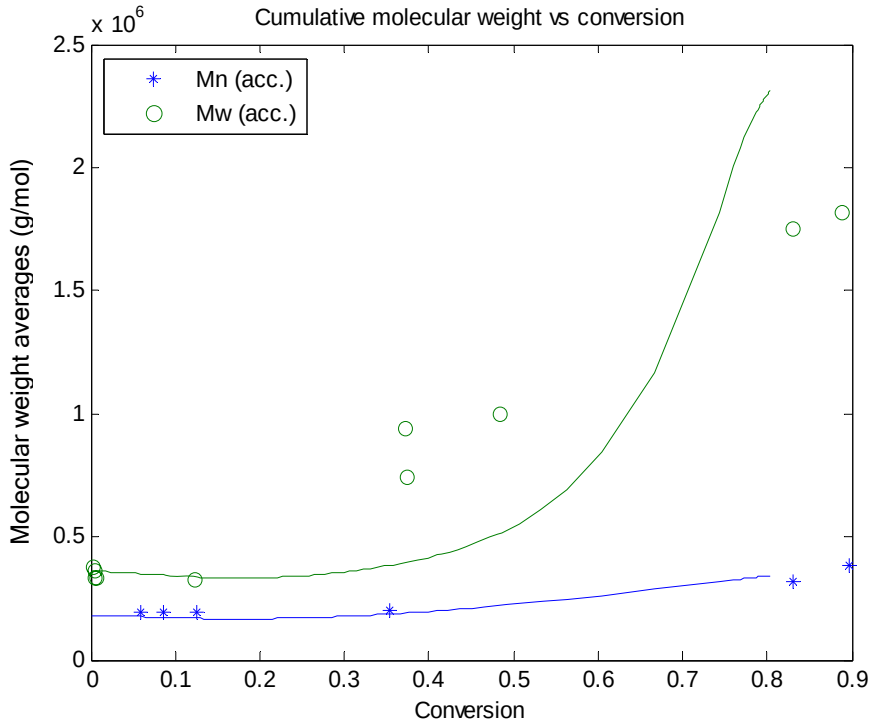

Figure 5.9. Molecular weight predictions for MMA polymerization at 70℃, $[AIBN]_0$ = 0.01548 M

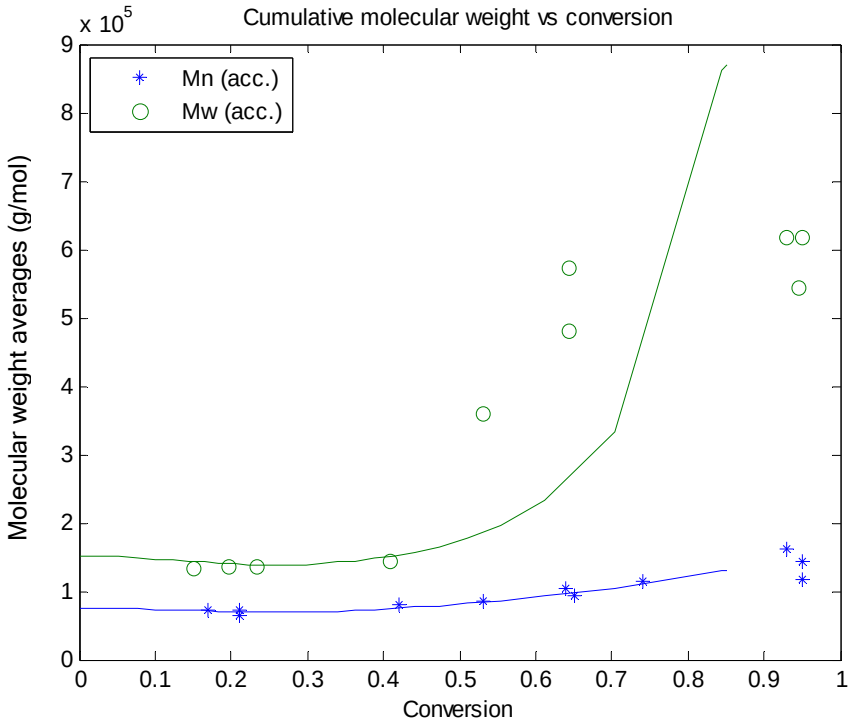

Figure 5.10. Molecular weight predictions for MMA polymerization at 90℃, $[AIBN]_0$ = 0.01548 M

5.3 EA *homo*-polymerization

Figures 5.11 to 5.13 show good agreement between model predictions and experimental data obtained by McIsaac (1994). Two initiator concentration levels (0.0002 mol/L and 0.0008 mol/L) and three temperature levels (40, 50, and 60℃) were used for the recipes. It is reported that the molecular weight of the polymer formed in bulk EA *homo*-polymerization is very high, and the system becomes highly viscous shortly after the reaction starts. This is the clue that EA exhibits a strong autoacceleration starting at low conversion levels with no limiting conversion. Considerable branching takes place during the reaction due to transfer to polymer and terminal double bond polymerization. However, the parameters involved in branching reactions (transfer to polymer and terminal double bond polymerization) are not well known.

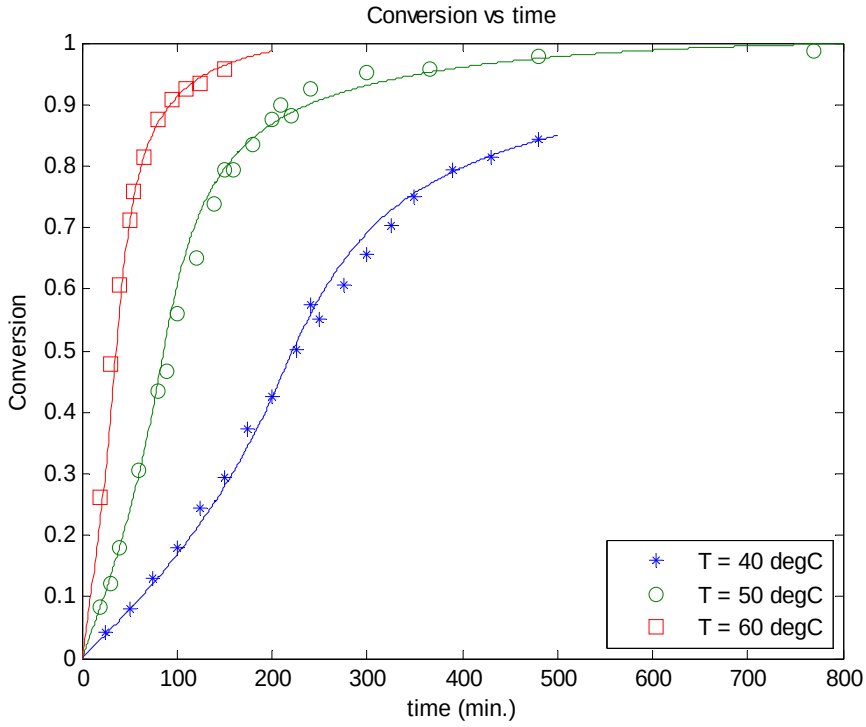

Figure 5.11. Simulation of bulk polymerizations of EA, $[AIBN]_0$ = 0.0008 M

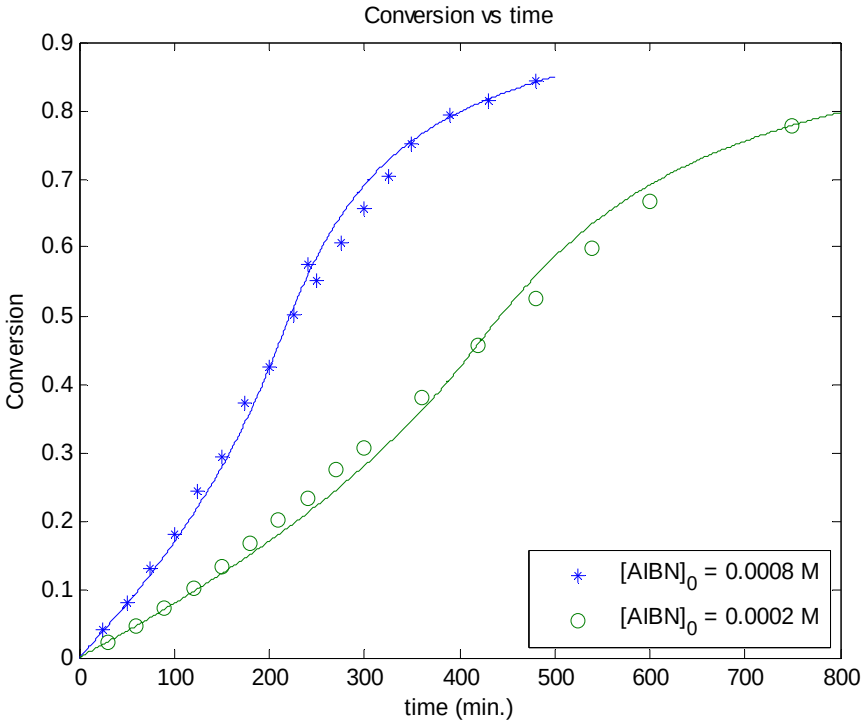

Figure 5.12. Simulation of bulk EA polymerizations at 40℃

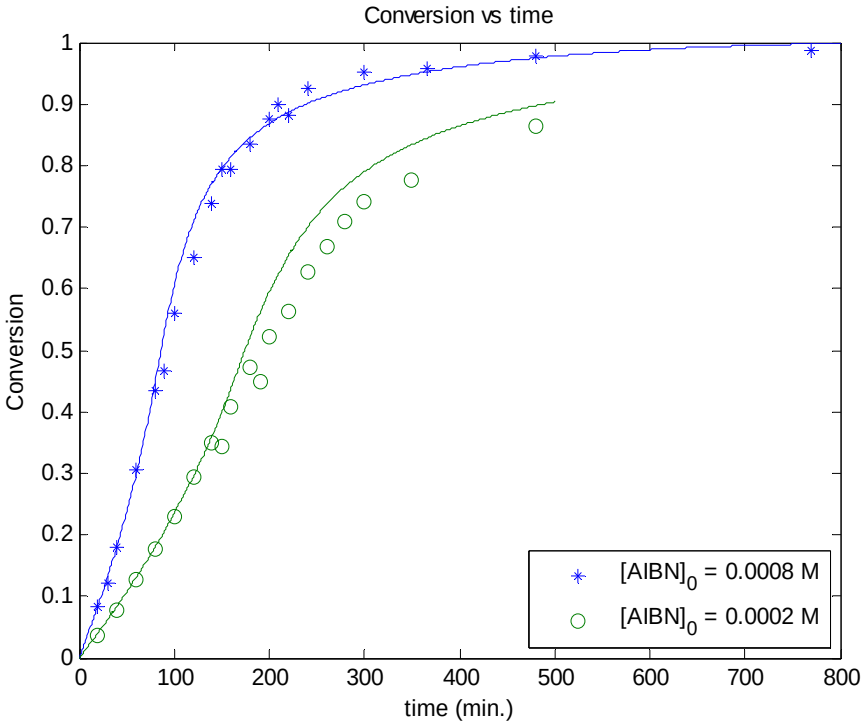

Figure 5.13. Simulation of bulk EA polymerizations at 50℃

5.4 AN *homo*-polymerization

Figure 5.14 shows model predictions and experimental data at three different sets of temperature (40, 60, and 80℃) and initiator concentrations (2, 0.2, and 0.05 wt%) from Garcia-Rubio *et al*. (1979). Despite the reasonable trends, what should be noted is that AN polymerization is a heterogeneous reaction. In bulk polymerization, polymer precipitates in the reaction medium (monomer) and forms a polymer-rich phase, which makes some kinetic rate constants different from those in a homogeneous reaction. The complex mechanism of phase separation is not completely understood.

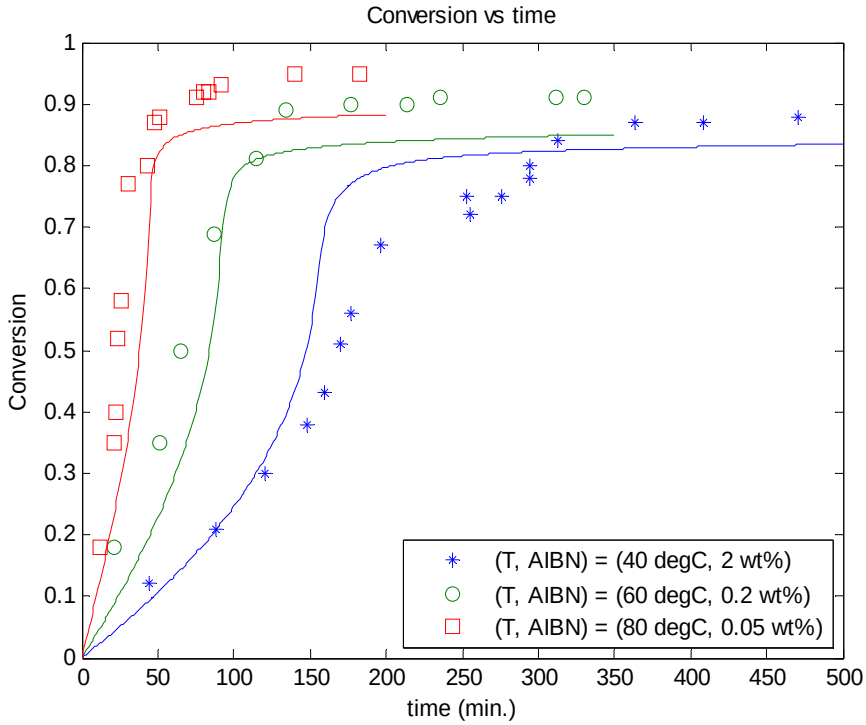

Figure 5.14. Simulation of bulk polymerizations of AN

5.5 VAc *homo*-polymerization

Vinyl acetate (VAc) is characterized by long-chain branching formation. Figure 5.15 shows model predictions and experimental results at 50℃ and 0.004 mol/L of AIBN from Friis and Nyhagen (1973). The rate of polymerization begins to increase mildly around 30% conversion level and no limiting conversion is observed. Our model predictions are again satisfactory.

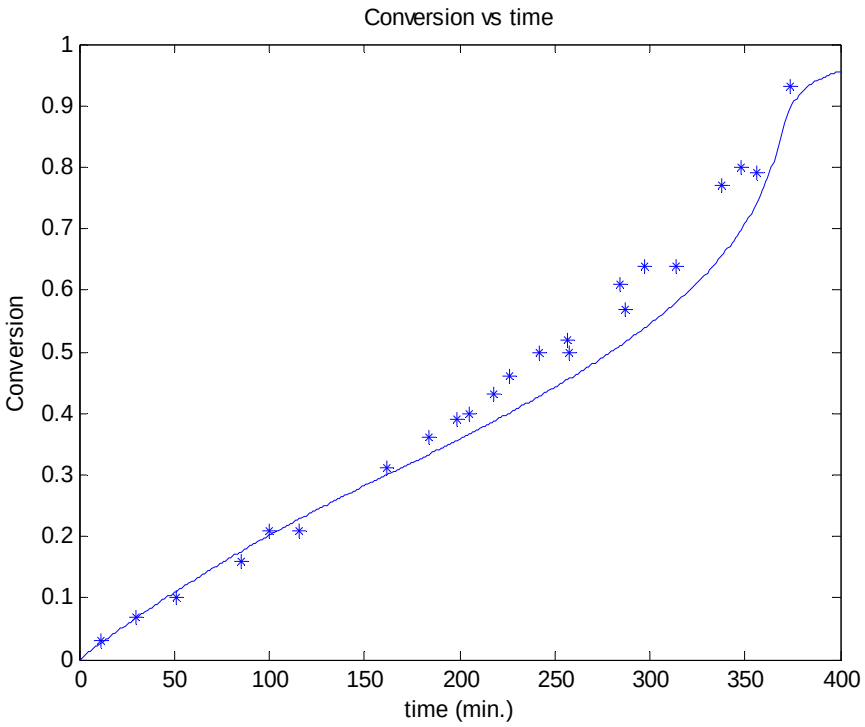

Figure 5.15. Simulation of bulk polymerization of VAc at 50℃, $[AIBN]_0$ = 0.004 mol/L

5.6 Sty/EA *co*-polymerization

Full conversion range experiments of Sty/EA *co*-polymerization were conducted in our research group (McManus and Penlidis, 1996) for the first time. Sty and EA monomers are different from each other in physical and chemical properties (like in Sty/BA case) and the *co*-polymer properties also largely depend on the dominant monomer content. The reactivity ratios are $r_{\text{Sty-EA}} = 0.717$, $r_{\text{EA-Sty}} = 0.128$, estimated by the EVM method. Figures 5.16 and 5.17 represent conversion and polymer composition profiles as a function of Sty (monomer 1) content in the feed ($f_{10} = f_{\text{Sty0}} = 0.152$, 0.463, and 0.762) at 50℃ with $[\text{AIBN}]_0 = 0.05$ mol/L. Figure 5.16 shows that polymerization rate becomes slower as Sty becomes more dominant in the monomer feed ratio. Simulation results show reasonable agreement with experimental data throughout the entire conversion when $f_{10} = f_{\text{Sty0}} = 0.152$ and 0.453. However, some discrepancies are observed from around 40% of conversion in the azeotropic composition case ($f_{\text{Sty0}} = 0.762$). The model prediction of accumulated polymer composition of Sty explains the experimental data well in Figure 5.17.

Sahloul (2004) conducted solution *co*-polymerization (Sty/EA = 50/50 wt% in the feed) at 130℃, with m-Xylene as solvent (60 wt% of total mixture), *tert*-butyl peroxybenzoate (TBPB) as initiator (1.5 wt% of total mixture), and octanethiol (0.5 wt% of total mixture) as CTA. The model follows the *co*-polymerization trends satisfactorily in Figures 5.18 and 5.19.

The calculation of the amounts of monomers, solvent, and initiator in this *co*-polymerization recipe is as follows.

Total monomer amounts (grams): 100 (Sty/EA = 50/50)

Total mixture amounts (grams): 100 + x (solvent) + y (initiator) + z (CTA)

Ratio of solvent in total mixture: $\dfrac{x}{x+100+y+z} = 0.6$

Ratio of initiator in total mixture: $\dfrac{y}{x+100+y+z} = 0.015$

Ratio of CTA in total mixture: $\dfrac{z}{x+100+y+z} = 0.005$

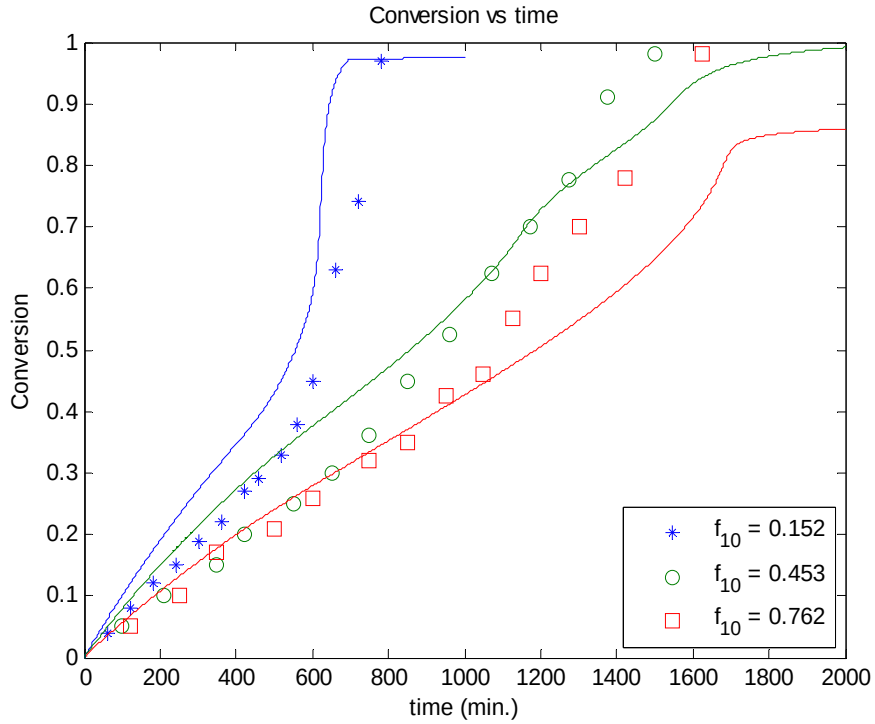

Figure 5.16. Simulation of bulk *co*-polymerizations of Sty/EA at T = 50℃, $[AIBN]_0$ = 0.05 M (1 = Sty)

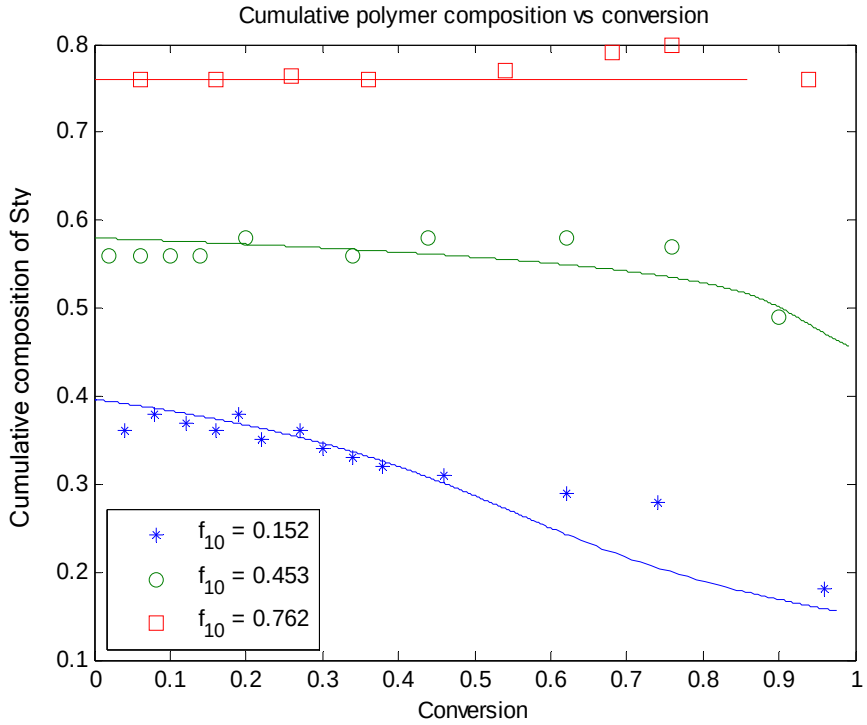

Figure 5.17. Cumulative polymer composition of Sty in Sty/EA *co*-polymerization T = 50℃ and $[AIBN]_0$ = 0.05 M (1 = Sty)

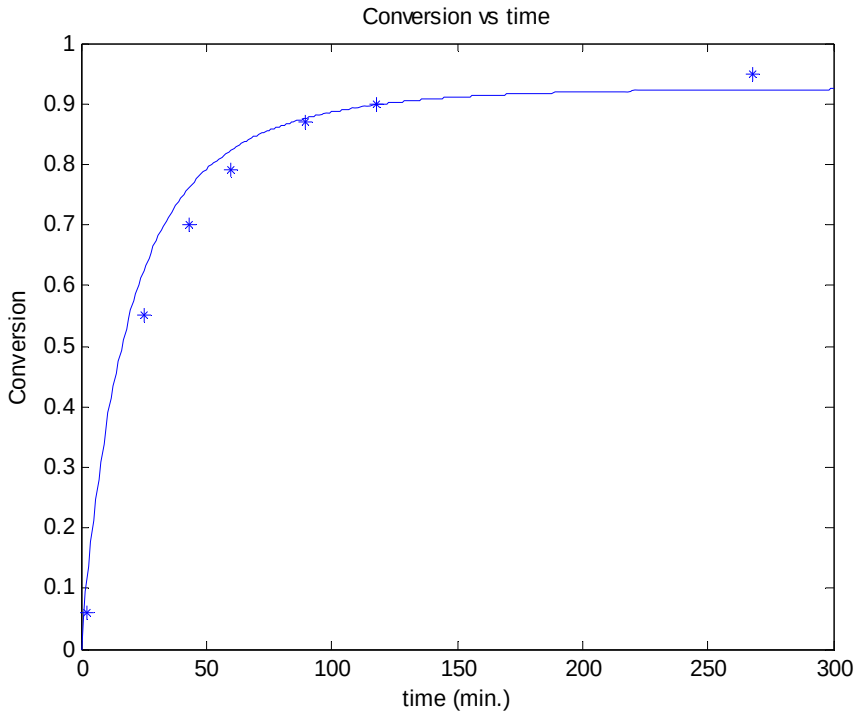

Figure 5.18. Simulation of solution *co*-polymerization of Sty/EA (50/50 wt%)
T = 130℃, m-Xylene = 60 wt% of total mixture, TBPB = 1.5 wt% and Octanethiol = 0.5 wt% of total monomer

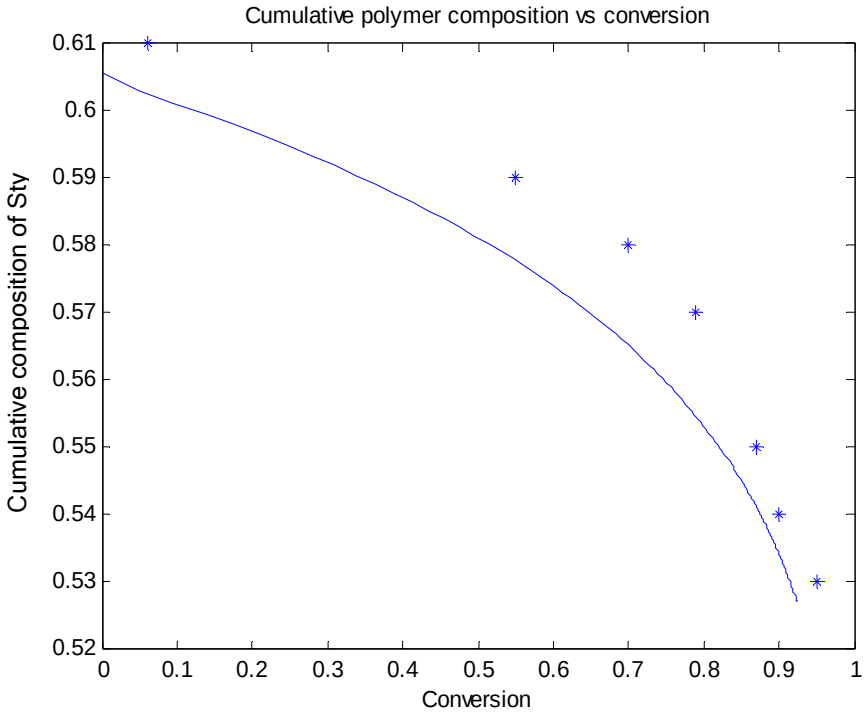

Figure 5.19. Cumulative polymer composition of Sty in Sty/EA (50/50 wt%) *co*-polymerization
T = 130℃, m-Xylene = 60 wt% of total mixture, TBPB = 1.5 wt% and Octanethiol = 0.5 wt% of total monomer

5.7 Sty/AN *co*-polymerization

Sty/AN *co*-polymer product is used as a common thermoplastic with good mechanical/chemical properties, and easy to process as well. Sty and AN monomers are also often polymerized with butadiene to produce ABS rubber. In spite of the academic/industrial interest, its full conversion kinetics have been largely unstudied. Garcia-Rubio *et al*. (1985) reported the reactivity ratios as ($r_{\text{Sty-AN}}$, $r_{\text{AN-Sty}}$) = (0.36, 0.078) along with full conversion experimental data.

As mentioned earlier, AN exhibits heterogeneous *homo*-polymerization and this may affect *co*-polymerization too. Garcia-Rubio *et al*. (1985) observed that Sty/AN in bulk is a homogeneous process throughout most of the conversion range when the Sty (monomer 1) initial feed composition is higher than 0.5, hence it was possible to test our model with the experimental data. Figure 5.20 represents conversion profiles of bulk *co*-polymerization changing f_{Sty0} (f_{10}) from 0.5 to 0.9. Discrepancies start manifesting themselves at Sty content of 70 %.

In Figure 5.21, our model predictions of residual Sty monomer mole fraction acceptably follow experimental data. It should be noted that the azeotropic point ($f_{\text{azeo.}}$) of this system is expected to exist between 0.5 and 0.6, after which the decreasing trend of residual monomer starts to reverse in Figure 5.21. This is an important point indicating which monomer is preferentially incorporated into the polymer, determined by reactivity ratios. AN has basically about five times faster a *homo*-propagation rate constant than Sty, and the *cross*-propagation rate of AN radical with Sty monomer is about twenty times more favored than the reverse *cross*-propagation. In this system, Sty monomer is more readily incorporated into polymer than AN monomer when f_{Sty0} is 0.5, a case slightly lower than the azeotropic point and the opposite phenomenon happens at mole fractions higher than the azetrope. The trends are expected to level off at the limiting conversion, after which composition will stay constant.

Figure 5.22 shows accumulated number average sequence length of Sty (predictions and experimental data). This plot helps to understand how Sty/AN microstructure will change

throughout the entire conversion. When Sty and AN molar contents are similar in the system, Sty average sequence length is located slightly above one and the chain develops almost like an alternating co-polymer (-ABABAB-). As f_{Sty0} increases, the sequence length also increases, especially at high conversion. Then the monomer sequencing patterns resemble those of a block co-polymer (-AAABBBAA-). Model trends agree well with the experimental data.

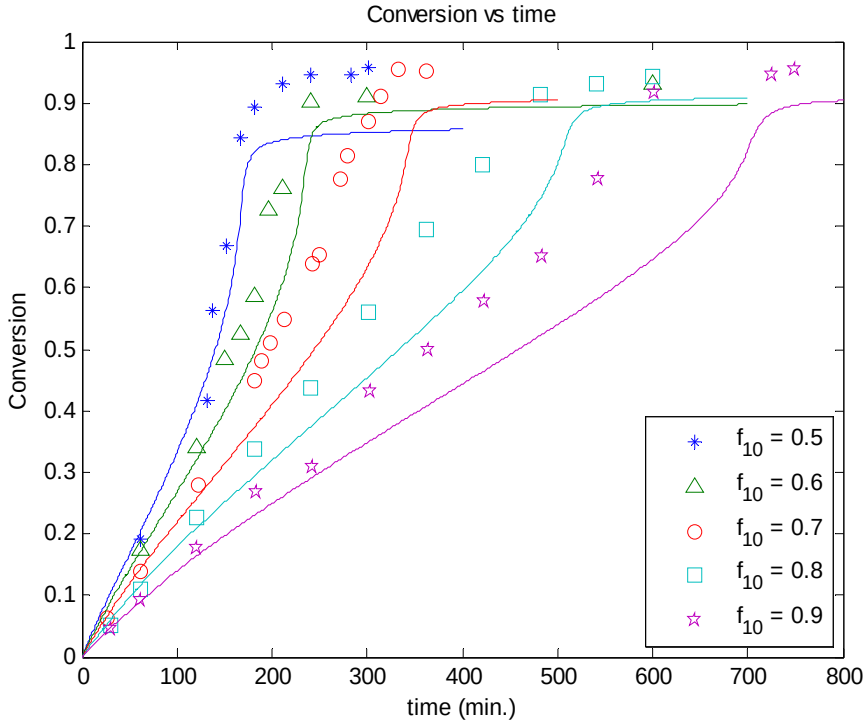

Figure 5.20. Simulation of bulk *co*-polymerizations of Sty/AN
T = 60℃ and $[AIBN]_0$ = 0.05 M (1 = Sty)

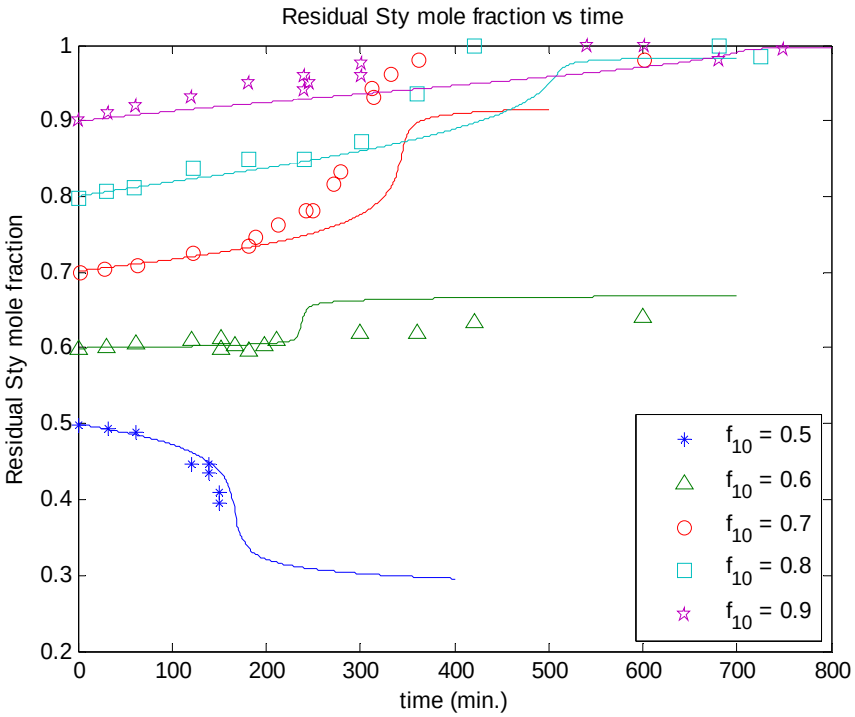

Figure 5.21. Simulation of residual mole fractions of Sty in Sty/AN *co*-polymerization T = 60℃ and $[AIBN]_0$ = 0.05 M (1 = Sty)

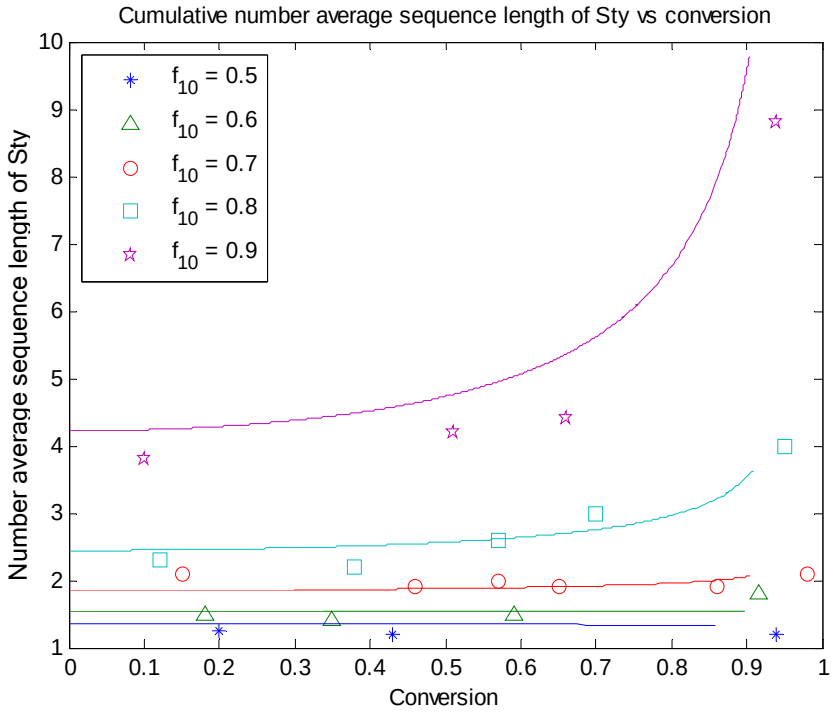

Figure 5.22. Simulation of accumulated number average sequence lengths of Sty in Sty/AN *co*-polymerization, T = 60℃ and $[AIBN]_0$ = 0.05 M (1 = Sty)

5.8 BA/VAc *co*-polymerization

Using EVM, the reactivity ratios were estimated as ($r_{BA\text{-}VAc}$, $r_{VAc\text{-}BA}$) = (5.939, 0.026) by Dubé *et al*. (1995). No azeotropic composition exists in this monomer system. Figure 5.23 shows the conversion profile of bulk *co*-polymerization at 60℃ with $[AIBN]_0$ = 0.00054 mol/L and f_{BA0} = 0.80. The general trend looks like solution polymerization. Some discrepancies between model predictions and experimental data are observed over 70% conversion. Due to the presence of VAc monomer, reactivity ratios differ widely from each other, and much more BA monomer is consumed at the early stages of the reaction. VAc is incorporated into the polymer after the majority of BA is depleted in the reaction mixture. The corresponding polymer composition over conversion is depicted in Figure 5.24. Model predictions generally follow the trend of composition drift.

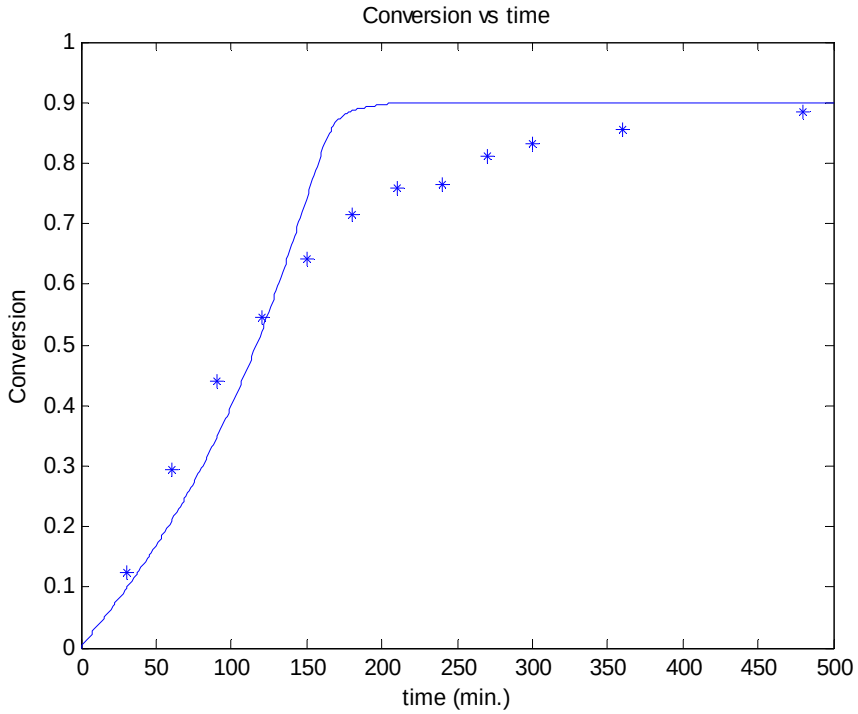

Figure 5.23. Simulation of bulk *co*-polymerization of BA/VAc
T = 60℃, $[AIBN]_0$ = 0.00054 M, and f_{BA0} = 0.80

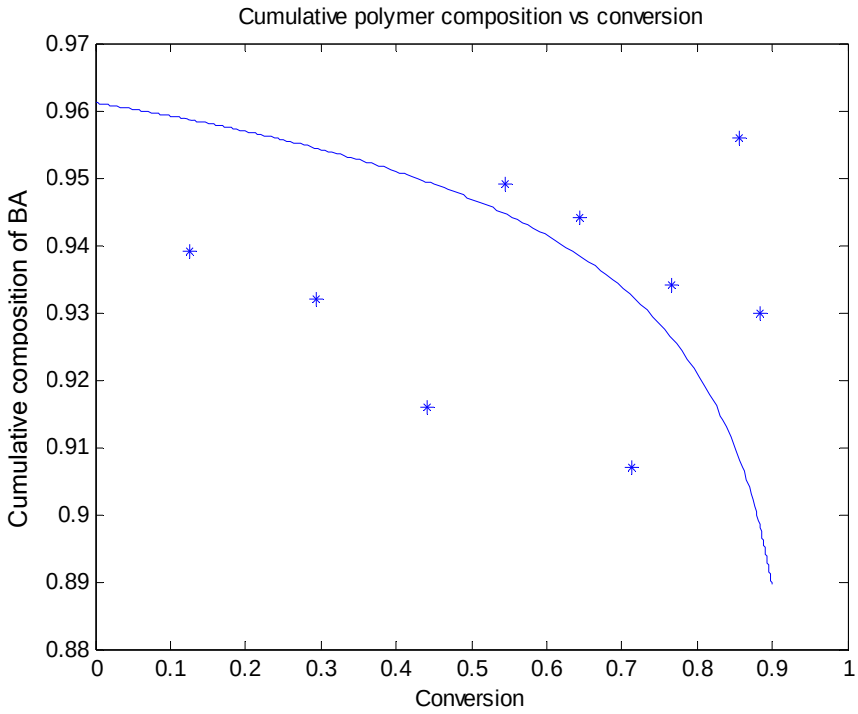

Figure 5.24. Cumulative polymer composition of BA in BA/VAc *co*-polymerization T = 60℃, $[AIBN]_0$ = 0.00054 M, and f_{BA0} = 0.80

5.9 MMA/VAc *co*-polymerization

MMA and VAc *homo*-polymerizations show different kinetic behaviours. MMA polymer is linear and reacts much slower than VAc, which exhibits significant long-chain branching. Reactivity ratios are ($r_{MMA\text{-}VAc}$, $r_{Vac\text{-}MMA}$) = (24.0254, 0.026107) (by EVM method, Dubé *et al*. (1995)). Due to the large difference between reactivity ratios, both MMA and VAc radicals prefer to react with MMA monomer and this leads to a significant composition drift and a two-stage 'double rate phenomenon'.

Figure 5.25 exhibits this effect very well. Experimental conditions were set as T = 60℃, $[AIBN]_0$ = 0.01 mol/L, and f_{MMA0} = 0.30. Almost a virtual MMA "*homo*-polymerization" prevails at the early stage of the reaction, up to about 30% conversion level, whereas the second stage is dominated by VAc "*homo*-polymerization". There is a drastically rapid increase in conversion starting at the second stage because the VAc propagation rate constant is much higher than that of MMA. In Figures 5.26 and 5.27, severe polymer composition drift and a steep increase in weight average molecular weight are also observed after the second stage due to the double rate phenomenon and branching reactions of VAc by transfer to polymer and terminal double bond polymerization. Our model follows these trends satisfactorily.

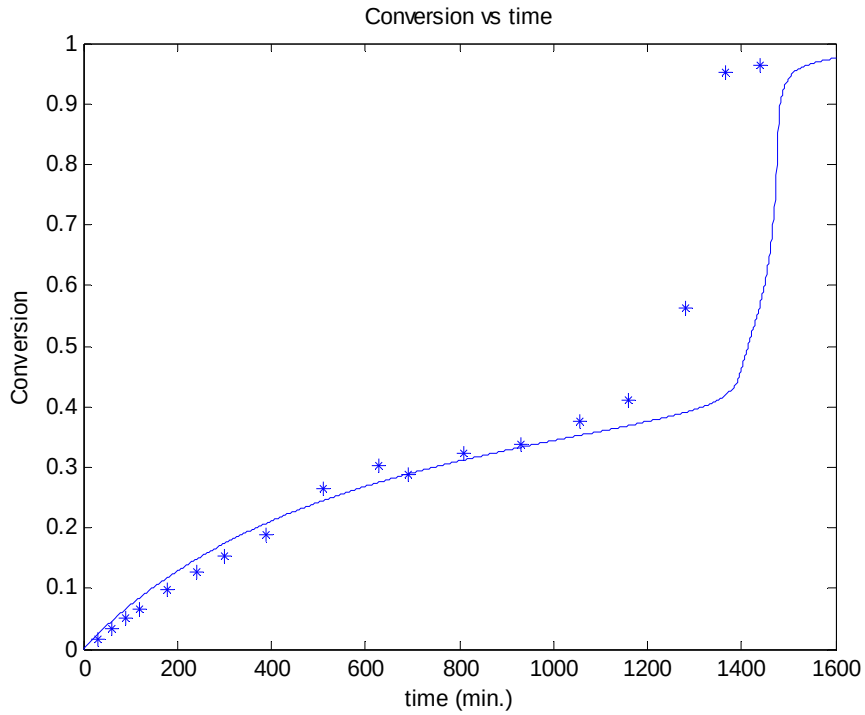

Figure 5.25. Simulation of bulk *co*-polymerization of MMA/VAc
T = 60℃, $[AIBN]_0$ = 0.01 M, and f_{MMA0} = 0.30

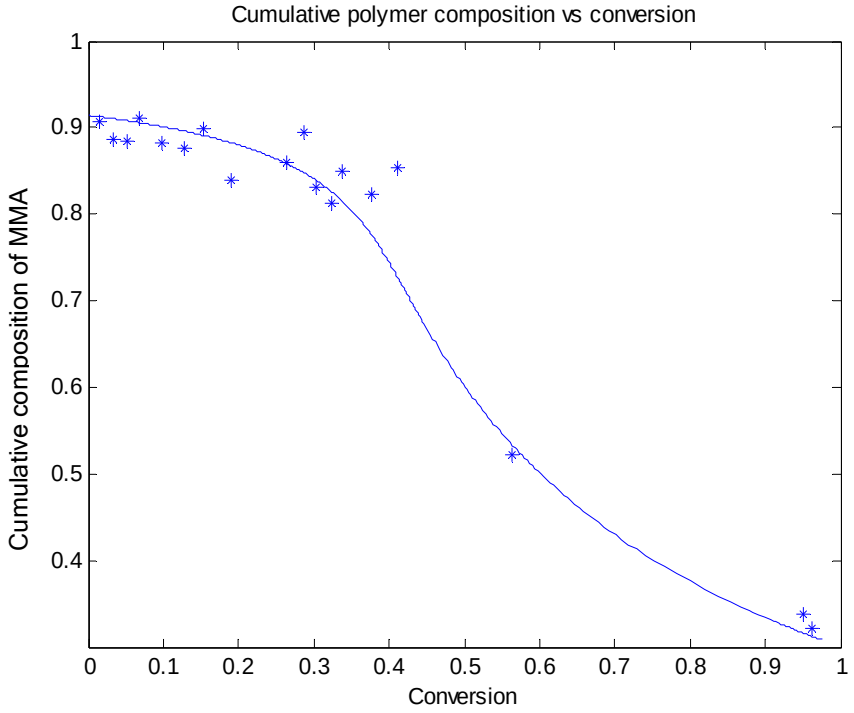

Figure 5.26. Cumulative polymer composition of MMA in MMA/VAc *co*-polymerization
T = 60℃, $[AIBN]_0$ = 0.01 M, and f_{MMA0} = 0.30

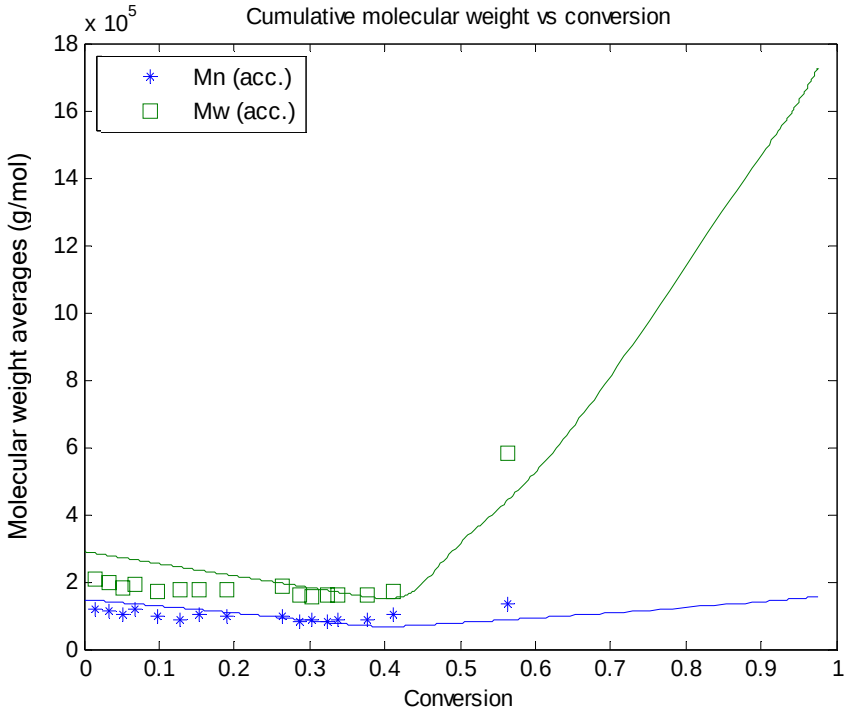

Figure 5.27. Molecular weight averages of MMA/VAc *co*-polymerization T = 60℃, $[AIBN]_0$ = 0.01 M, and f_{MMA0} = 0.30

Chapter 6

Multi-component Modeling Case Studies

In this chapter, the multi-component polymerization model is tested with experimental data which are more relevant to the recipe mentioned in chapter 4: *homo*-polymerizations of BA, BMA, and HEA, *co*-polymerizations of Sty/BA, BA/MMA, and Sty/HEA, *ter*-polymerizations of BA/MMA/VAc, Sty/EA/HEA, Sty/EA/MAA, EA/HEA/MAA, and finally, *tetra*-polymerization of Sty/EA/HEA/MAA.

6.1 BA *homo*-polymerization

Kinetic information on BA is not well known and experimental information is not as readily available as for Sty or MMA. Dubé *et al*. (1991) performed full conversion range experiments of BA polymerization using a 2^2 factorial design (T = 50 and 60℃, and $[AIBN]_0$ = 0.001 M, 0.00025 M). BA polymerization is fast, with a high k_p value, and exhibits gel effect but no limiting conversion, as shown in Figures 6.1 and 6.2. It is reported that the glass transition temperature of a BA polymer is low (about -50℃) and there is significant branching formation via transfer to polymer and terminal double bond polymerization. The model follows the experimental data well at low to medium conversion levels, but some discrepancies are observed at high conversion level. Due to complete lack of data in the literature, the number/weight average molecular weight predictions could not be compared.

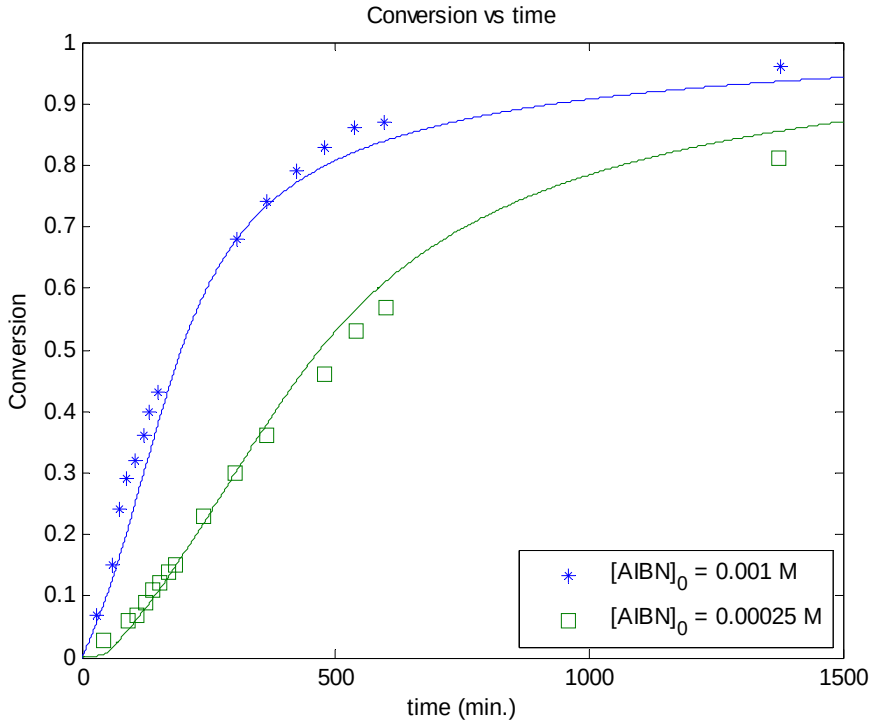

Figure 6.1. Simulation of bulk polymerizations of BA at 50℃

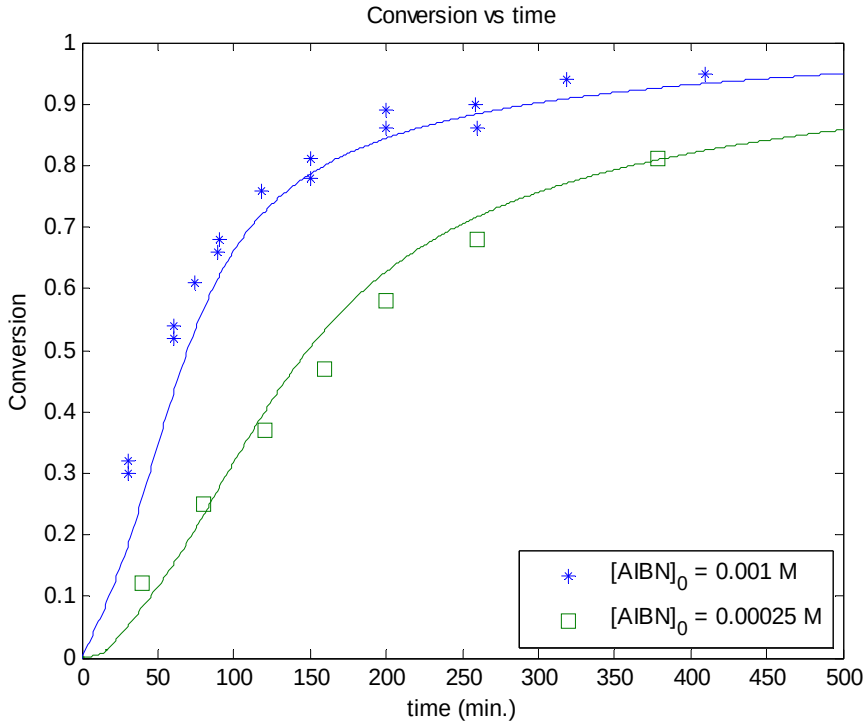

Figure 6.2. Simulation of bulk polymerizations of BA at 60℃

6.2 BMA *homo*-polymerization

Model predictions are compared with experimental data reported by Nair and Muthana (1961). They obtained conversion data at 60℃ using two kinds of initiators, 2,2'-azo-bis-isobutyonitrile (AIBN) and benzoyl peroxide (BPO). Figures 6.3 and 6.4 represent the bulk polymerization results at different concentration levels of AIBN and BPO, respectively. Autoacceleration starts around 30% conversion and there is no limiting conversion. The model predictions are good.

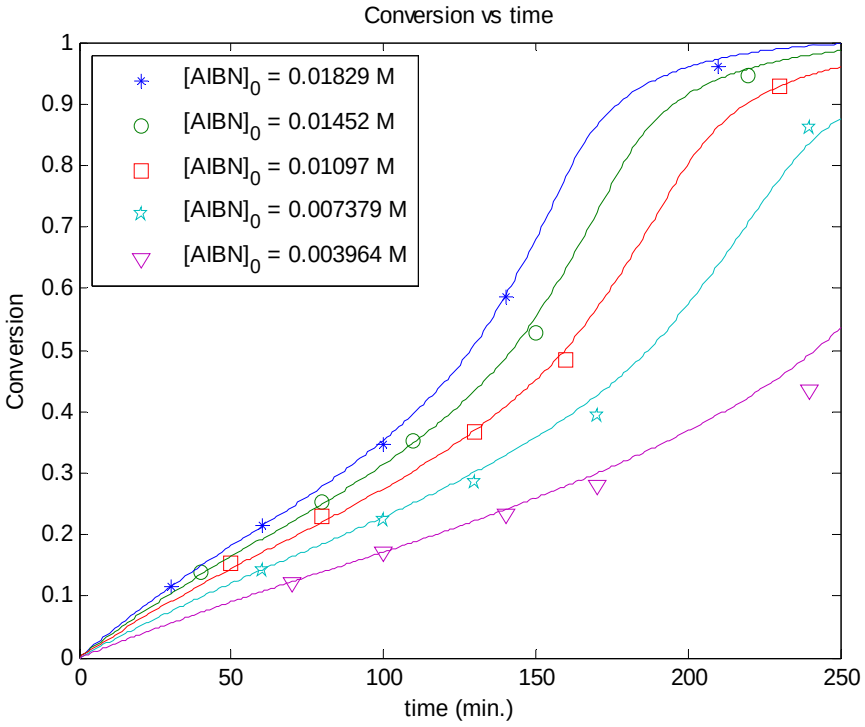

Figure 6.3. Simulation of bulk polymerizations of BMA at 60℃, AIBN as initiator

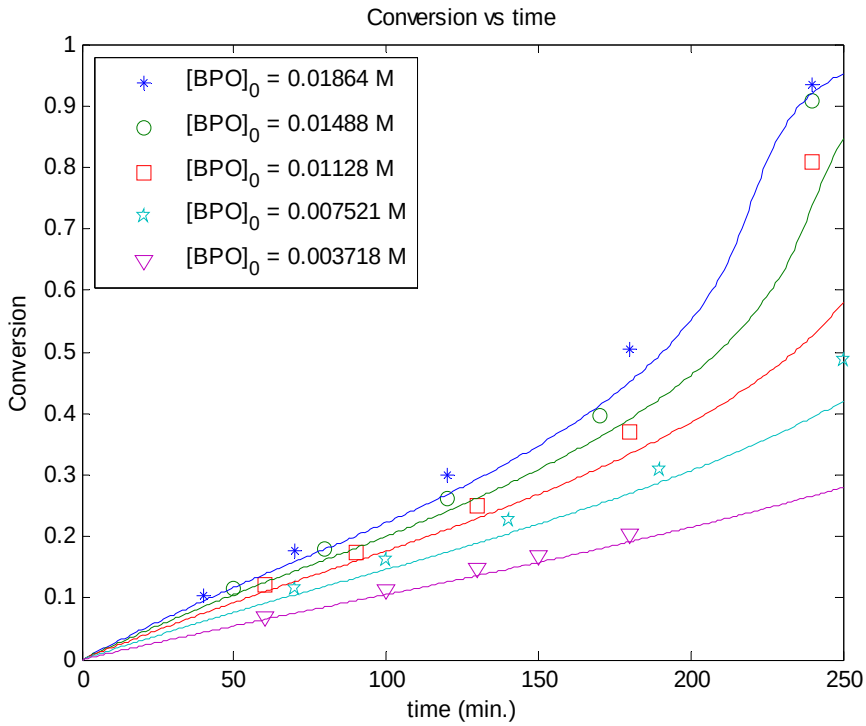

Figure 6.4. Simulation of bulk polymerizations of BMA at 60℃, BPO as initiator

6.3 HEA *homo*-polymerization

Kim (1994) studied Sty/HEA *co*-polymerization kinetics. Based on his data, we estimated the HEA *homo*-polymerization kinetic data. Our model was also compared with experimental data at three different temperature levels (50, 60, and 70℃) with 6.6E-5 moles of BPO of Vargün and Usanmaz (2005) in Figure 6.5. Fast reaction, strong autoacceleration, and no limiting conversion are observed in the plot and some discrepancies are found at high conversion level and higher temperature (60 and 70℃). This monomer is used later for further model testing of *co*-, *ter*-, and *tetra*-polymerizations.

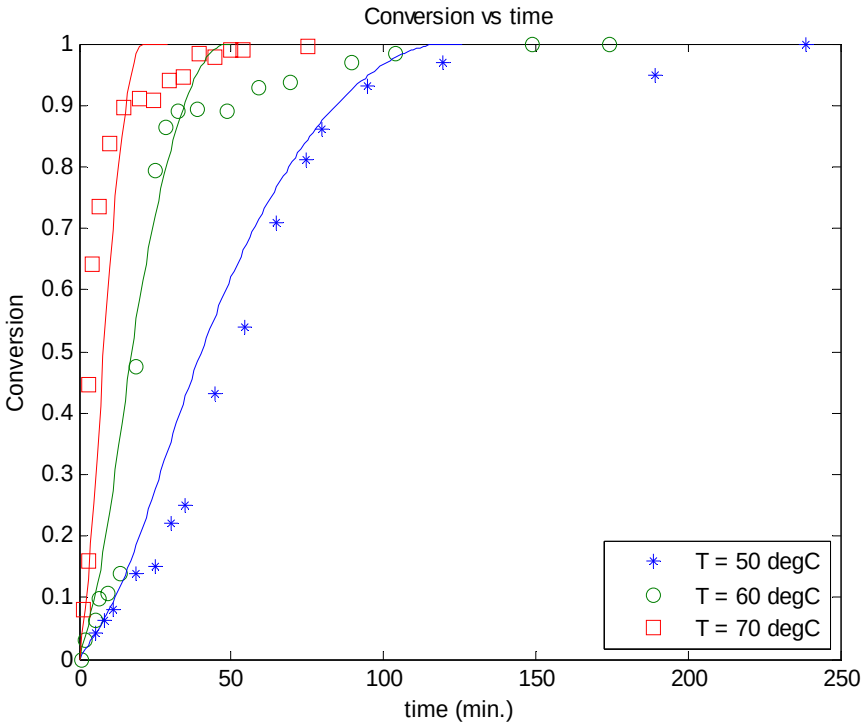

Figure 6.5. Simulation of bulk polymerizations of HEA, BPO = 6.6E-5 mol

6.4 Sty/BA *co*-polymerization

The two monomers show fairly different polymerization characteristics. Sty *homo*-polymer is hard and tough with high glass transition temperature (T_g) around 105℃, while BA is flexible and rubbery with low T_g, around -45℃. BA *hom*o-polymerization exhibits its gel effect early with no limiting conversion and Sty *hom*o-polymerization shows the opposite behaviour. Therefore, the overall kinetic behaviour of *co*-polymerization mainly relies on which monomer is more dominant in the monomer feed.

Dubé *et al*. (1990) investigated Sty/BA *co*-polymerization kinetics and carried out full conversion range experiments under a variety of reaction conditions. The estimated reactivity ratios are $r_{\text{Sty-BA}} = 0.956$, $r_{\text{BA-Sty}} = 0.183$. Figures 6.6 to 6.11 represent simulation of bulk *co*-polymerizations with three initial monomer feed compositions (f_{Sty0} = 0.258, 0.600, and 0.942) at 50℃ and two initiator concentration levels, $[\text{AIBN}]_0$ = 0.05 and 0.1 mol/L. In Figures 6.6 and 6.7, as Sty content becomes more dominant in the monomer feed composition, we can see that polymerization rate becomes slower. This makes sense because Sty *homo*-polymerization rate is slower than BA *homo*-polymerization.

Figures 6.8 and 6.9 show the average cumulative composition of Sty monomer in the *co*-polymer throughout the entire conversion. As Sty content increases in the reaction medium, the extent of 'composition drift' is observed to decrease. Looking at the reactivity ratios, the value of $r_{\text{Sty-BA}}$ is almost equal to one, which means that the probability of reaction of Sty radical and BA monomer is the same as that of Sty radical and Sty monomer. On the other hand, the low value of $r_{\text{BA-Sty}}$ means BA radical favors Sty monomer over its own monomer species. Therefore, it is expected that Sty monomer is incorporated into the polymer at the early stages of the reaction and hence the Sty cumulative composition ($\overline{F_{Sty}}$) decreases when the Sty monomer feed content (f_{Sty0}) is lower. At f_{Sty0} = 0.942, the cumulative composition does not fall because it is the azeotropic composition of the *co*-polymer.

Figures 6.10 and 6.11 are simulations of molecular weight averages of the *co*-polymer when f_{Sty} is 0.942. Predictions generally agree with the experimental data but some

discrepancies are observed at very high conversion. However, these may be due to erroneous measurements equally well.

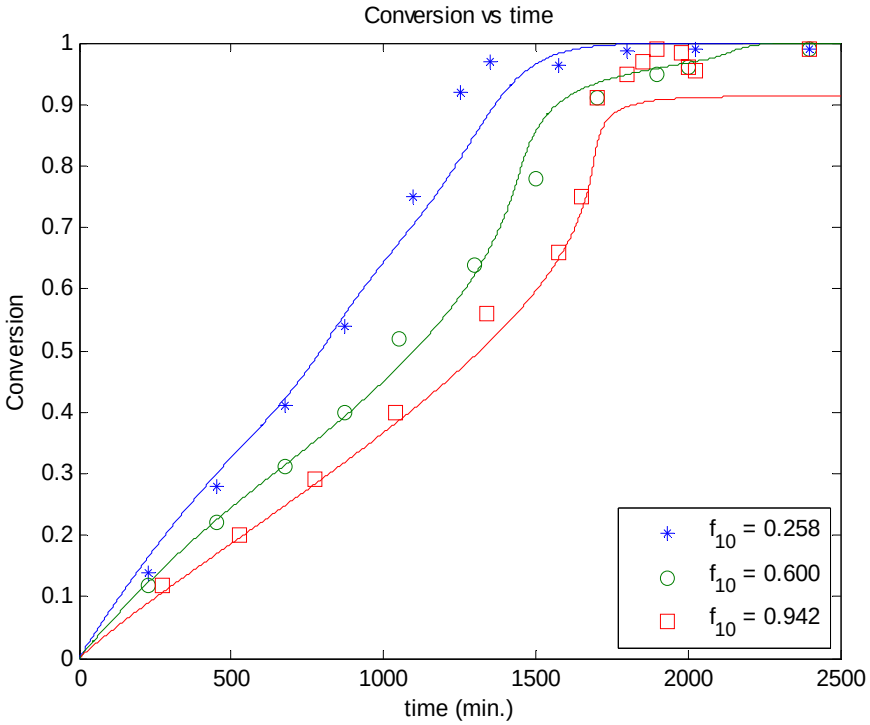

Figure 6.6. Simulation of bulk *co*-polymerizations of Sty/BA, T = 50℃ and $[AIBN]_0$ = 0.05 M (1 = Sty)

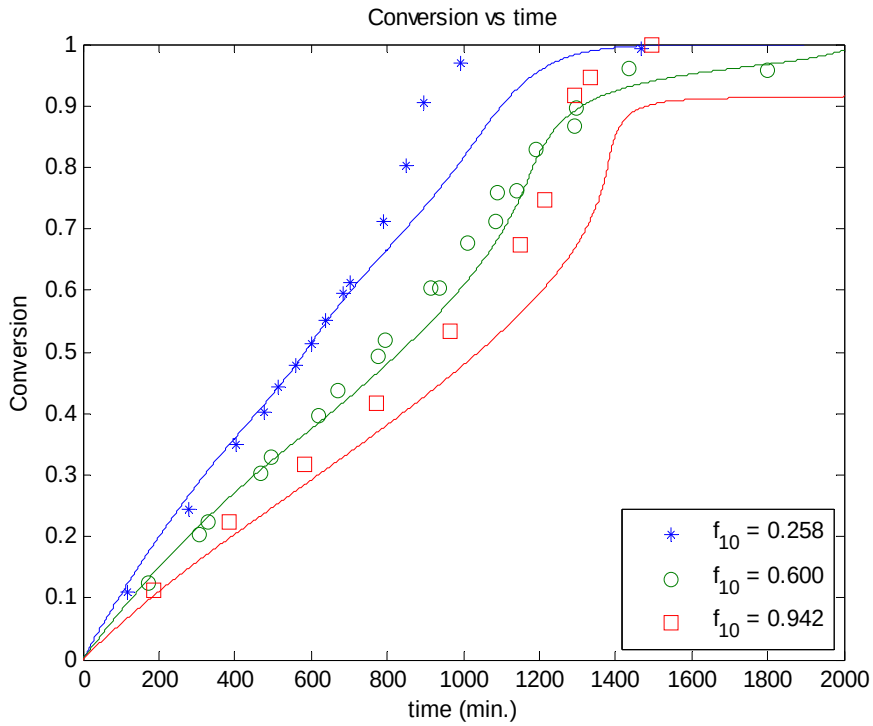

Figure 6.7. Simulation of bulk *co*-polymerizations of Sty/BA, T = 50℃ and $[AIBN]_0$ = 0.1 M (1 = Sty)

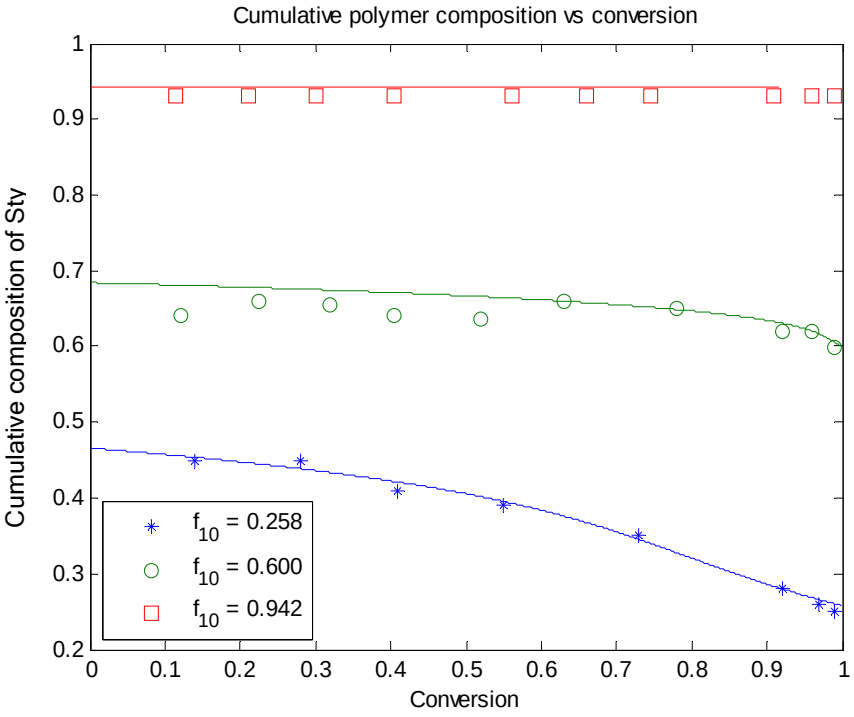

Figure 6.8. Cumulative polymer compositions of Sty in Sty/BA *co*-polymerization T = 50℃ and $[AIBN]_0$ = 0.05 M (1 = Sty)

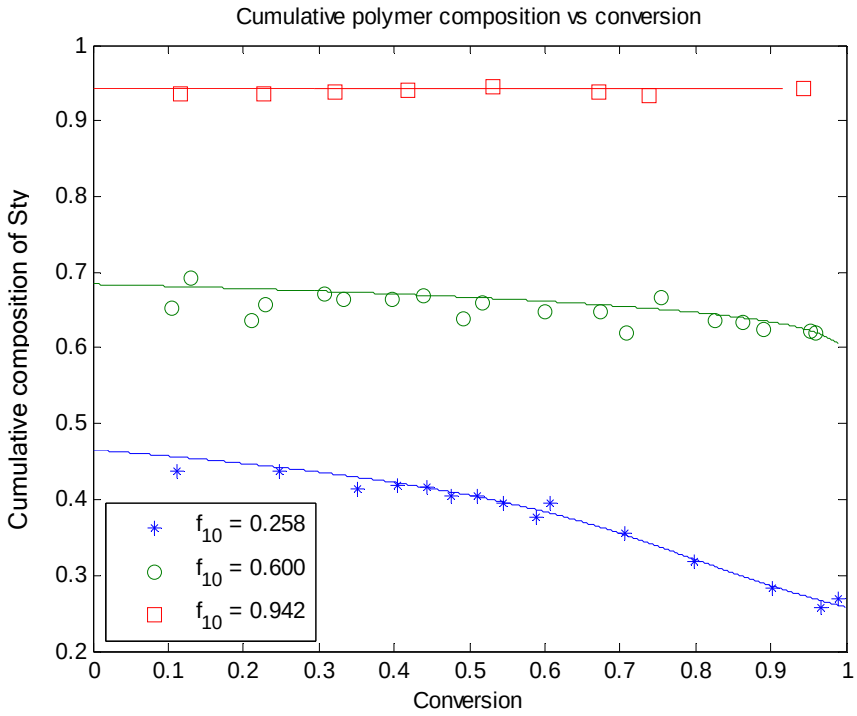

Figure 6.9. Cumulative polymer compositions of Sty in Sty/BA *co*-polymerization T = 50℃ and $[AIBN]_0$ = 0.1 M (1 = Sty)

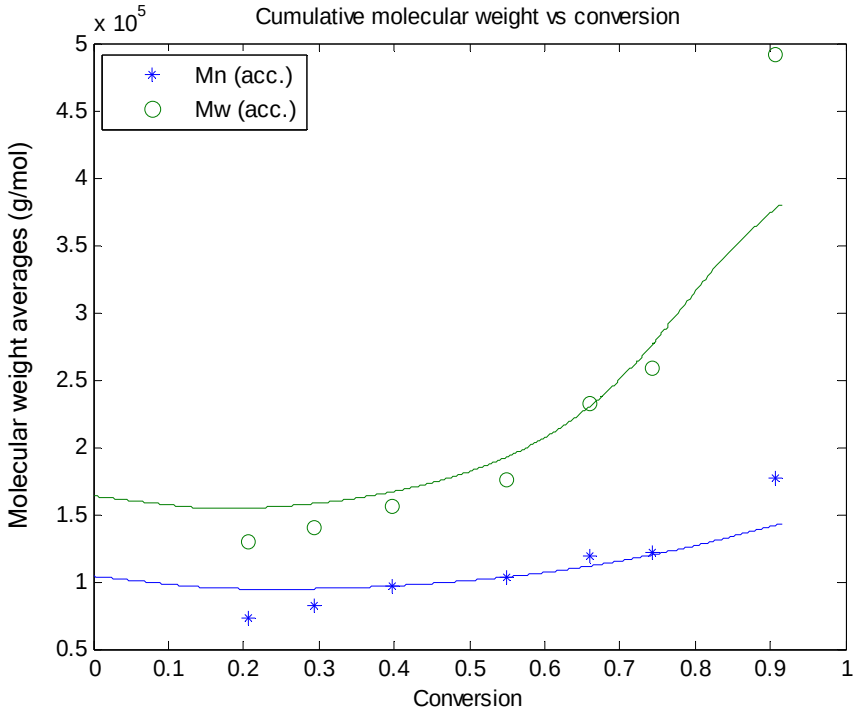

Figure 6.10. Molecular weight averages of Sty/BA *co*-polymerization T = 50℃, $[AIBN]_0$ = 0.05 M, and f_{Sty0} = 0.942

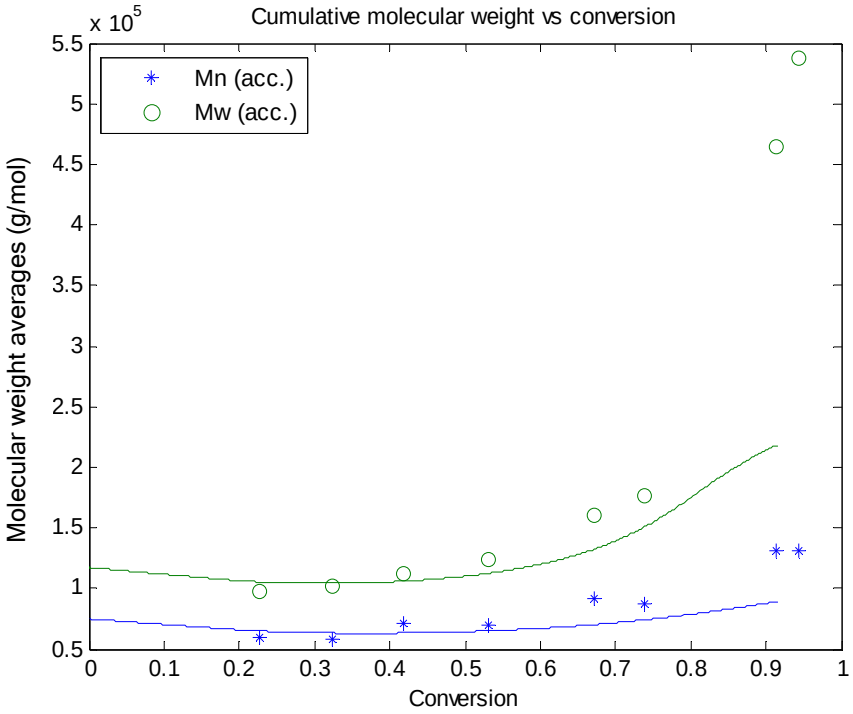

Figure 6.11. Molecular weight averages of Sty/BA *co*-polymerization T = 50℃, $[AIBN]_0$ = 0.1 M, and f_{Sty0} = 0.942

6.5 BA/MMA *co*-polymerization

Dubé *et al*. (1995) investigated BA/MMA, BA/VAc, and MMA/VAc *co*-polymer systems as part of a MMA/BA/VAc *ter*-polymerization study. Reactivity ratios were estimated as $r_{MMA\text{-}BA}$ = 1.789 and $r_{BA\text{-}MMA}$ = 0.297 (by EVM method), which means that there is no azeotropic composition in this system and hence composition drift is expected for all monomer feed compositions. Figures 6.12 and 6.13 represent conversion profiles as a function of BA feed fractions (f_{BA0} = 0.439 and 0.163) at 60℃ with two initiator levels ($[AIBN]_0$ = 0.05 and 0.1 mol/L). For the low BA content experiment (f_{BA0} = 0.163), a limiting conversion is observed in the model prediction plots, which disagrees with the experimental data.

Figures 6.14 and 6.15 show the composition drift of BA in the polymer. Initiator concentration change does not affect the drift and more drift is observed at f_{BA0} = 0.439 (Figure 6.14) than f_{BA0} = 0.163 (Figure 6.15). Figures 6.16 to 6.19 are the measured average molecular weights and prediction plots. Comparing Figures 6.16 and 6.17, and Figures 6.18 and 6.19, the higher initiator amount reduces molecular weights in both cases. More discrepancies are observed at low BA feed fractions, consistent with the conversion discrepancies above. Model predictions, however, give reasonable trends for this system.

Alb *et al*. (2006) conducted BA/MMA solution *co*-polymerization with 70 wt% of butyl acetate solvent and 2 wt% of AIBN initiator at 66℃ under different initial monomer feed ratios (weight basis) using an automatic continuous online spectrum monitoring technique, which enables to calculate instantaneous polymer compositions. Note that Figure 6.20 represents the instantaneous (not cumulative) composition drift of BA as a function of conversion. Looking at the reactivity ratios, it is evident that MMA incorporation into the polymer is more favored than BA, which leads to larger composition drift at lower initial BA feed ratios because MMA is depleted earlier than BA.

This can also be verified with the corresponding differential *co*-polymer composition distribution in Figure 6.21. The values of the y-axis represent the absolute values of the infinitesimal change of total conversion divided by the infinitesimal change of instantaneous

polymer composition of BA, namely the values of inverse slope in Figure 6.20. At the early stages of reaction, more MMA monomer is incorporated into the *co*-polymer than BA monomer and this does not change much the polymer composition of BA. Therefore, it is observed that with a higher initial MMA content in the system, the slope $|dF_{BA}/dX|$ becomes smaller in Figure 6.20, while the inverse slope $|dX/dF_{BA}|$ (the y-value, calculated as $|\Delta X/\Delta F_{BA}|$ numerically) becomes larger in Figure 6.21 (the prediction curves are also changing from 'J-shape' to 'U-shape').

It has been reported by Meyer and Lowry (1965) that this 'U-shaped' differential *co*-polymer composition distribution is considered as characteristic of "incompatible" *co*-polymerizations when the differences between reactivity ratios are large. During the entire reaction, the virtual "*homo*-polymerization" of the more reactive monomer species is favored initially, while the "*homo*-polymerization" of the other one happens during the final stages of *co*-polymerization. This also applies to the 'double rate phenomenon' case of MMA/VAc *co*-polymerization in section 5.9.

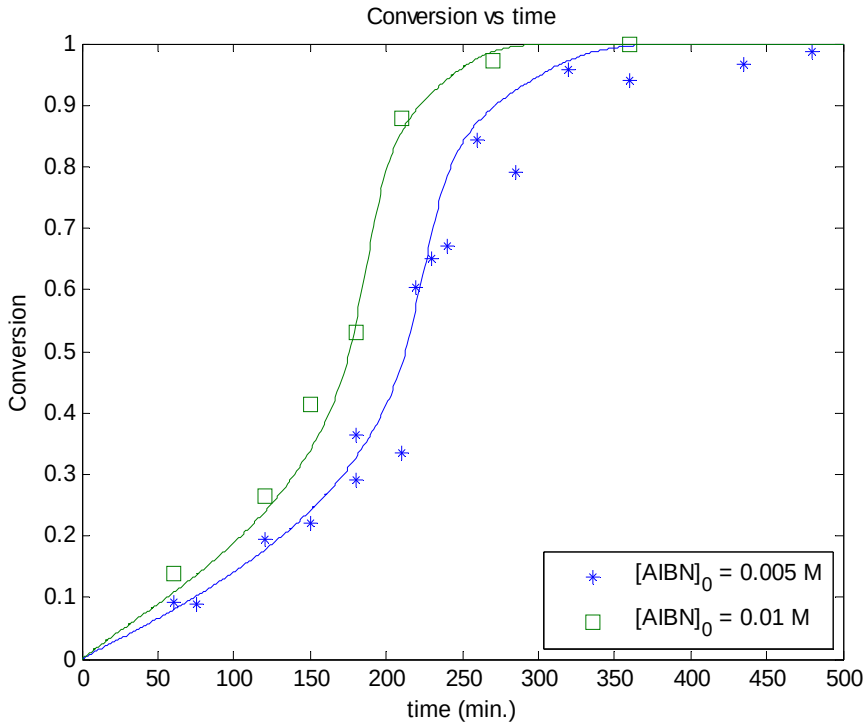

Figure 6.12. Simulation of bulk *co*-polymerizations of BA/MMA, T = 60℃, f_{BA0} = 0.439

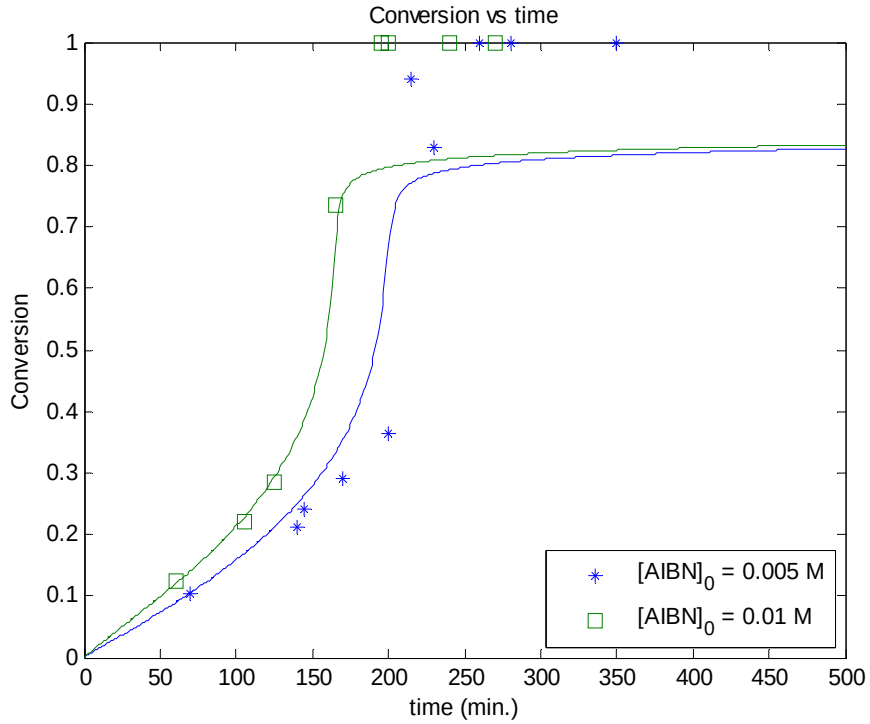

Figure 6.13. Simulation of bulk BA/MMA *co*-polymerizations, T = 60℃ and f_{BA0} = 0.163

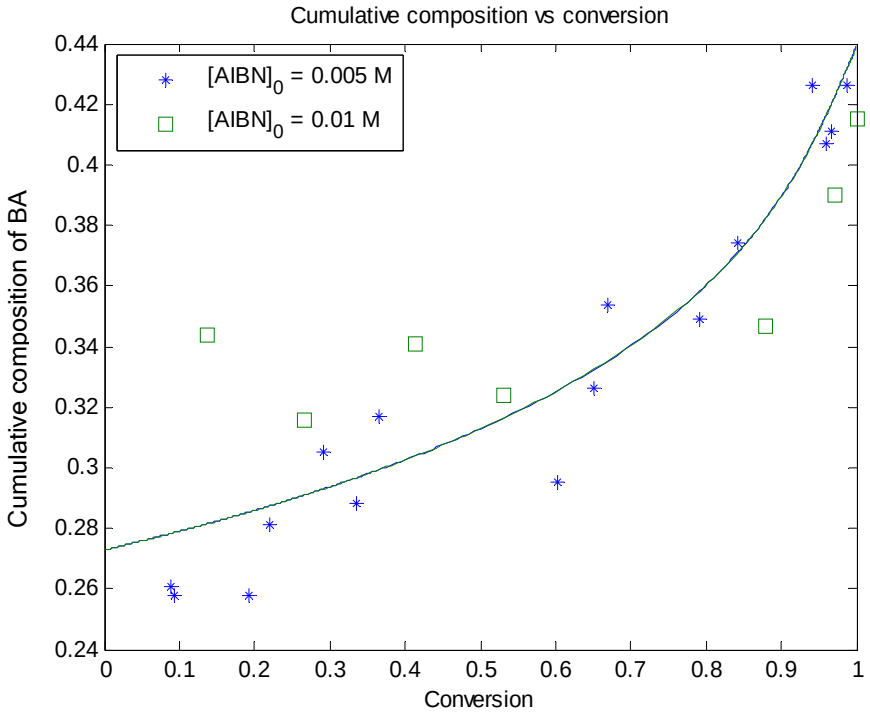

Figure 6.14. Cumulative polymer composition of BA in BA/MMA *co*-polymerization T = 60℃ and f_{BA0} = 0.439

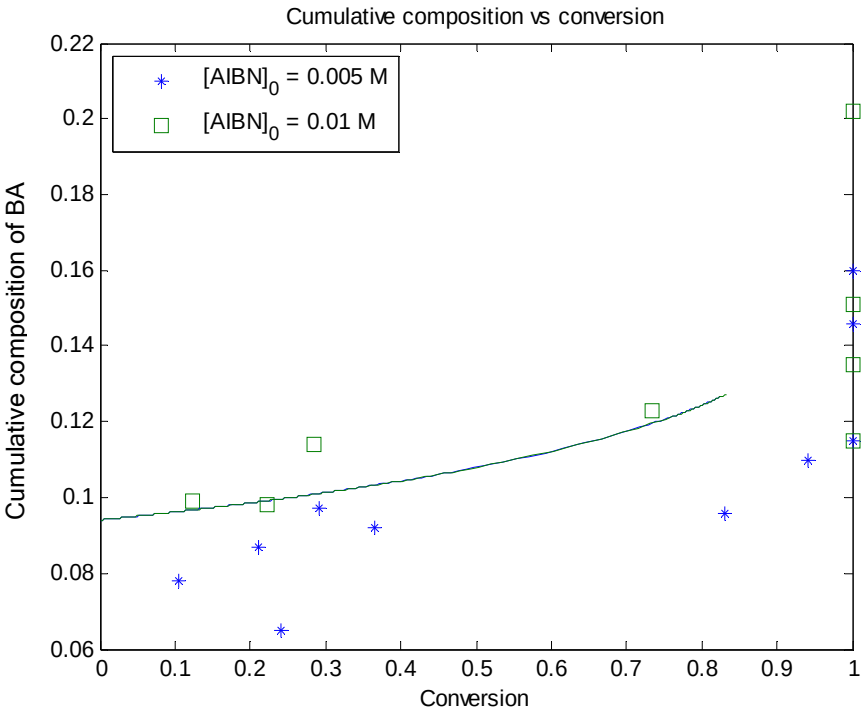

Figure 6.15. Cumulative polymer composition of BA in BA/MMA *co*-polymerization T = 60℃ and f_{BA0} = 0.163

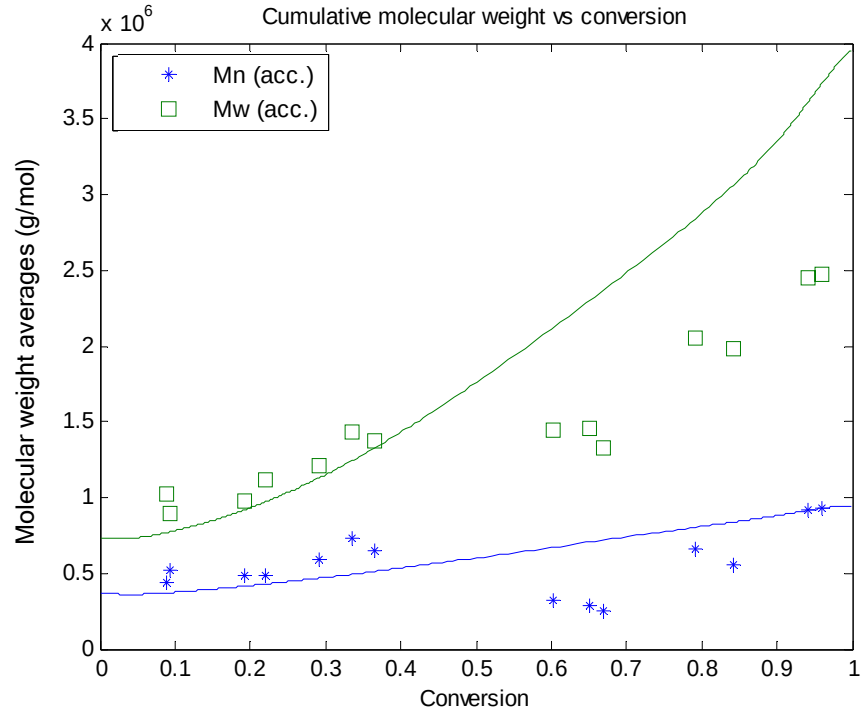

Figure 6.16. Molecular weight averages of BA/MMA *co*-polymerization T = 60℃, $[AIBN]_0$ = 0.005 M, and f_{BA0} = 0.439

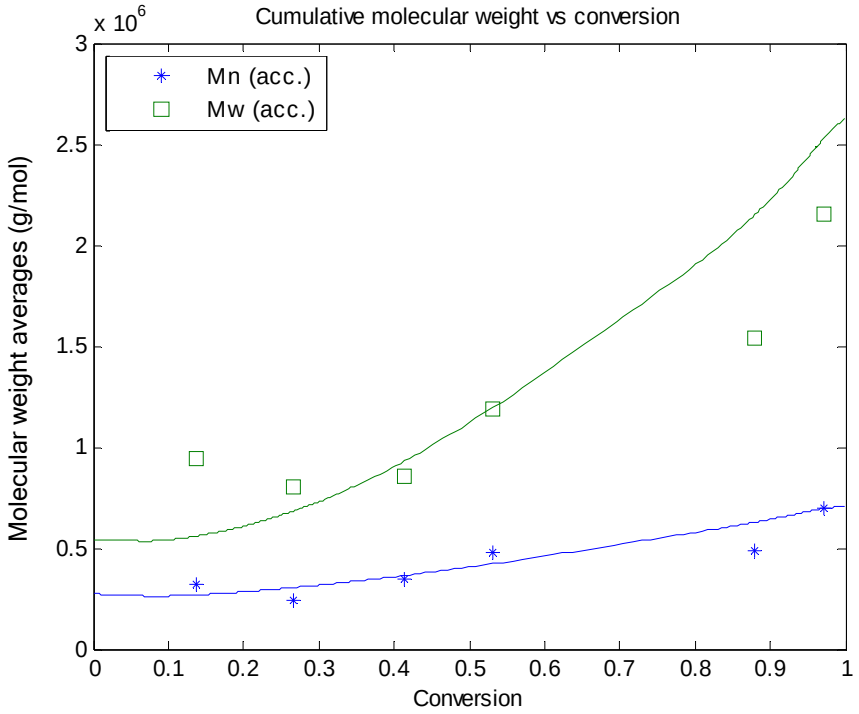

Figure 6.17. Molecular weight averages of BA/MMA *co*-polymerization T = 60℃, $[AIBN]_0$ = 0.01 M, and f_{BA0} = 0.439

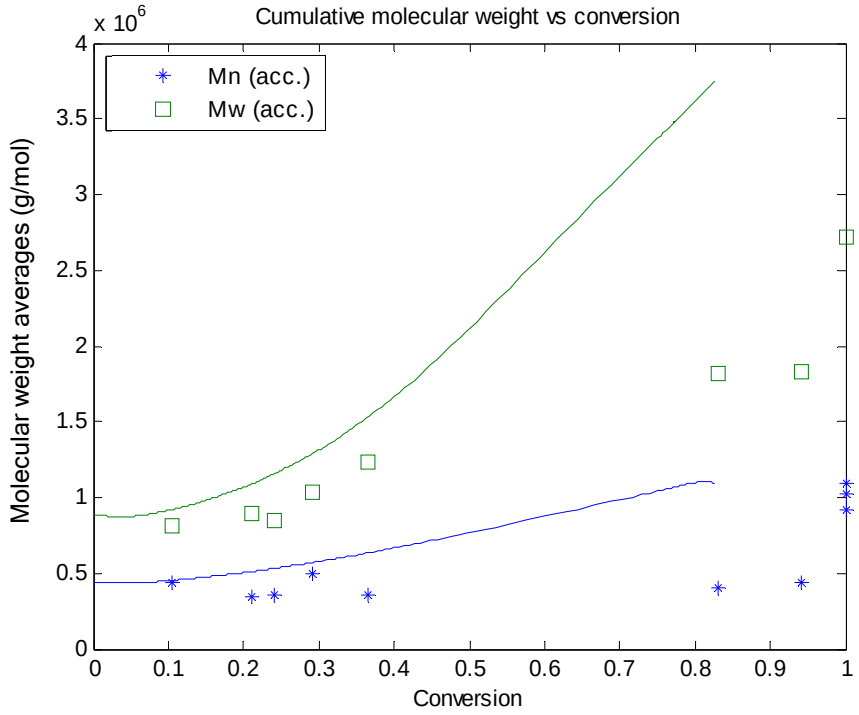

Figure 6.18. Molecular weight averages of BA/MMA *co*-polymerization T = 60℃, $[AIBN]_0$ = 0.005 M, and f_{BA0} = 0.163

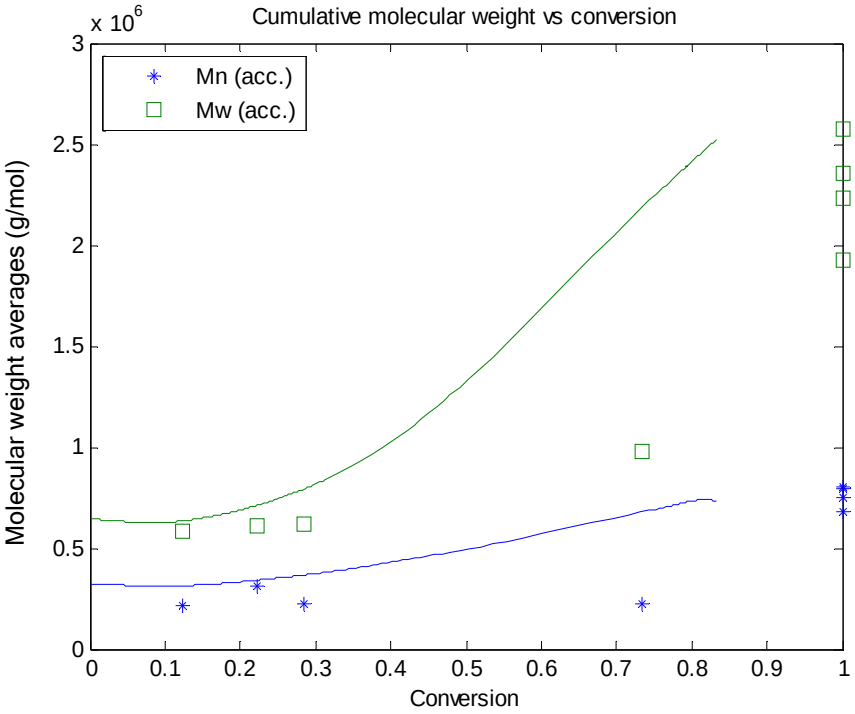

Figure 6.19. Molecular weight averages of BA/MMA *co*-polymerization
T = 60℃, $[AIBN]_0$ = 0.01 M, and f_{BA0} = 0.163

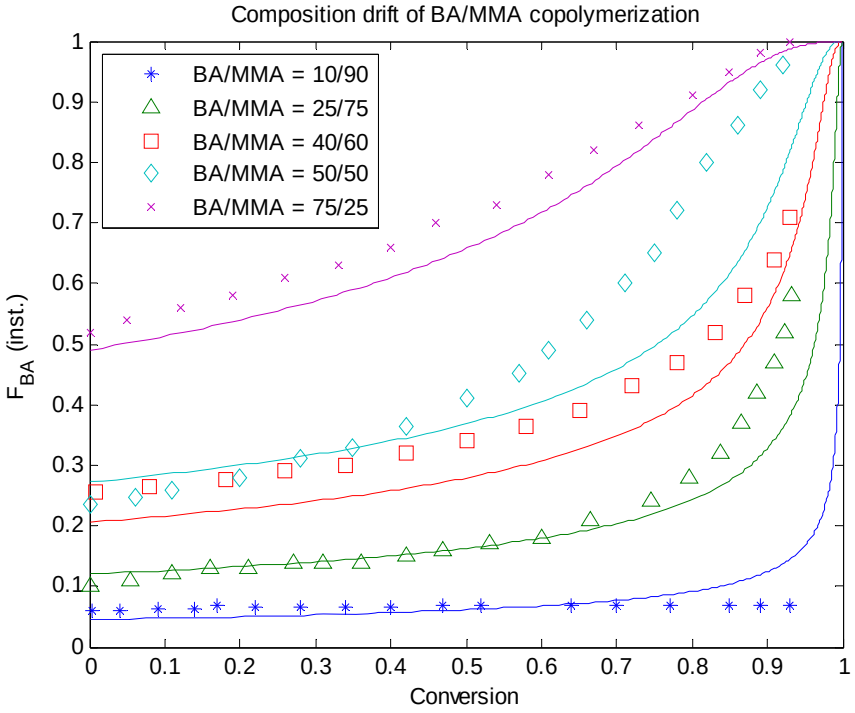

Figure 6.20. Simulation of composition drift of instantaneous F_{BA} in BA/MMA *co*-polymerization
T = 66℃, Butyl acetate (solvent) = 70 wt%, and AIBN = 2 wt% of total mixture

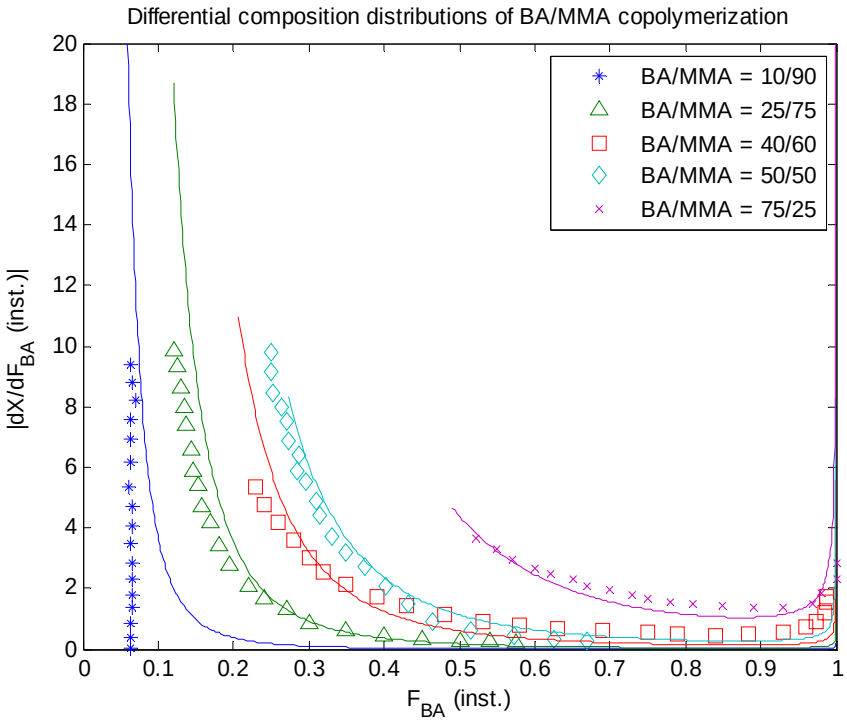

Figure 6.21. Differential instantaneous *co*-polymer composition distributions of BA in BA/MMA *co*-polymerization
T = 66℃, Butyl acetate (solvent) = 70 wt%, and AIBN = 2 wt% of total mixture

6.6 Sty/HEA *co*-polymerization

Sty/HEA full conversion range experiments were conducted by Kim (1994). Kinetic studies of any polymerization involving HEA are extremely scarce. HEA polymerization exhibits high molecular weight products through crosslinking reactions by polymerization of divinyl impurities, which are side products in the hydroxylalkyl acrylate polymerization, and transfer to polymer. This leads to difficulties in the analysis of its polymer characteristics.

Some research groups have given approximate estimates for the reactivity ratios of Sty/HEA *co*-polymerization, but our model uses $r_{\text{Sty-HEA}} = 0.254$ and $r_{\text{HEA-Sty}} = 0.279$ from Kim (1994), whose study was more systematic. A 2^3 factorial design was conducted to investigate the effect of temperature (40 and 50℃), initiator concentration ($[\text{AIBN}]_0 = 0.025$ and 0.05 mol/L), and initial monomer feed composition ($f_{10} = f_{\text{Sty0}} = 0.515$, and 0.840). Results are shown in Figures 6.22 to 6.25. Some discrepancies are observed at high conversion. Other than that, our model trends show good agreement with experimental data.

McManus *et al*. (1998) conducted not only Sty/HEA *co*-polymerization (T = 50℃, $[\text{AIBN}]_0 = 0.025$ M, and $f_{10} = f_{\text{Sty0}} = 0.601$) but also Sty/EA/HEA *ter*-polymerization experiments. Their *co*-polymerization data are plotted along with the data from Kim (1994) in Figure 6.25. Again, the model follows the experimental trends well. Model testing with the *ter*-polymerization experimental data will be discussed later.

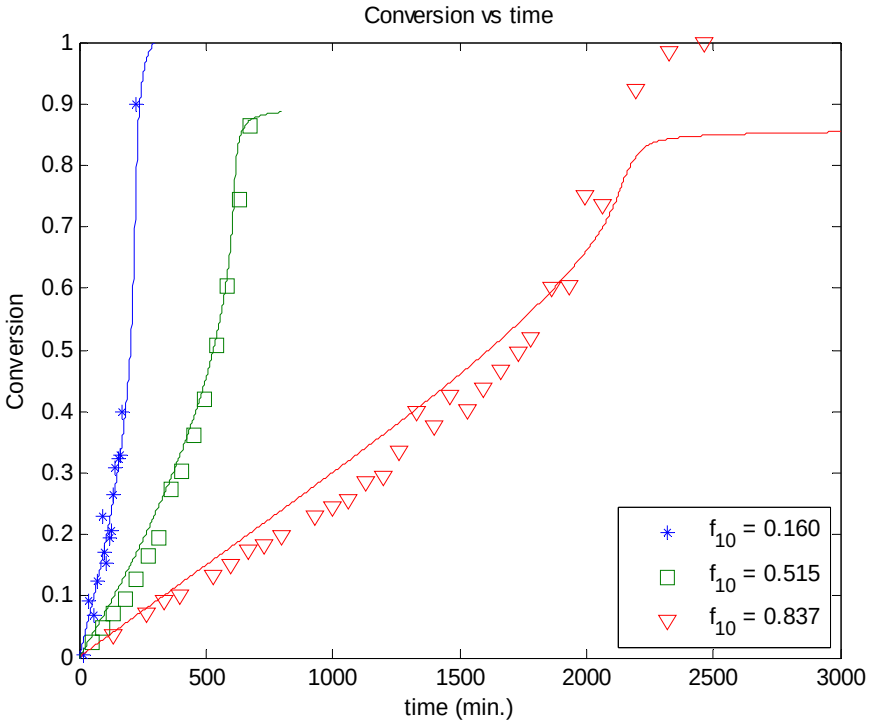

Figure 6.22. Simulation of Sty/HEA bulk *co*-polymerizations at T = 40℃, $[AIBN]_0$ = 0.05 M (1 = Sty)

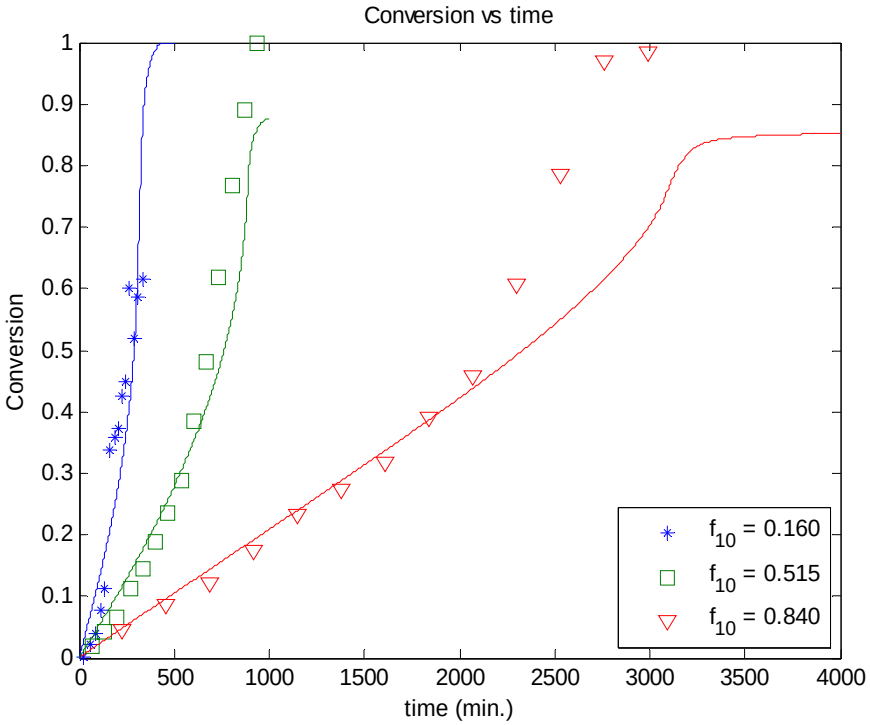

Figure 6.23. Simulation of Sty/HEA bulk *co*-polymerizations at T = 40℃, $[AIBN]_0$ = 0.025 M (1 = Sty)

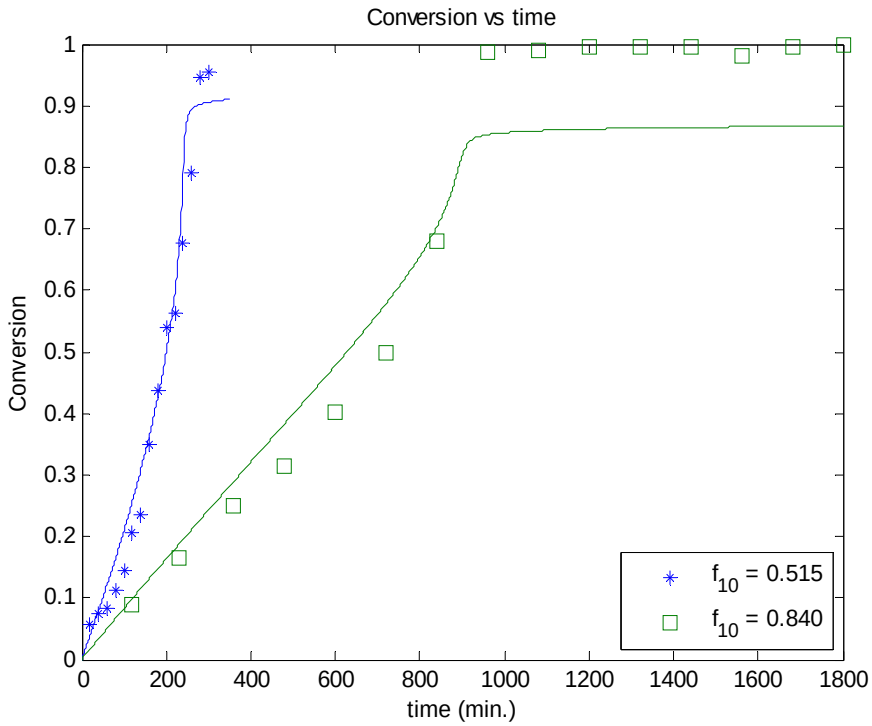

Figure 6.24. Simulation of Sty/HEA bulk *co*-polymerizations at T = 50℃, $[AIBN]_0$ = 0.05 M (1 = Sty)

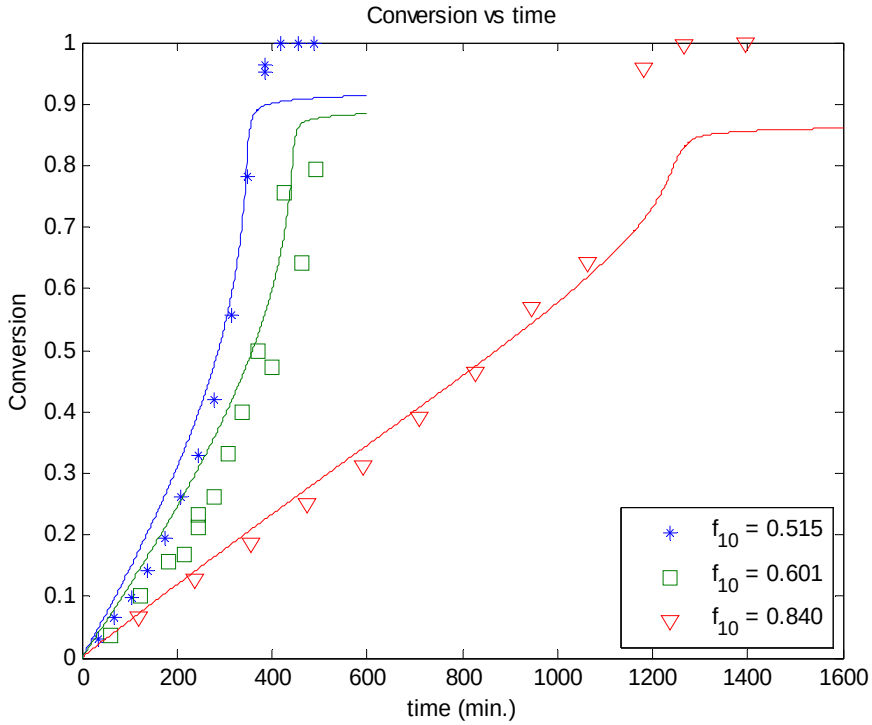

Figure 6.25. Simulation of Sty/HEA bulk *co*-polymerizations at T = 50℃, $[AIBN]_0$ = 0.025 M (1 = Sty)

6.7 BA/MMA/VAc *ter*-polymerization

The simulations of *ter*- and higher multi-component polymerizations can be obtained by utilizing the existing *homo*- and *co*-polymerization database without any additional changes thanks to the pseudo rate constant method. All model predictions in Figures 6.26 to 6.35 are based on the same database used by the previous *homo*- and *co*-polymerizations of BA, MMA, and VAc. Dubé and Penlidis (1995b) conducted factorial design experiments over the full conversion range for bulk *ter*-polymerizations at T = 50 and 70℃, and $[AIBN]_0$ = 0.01 and 0.071 mol/L under 30/30/40 wt% of BA/MMA/VAc initial monomer feed ratio.

Examining Figures 6.26 and 6.27, the polymerization behaviour can be divided into two stages. The rate is more or less constant up to about 60% conversion (first stage), after which it shows a dramatic increase (second stage). A 'double rate phenomenon' is observed. The *co*-polymer composition plots (Figures 6.29 to 6.32) and average molecular weight plots (Figures 6.33 to 6.36) also corroborate the "double rate" phenomenon and our model satisfactorily describes the behaviour.

It was reported in Dubé and Penlidis (1995b) that the samples taken out at higher conversions during the experiment at 70℃ contained a solid core surrounded by a lower viscosity liquid, and a feasible explanation was that a mild non-isothermal behaviour had occurred. This points to possible discrepancies between model predictions and experimental data at mid- and high conversion levels, as shown in Figure 6.27 ($[AIBN]_0$ = 0.01 M case). However, if one uses a non-isothermal profile (which is what really happened in this case), then one can obtain very good agreement, as shown in Figure 6.28. This is another example of the great uses of a mathematical model, with respect to troubleshooting process behaviour. At first glance, if a discrepancy exists between experimental data and model predictions, the natural tendency is to fault the model. This case is indeed a counter-example, where actually the model is doing very well if fed the appropriate input information.

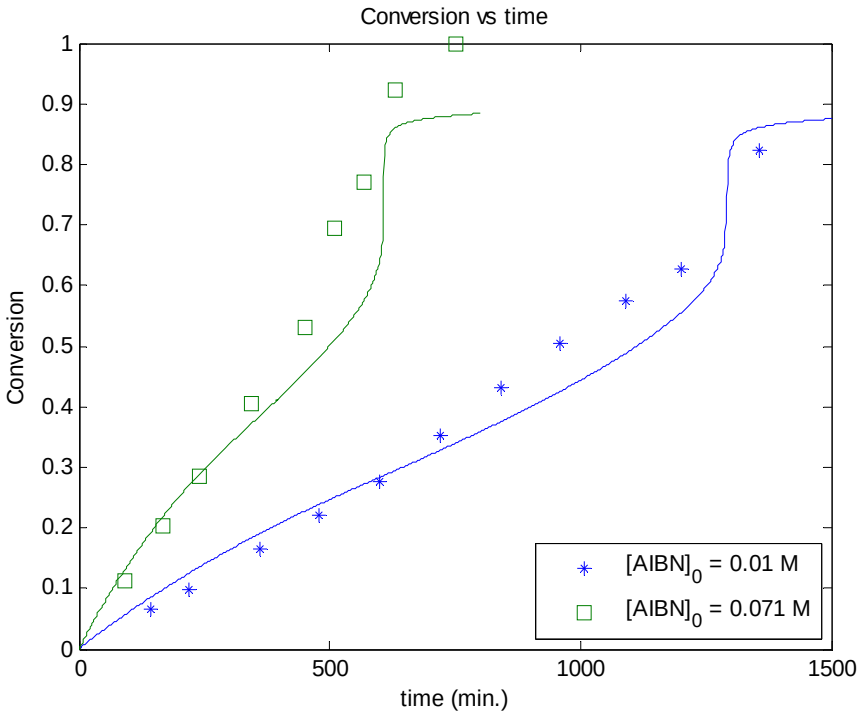

Figure 6.26. Simulation of bulk *ter*-polymerizations of BA/MMA/VAc T = 50℃ and (BA/MMA/VAc) = (30/30/40 wt%)

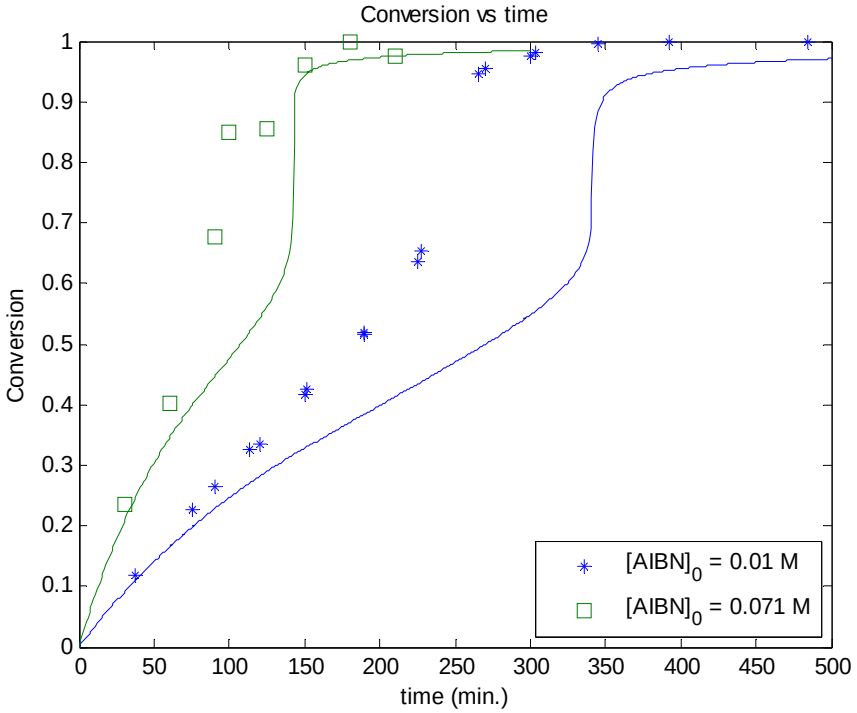

Figure 6.27. Simulation of bulk *ter*-polymerizations of BA/MMA/VAc T = 70℃ and (BA/MMA/VAc) = (30/30/40 wt%)

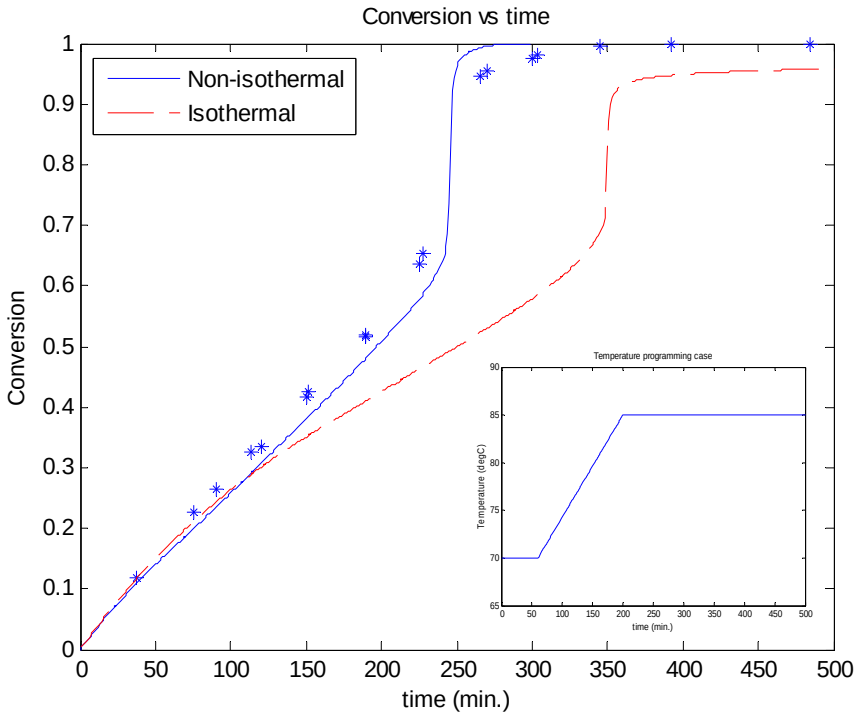

Figure 6.28. Simulation of bulk *ter*-polymerization of BA/MMA/VAc $[AIBN]_0$ = 0.01 M, (BA/MMA/VAc) = (30/30/40 wt%), non-isothermal profile

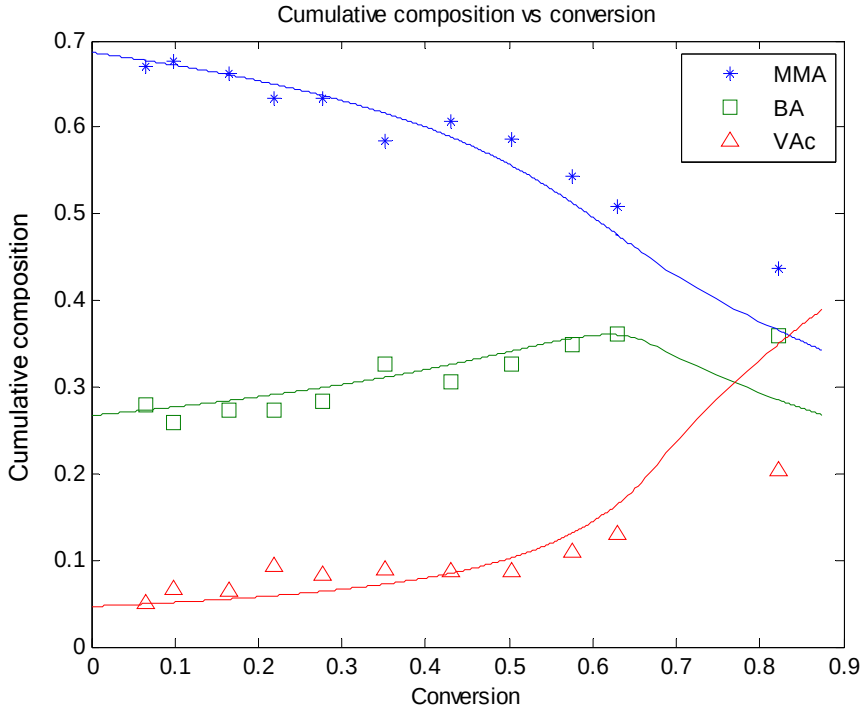

Figure 6.29. Cumulative polymer composition in BA/MMA/VAc *ter*-polymerization T = 50℃, $[AIBN]_0$ = 0.01 M, and (BA/MMA/VAc) = (30/30/40 wt%)

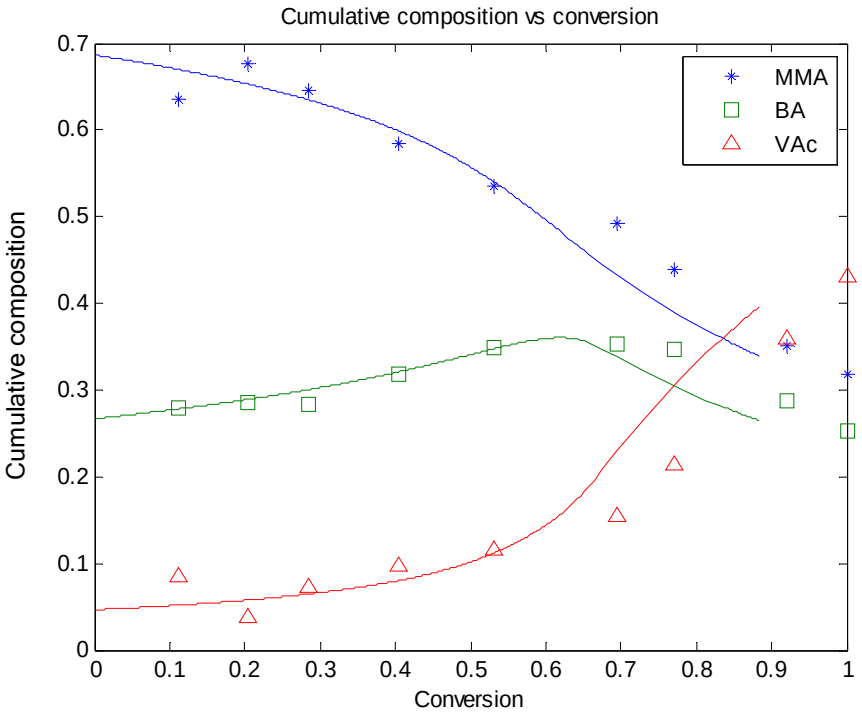

Figure 6.30. Cumulative polymer composition in BA/MMA/VAc *ter*-polymerization T = 50℃, $[AIBN]_0$ = 0.071 M, and (BA/MMA/VAc) = (30/30/40 wt%)

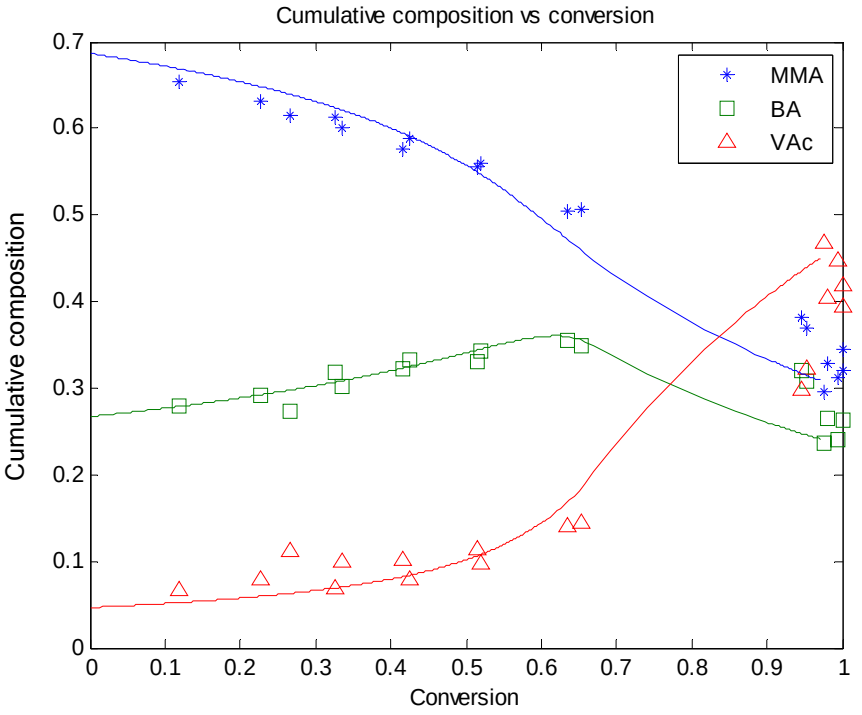

Figure 6.31. Cumulative polymer composition in BA/MMA/VAc *ter*-polymerization T = 70℃, $[AIBN]_0$ = 0.01 M, and (BA/MMA/VAc) = (30/30/40 wt%)

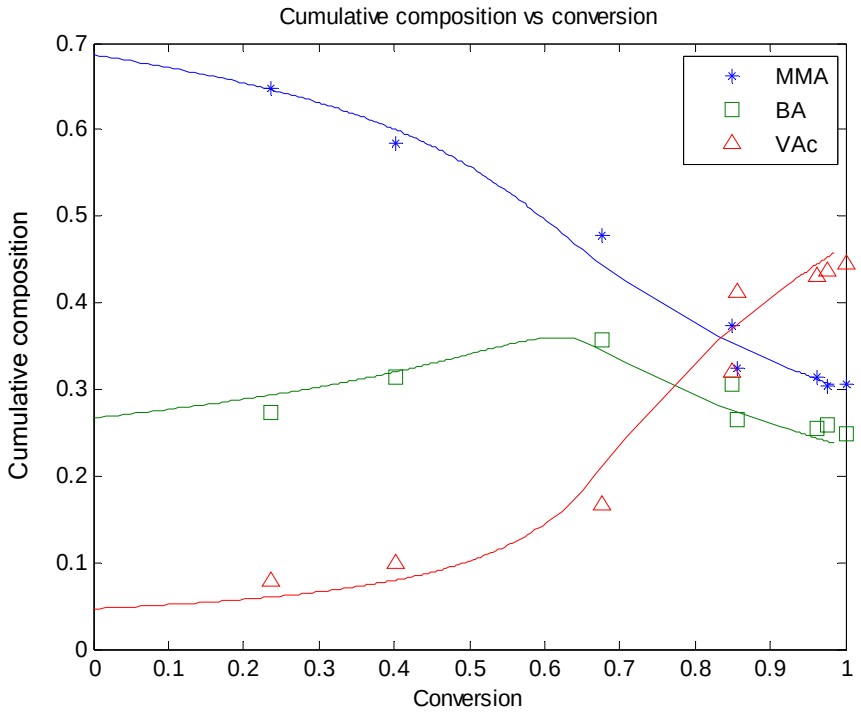

Figure 6.32. Cumulative polymer composition in BA/MMA/VAc *ter*-polymerization T = 70℃, $[AIBN]_0$ = 0.071 M, and (BA/MMA/VAc) = (30/30/40 wt%)

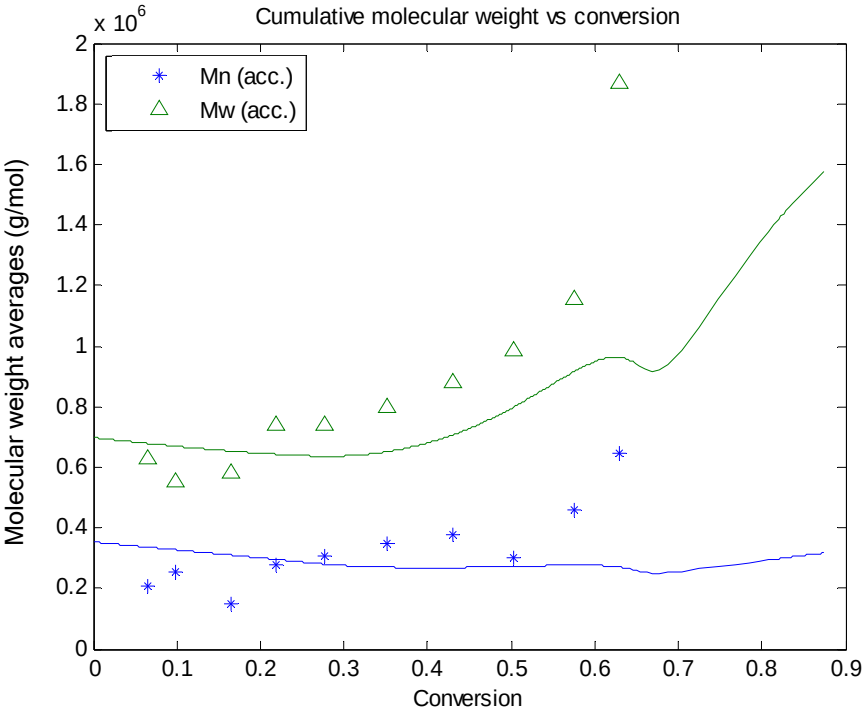

Figure 6.33. Molecular weight averages of BA/MMA/VAc *ter*-polymerization T = 50℃, $[AIBN]_0$ = 0.01 M, and (BA/MMA/VAc) = (30/30/40 wt%)

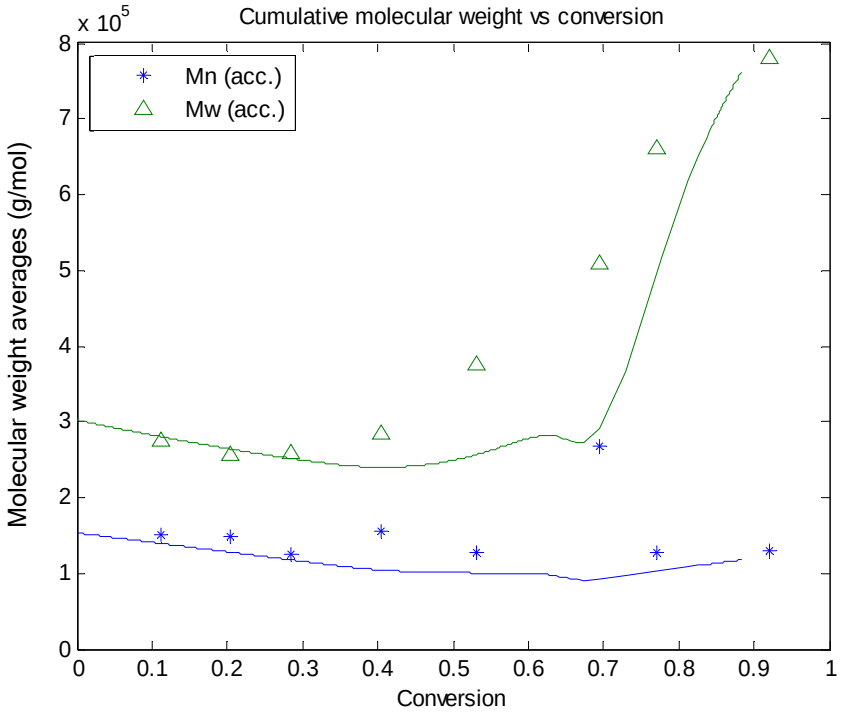

Figure 6.34. Molecular weight averages of BA/MMA/VAc *ter*-polymerization T = 50℃, $[AIBN]_0$ = 0.071 M, and (BA/MMA/VAc) = (30/30/40 wt%)

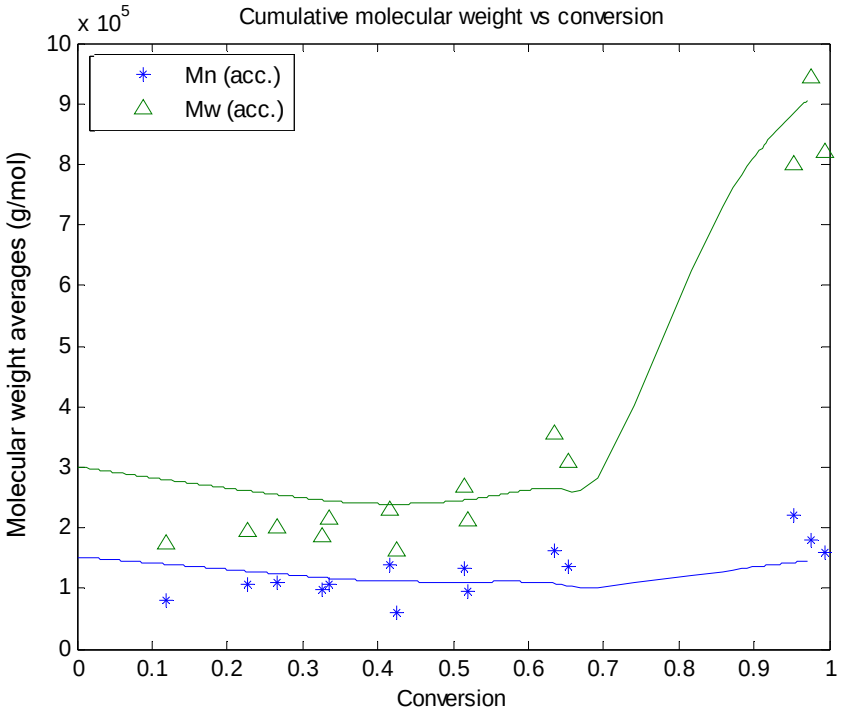

Figure 6.35. Molecular weight averages of BA/MMA/VAc *ter*-polymerization T = 70℃, $[AIBN]_0$ = 0.01 M, and (BA/MMA/VAc) = (30/30/40 wt%)

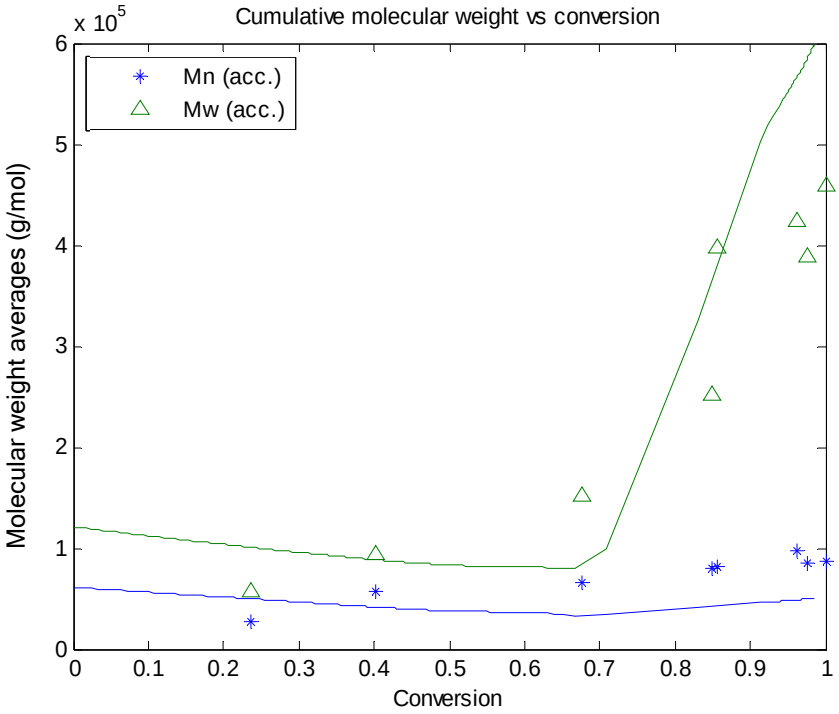

Figure 6.36. Molecular weight averages of BA/MMA/VAc *ter*-polymerization T = 70℃, $[AIBN]_0$ = 0.071 M, and (BA/MMA/VAc) = (30/30/40 wt%)

6.8 Sty/EA/HEA *ter*-polymerization

Sty/EA/HEA and Sty/EA/MAA *ter*-polymers are used in the paint and surface coatings industry. McManus *et al*. (1998) performed Sty/EA/HEA bulk *ter*-polymerization at 60℃, $[AIBN]_0$ = 0.05 mol/L and two levels of monomer initial feed ratios (Sty/EA/HEA = 50/45/5 wt% and 50/40/10 wt%). Experiments were limited to maintaining a low HEA level because it was difficult to isolate residual HEA monomer from the polymer when the feed mole fraction of HEA was greater than 0.5, as this would have increased the experimental error. Figure 6.37 represents model predictions and experimental data, which agree with each other. As HEA content increases, polymerization rate increases.

Sahloul (2004) also studied this system at elevated temperature. She started with Sty/EA *co*-polymerization and extended it up to Sty/EA/HEA/MAA solution *tetra*-polymerization. A 2^2 factorial design was performed to test the effect of temperature (100 and 130℃) and the presence of 0.5 wt% chain transfer agent (octanethiol). Feed composition ratio was Sty/EA/HEA = 42/42/16 wt%, *tert*-butyl peroxybenzoate (TBPB) initiator at 1.5 wt% of total monomer mixture, and m-xylene solvent at 60 wt% of total reaction mixture. The reactivity ratios estimated at elevated temperature were ($r_{Sty\text{-}EA}$, $r_{EA\text{-}Sty}$) = (0.8996, 0.2083), ($r_{Sty\text{-}HEA}$, $r_{HEA\text{-}Sty}$) = (0.5527, 0.2347), and ($r_{EA\text{-}HEA}$, $r_{HEA\text{-}EA}$) = (0.7498, 2.2361) at 100℃; ($r_{Sty\text{-}EA}$, $r_{EA\text{-}Sty}$) = (0.9305, 0.1996), ($r_{Sty\text{-}HEA}$, $r_{HEA\text{-}Sty}$) = (0.6193, 0.2408), and ($r_{EA\text{-}HEA}$, $r_{HEA\text{-}EA}$) = (0.6517, 1.4214) at 130℃.

In Figures 6.38 and 6.39, model predictions show good agreement with conversion experimental data and CTA effects are negligible on reaction rate. As expected, reaction rate becomes faster as temperature increases. However, some significant discrepancies were observed in *ter*-polymer composition in Figures 6.40 to 6.43. Most of the experimental error is definitely due to the highly branched and potentially crosslinked chains, as this would affect polymer composition characterized by solution ^{1}H-NMR.

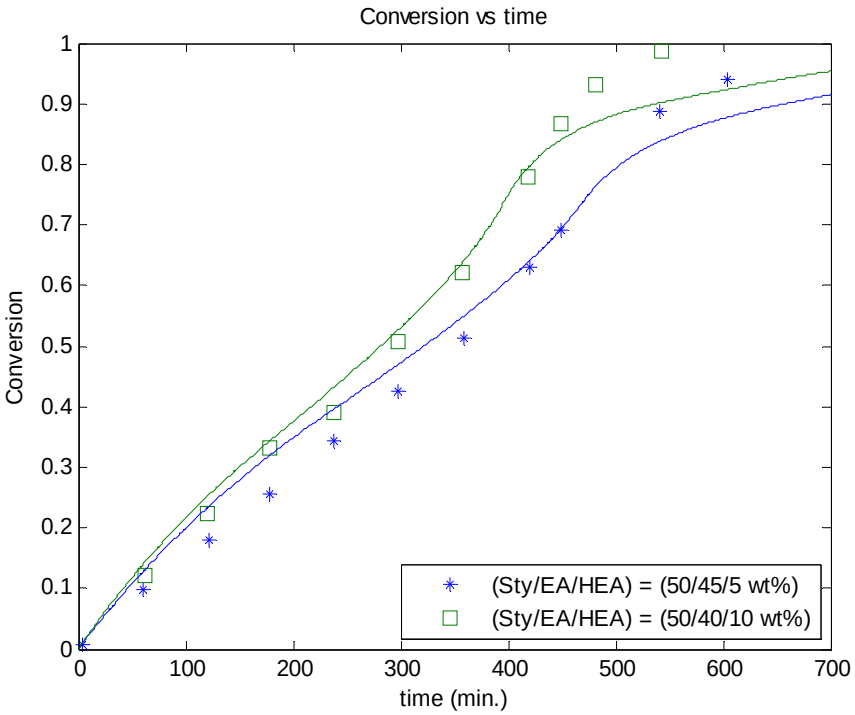

Figure 6.37. Simulation of bulk *ter*-polymerizations of Sty/EA/HEA T = 60℃ and $[AIBN]_0$ = 0.05 M

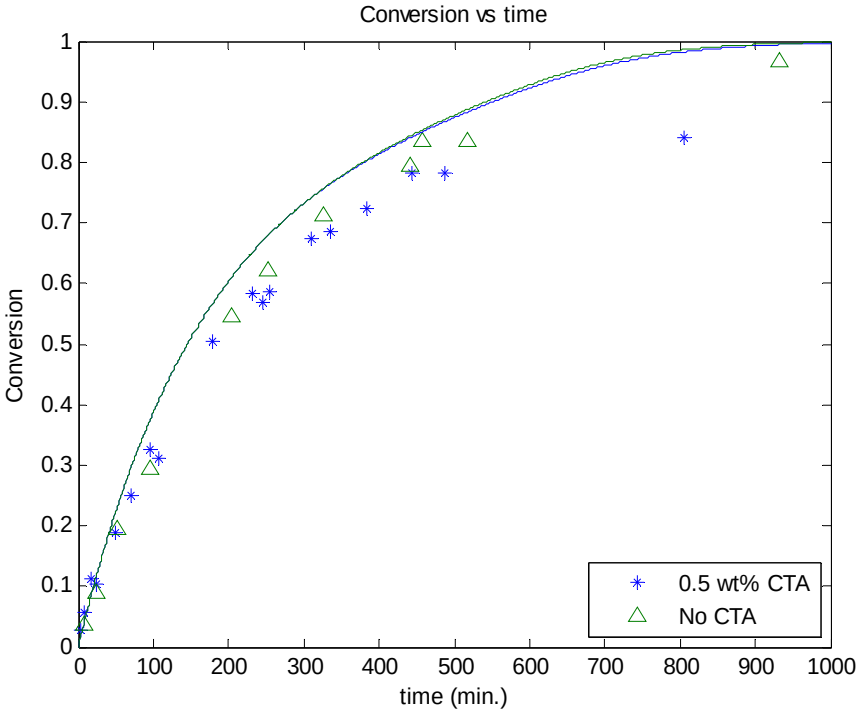

Figure 6.38. Simulation of solution *ter*-polymerization of Sty/EA/HEA (42/42/16 wt%) T = 100℃, m-Xylene = 60 wt% of total mixture, and TBPB = 1.5 wt% of total monomer

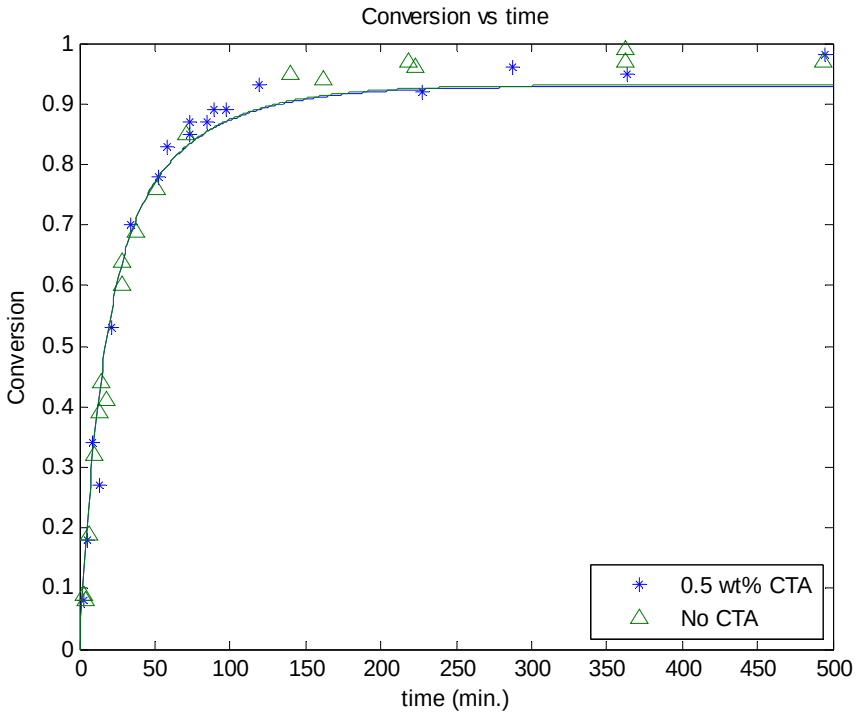

Figure 6.39. Simulation of solution *ter*-polymerization of Sty/EA/HEA (42/42/16 wt%) T = 130℃, m-Xylene = 60 wt% of total mixture, and TBPB = 1.5 wt% of total monomer

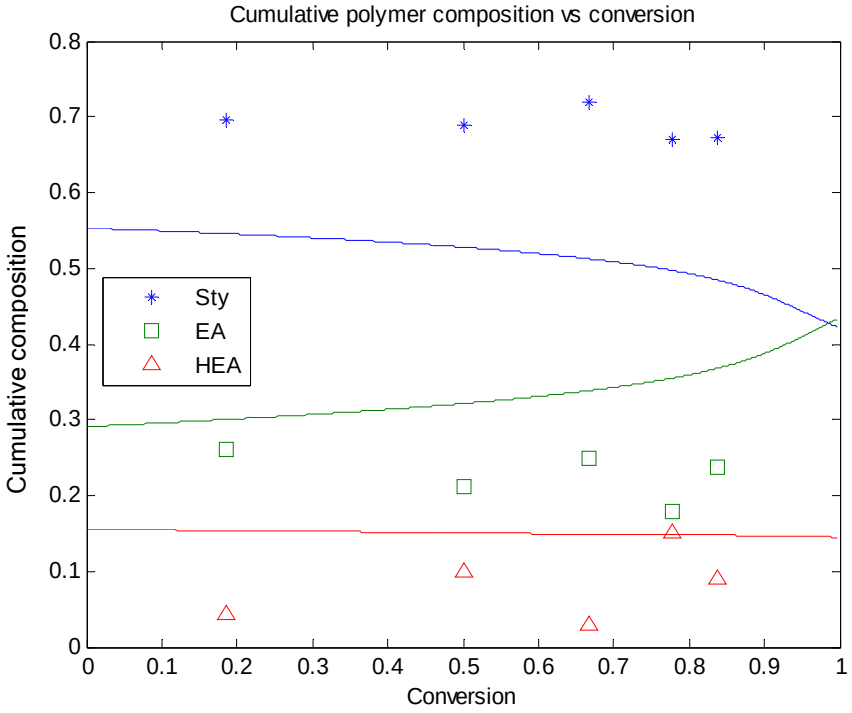

Figure 6.40. Cumulative polymer composition in Sty/EA/HEA (42/42/16 wt%) *ter*-polymerization
T = 100℃, m-Xylene = 60 wt% of total mixture, Octanethiol = 0.5 wt% and TBPB = 1.5 wt% of total monomer

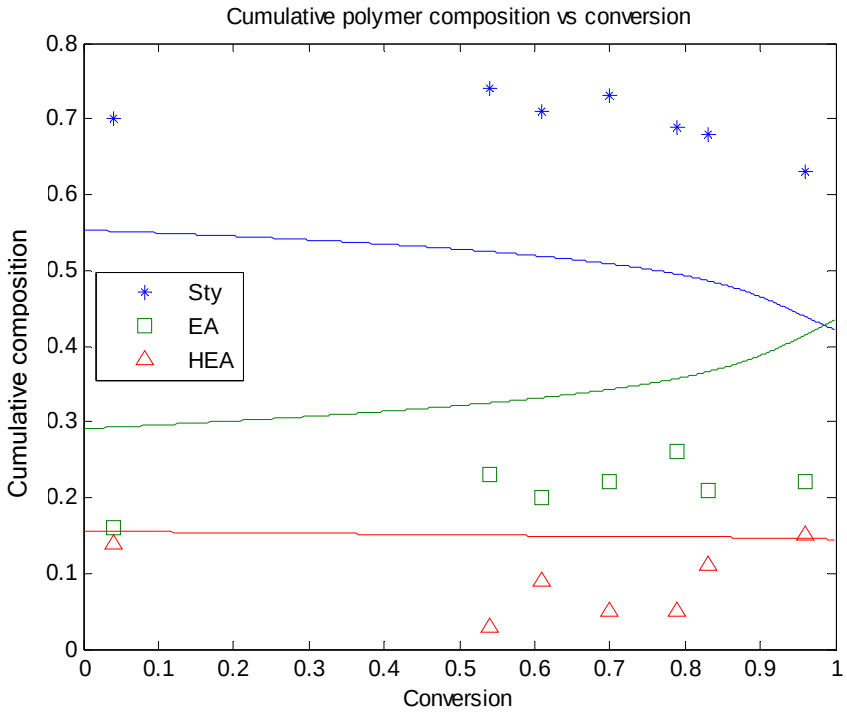

Figure 6.41. Cumulative polymer composition in Sty/EA/HEA (42/42/16 wt%) *ter*-polymerization
T = 100℃, m-Xylene = 60 wt% of total mixture, No octanethiol and TBPB = 1.5 wt% of total monomer

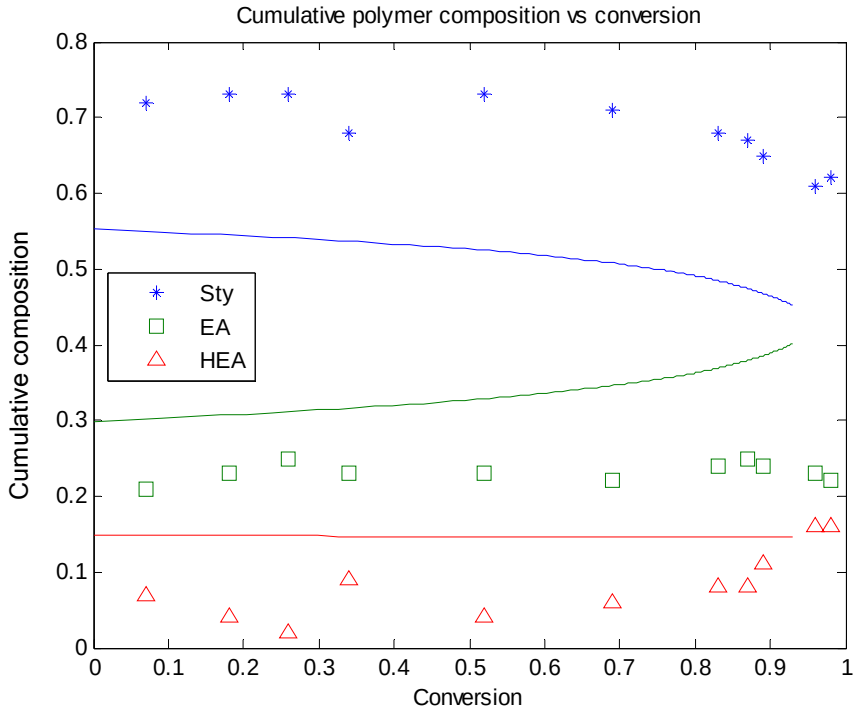

Figure 6.42. Cumulative polymer composition in Sty/EA/HEA (42/42/16 wt%) *ter*-polymerization
T = 130℃, m-Xylene = 60 wt% of total mixture, Octanethiol = 0.5 wt% and TBPB = 1.5 wt% of total monomer

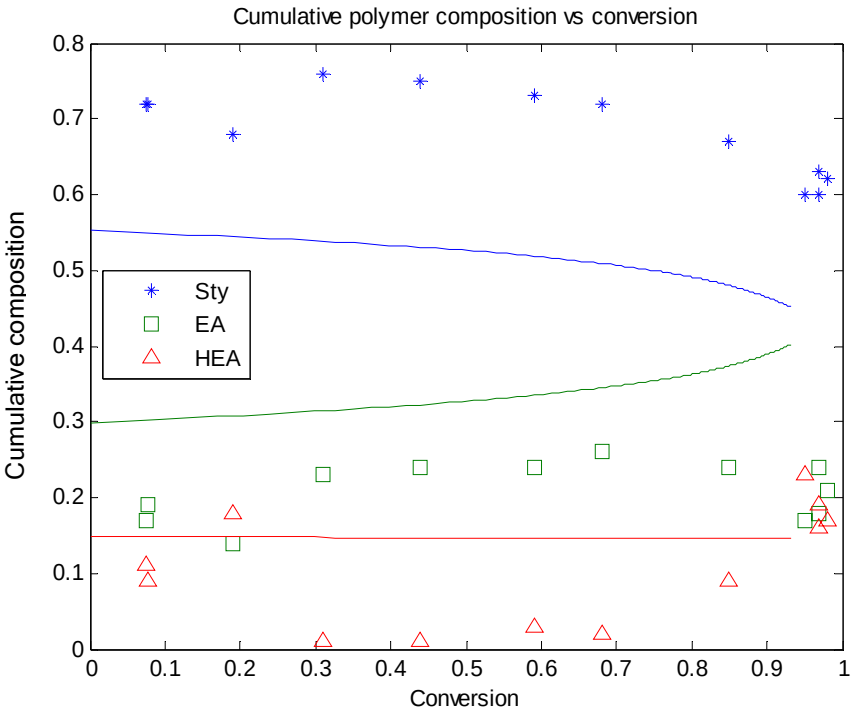

Figure 6.43. Cumulative polymer composition in Sty/EA/HEA (42/42/16 wt%) *ter*-polymerization
T = 130℃, m-Xylene = 60 wt% of total mixture, No octanethiol and TBPB = 1.5 wt% of total monomer

6.9 Sty/EA/MAA *ter*-polymerization

Full conversion range experiments for this system were conducted by Sahloul (2004) at feed composition ratios of (Sty/EA/MAA) = (49/49/2 wt% and 47.5/47.5/5 wt%) with *tert*-butyl peroxybenzoate (TBPB) and octanethiol (1.5 and 0.5 wt% of total monomer mixture, respectively) in m-xylene solvent (60 wt% of total reaction mixture) at 130℃. The estimated reactivity ratios were ($r_{Sty\text{-}MAA}$, $r_{MAA\text{-}Sty}$) = (0.2221, 0.5717), ($r_{MAA\text{-}EA}$, $r_{EA\text{-}MAA}$) = (4.3616, 0.4295). Figure 6.44 represents conversion plots of different feed compositions of Sty/EA/MAA *ter*-polymer, which almost overlap with each other. The model predictions are good. Cumulative polymer composition plots are shown in Figures 6.45 and 6.46. As the monomer feed ratio of MAA increases, more MAA is incorporated into the polymer and the contents of Sty and EA slightly decrease. Some discrepancies do exist in Figures 6.45 and 6.46, but the trends are the same, which indicates possible experimental bias. Figure 6.47 is the first attempt in the literature to both show and try to predict average molecular weights for the system. Despite serious experimental difficulties with gel permeation chromatography for this (and other similar *ter*-polymers with EA/MAA), the trends seem satisfactory, although experimental error (data point fluctuation) is evident. The glass transition temperature in Figure 6.48 was determined from differential scanning calorimetry (DSC) and the model explains the trend relatively well.

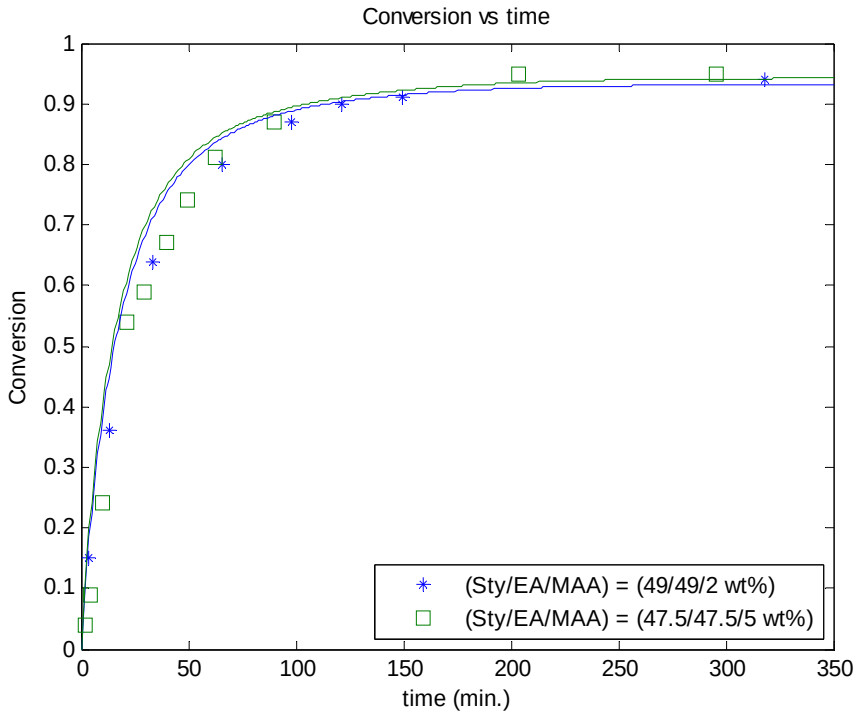

Figure 6.44. Simulation of solution *ter*-polymerization of Sty/EA/MAA
T = 130℃, m-Xylene = 60 wt% of total mixture, Octanethiol = 0.5 wt%, and TBPB = 1.5 wt% of total monomer

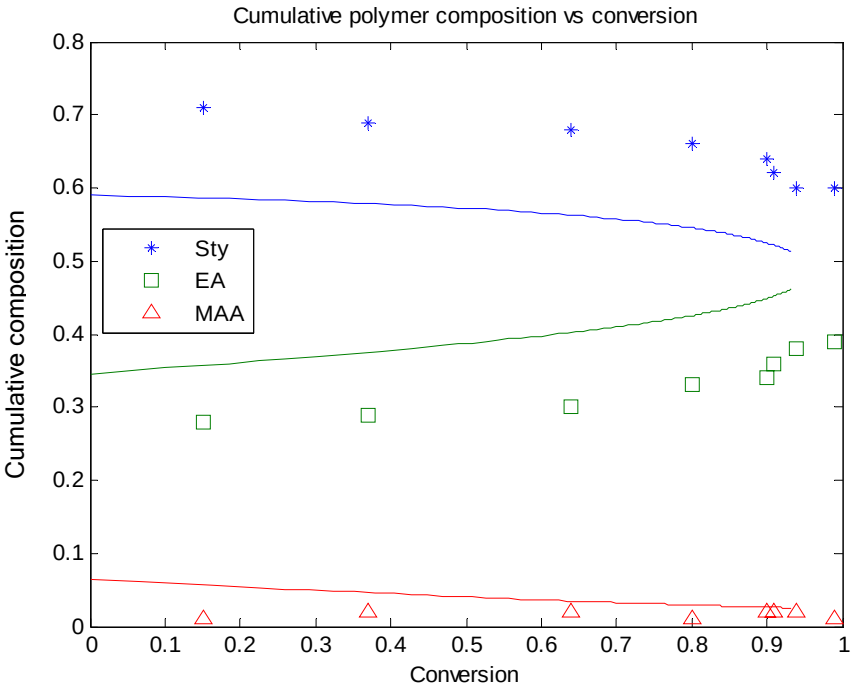

Figure 6.45. Cumulative polymer composition in Sty/EA/MAA (49/49/2 wt%) *ter*-polymerization
T = 130℃, m-Xylene = 60 wt% of total mixture, Octanethiol = 0.5 wt%, and TBPB = 1.5 wt% of total monomer

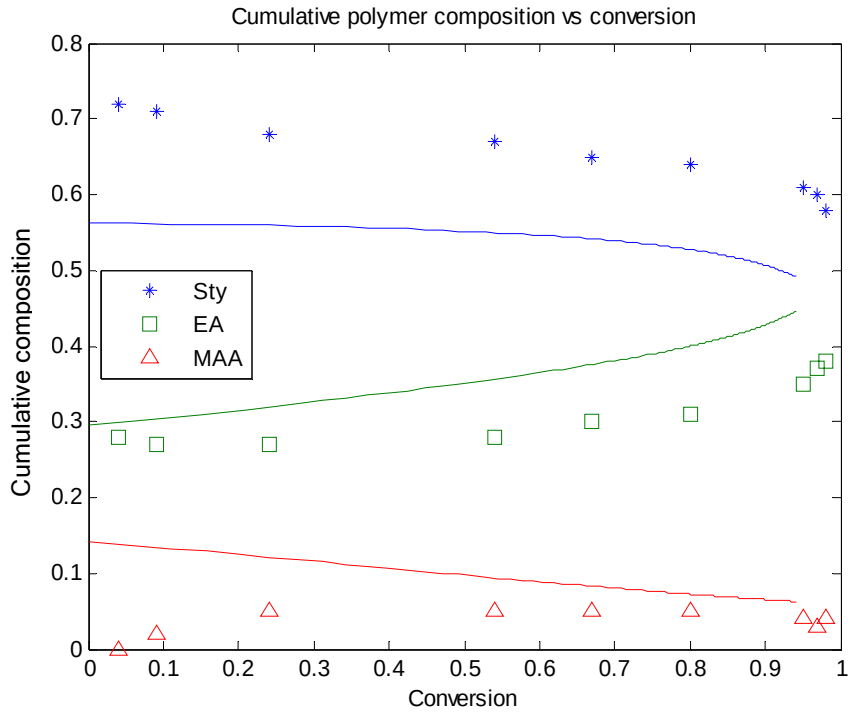

Figure 6.46. Cumulative polymer composition in Sty/EA/MAA (47.5/47.5/5 wt%) *ter*-polymerization
T = 130℃, m-Xylene = 60 wt% of total mixture, Octanethiol = 0.5 wt%, and TBPB = 1.5 wt% of total monomer

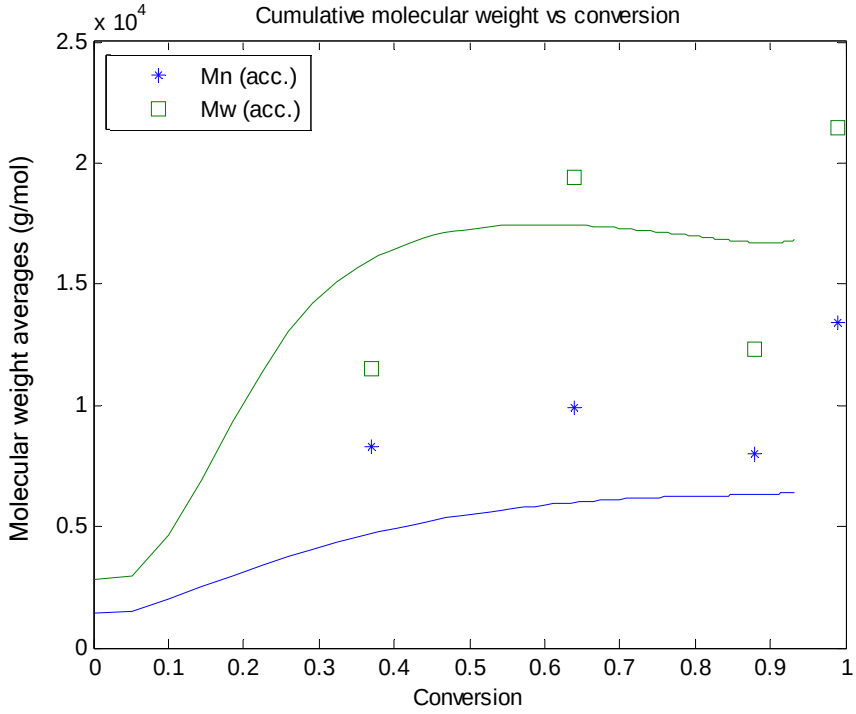

Figure 6.47. Molecular weight averages of Sty/EA/MAA (49/49/2 wt%) *ter*-polymerization
T = 130℃, m-Xylene = 60 wt% of total mixture, Octanethiol = 0.5 wt%, and TBPB = 1.5 wt% of total monomer

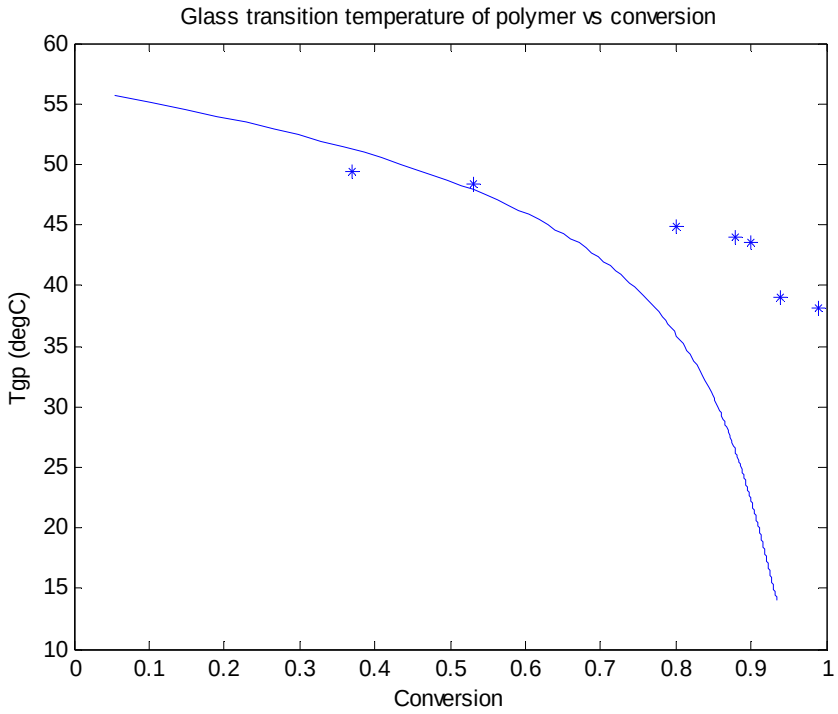

Figure 6.48. Glass transition temperature of Sty/EA/MAA (49/49/2 wt%) *ter*-polymer
T = 130℃, m-Xylene = 60 wt% of total mixture, Octanethiol = 0.5 wt%, and TBPB = 1.5 wt% of total monomer

6.10 EA/HEA/MAA *ter*-polymerization

We were able to locate only one experimental run with EA/HEA/MAA from Sahloul (2004) conducted in solution using CTA and initiator at 130℃. The reactivity ratios estimated were ($r_{MAA\text{-}HEA}$, $r_{HEA\text{-}MAA}$) = (0.568, 0.2592). Polymerization was carried out with 60 wt% solvent (m-xylene), 1.5 wt% initiator (TBPB), and 0.5 wt% CTA (octanethiol). Weight percentages above refer to the total reaction mixture. The monomer feed composition was (EA/HEA/MAA) = (84/11/5 wt% of total monomer). Figure 6.49 shows a dramatic increase of conversion in a short time, i.e., very fast reaction. Because of this, measurement data at low conversion levels were unavailable. Polymer composition was characterized by utilizing gel phase ^{1}H-NMR (a tedious measurement in itself), and our model successfully agrees with the data in Figure 6.50.

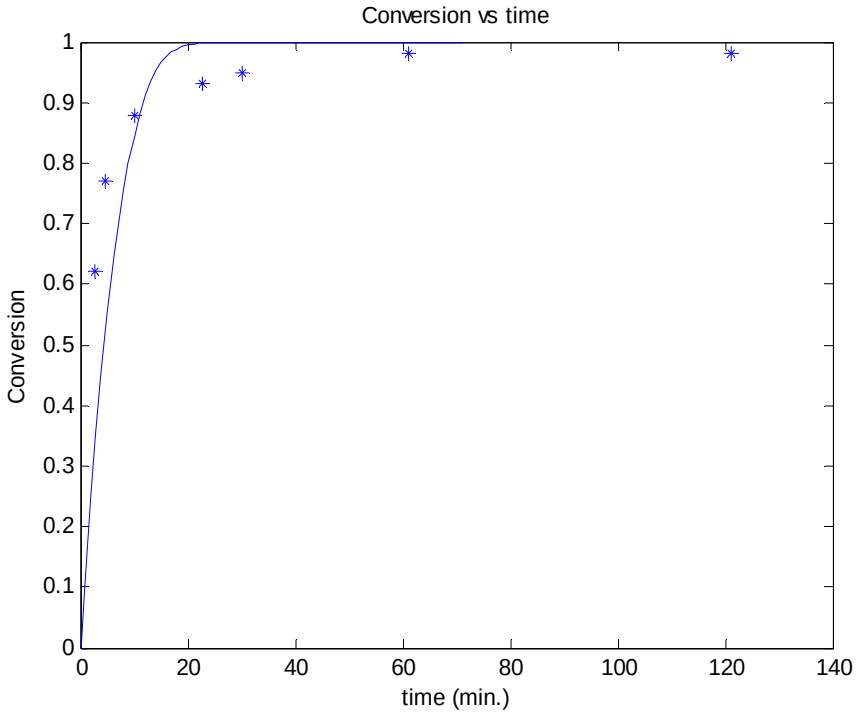

Figure 6.49. Simulation of solution *ter*-polymerization of EA/HEA/MAA (84/11/5 wt%)
T = 130℃, m-Xylene = 60 wt% of total mixture, Octanethiol = 0.5 wt%, and TBPB = 1.5 wt% of total monomer

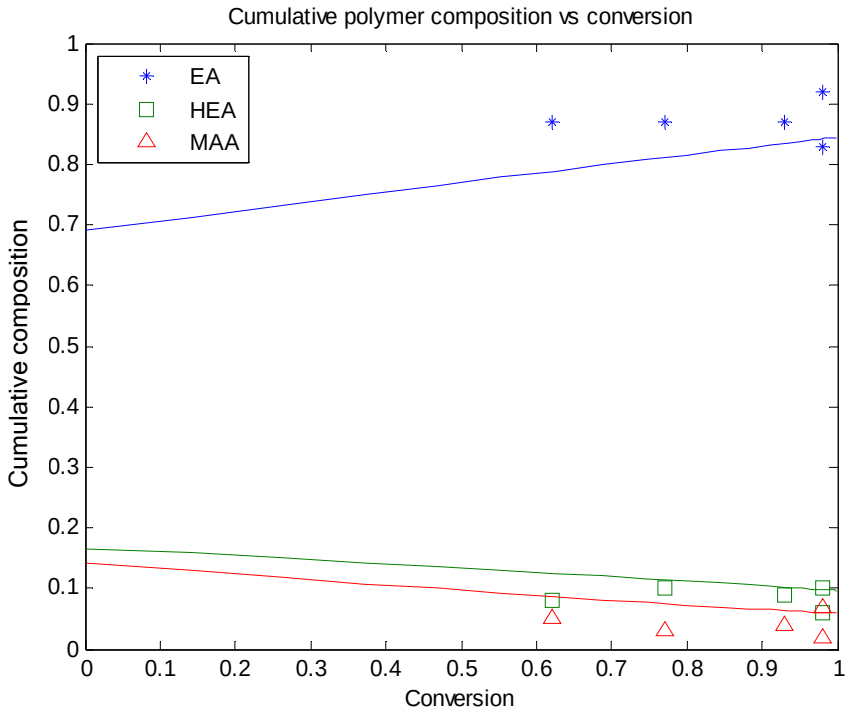

Figure 6.50. Cumulative polymer composition in EA/HEA/MAA (84/11/5 wt%) *ter*-polymerization
T = 130℃, m-Xylene = 60 wt% of total mixture, Octanethiol = 0.5 wt%, and TBPB = 1.5 wt% of total monomer

6.11 Sty/EA/HEA/MAA *tetra*-polymerization

This monomer system represents the highest degree of multi-component polymerization model testing that we have found so far. Solution polymerizations were conducted by Sahloul (2004) using 2^3 factorial design experiments. m-Xylene was used as solvent with two levels of temperature (100 and 130℃) and the presence of CTA (octanethiol) and initiator (*tert*-butyl peroxybenzoate, TBPB). Feed composition was set as (Sty/EA/HEA/MAA) = (41/41/16/2 wt%) and the amounts of solvent, CTA, and initiator were 60 wt%, 0.5 wt%, and 1.5 wt% of the total reaction mixture. Extra monomer feed compositions were further utilized, such as (Sty/EA/HEA/MAA) = (42/42/14/2, 42/42/11/5, and 39.5/39.5/16/5 wt%).

Figures 6.51 to 6.54 are conversion plots at 100/130℃, with or without CTA/initiator. CTA effect is not significant on the polymerization rate in the chemical initiation cases (Figures 6.51 and 6.53). However, the experimental data using CTA show slower rate than the ones without CTA in Figures 6.52 and 6.54. Our model prediction is poor during thermal initiation because the model contains the thermal initiation option for styrenics only. This can be a clue that other significant thermal initiation "contributions" may happen at elevated temperatures with systems other than styrene.

In cumulative polymer composition plots (Figures 6.55 to 6.62), it is clear that temperature and CTA effects are negligible. Model prediction trends are similar to the ones of the experimental data but some discrepancies are observed. Sahloul (2004) reported that the polymer samples contained microgel and were not completely dissolved during NMR analysis, hence this acted as a source of error in both composition calculations (scattered points) and reactivity ratio estimation.

Figure 6.63 shows conversion profiles from additional experiments (change of monomer feed compositions). There are almost no differences among polymerization rates and the model predictions are good. Figures 6.64 to 6.66 are cumulative polymer composition plots corresponding to the feed compositions in Figure 6.63. Again, model trends are similar but some discrepancies exist due to the reasons discussed above.

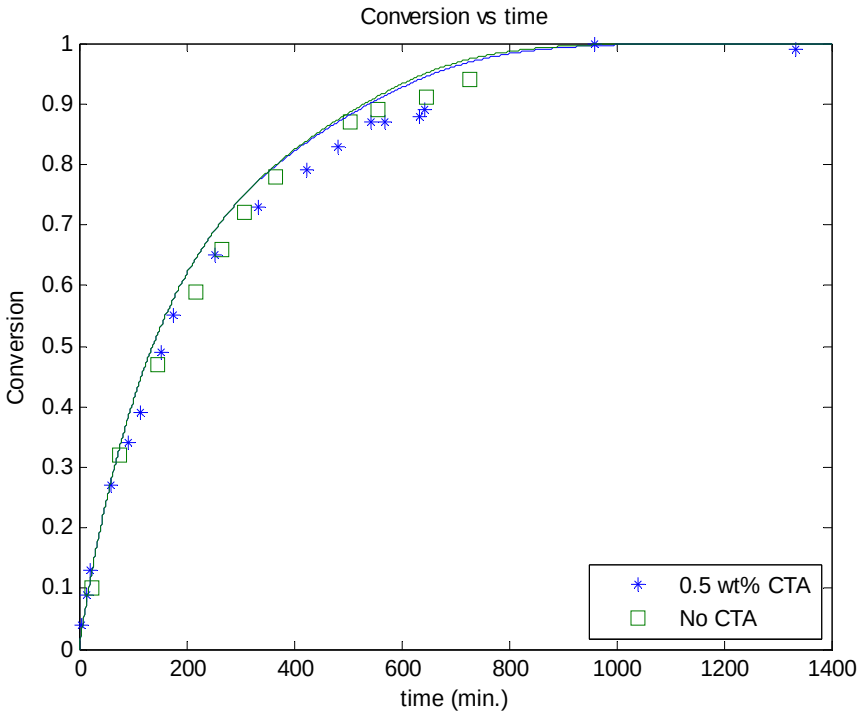

Figure 6.51. Simulation of solution *tetra*-polymerization of Sty/EA/HEA/MAA (41/41/16/2 wt%) T = 100℃, m-Xylene = 60 wt% of total mixture, and TBPB = 1.5 wt% of total monomer

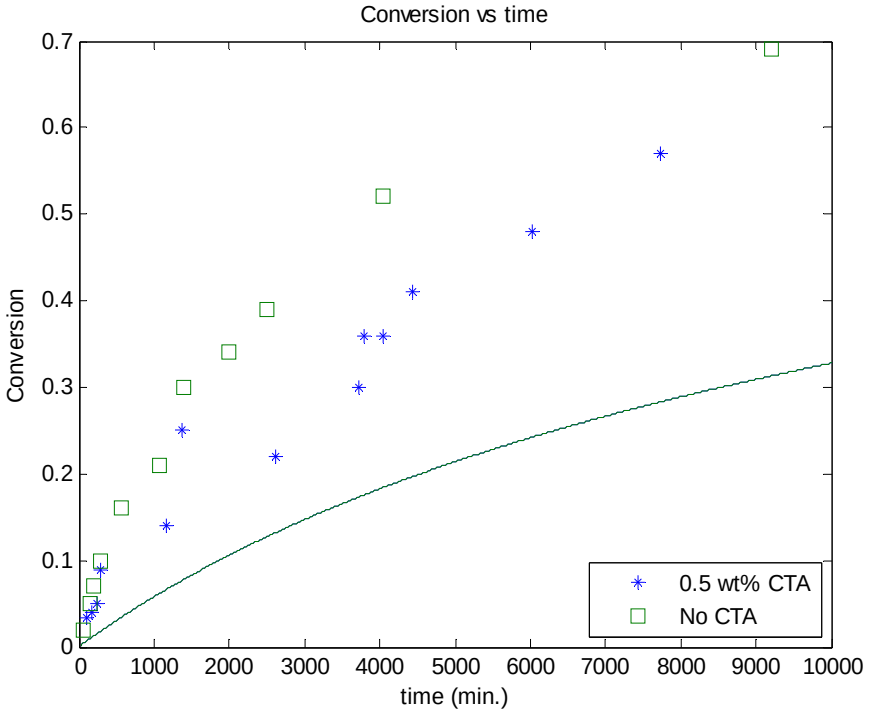

Figure 6.52. Simulation of solution *tetra*-polymerization of Sty/EA/HEA/MAA (41/41/16/2 wt%) T = 100℃, m-Xylene = 60 wt% of total mixture, No TBPB

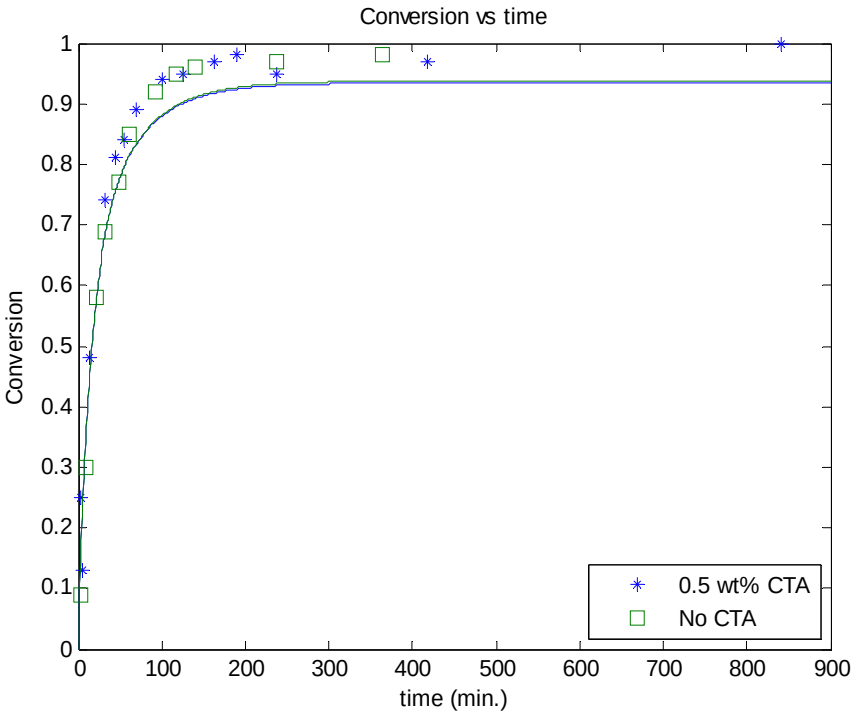

Figure 6.53. Simulation of solution *tetra*-polymerization of Sty/EA/HEA/MAA (41/41/16/2 wt%) T = 130℃, m-Xylene = 60 wt% of total mixture, and TBPB = 1.5 wt% of total monomer

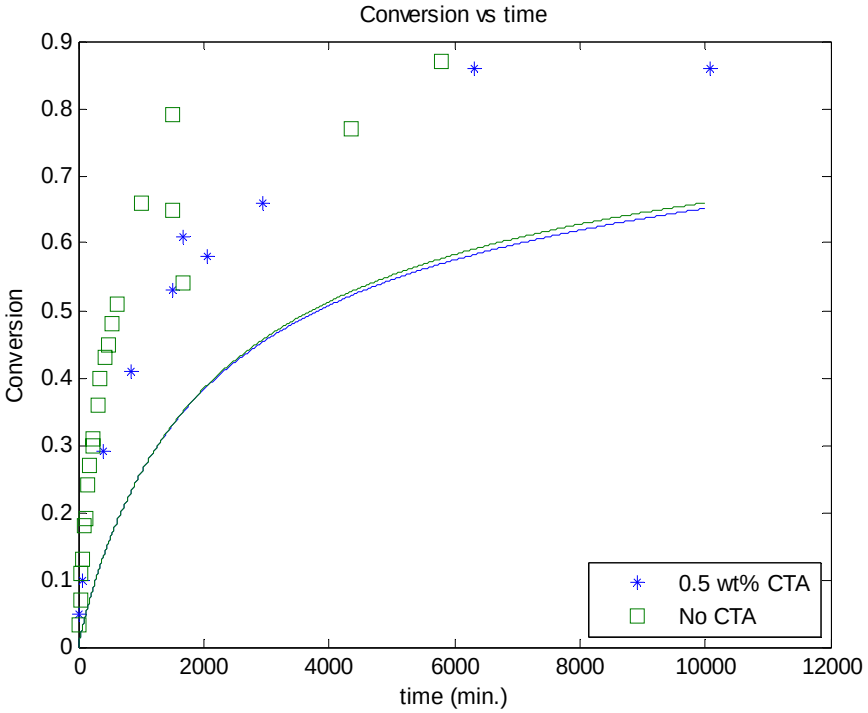

Figure 6.54. Simulation of solution *tetra*-polymerization of Sty/EA/HEA/MAA (41/41/16/2 wt%) T = 130℃, m-Xylene = 60 wt% of total mixture, No TBPB

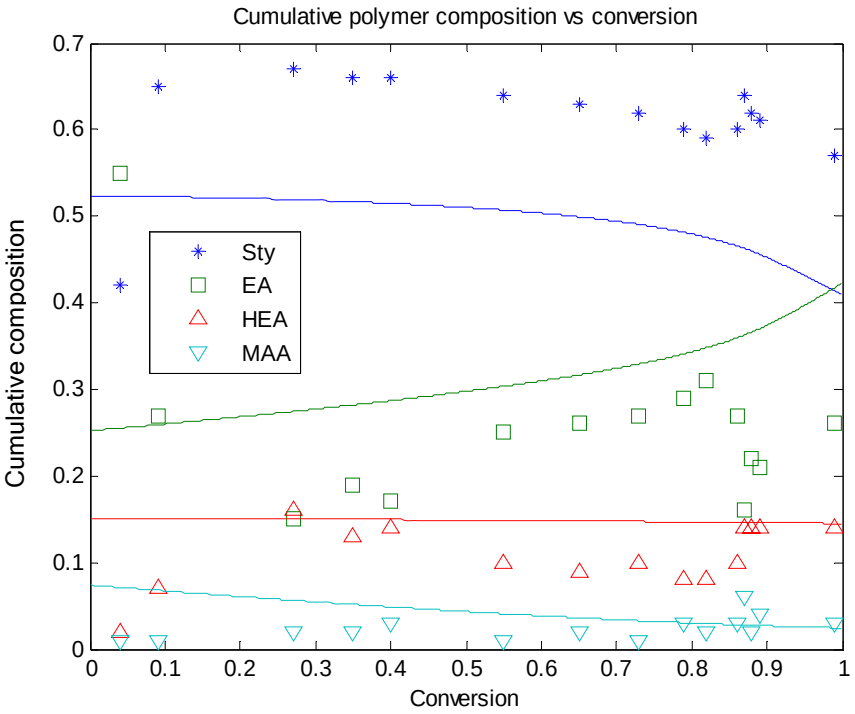

Figure 6.55. Cumulative polymer composition in Sty/EA/HEA/MAA (41/41/16/2 wt%) *tetra*-polymerization T = 100℃, m-Xylene = 60 wt% of total mixture, Octanethiol = 0.5 wt%, and TBPB = 1.5 wt% of total monomer

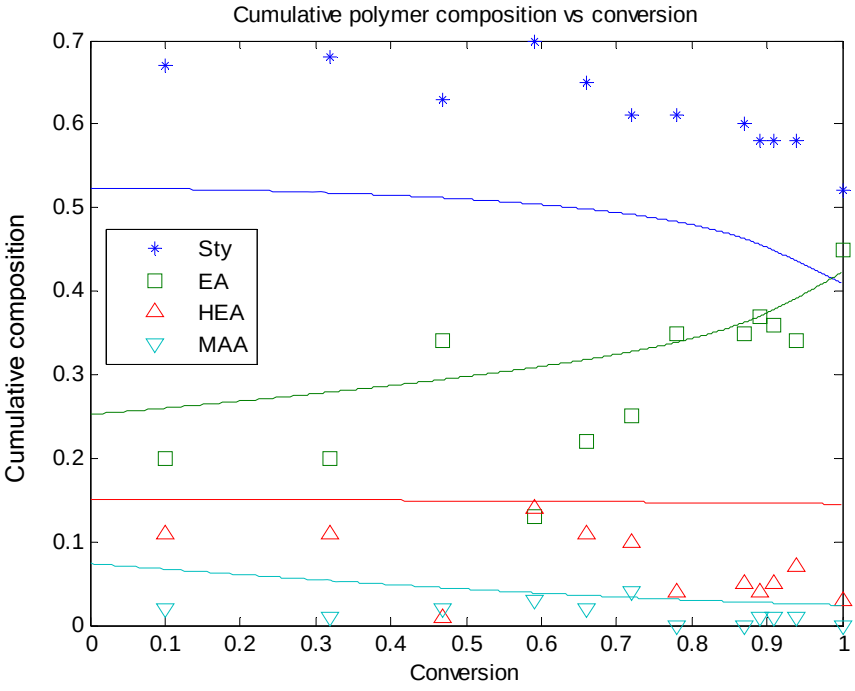

Figure 6.56. Cumulative polymer composition in Sty/EA/HEA/MAA (41/41/16/2 wt%) *tetra*-polymerization T = 100℃, m-Xylene = 60 wt% of total mixture, No octanethiol, and TBPB = 1.5 wt% of total monomer

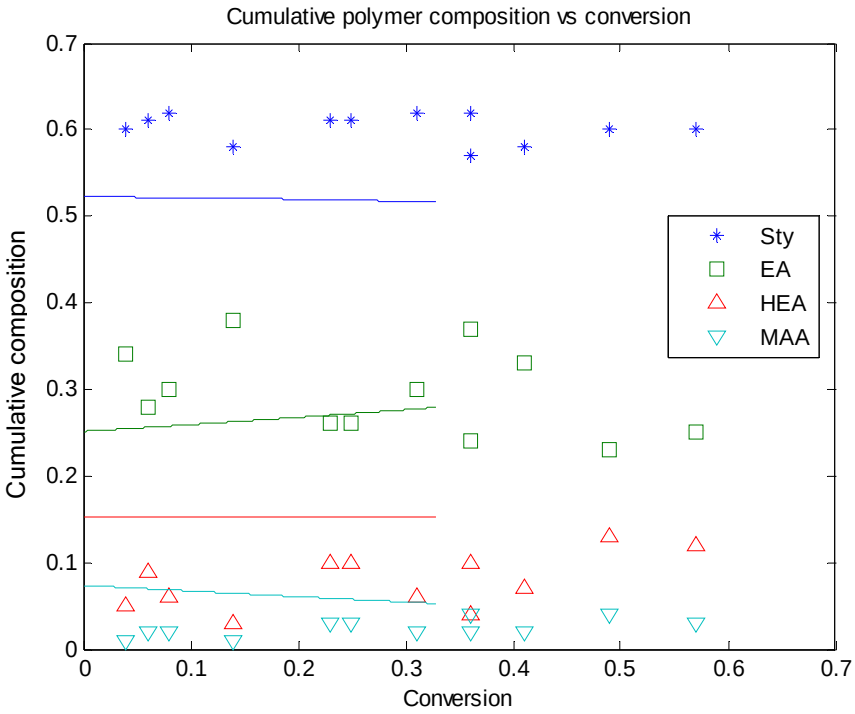

Figure 6.57. Cumulative polymer composition in Sty/EA/HEA/MAA (41/41/16/2 wt%) *tetra*-polymerization T = 100℃, m-Xylene = 60 wt% of total mixture, Octanethiol = 0.5 wt%, and No TBPB

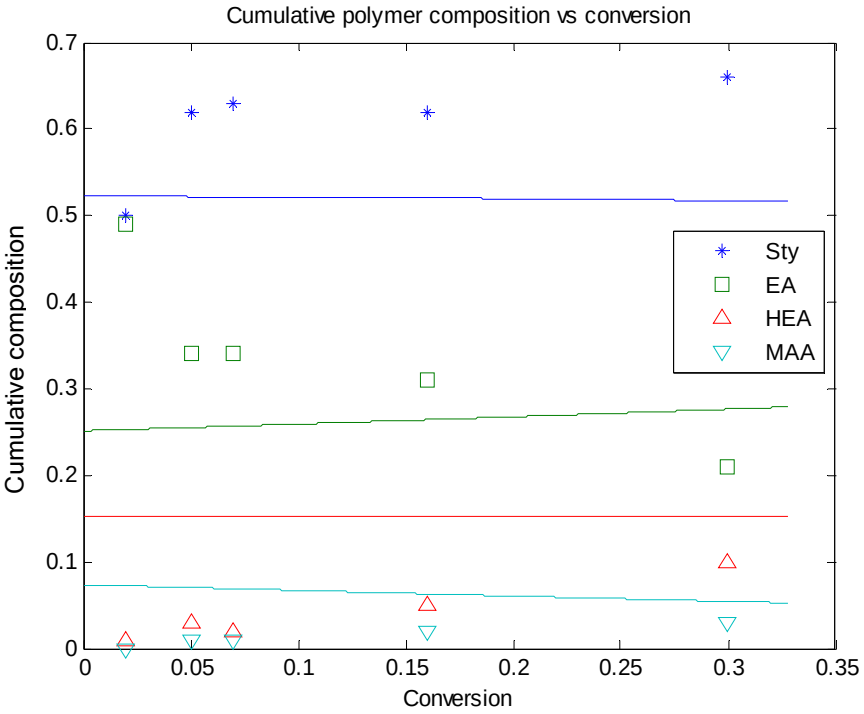

Figure 6.58. Cumulative polymer composition in Sty/EA/HEA/MAA (41/41/16/2 wt%) *tetra*-polymerization T = 100℃, m-Xylene = 60 wt% of total mixture, No octanethiol and TBPB

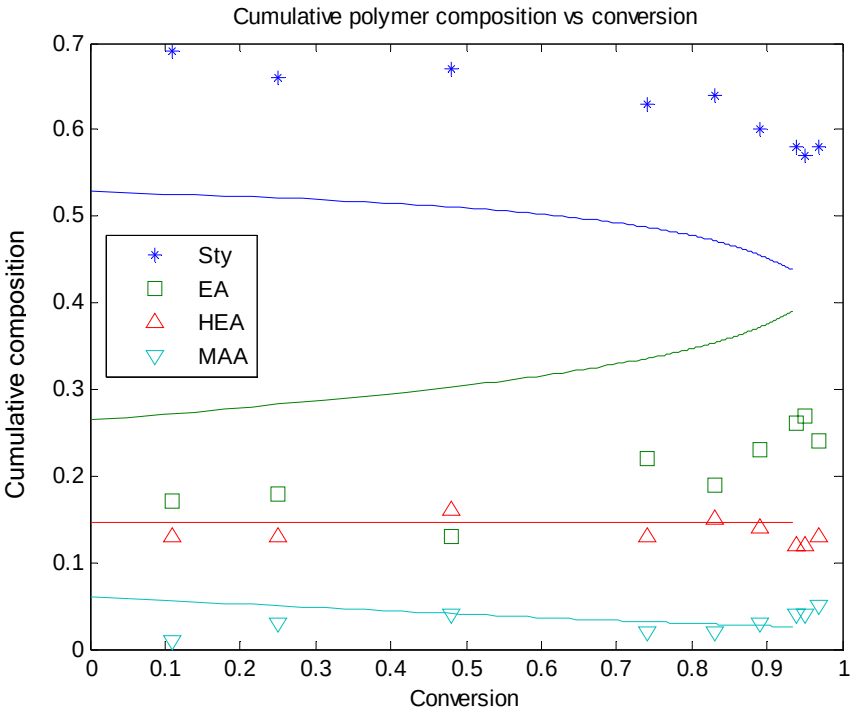

Figure 6.59. Cumulative polymer composition in Sty/EA/HEA/MAA (41/41/16/2 wt%) *tetra*-polymerization T = 130℃, m-Xylene = 60 wt% of total mixture, Octanethiol = 0.5 wt%, and TBPB = 1.5 wt% of total monomer

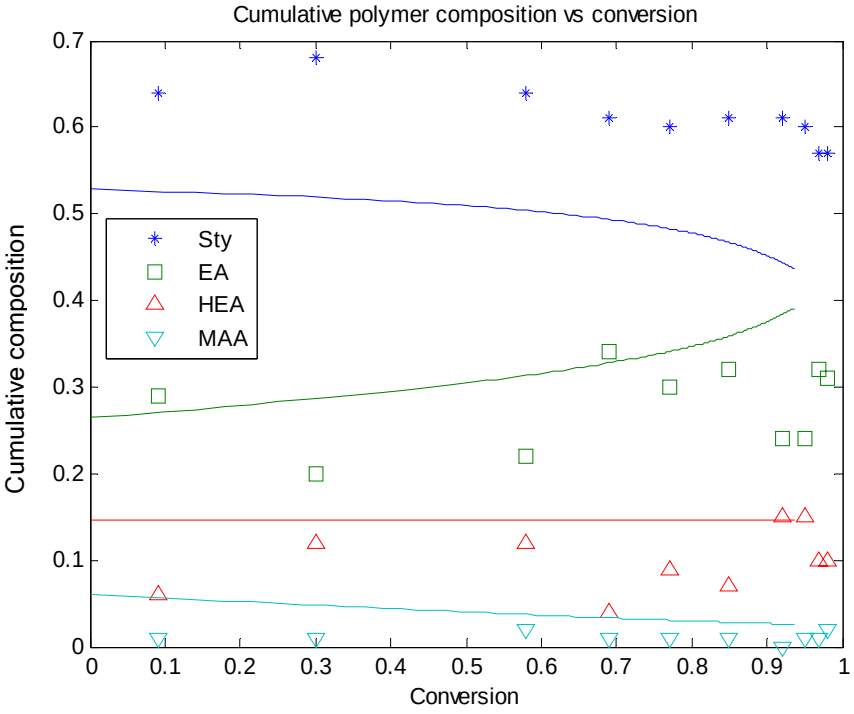

Figure 6.60. Cumulative polymer composition in Sty/EA/HEA/MAA (41/41/16/2 wt%) *tetra*-polymerization T = 130℃, m-Xylene = 60 wt% of total mixture, No octanethiol, and TBPB = 1.5 wt% of total monomer

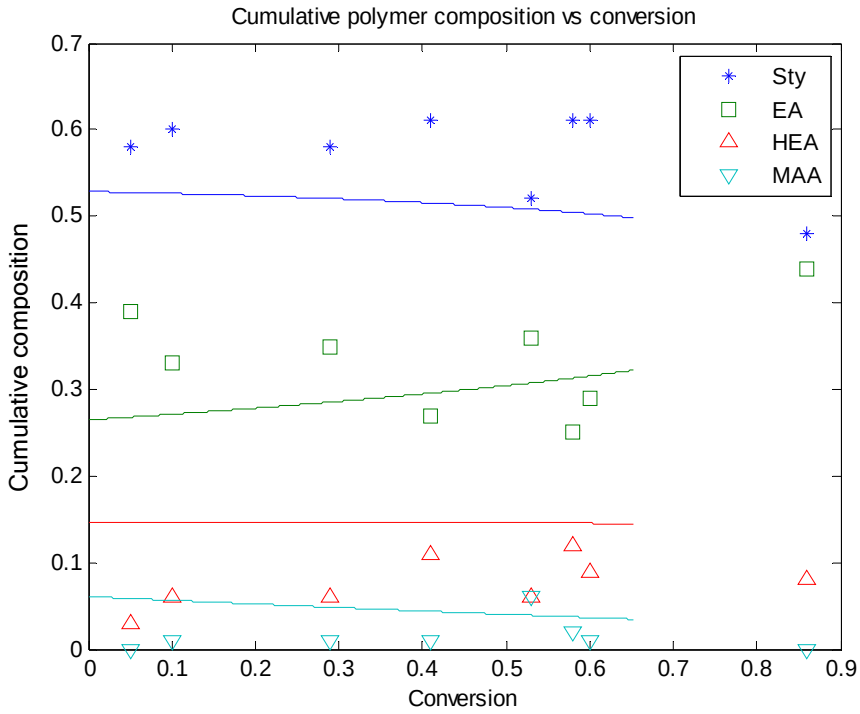

Figure 6.61. Cumulative polymer composition in Sty/EA/HEA/MAA (41/41/16/2 wt%) *tetra*-polymerization T = 130℃, m-Xylene = 60 wt% of total mixture, Octanethiol = 0.5 wt%, and No TBPB

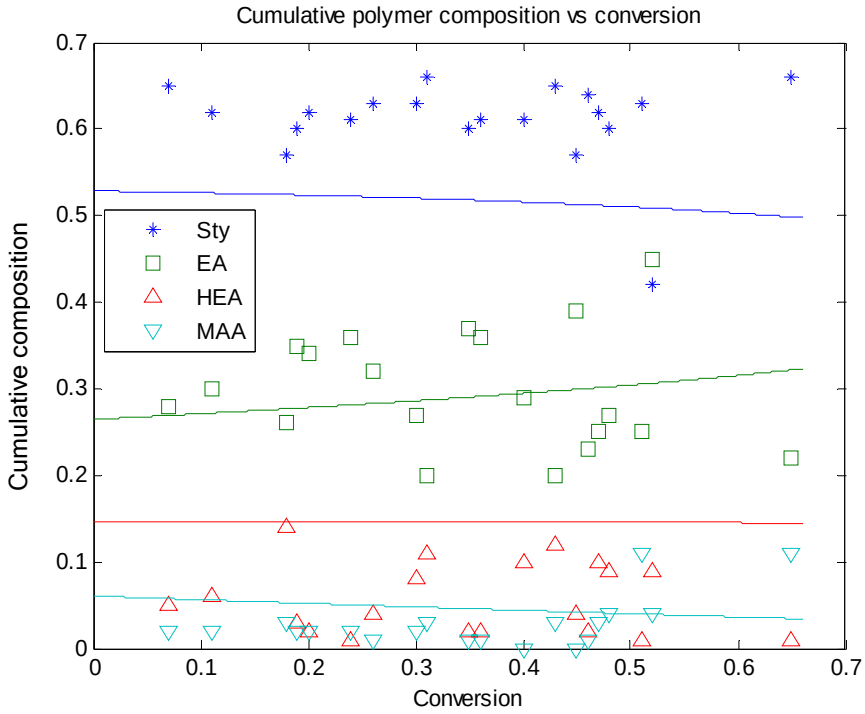

Figure 6.62. Cumulative polymer composition in Sty/EA/HEA/MAA (41/41/16/2 wt%) *tetra*-polymerization T = 130℃, m-Xylene = 60 wt% of total mixture, No octanethiol and TBPB

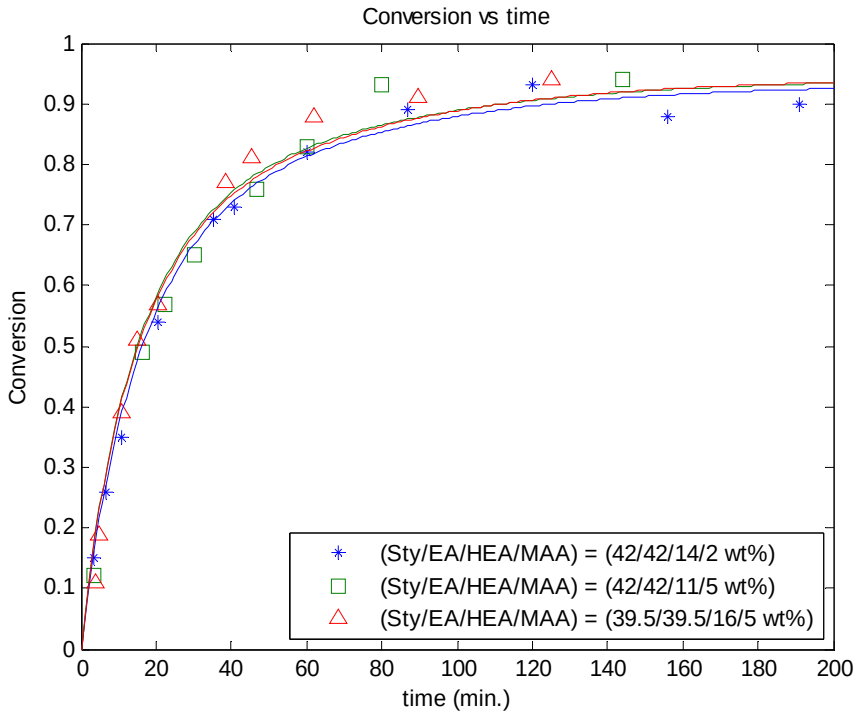

Figure 6.63. Simulation of solution *tetra*-polymerization of Sty/EA/HEA/MAA
T = 130℃, m-Xylene = 60 wt% of total mixture, Octanethiol = 0.5 wt%, and TBPB = 1.5 wt% of total monomer

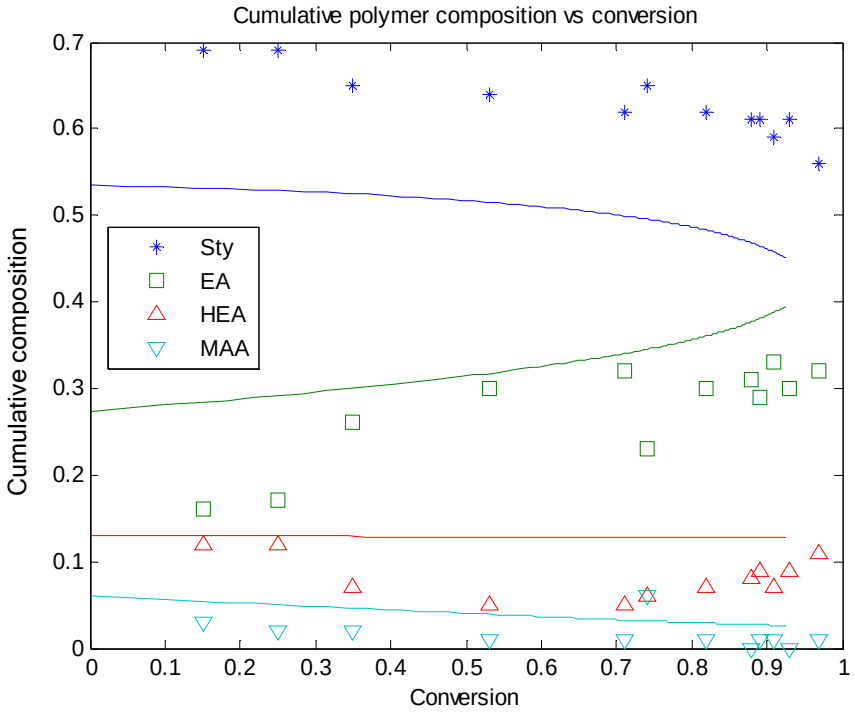

Figure 6.64. Cumulative polymer composition in Sty/EA/HEA/MAA (42/42/14/2 wt%) *tetra*-polymerization
T = 130℃, m-Xylene = 60 wt% of total mixture, Octanethiol = 0.5 wt%, and TBPB = 1.5 wt% of total monomer

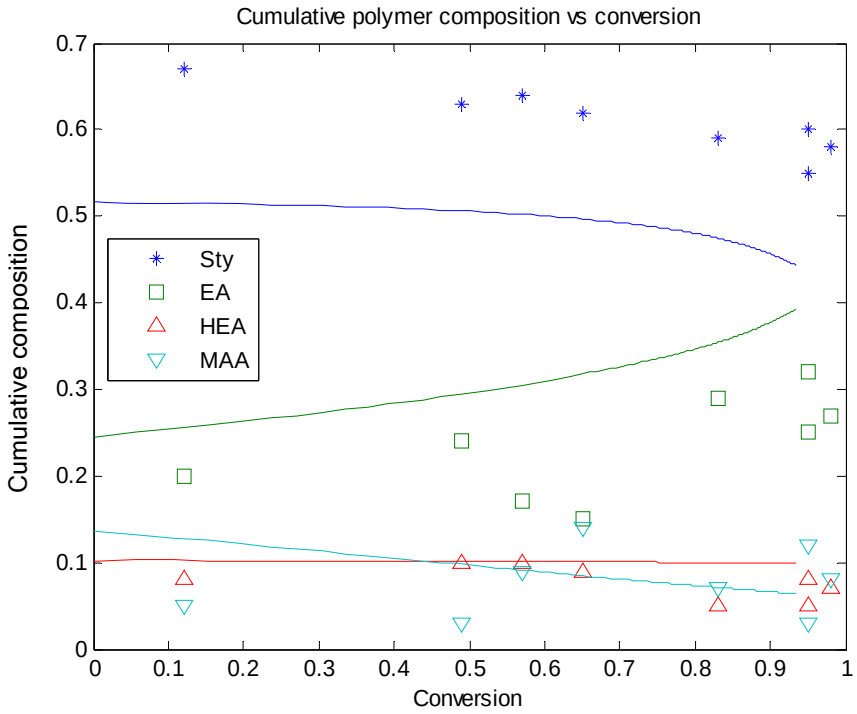

Figure 6.65. Cumulative polymer composition in Sty/EA/HEA/MAA (42/42/11/5 wt%) *tetra*-polymerization T = 130℃, m-Xylene = 60 wt% of total mixture, Octanethiol = 0.5 wt%, and TBPB = 1.5 wt% of total monomer

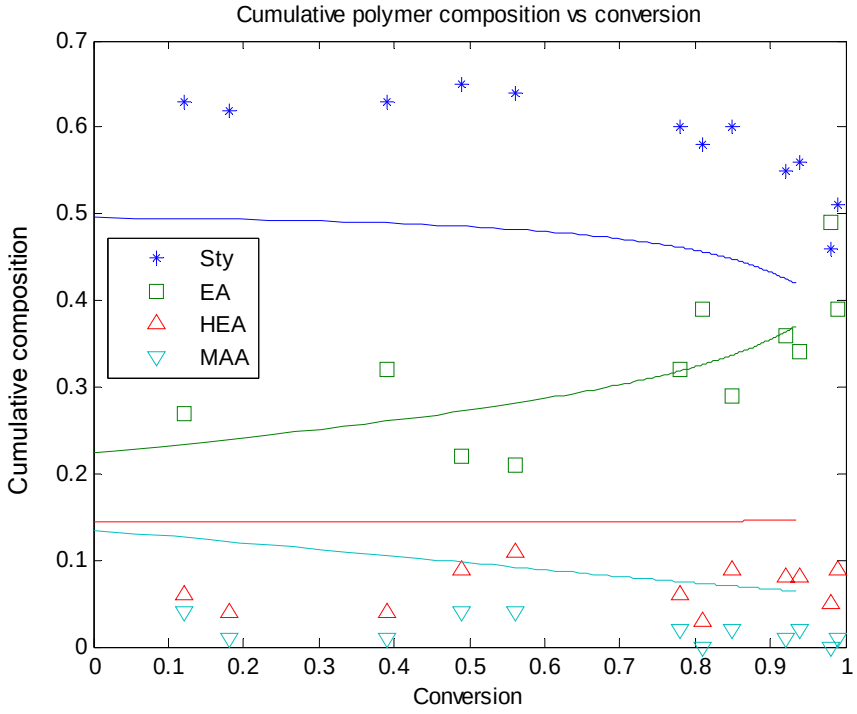

Figure 6.66. Cumulative polymer composition in Sty/EA/HEA/MAA (39.5/39.5/16/5 wt%) *tetra*-polymerization T = 130℃, m-Xylene = 60 wt% of total mixture, Octanethiol = 0.5 wt%, and TBPB = 1.5 wt% of total monomer

Chapter 7

Six-component Recipe Trends

Typical prediction trends with the full multi-component bulk and solution polymerization model in a batch and semi-batch reactor (refer to the six-component recipe in Chapter 4) are presented herein. Due to the complete absence from the literature of information concerning HBA kinetics, the six monomer recipe cited in Chapter 4 was modified such that HBA monomer was replaced with the same amount of EA monomer (Sty/BA/EA/BMA/HEA/AA = 10/30/20/15/20/5 wt% of total monomer). Xylene solvent and *di-tert*-butyl peroxide initiator amounts were fixed at 66 and 0.6 wt% of total reaction mixture, respectively. Table 7.1 summarizes the reactivity ratios ($r_{\text{Monomer 1-Monomer 2}}$) used in this six component system at 120℃. The three pairs of reactivity ratios ($r_{\text{BA-EA}}$, $r_{\text{EA-BA}}$), ($r_{\text{BMA-HEA}}$, $r_{\text{HEA-BMA}}$), and ($r_{\text{HEA-AA}}$, $r_{\text{AA-HEA}}$) were impossible to locate in the literature. Therefore, these unknown values were approximated using the *Q-e* scheme.

		Monomer 1					
		Sty	**BA**	**EA**	**BMA**	**HEA**	**AA**
Monomer 2	**Sty**		**0.183**	**0.218**	**0.42**	**0.317**	**0.18**
	BA	**0.956**		**1.273**	**1.694**	**0.9**	**0.58**
	EA	**0.937**	**0.718**		**2.43**	**1.657**	**0.91**
	BMA	**0.61**	**0.376**	**0.22**		**0.777**	**0.29**
	HEA	**0.497**	**0.3**	**0.687**	**0.284**		**0.354**
	AA	**0.25**	**1.07**	**1.02**	**3.67**	**1.899**	

Table 7.1. Reactivity ratios ($r_{\text{Monomer 1-Monomer 2}}$) for six component system at 120℃

Figure 7.1 shows conversion curves for six-component solution polymerizations at 120, 150, and 180℃. The reaction rate increases at higher temperature level without limiting conversion. Especially, as the reaction temperature changes from 120 to 150℃, the rate of polymerization is dramatically increased. For a further analysis of *hexa*-polymerization, the reaction temperature of 120℃ was selected as the base case.

Bulk and solution conversion profiles at 120℃ are compared in Figure 7.2. Distinct autoacceleration is observed in the bulk case because the absence of solvent makes the reaction mixture highly viscous. The differences between bulk and solution polymerizations are also recognizable in the number/weight average molecular weights shown in Figures 7.3 and 7.4. Due to the presence of solvent and transfer reactions with it, molecular weight averages in the solution case are much lower than those in the bulk case. In addition, the molecular weight averages are increasing in bulk while they are decreasing in solution, as expected from typical polymerization behaviour (diffusion-controlled kinetics). Partial conversion plots at 120℃ are depicted in Figure 7.5. It is observed that Sty is polymerizing faster than any other monomer in this system and the initial rates can be ordered as: Sty > HEA ≈ BMA > AA ≈ BA ≈ EA, as governed by the corresponding monomer reactivities and reactivity ratios.

Figure 7.6 is a *ter*-polymerization conversion plot for Sty/EA/HEA shown earlier in Chapter 6 (Figure 6.39). This plot was reproduced here by using the six-component computer program, adjusting the recipe (i.e. solvent and CTA values) and setting certain monomer concentrations, namely BA, BMA, and AA, to zero. This clearly indicates that our six-component model can successfully be reduced to the three-component one and shows the flexibility of the code to handle *homo*- to *hexa*-polymerizations thanks to code generalization.

In order to illustrate another important feature of our model, we have run a six-component semi-batch simulation to show the difference in the polymerization behaviour compared to a batch reactor (simply a straightforward direct comparison without trying to optimize any properties). In Figure 7.7, monomers (Sty/BA/EA/BMA/HEA/AA = 10/30/20/15/20/5 wt%) were fed into the reactor with fixed rates over 180 minutes. Solvent

(m-xylene, 66 wt% of total mixture), and initiator (*di-tert*-butyl peroxide, 0.6 wt% of total mixture) were fed concurrently with monomers, but for an additional 20 minutes in order to drive the final amount of residual monomer to a low level.

With this recipe, the semi-batch conversion profile was produced and compared with the previous batch case in Figure 7.8. The reaction rate was not as fast as the one in batch polymerization due to the low amount of monomers in the mixture and the final conversion was calculated as 82%, while 100% was attained in the batch reactor. Figures 7.9 and 7.10 show the monomer profiles for the batch and semi-batch reactions, respectively. Differences in the monomer profile will affect the residual monomer fractions, cumulative polymer compositions, and number average sequence lengths. In Figure 7.9, there was no inflow of monomers into the reactor during the polymerization and therefore, all are decreasing. On the other hand, in Figure 7.10, fresh monomers were continuously fed up to 180 minutes.

Figures 7.11 and 7.12 show residual monomer mole fractions vs conversion curves in batch and semi-batch, respectively. Along with the partial conversion curves in Figure 7.5, the residual monomer fractions, namely the relative amounts of unreacted monomers, are clearly indicating the differences of monomer reactivities in the mixture. The fractions of BA, EA, and AA are increasing, whereas Sty, HEA, and BMA show decreasing trends because the former monomers are more slowly incorporated into the polymer compared with the latter ones at the early stages of polymerization. It is interesting that the EA fraction starts to decrease above 90% conversion indicating rapid consumption of EA monomer at that point. The ranges of monomer fractions in the semi-batch reactor (Figure 7.12) are narrower than in the batch case over the entire conversion.

The cumulative (six component) polymer compositions in batch and semi-batch reactors are plotted over the entire conversion range in Figures 7.13 and 7.14, respectively. Again, the observed composition trends are similar to the residual monomer fraction plots (BA, EA and AA compositions are drifting up, while Sty, HEA, and BMA are drifting down as a function of conversion). The reason for the ‘composition drift’ is that polymer composition is a function of not only reactivity ratios but also residual monomer fractions. Once the faster monomers are incorporated into the polymer backbone (more than the slower ones initially),

their residual amounts will be decreased, and finally, their polymer composition will be drifting towards lower levels as polymerization proceeds. Among the three fast monomers (10wt% of Sty, 20wt% of HEA, and 15wt% of BMA), Sty shows the most distinctive composition drift, which means that it is the fastest monomer because its *cross*-propagation rate constants with other radical species are largest. On the contrary, the composition of 5 wt% of AA remained almost constant and it is the slowest monomer. On the other hand, the drifting tendencies in the semi-batch reactor (Figure 7.14) were less than in the batch case (Figure 7.13). If the purpose of the semi-batch operation is to minimize the composition drift affecting polymer's physical/chemical properties, then optimizing the monomer feed profiles in Figure 7.7 will be necessary in order to control polymer composition to a more steady level.

Figures 7.15 and 7.16 exhibit the cumulative number average sequence lengths of solution *hexa*-polymerization in batch and semi-batch reactors, respectively. All the sequence lengths did not exceed 1.3. This means that the probabilities of attaching the same kinds of monomers were low in this system. The sequence lengths of the three fast monomers (Sty, HEA, and BMA) slightly decreased, while the others gradually increased during polymerization (EA and BA showed the most distinctive increases). As these residual monomers are increasing, the sequence probabilities are also expected to increase and the average lengths will be greater as well.

In Figures 7.17 to 7.21, examples of internal "hidden" variables are plotted and compared in batch and semi-batch cases. Once more, we cite these plots in order to demonstrate the wealth of information one can obtain from such a mathematical model, that otherwise may not be readily apparent. Among them, the initiator concentration profiles (Figure 7.17), overall termination rate constants (Figure 7.18), and radical concentration profiles (Figure 7.19) are highly related with one another. In the batch case, initiator decomposes and its concentration is decreasing. The overall termination rate constant in the batch case shows diffusion control regions, which are segmental (zero to about 20% conversion), translational (20% to 90%), and finally, reaction-diffusion (after 90%). Accordingly, the radical concentration increases after the onset of translational diffusion control region and decreases

again at very high conversion. On the other hand, in the semi-batch case, initiator concentration increases quickly to around 0.11 M, after which point the initiator gradually decomposes until the monomer feed is stopped. The fact that initiator is fed into the reactor keeps the initiator level in the reactor almost constant, and one can see the initiator concentration increasing at about 180 minutes, when the monomer feed ceases. The overall termination rate constant shows an increasing trend and it never seems to enter the diffusion-controlled region until about 70% conversion. The radical concentration in the semi-batch case is changing similarly to the initiator profile and also shows higher levels than the batch case.

The glass transition temperature of polymer (T_{gpoly}) is plotted in Figure 7.20 versus conversion. The profiles indicate that T_{gpoly} in batch is higher than in the semi-batch case. This is because T_{gpoly} is affected in an inverse way by the weight fractions of monomers incorporated into the polymer (see equation (3-59)), and therefore, since the fractions in the semi-batch are generally higher than in the batch case, the glass transition temperature is lower in semi-batch.

Figure 7.21 shows the average number of trifunctional branches per molecule in batch vs semi-batch reactor. Both are increasing as polymerization proceeds, but the batch case produces more branches at the early stages of the reaction, based on the accumulated weight fraction of polymer.

Finally, *hexa*-polymerization behaviour using depropagating and non-depropagating options at 140℃ are compared in Figures 7.22 to 7.24. BMA monomer is the one which depropagates at elevated temperature levels. However, due to the limited literature on multi-component systems, its kinetic parameters were unavailable and we thus assumed reasonable values for the *homo*- and *cross*-depropagation rate constants to check our model trends. The conversion levels with depropagation are lower than those with no depropagation in Figure 7.22. Accordingly, the number/weight average molecular weights with depropagation are also lower in Figures 7.23 and 7.24, which indicates that our multi-component model is in agreement with polymerization theory.

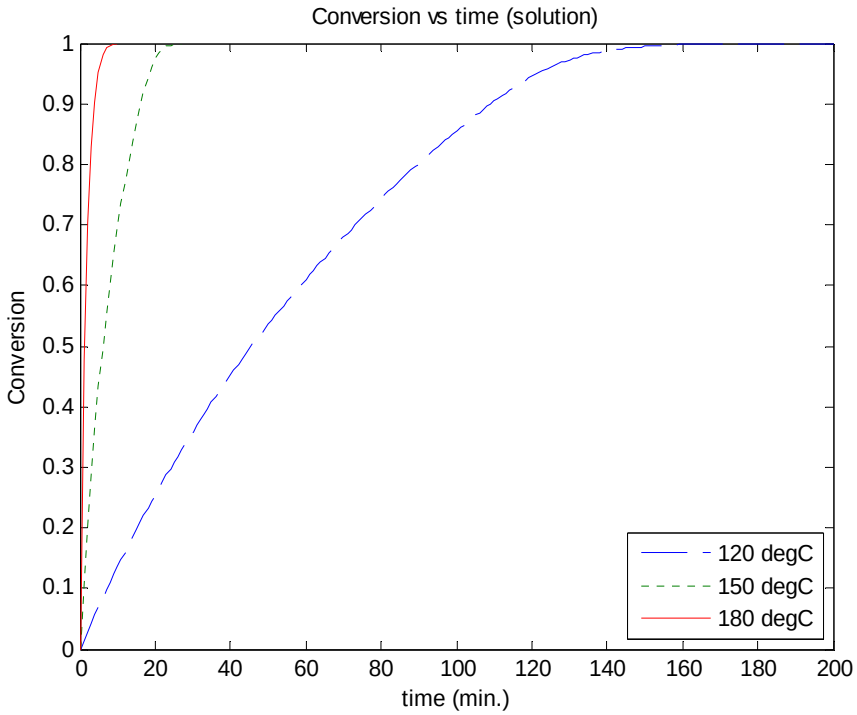

Figure 7.1. Simulation of solution *hexa*-polymerization of Sty/BA/EA/BMA/HEA/AA (10/30/20/15/20/5 wt%) m-Xylene = 60 wt%, *di-tert*-butyl peroxide = 0.6 wt% of total mixture

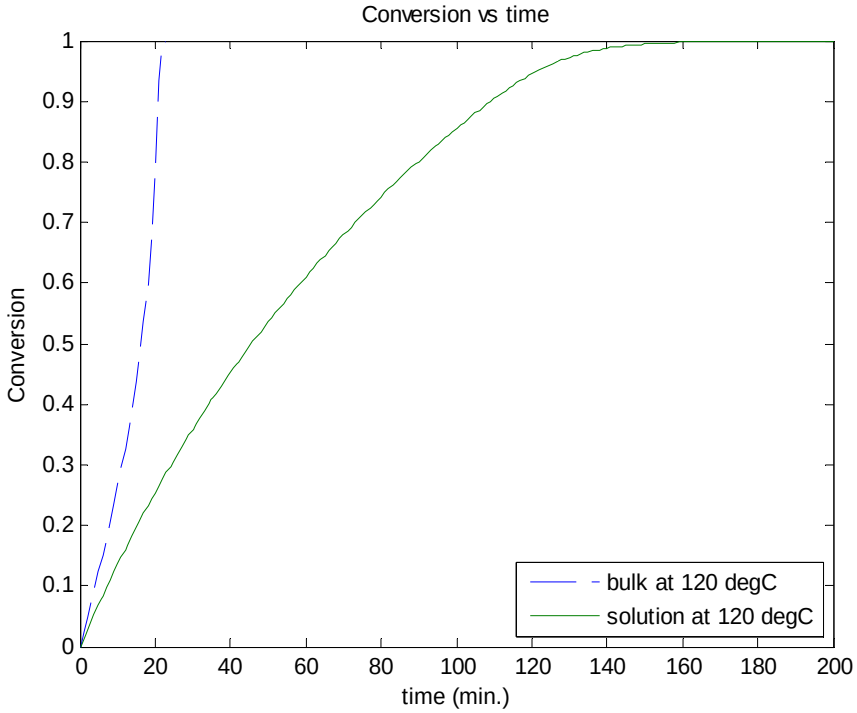

Figure 7.2. Bulk vs solution *hexa*-polymerization of Sty/BA/EA/BMA/HEA/AA (10/30/20/15/20/5 wt%) T = 120℃, m-Xylene = 60 wt% (solution case) *di-tert*-butyl peroxide = 0.6 wt% of total mixture

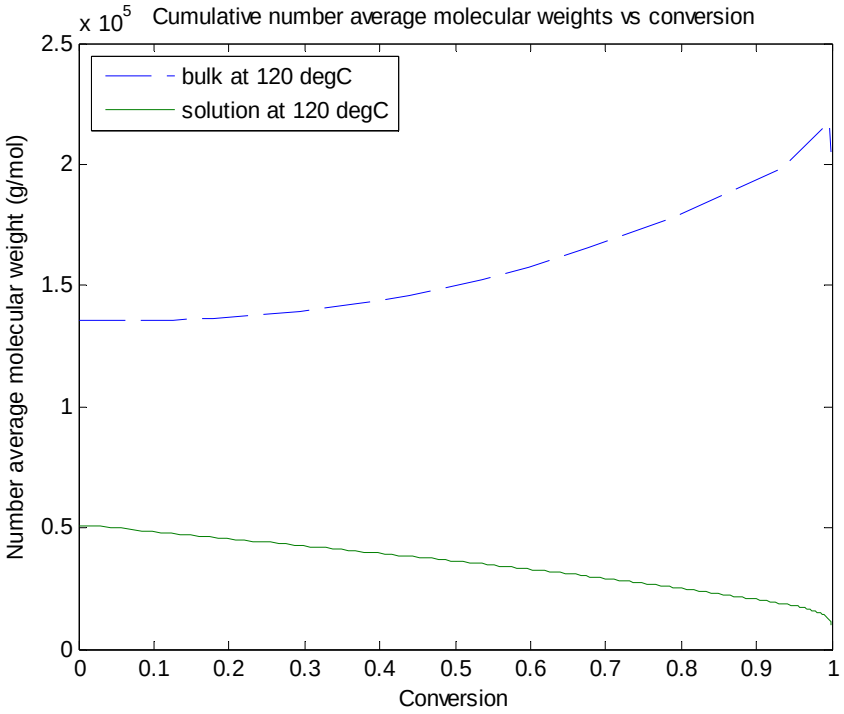

Figure 7.3. Mn of bulk and solution *hexa*-polymerization of Sty/BA/EA/BMA/HEA/AA (10/30/20/15/20/5 wt%) T = 120℃, m-Xylene = 60 wt% (solution case) *di-tert*-butyl peroxide = 0.6 wt% of total mixture

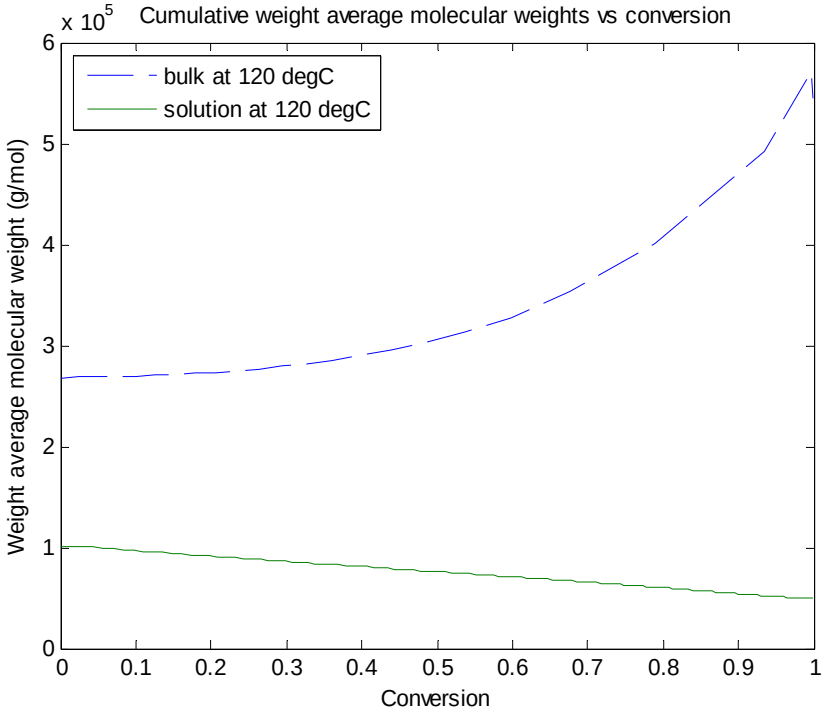

Figure 7.4. Mw of bulk and solution *hexa*-polymerization of Sty/BA/EA/BMA/HEA/AA (10/30/20/15/20/5 wt%) T = 120℃, m-Xylene = 60 wt% (solution case) *di-tert*-butyl peroxide = 0.6 wt% of total mixture

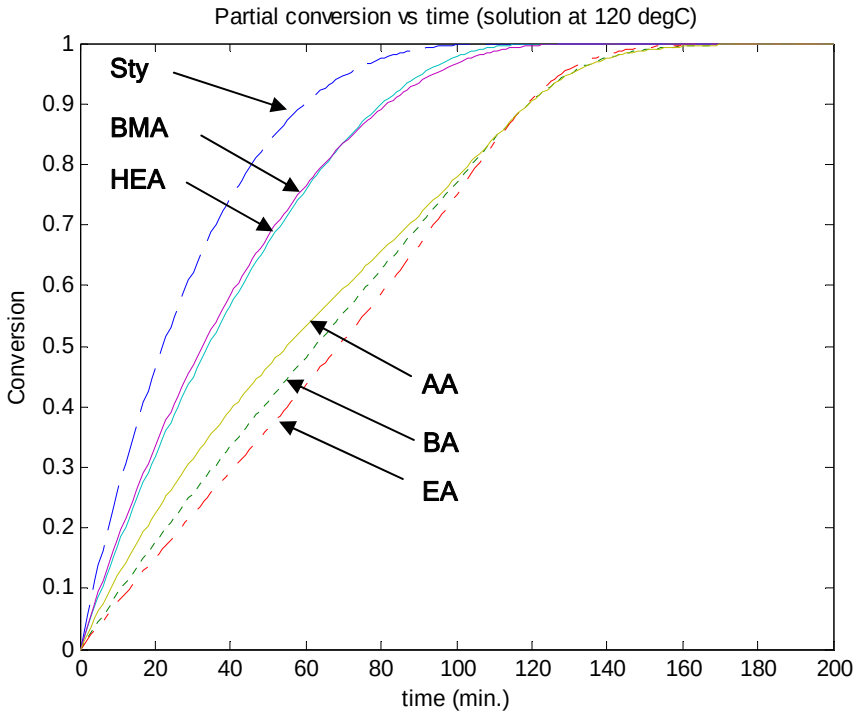

Figure 7.5. Partial conversions of solution *hexa*-polymerization of Sty/BA/EA/BMA/HEA/AA (10/30/20/15/20/5 wt%) T = 120℃, m-Xylene = 60 wt%, *di-tert*-butyl peroxide = 0.6 wt% of total mixture

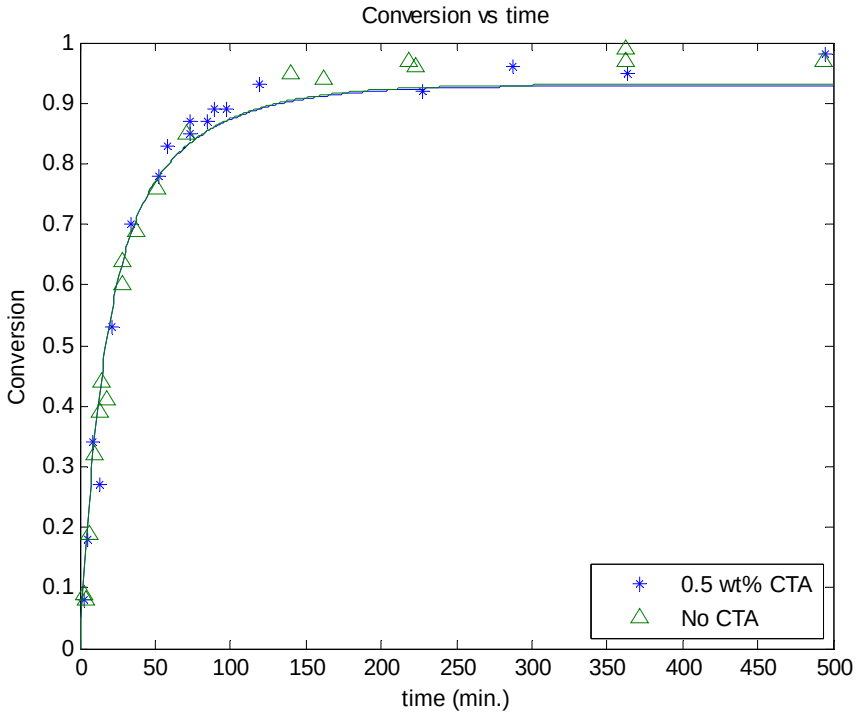

Figure 7.6. Simulation of solution *ter*-polymerization of Sty/EA/HEA (42/42/16 wt%) T = 130℃, m-Xylene = 60 wt% of total mixture, and TBPB = 1.5 wt% of total monomer

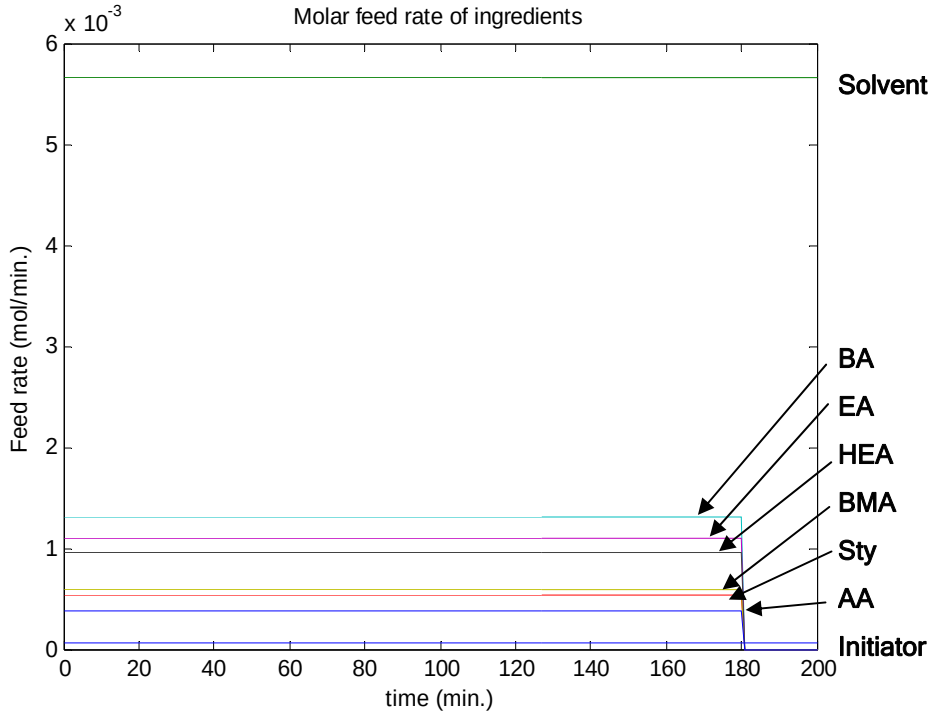

Figure 7.7. Molar feed rates of solvent, initiator, and monomers for semi-batch solution *hexa*-polymerization

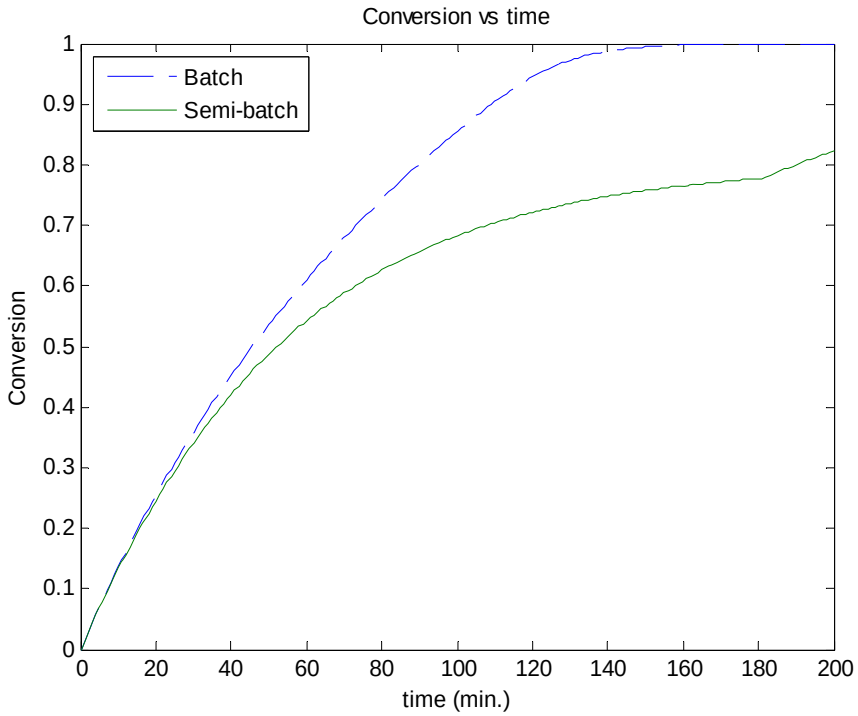

Figure 7.8. Batch vs semi-batch solution *hexa*-polymerization of Sty/BA/EA/BMA/HEA/AA (10/30/20/15/20/5 wt%) T = 120℃, according to the recipe of Figure 7.7

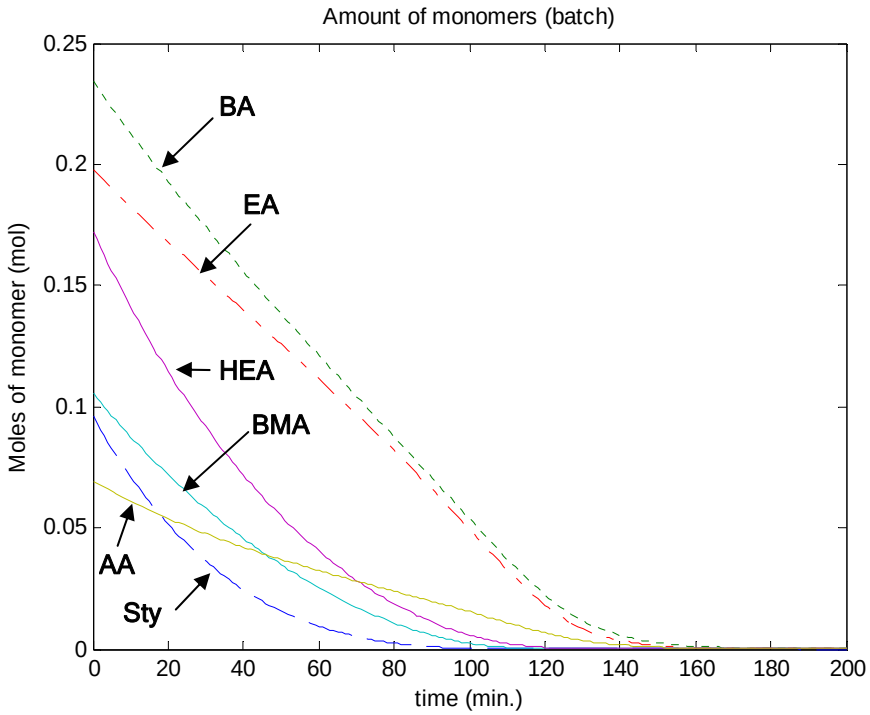

Figure 7.9. Moles of monomer profiles of Sty/BA/EA/BMA/HEA/AA (10/30/20/15/20/5 wt%) batch solution *hexa*-polymerization, T = 120℃, m-Xylene = 60 wt%, *di-tert*-butyl peroxide = 0.6 wt% of total mixture

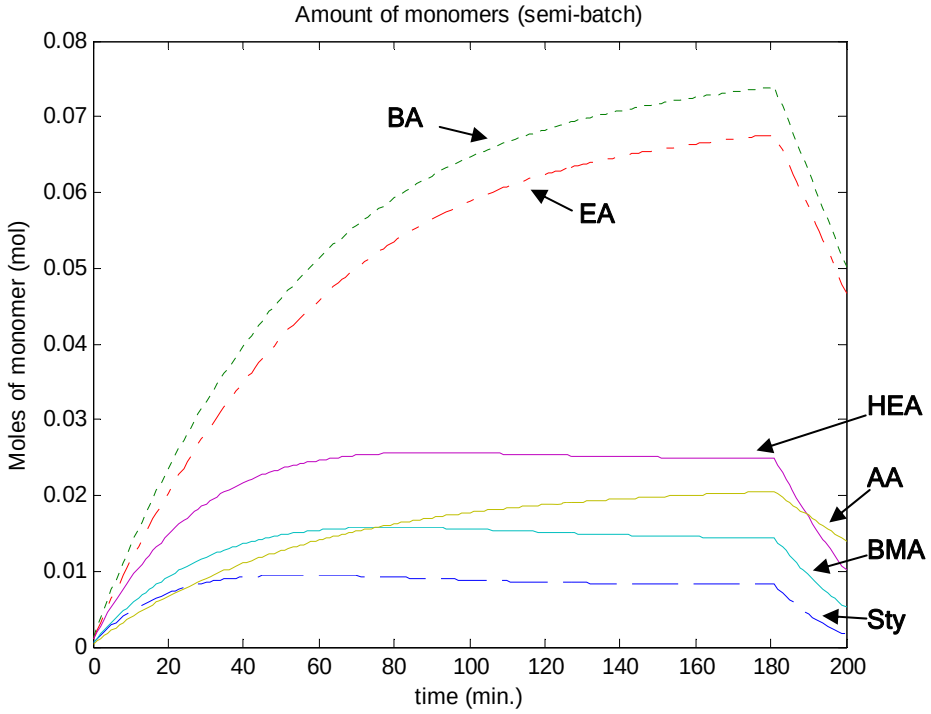

Figure 7.10. Moles of monomer profiles of Sty/BA/EA/BMA/HEA/AA (10/30/20/15/20/5 wt%) semi-batch solution *hexa*-polymerization, T = 120℃, according to the recipe of Figure 7.7

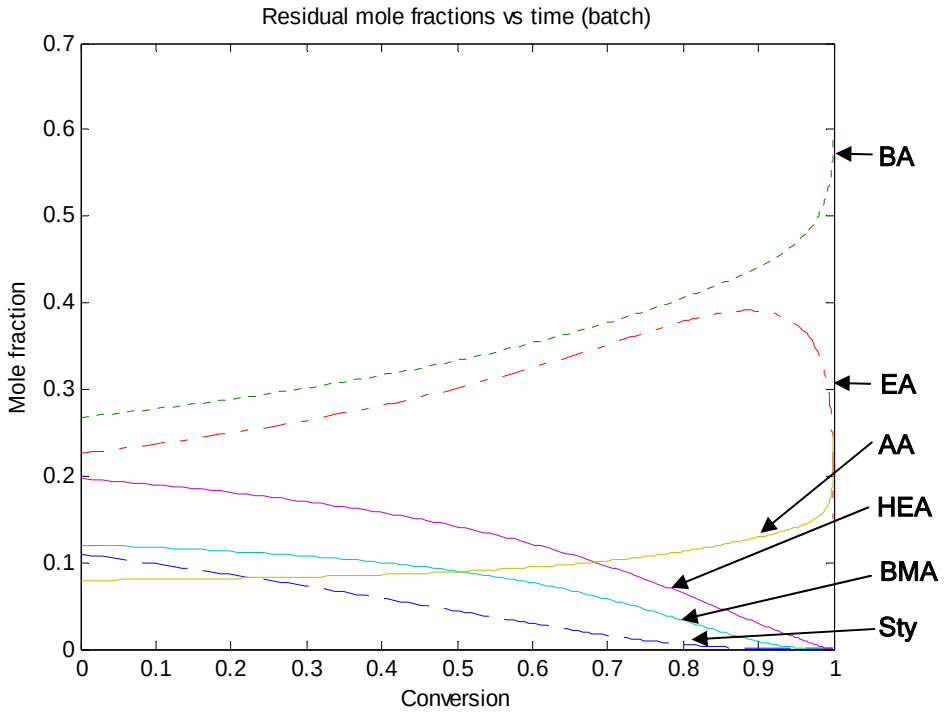

Figure 7.11. Residual monomer mole fractions of Sty/BA/EA/BMA/HEA/AA (10/30/20/15/20/5 wt%) batch solution *hexa*-polymerization, T = 120℃, m-Xylene = 60 wt%, *di-tert*-butyl peroxide = 0.6 wt% of total mixture

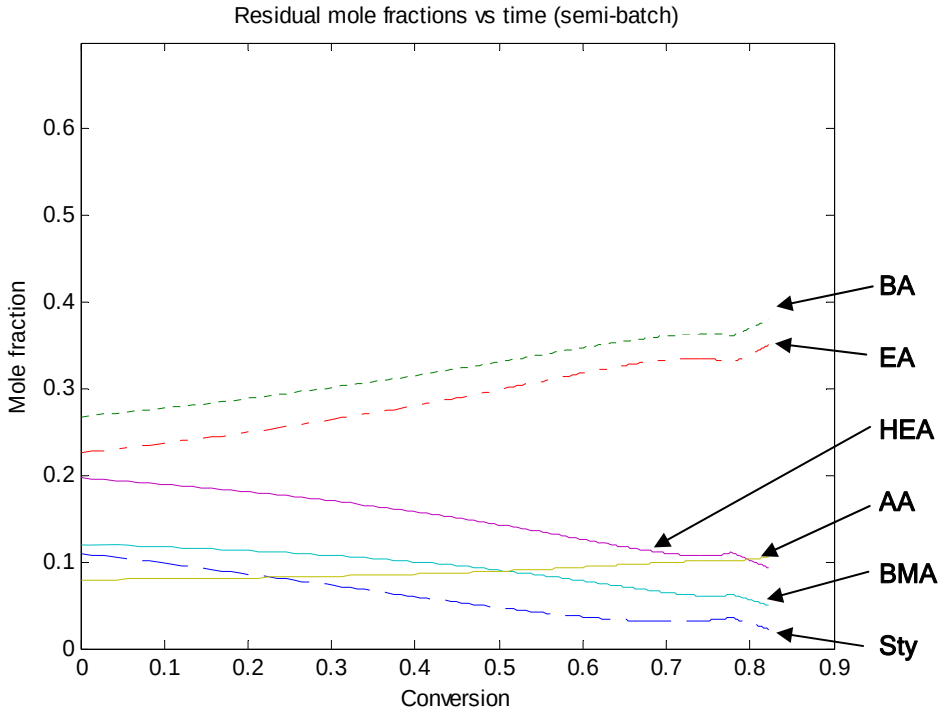

Figure 7.12. Residual monomer mole fractions of Sty/BA/EA/BMA/HEA/AA (10/30/20/15/20/5 wt%) semi-batch solution *hexa*-polymerization, T = 120℃, according to the recipe of Figure 7.7

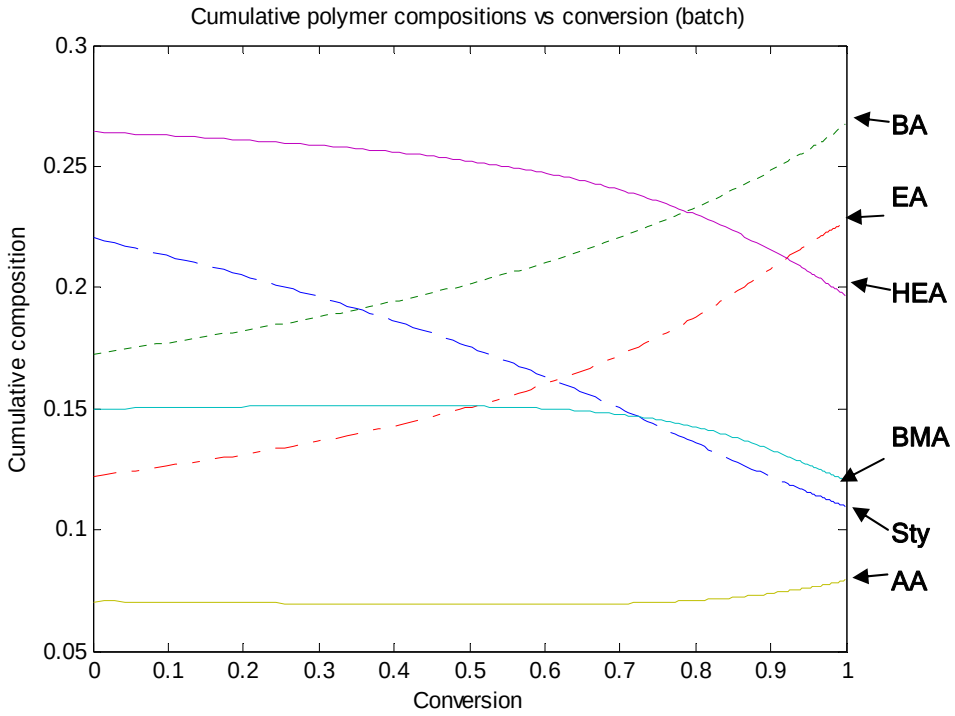

Figure 7.13. Cumulative polymer composition of Sty/BA/EA/BMA/HEA/AA (10/30/20/15/20/5 wt%) batch solution *hexa*-polymerization, T = 120℃, m-Xylene = 60 wt%, *di-tert*-butyl peroxide = 0.6 wt% of total mixture

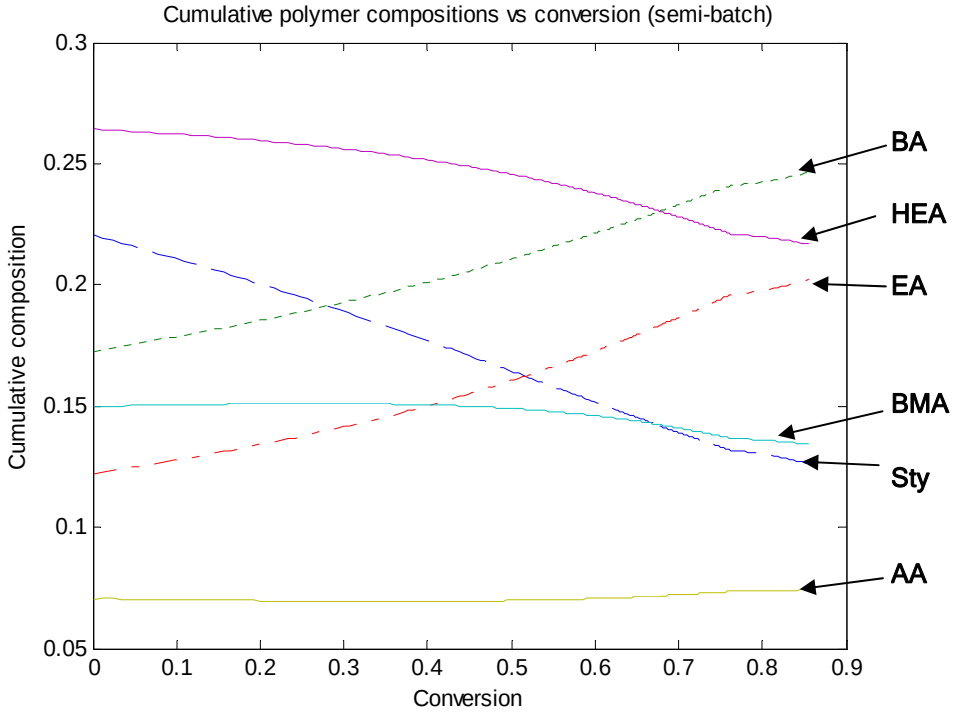

Figure 7.14. Cumulative polymer composition of Sty/BA/EA/BMA/HEA/AA (10/30/20/15/20/5 wt%) semi-batch solution *hexa*-polymerization, T = 120℃, according to the recipe of Figure 7.7

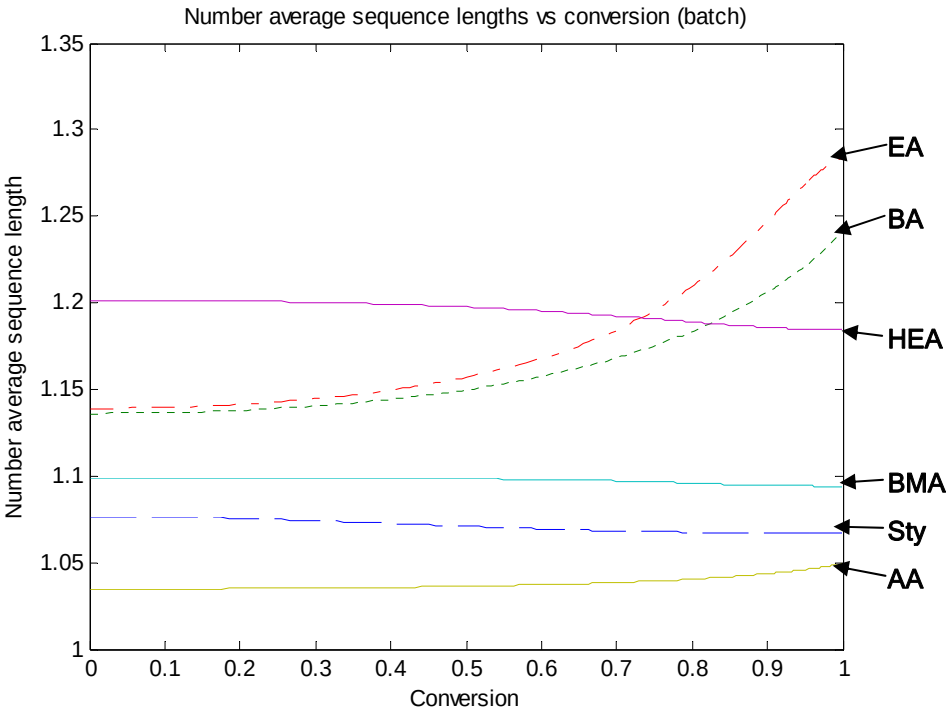

Figure 7.15. Cumulative number average sequence lengths of Sty/BA/EA/BMA/HEA/AA (10/30/20/15/20/5 wt%) batch solution *hexa*-polymerization, T = 120℃, m-Xylene = 60 wt%, *di-tert*-butyl peroxide = 0.6 wt% of total mixture

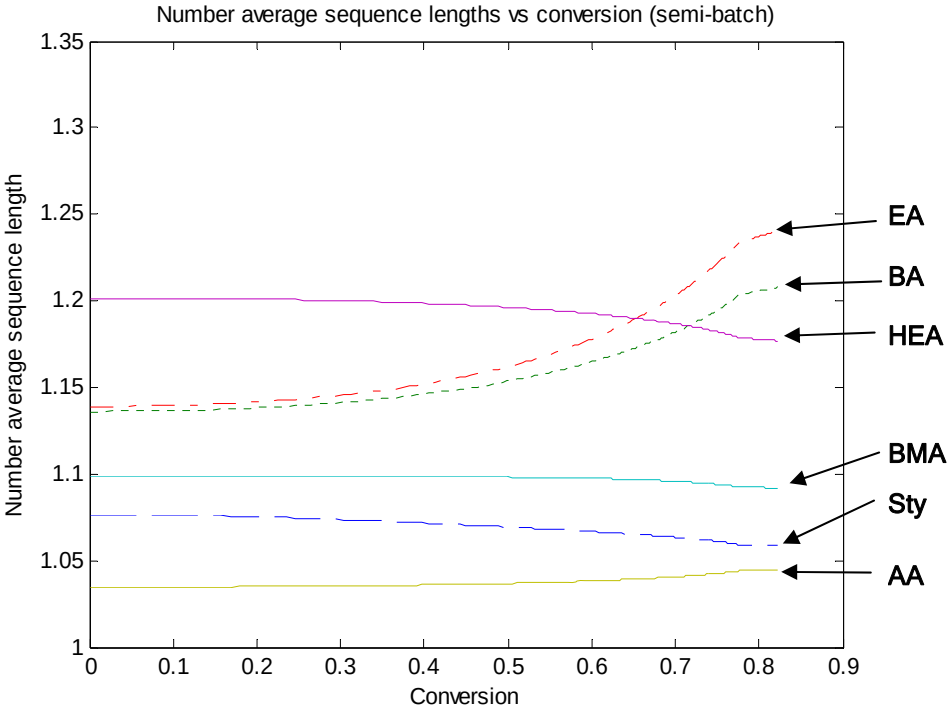

Figure 7.16. Cumulative number average sequence lengths of Sty/BA/EA/BMA/HEA/AA (10/30/20/15/20/5 wt%) semi-batch solution *hexa*-polymerization, T = 120℃, according to the recipe of Figure 7.7

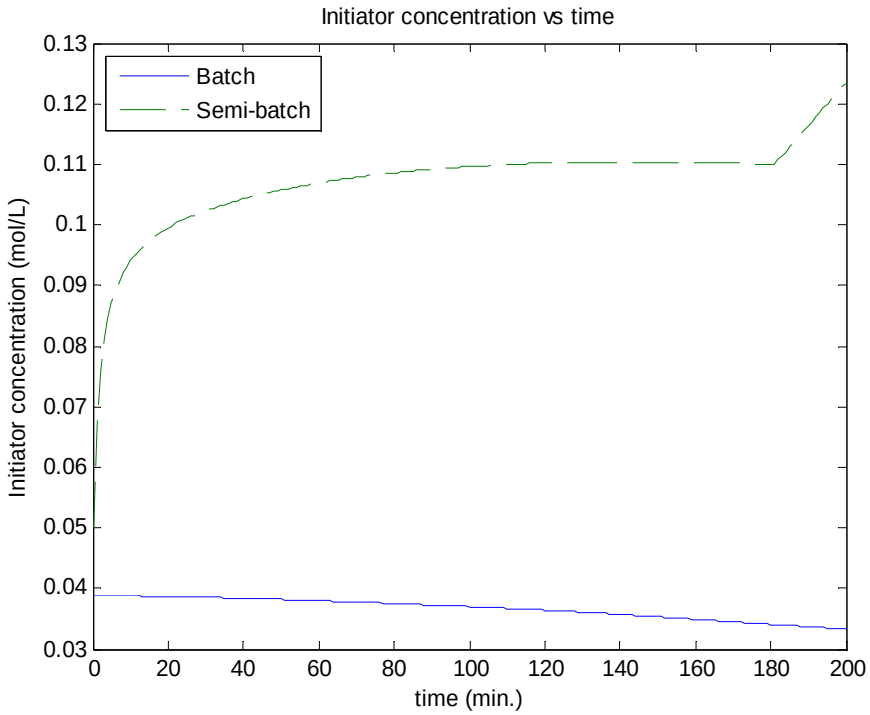

Figure 7.17. Initiator concentration profile in batch vs semi-batch reactor T= 120℃, according to the recipe of Figure 7.7

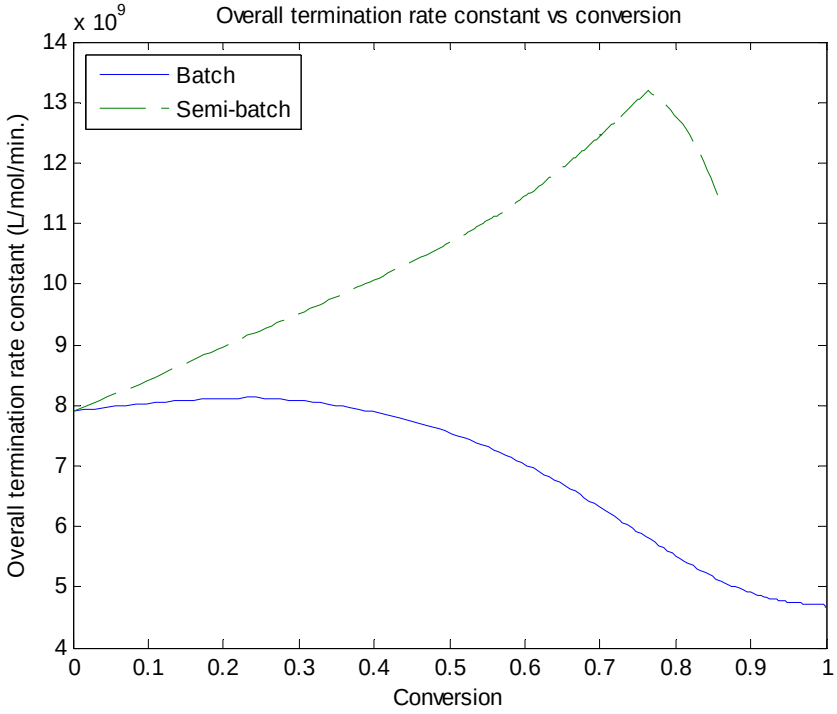

Figure 7.18. Overall termination rate constant in batch vs semi-batch reactor T = 120℃, according to the recipe of Figure 7.7

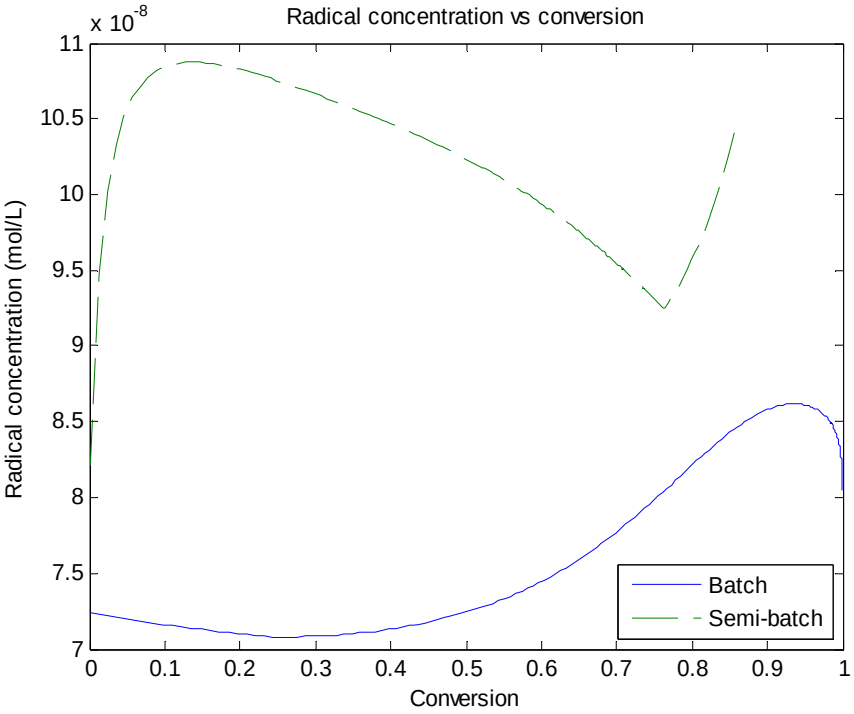

Figure 7.19. Radical concentration profile in batch vs semi-batch reactor
T = 120℃, according to the recipe of Figure 7.7

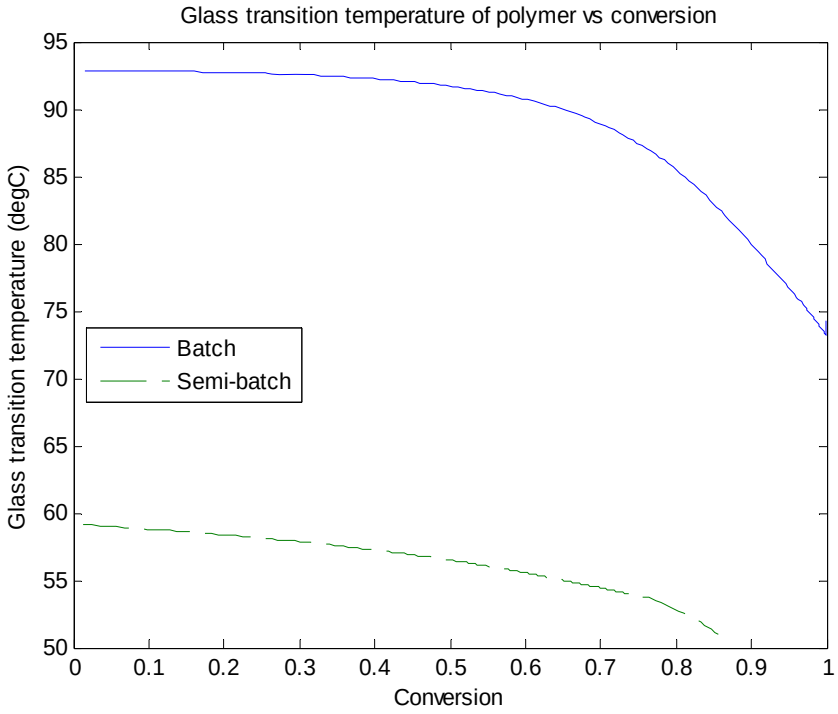

Figure 7.20. Glass transition temperature of *hexa*-polymer in batch vs semi-batch reactor
T = 120℃, according to the recipe of Figure 7.7

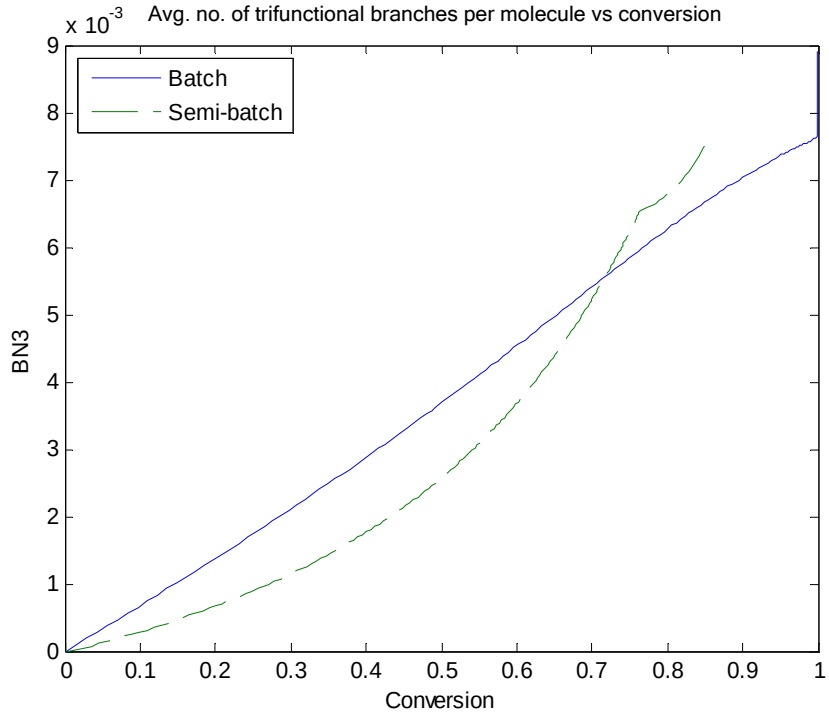

Figure 7.21. Average number of trifunctional branches per molecule in batch vs semi-batch reactor T = 120℃, according to the recipe of Figure 7.7

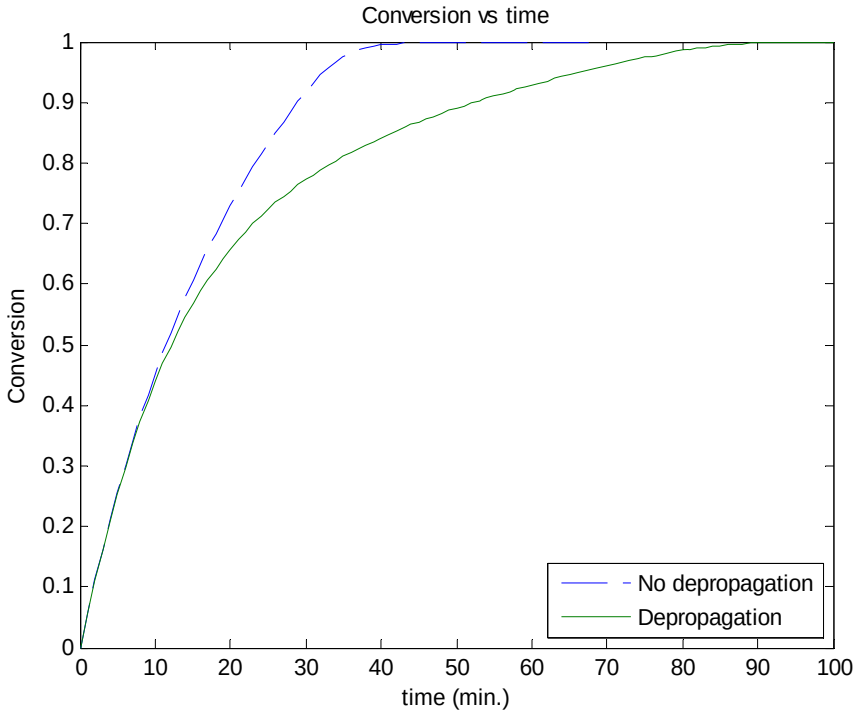

Figure 7.22. Depropagating and non-depropagating solution *hexa*-polymerization of Sty/BA/EA/BMA/HEA/AA (10/30/20/15/20/5 wt%), T = 140℃, m-Xylene = 60 wt%, *di-tert*-butyl peroxide = 0.6 wt% of total mixture

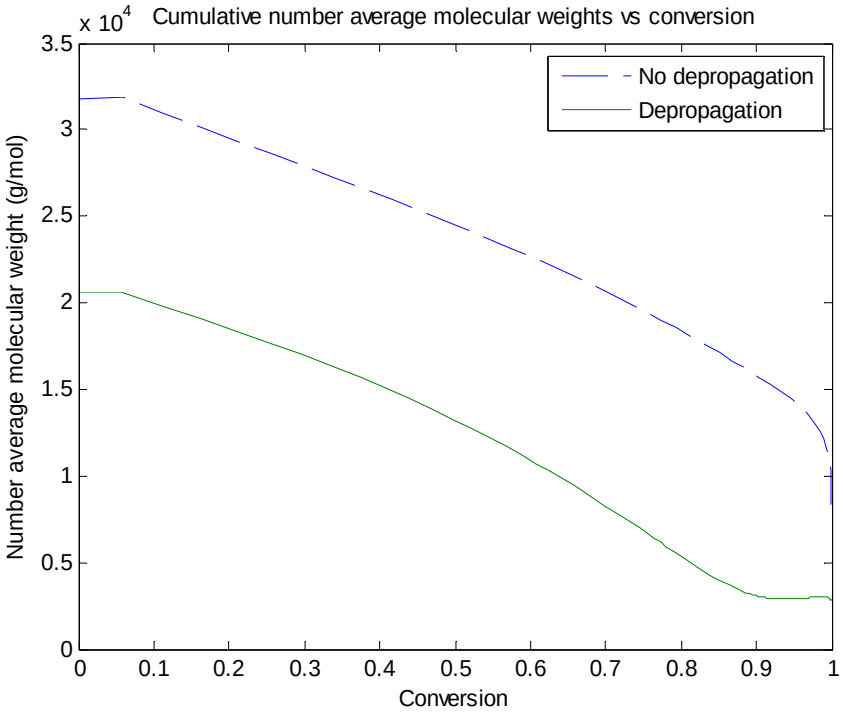

Figure 7.23. Mn of solution *hexa*-polymerization of Sty/BA/EA/BMA/HEA/AA (10/30/20/15/20/5 wt%), T = 140℃, m-Xylene = 60 wt%, *di-tert*-butyl peroxide = 0.6 wt% of total mixture

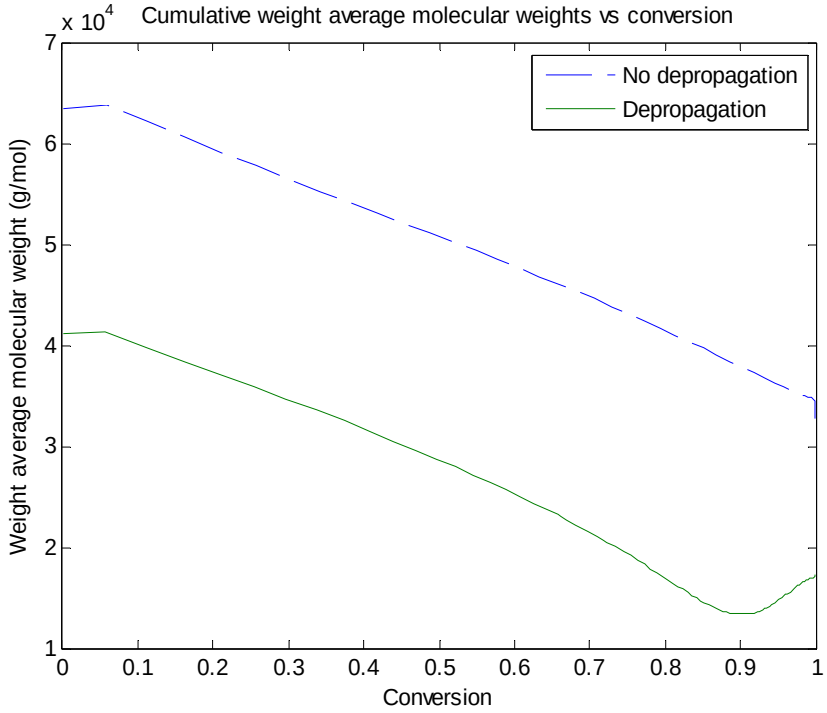

Figure 7.24. Mw of solution *hexa*-polymerization of Sty/BA/EA/BMA/HEA/AA (10/30/20/15/20/5 wt%), T = 140℃, m-Xylene = 60 wt%, di-tert-butyl peroxide = 0.6 wt% of total mixture

Chapter 8

Concluding Remarks and Recommendations

8.1 Concluding Remarks

A reactor model for batch/semi-batch multi-component bulk/solution free-radical polymerizations was developed and tested. Initially benchmarked with the WATPOLY simulator/database package (Gao and Penlidis, 1996, 1998, 2000; Chemical Engineering, University of Waterloo), the model was extended to a six-monomer system from each monomer's *homo*- and *co*-polymerization kinetic database with enhanced features. It was designed by code generalization to cover flexibly cases from *homo*- to *hexa*-polymerization, and to make future extensions easier. The idea of using a kinetic database separate from the model equations is helpful in handling the simulator program because it makes it more user-friendly and allows for versatile combinations of any monomers in the database. Of course, another contribution in parallel, equally important to developing the model equations, was to develop the accompanying detailed database of physico-chemical monomer characteristics (Appendix C).

An extensive literature search was conducted for multi-component modeling, kinetics and model testing. A general polymerization reaction mechanism was translated into a detailed mathematical model, and the equations were directly transformed into MATLAB code. Free volume theory and the pseudo kinetic rate constant method were adopted for diffusion-controlled kinetics and multi-component cases, respectively. Several options regarding polymer composition and molecular weight calculations are available in the model. In addition, polymerization behaviour options at elevated temperatures were also included:

thermal self initiation and depropagation. As a result, the developed model can predict a lot of important information over the full conversion range, such as reaction rates, molecular weights, and monomer compositions/sequences either at regular or elevated temperatures (Chapter 4).

A lot of effort has been focused on model reliability testing by comparing model predictions with various multi-component polymerization experimental data obtained from the literature. This is presented in Chapters 5 and 6. Code generalization not only increases the model flexibility in handling *homo*- to multi-component bulk and solution polymerizations, but also enables easy extensions to deal with systems composed of more than six monomers. Also, we have attempted full conversion model testing of HEA monomer systems (*homo*- to *tetra*-polymerizations) for the first time quite satisfactorily.

Our model has shown successful prediction results and proved to be useful for better understanding of the multi-component polymerization process. It will serve as an excellent tool for industrial, academic, and educational purposes.

8.2 Future Recommendations

Several recommendations for future work are suggested herein and divided into immediate and long-term steps.

8.2.1 Immediate steps

1. Full conversion depropagation model testing is required. BMA monomer is known to exhibit depropagation at high temperature and its *homo*-depropagation rate constant has been estimated by Grady *et al*. (2002). However, in multi-component polymerization, further investigations should be conducted to determine which *cross*-propagations are reversible and their rates should be determined/measured accordingly. The ability of BMA to depropagate depends upon what monomer species is attached at the penultimate position of a radical, since not all BMA

radicals in the terminal position may undergo depropagation. The extended Krüger's model developed in this thesis will be able to work effectively once these parameter values are obtained.

2. Along with depropagation, the secondary reaction mechanism (backbiting and β-scission) of acrylate monomers (BA and EA) becomes significant at elevated temperature and affects MWD due to the short chain branching (Quan *et al*., 2005). The model should be able to explain this because the amount of BA in the feed is greater than any other monomer in the recipe (Chapter 4).
3. Finally, the semi-batch part of the model could be tested further with data and different operating scenarios. In general, the basic limitation in this thesis, like in any other polymerization modeling effort, is the lack of experimental data and reliable parameter values, especially for multi-component cases (certainly for *ter*- and higher-, but also for many *co*-polymerizations).

8.2.2 Long-term steps

1. The kinetic database of HBA *homo*-polymerization and its relevant *co*-polymer reactivity ratios are required for the complete *hexa*-polymerization recipe. As more physico-chemical parameters are estimated for this monomer through experiments, further database development and model testing can be performed.
2. The kinetic parameters of AA employed by Gao (1992) are based on *homo*-polymerization experimental data in water. It is necessary to verify whether or not they are also applicable to bulk and (organic) solution polymerization in our model.
3. Further (replicate) experiments are recommended in aid of model testing for measuring average molecular weights in Sty/EA/HEA/MAA *tetra*-polymerization (Sahloul, 2004) in Chapter 6. The measured weight average molecular weights were reported considerably higher than those of Sty/EA/MAA *ter*-polymerization in Figure 6.47 under the same reaction conditions, but without any replication.

This could be clarified experimentally in the future. In addition, the persistent bias between predictions and measurements in *co*-polymer composition (as, for instance, one can see in Figure 6.46 for a Sty/EA/MAA *ter*-polymer and in Figure 6.55 for a Sty/EA/HEA/MAA *tetra*-polymer) should also be clarified/revisited (i.e. is it due to very large experimental error or due to inconsistent model parameters?).

Appendix A

Multi-component Polymer Composition Models

Several instantaneous polymer composition equations developed for multi-component polymerization cases are compared in this Appendix. The available options mentioned in Chapter 3 are the equations by rate incorporation, by the extended Walling and Briggs (WB) model, by the extended Valvassori and Sartori (VS) approach, and finally, by the extended Hocking and Klimchuk (HK) model. The extended WB model showed exactly the same results as the rate incorporation equations while certain deviations were observed with the other two approaches.

A.1 Rate incorporation equations

The model here is based on the rate of polymerization of individual monomer species. We chose it as a criterion for model testing because it is the mathematical definition of multi-component polymer composition.

$$R_{pj} = \left(\sum_{i=1}^{6} k_{pij} [R_i \cdot] \right) [M_j]$$
$$R_p = \sum_{j=1}^{6} R_{pj} \tag{A-1}$$

$$F_j = \frac{R_{pj}}{R_p} = \frac{\left(\sum_{i=1}^{6} k_{pij} \Phi_i^{\bullet} \right) f_j}{\sum_{i=1}^{6} \sum_{j=1}^{6} \left(k_{pij} \Phi_i^{\bullet} f_j \right)} \tag{A-2}$$

A.2 Extended Walling and Briggs (WB) model

This is an extension of the *ter*-polymer composition equation from Walling and Briggs (1945). The symbol |**A**| below stands for the determinant of the corresponding matrix **A**.

$$d[M_1]=[M_1]\begin{vmatrix} -\frac{1}{r_{61}} & \frac{1}{r_{21}} & \frac{1}{r_{31}} & \frac{1}{r_{41}} & \frac{1}{r_{51}} \\ -\frac{[M_2]}{r_{62}} & A & \frac{[M_2]}{r_{32}} & \frac{[M_2]}{r_{42}} & \frac{[M_2]}{r_{52}} \\ -\frac{[M_3]}{r_{63}} & \frac{[M_3]}{r_{23}} & B & \frac{[M_3]}{r_{43}} & \frac{[M_3]}{r_{53}} \\ -\frac{[M_4]}{r_{64}} & \frac{[M_4]}{r_{24}} & \frac{[M_4]}{r_{34}} & C & \frac{[M_4]}{r_{54}} \\ -\frac{[M_5]}{r_{65}} & \frac{[M_5]}{r_{25}} & \frac{[M_5]}{r_{35}} & \frac{[M_5]}{r_{45}} & D \end{vmatrix} \left\{[M_1]+\frac{[M_2]}{r_{12}}+\frac{[M_3]}{r_{13}}+\frac{[M_4]}{r_{14}}+\frac{[M_5]}{r_{15}}+\frac{[M_6]}{r_{16}}\right\} \quad \text{(A-3)}$$

where:

$$A=-\left(\frac{[M_1]}{r_{21}}+\frac{[M_3]}{r_{23}}+\frac{[M_4]}{r_{24}}+\frac{[M_5]}{r_{25}}+\frac{[M_6]}{r_{26}}\right),\ B=-\left(\frac{[M_1]}{r_{31}}+\frac{[M_2]}{r_{32}}+\frac{[M_4]}{r_{34}}+\frac{[M_5]}{r_{35}}+\frac{[M_6]}{r_{36}}\right)$$

$$C=-\left(\frac{[M_1]}{r_{41}}+\frac{[M_2]}{r_{42}}+\frac{[M_3]}{r_{43}}+\frac{[M_5]}{r_{45}}+\frac{[M_6]}{r_{46}}\right),\ D=-\left(\frac{[M_1]}{r_{51}}+\frac{[M_2]}{r_{52}}+\frac{[M_3]}{r_{53}}+\frac{[M_4]}{r_{54}}+\frac{[M_6]}{r_{36}}\right)$$

$$d[M_2]=[M_2]\begin{vmatrix} -\frac{1}{r_{12}} & \frac{1}{r_{32}} & \frac{1}{r_{42}} & \frac{1}{r_{52}} & \frac{1}{r_{62}} \\ -\frac{[M_3]}{r_{13}} & E & \frac{[M_3]}{r_{43}} & \frac{[M_3]}{r_{53}} & \frac{[M_3]}{r_{63}} \\ -\frac{[M_4]}{r_{14}} & \frac{[M_4]}{r_{34}} & F & \frac{[M_4]}{r_{54}} & \frac{[M_4]}{r_{64}} \\ -\frac{[M_5]}{r_{15}} & \frac{[M_5]}{r_{35}} & \frac{[M_5]}{r_{45}} & G & \frac{[M_5]}{r_{65}} \\ -\frac{[M_6]}{r_{16}} & \frac{[M_6]}{r_{36}} & \frac{[M_6]}{r_{46}} & \frac{[M_6]}{r_{56}} & H \end{vmatrix} \left\{[M_2]+\frac{[M_1]}{r_{21}}+\frac{[M_3]}{r_{23}}+\frac{[M_4]}{r_{24}}+\frac{[M_5]}{r_{25}}+\frac{[M_6]}{r_{26}}\right\} \quad \text{(A-4)}$$

where:

$$E=-\left(\frac{[M_1]}{r_{31}}+\frac{[M_2]}{r_{32}}+\frac{[M_4]}{r_{34}}+\frac{[M_5]}{r_{35}}+\frac{[M_6]}{r_{36}}\right),\ F=-\left(\frac{[M_1]}{r_{41}}+\frac{[M_2]}{r_{42}}+\frac{[M_3]}{r_{43}}+\frac{[M_5]}{r_{45}}+\frac{[M_6]}{r_{46}}\right)$$

$$G=-\left(\frac{[M_1]}{r_{51}}+\frac{[M_2]}{r_{52}}+\frac{[M_3]}{r_{53}}+\frac{[M_4]}{r_{54}}+\frac{[M_6]}{r_{56}}\right),\ G=-\left(\frac{[M_1]}{r_{61}}+\frac{[M_2]}{r_{62}}+\frac{[M_3]}{r_{63}}+\frac{[M_4]}{r_{64}}+\frac{[M_5]}{r_{65}}\right)$$

$$d[M_3]=[M_3]\begin{vmatrix} -\frac{1}{r_{23}} & \frac{1}{r_{43}} & \frac{1}{r_{53}} & \frac{1}{r_{63}} & \frac{1}{r_{13}} \\ -\frac{[M_4]}{r_{24}} & I & \frac{[M_4]}{r_{54}} & \frac{[M_4]}{r_{64}} & \frac{[M_4]}{r_{14}} \\ -\frac{[M_5]}{r_{25}} & \frac{[M_5]}{r_{45}} & J & \frac{[M_5]}{r_{65}} & \frac{[M_5]}{r_{15}} \\ -\frac{[M_6]}{r_{26}} & \frac{[M_6]}{r_{46}} & \frac{[M_6]}{r_{56}} & K & \frac{[M_6]}{r_{16}} \\ -\frac{[M_1]}{r_{21}} & \frac{[M_1]}{r_{41}} & \frac{[M_1]}{r_{51}} & \frac{[M_1]}{r_{61}} & L \end{vmatrix}\left\{[M_3]+\frac{[M_1]}{r_{31}}+\frac{[M_2]}{r_{32}}+\frac{[M_4]}{r_{34}}+\frac{[M_5]}{r_{35}}+\frac{[M_6]}{r_{36}}\right\} \quad \text{(A-5)}$$

where:

$$I=-\left(\frac{[M_1]}{r_{41}}+\frac{[M_2]}{r_{42}}+\frac{[M_3]}{r_{43}}+\frac{[M_5]}{r_{45}}+\frac{[M_6]}{r_{46}}\right),\ J=-\left(\frac{[M_1]}{r_{51}}+\frac{[M_2]}{r_{52}}+\frac{[M_3]}{r_{53}}+\frac{[M_4]}{r_{54}}+\frac{[M_6]}{r_{56}}\right)$$

$$K=-\left(\frac{[M_1]}{r_{61}}+\frac{[M_2]}{r_{62}}+\frac{[M_3]}{r_{63}}+\frac{[M_4]}{r_{64}}+\frac{[M_5]}{r_{65}}\right),\ L=-\left(\frac{[M_2]}{r_{12}}+\frac{[M_3]}{r_{13}}+\frac{[M_4]}{r_{14}}+\frac{[M_5]}{r_{15}}+\frac{[M_6]}{r_{16}}\right)$$

$$d[M_4]=[M_4]\begin{vmatrix} -\frac{1}{r_{34}} & \frac{1}{r_{54}} & \frac{1}{r_{64}} & \frac{1}{r_{14}} & \frac{1}{r_{24}} \\ -\frac{[M_5]}{r_{35}} & M & \frac{[M_5]}{r_{65}} & \frac{[M_5]}{r_{15}} & \frac{[M_5]}{r_{25}} \\ -\frac{[M_6]}{r_{36}} & \frac{[M_6]}{r_{56}} & N & \frac{[M_6]}{r_{16}} & \frac{[M_6]}{r_{26}} \\ -\frac{[M_1]}{r_{31}} & \frac{[M_1]}{r_{51}} & \frac{[M_1]}{r_{61}} & O & \frac{[M_1]}{r_{21}} \\ -\frac{[M_2]}{r_{32}} & \frac{[M_2]}{r_{52}} & \frac{[M_2]}{r_{62}} & \frac{[M_2]}{r_{12}} & P \end{vmatrix}\left\{[M_4]+\frac{[M_1]}{r_{41}}+\frac{[M_2]}{r_{42}}+\frac{[M_3]}{r_{43}}+\frac{[M_5]}{r_{45}}+\frac{[M_6]}{r_{46}}\right\} \quad \text{(A-6)}$$

where:

$$M=-\left(\frac{[M_1]}{r_{51}}+\frac{[M_2]}{r_{52}}+\frac{[M_3]}{r_{53}}+\frac{[M_4]}{r_{54}}+\frac{[M_6]}{r_{56}}\right),\ N=-\left(\frac{[M_1]}{r_{61}}+\frac{[M_2]}{r_{62}}+\frac{[M_3]}{r_{63}}+\frac{[M_4]}{r_{64}}+\frac{[M_5]}{r_{65}}\right)$$

$$O=-\left(\frac{[M_2]}{r_{12}}+\frac{[M_3]}{r_{13}}+\frac{[M_4]}{r_{14}}+\frac{[M_5]}{r_{15}}+\frac{[M_6]}{r_{16}}\right),\ P=-\left(\frac{[M_1]}{r_{21}}+\frac{[M_3]}{r_{23}}+\frac{[M_4]}{r_{24}}+\frac{[M_5]}{r_{25}}+\frac{[M_6]}{r_{26}}\right)$$

$$d[M_5]=[M_5]\begin{vmatrix} -\frac{1}{r_{45}} & \frac{1}{r_{65}} & \frac{1}{r_{15}} & \frac{1}{r_{25}} & \frac{1}{r_{35}} \\ -\frac{[M_6]}{r_{46}} & Q & \frac{[M_6]}{r_{16}} & \frac{[M_6]}{r_{26}} & \frac{[M_6]}{r_{36}} \\ -\frac{[M_1]}{r_{41}} & \frac{[M_1]}{r_{61}} & R & \frac{[M_1]}{r_{21}} & \frac{[M_1]}{r_{31}} \\ -\frac{[M_2]}{r_{42}} & \frac{[M_2]}{r_{62}} & \frac{[M_2]}{r_{12}} & S & \frac{[M_2]}{r_{32}} \\ -\frac{[M_3]}{r_{43}} & \frac{[M_3]}{r_{63}} & \frac{[M_3]}{r_{13}} & \frac{[M_3]}{r_{23}} & T \end{vmatrix}\left\{[M_5]+\frac{[M_1]}{r_{51}}+\frac{[M_2]}{r_{52}}+\frac{[M_3]}{r_{53}}+\frac{[M_4]}{r_{54}}+\frac{[M_6]}{r_{56}}\right\} \quad \text{(A-7)}$$

where:

$$Q=-\left(\frac{[M_1]}{r_{61}}+\frac{[M_2]}{r_{62}}+\frac{[M_3]}{r_{63}}+\frac{[M_4]}{r_{64}}+\frac{[M_5]}{r_{65}}\right),\ R=-\left(\frac{[M_2]}{r_{12}}+\frac{[M_3]}{r_{13}}+\frac{[M_4]}{r_{14}}+\frac{[M_5]}{r_{15}}+\frac{[M_6]}{r_{16}}\right)$$

$$S=-\left(\frac{[M_1]}{r_{21}}+\frac{[M_3]}{r_{23}}+\frac{[M_4]}{r_{24}}+\frac{[M_5]}{r_{25}}+\frac{[M_6]}{r_{26}}\right),\ T=-\left(\frac{[M_1]}{r_{31}}+\frac{[M_2]}{r_{32}}+\frac{[M_4]}{r_{34}}+\frac{[M_5]}{r_{35}}+\frac{[M_6]}{r_{36}}\right)$$

$$d[M_6]=[M_6]\begin{vmatrix} -\frac{1}{r_{56}} & \frac{1}{r_{16}} & \frac{1}{r_{26}} & \frac{1}{r_{36}} & \frac{1}{r_{46}} \\ -\frac{[M_1]}{r_{51}} & U & \frac{[M_1]}{r_{21}} & \frac{[M_1]}{r_{31}} & \frac{[M_1]}{r_{41}} \\ -\frac{[M_2]}{r_{52}} & \frac{[M_2]}{r_{12}} & V & \frac{[M_2]}{r_{32}} & \frac{[M_2]}{r_{42}} \\ -\frac{[M_3]}{r_{53}} & \frac{[M_3]}{r_{13}} & \frac{[M_3]}{r_{23}} & W & \frac{[M_3]}{r_{43}} \\ -\frac{[M_4]}{r_{54}} & \frac{[M_4]}{r_{14}} & \frac{[M_4]}{r_{24}} & \frac{[M_4]}{r_{34}} & X \end{vmatrix}\left\{[M_6]+\frac{[M_1]}{r_{61}}+\frac{[M_2]}{r_{62}}+\frac{[M_3]}{r_{63}}+\frac{[M_4]}{r_{64}}+\frac{[M_5]}{r_{65}}\right\} \quad \text{(A-8)}$$

where:

$$U=-\left(\frac{[M_2]}{r_{12}}+\frac{[M_3]}{r_{13}}+\frac{[M_4]}{r_{14}}+\frac{[M_5]}{r_{15}}+\frac{[M_6]}{r_{16}}\right),\ V=-\left(\frac{[M_1]}{r_{21}}+\frac{[M_3]}{r_{23}}+\frac{[M_4]}{r_{24}}+\frac{[M_5]}{r_{25}}+\frac{[M_6]}{r_{26}}\right)$$

$$W=-\left(\frac{[M_1]}{r_{31}}+\frac{[M_2]}{r_{32}}+\frac{[M_4]}{r_{34}}+\frac{[M_5]}{r_{35}}+\frac{[M_6]}{r_{36}}\right),\ X=-\left(\frac{[M_1]}{r_{41}}+\frac{[M_2]}{r_{42}}+\frac{[M_3]}{r_{43}}+\frac{[M_5]}{r_{45}}+\frac{[M_6]}{r_{46}}\right)$$

The multi-component polymer composition is calculated by,

$$F_i=d[M_i]/\sum_{i=1}^{6}d[M_i] \quad \text{(A-9)}$$

A.3 Extended Valvassori and Sartori (VS) model

This is an extension of the *ter*-polymer composition equation by Valvassori and Sartori (1967) to a six monomer system, which is simpler and more readily extendable than the WB equation (1945), due to certain approximations.

$$d[M_1] = [M_1]\left\{[M_1] + \frac{[M_2]}{r_{12}} + \frac{[M_3]}{r_{13}} + \frac{[M_4]}{r_{14}} + \frac{[M_5]}{r_{15}} + \frac{[M_6]}{r_{16}}\right\} \tag{A-10}$$

$$d[M_2] = \frac{[M_2]}{r_{12}} r_{21}\left\{\frac{[M_1]}{r_{21}} + [M_2] + \frac{[M_3]}{r_{23}} + \frac{[M_4]}{r_{24}} + \frac{[M_5]}{r_{25}} + \frac{[M_6]}{r_{26}}\right\} \tag{A-11}$$

$$d[M_3] = \frac{[M_3]}{r_{13}} r_{31}\left\{\frac{[M_1]}{r_{31}} + \frac{[M_2]}{r_{32}} + [M_3] + \frac{[M_4]}{r_{34}} + \frac{[M_5]}{r_{35}} + \frac{[M_6]}{r_{36}}\right\} \tag{A-12}$$

$$d[M_4] = \frac{[M_4]}{r_{14}} r_{41}\left\{\frac{[M_1]}{r_{41}} + \frac{[M_2]}{r_{42}} + \frac{[M_3]}{r_{43}} + [M_4] + \frac{[M_5]}{r_{45}} + \frac{[M_6]}{r_{46}}\right\} \tag{A-13}$$

$$d[M_5] = \frac{[M_5]}{r_{15}} r_{51}\left\{\frac{[M_1]}{r_{51}} + \frac{[M_2]}{r_{52}} + \frac{[M_3]}{r_{53}} + \frac{[M_4]}{r_{54}} + [M_5] + \frac{[M_6]}{r_{56}}\right\} \tag{A-14}$$

$$d[M_6] = \frac{[M_6]}{r_{16}} r_{61}\left\{\frac{[M_1]}{r_{61}} + \frac{[M_2]}{r_{62}} + \frac{[M_3]}{r_{63}} + \frac{[M_4]}{r_{64}} + \frac{[M_5]}{r_{65}} + [M_6]\right\} \tag{A-15}$$

A.4 Extended Hocking and Klimchuk (HK) model

This is an extension of the *ter*-polymer composition equation by Hocking and Klimchuk (1996) to a six monomer system. This is considered as a more refined version of the VS equations above.

$$d[M_1] = [M_1]\left\{[M_1] + \frac{[M_2]}{r_{12}} + \frac{[M_3]}{r_{13}} + \frac{[M_4]}{r_{14}} + \frac{[M_5]}{r_{15}} + \frac{[M_6]}{r_{16}}\right\}\left\{1 + \frac{r_{12}}{r_{21}} + \frac{r_{13}}{r_{31}} + \frac{r_{14}}{r_{41}} + \frac{r_{15}}{r_{51}} + \frac{r_{16}}{r_{61}}\right\} \tag{A-16}$$

$$d[M_2] = [M_2]\left\{[M_2] + \frac{[M_3]}{r_{23}} + \frac{[M_4]}{r_{24}} + \frac{[M_5]}{r_{25}} + \frac{[M_6]}{r_{26}} + \frac{[M_1]}{r_{21}}\right\}\left\{\frac{r_{21}}{r_{12}} + 1 + \frac{r_{23}}{r_{32}} + \frac{r_{24}}{r_{42}} + \frac{r_{25}}{r_{52}} + \frac{r_{26}}{r_{62}}\right\} \tag{A-17}$$

$$d[M_3]=[M_3]\left\{[M_3]+\frac{[M_4]}{r_{34}}+\frac{[M_5]}{r_{35}}+\frac{[M_6]}{r_{36}}+\frac{[M_1]}{r_{31}}+\frac{[M_2]}{r_{32}}\right\}\left\{\frac{r_{31}}{r_{13}}+\frac{r_{32}}{r_{23}}+1+\frac{r_{34}}{r_{43}}+\frac{r_{35}}{r_{53}}+\frac{r_{36}}{r_{63}}\right\} \quad \text{(A-18)}$$

$$d[M_4]=[M_4]\left\{[M_4]+\frac{[M_5]}{r_{45}}+\frac{[M_6]}{r_{46}}+\frac{[M_1]}{r_{41}}+\frac{[M_2]}{r_{42}}+\frac{[M_3]}{r_{43}}\right\}\left\{\frac{r_{41}}{r_{14}}+\frac{r_{42}}{r_{24}}+\frac{r_{43}}{r_{34}}+1+\frac{r_{45}}{r_{54}}+\frac{r_{46}}{r_{64}}\right\} \quad \text{(A-19)}$$

$$d[M_5]=[M_5]\left\{[M_5]+\frac{[M_6]}{r_{56}}+\frac{[M_1]}{r_{51}}+\frac{[M_2]}{r_{52}}+\frac{[M_3]}{r_{53}}+\frac{[M_4]}{r_{54}}\right\}\left\{\frac{r_{51}}{r_{15}}+\frac{r_{52}}{r_{25}}+\frac{r_{53}}{r_{35}}+\frac{r_{54}}{r_{45}}+1+\frac{r_{56}}{r_{65}}\right\} \quad \text{(A-20)}$$

$$d[M_6]=[M_6]\left\{[M_6]+\frac{[M_1]}{r_{61}}+\frac{[M_2]}{r_{62}}+\frac{[M_3]}{r_{63}}+\frac{[M_4]}{r_{64}}+\frac{[M_5]}{r_{65}}\right\}\left\{\frac{r_{61}}{r_{16}}+\frac{r_{62}}{r_{26}}+\frac{r_{63}}{r_{36}}+\frac{r_{64}}{r_{46}}+\frac{r_{65}}{r_{56}}+1\right\} \quad \text{(A-21)}$$

A.5 Simulation results and discussion

Model simulation results of the instantaneous multi-component polymer composition of Sty over the full conversion range are presented in Figures A.1 to A.3. All of the models are successfully reduced to simpler monomer cases (*co*-polymerization in Figure A.1, *ter*-polymerization in Figure A.2, and *tetra*-polymerization in Figure A.3), although some differences are observed.

In Figure A.1, the HK model showed slightly higher values than the other ones, but the differences were not significant. On the other hand, in Figures A.2 and A.3, the VS result was located higher and the HK lower than the rate incorporation approach, but again the discrepancies were not considerable. The composition profile by the rate incorporation model completely overlapped with the one by the WB model in Figures A.1 to A.3, which means that the two equations give identical results with each other.

Comparing the composition trends, the differences among the four models are not significantly large relative to typically encountered experimental errors. The rate incorporation composition model is chosen as the default option in our model. Of course, the equations can easily be extended from six to more components, considering the equation patterns.

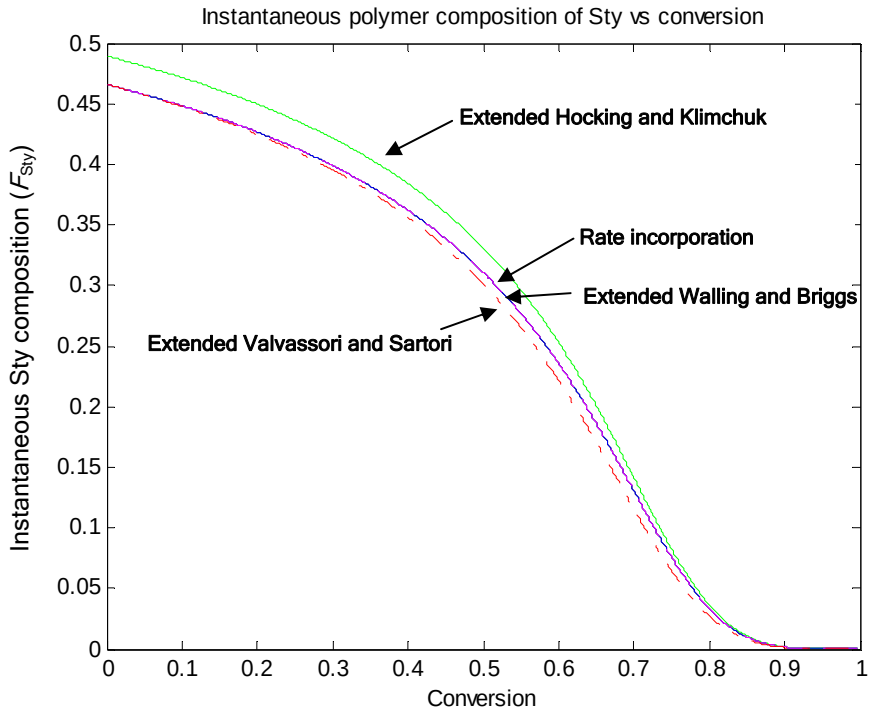

Figure A.1. Instantaneous polymer composition of Sty in Sty/BA bulk *co*-polymerization T = 50℃, f_{Sty0} = 0.258, and $[AIBN]_0$ = 0.05 M

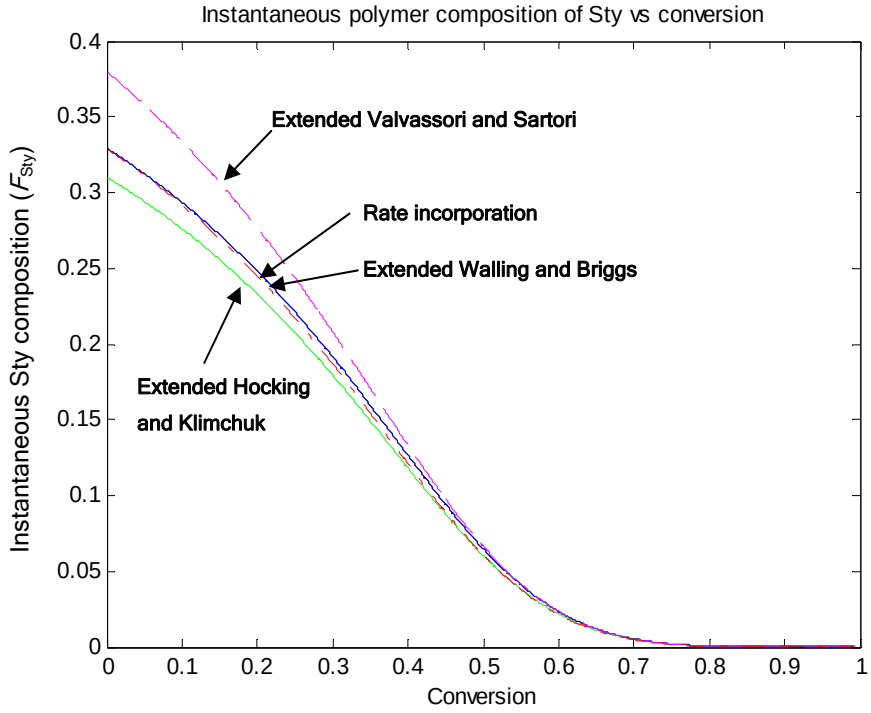

Figure A.2. Instantaneous polymer composition of Sty in Sty/BA/EA bulk *ter*-polymerization T = 60℃, f_{Sty0} = 0.112, f_{BA0} = 0.544, and $[AIBN]_0$ = 0.01 M

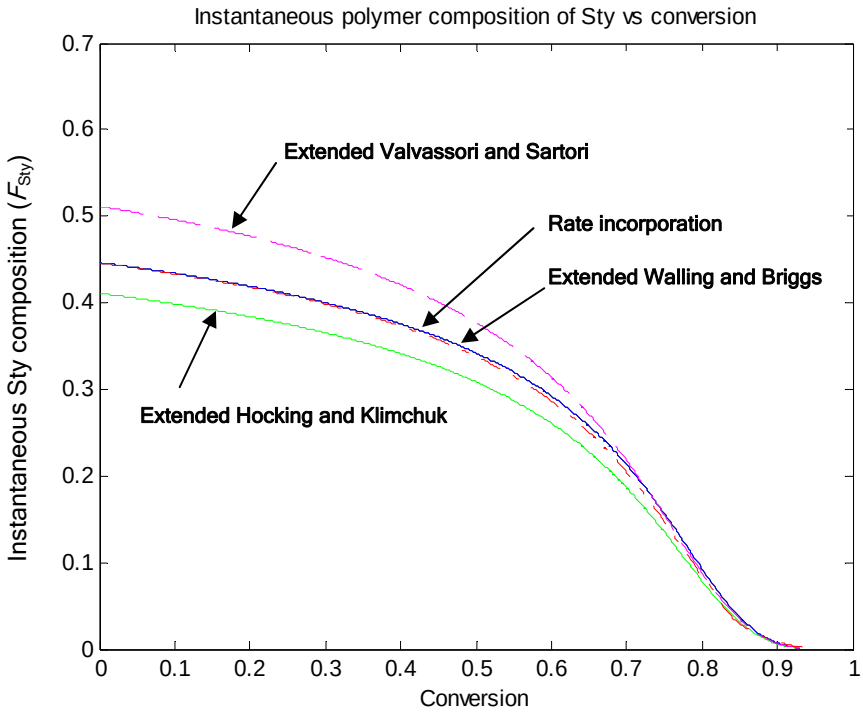

Figure A.3. Instantaneous polymer composition of Sty in Sty/BA/EA/BMA bulk *tetra*-polymerization T = 60℃, f_{Sty0} = 0.280, f_{BA0} = 0.227, f_{EA0} = 0.288, and $[AIBN]_0$ = 0.03 M

Appendix B

Method of Moments Calculations and Comparisons for Branched *Co*-polymers

In linear polymers, the integration of instantaneous molecular weights and the result of method of moments should be the same. Branched polymers are produced when at least one of the three following reactions are in effect: transfer to polymer molecules (k_{fp}), terminal double bond (k_p^*), and (or) internal double bond (k_p^{**}) polymerization. All of these reactions involve large dead polymer molecules. Several methods of moments calculations for number/weight average molecular weights of branched *co*-polymers are compared and discussed in this Appendix. We have already mentioned that there are two approaches for the moments calculation of the polymer molecule distribution (see relevant parts of Chapter 3).

Revisiting equations (3-43) to (3-44) and (3-48) to (3-50), the i^{th} moments of radical Y_i and polymer distribution Q_i are as follows.

$$Y_i = \sum_{r=1}^{\infty} r^i [R_r^\bullet] \tag{B-1}$$

$$Q_i = \sum_{r=1}^{\infty} r^i [P_r] \tag{B-2}$$

The zeroth, first, and second moments of radical distribution are given by,

$$Y_0 = \frac{1}{2}\left\{\left(\sqrt{\left(\frac{k_z[Z]}{k_t}\right)^2 + \frac{4R_i}{k_t}}\right) - \frac{k_z}{k_t}[Z]\right\} = [R^\bullet] \tag{B-3}$$

$$Y_1 = \frac{R_i + \left\{k_p[M] + k_{fm}[M] + k_{fCTA}[CTA] + k_{fS}[S] + \left(k_{fp} + k_p^{**}\right)Q_2 + k_p^{*}Q_1\right\}Y_0}{k_t Y_0 + k_{fm}[M] + k_{fCTA}[CTA] + k_{fS}[S] + k_{fZ}[Z] + k_{fp}Q_1 + k_p^{*}(Q_1 - Q_0)} \quad \text{(B-4)}$$

$$Y_2 = \frac{\left\{\begin{array}{l} R_i + \left(\begin{array}{l} k_p[M] + k_{fm}[M] + k_{fCTA}[CTA] + k_{fS}[S] \\ + k_{fp}Q_3 + k_p^{*}Q_2 + k_p^{**}Q_3 \end{array}\right)Y_0 \\ + 2\left(k_p[M] + k_p^{*}Q_1 + k_p^{**}Q_2\right)Y_1 \end{array}\right\}}{k_t Y_0 + k_{fm}[M] + k_{fCTA}[CTA] + k_{fS}[S] + k_{fZ}[Z] + k_{fp}Q_1 + k_p^{*}(Q_1 - Q_0)} \quad \text{(B-5)}$$

In order to calculate the moments of polymer molecule distribution, Kuindersma (1992) and Gao (1992) used the moments of radical distribution (Y_0, Y_1, and Y_2). On the other hand, Hamielec *et al*. (1987b), Dubé *et al*. (1991), and Xie and Hamielec (1993) used Y_0 only.

B.1 Kuindersma (1992) and Gao (1992)

The two sources used the same equations in the model for the moments of polymer molecule distribution. As mentioned earlier, all of the moments of the radical distribution are included in the differential equations.

$$\frac{d(VQ_0)}{dt} = \left\{\left(\frac{1}{2}k_{tc} + k_{td}\right)Y_0^2 + \left(k_{fm}[M] + k_{fCTA}[CTA] + k_{fS}[S] + k_{fZ}[Z] - k_p^{*}Q_0 - k_p^{**}Q_1\right)Y_0\right\}V \quad \text{(B-6)}$$

$$\frac{d(VQ_1)}{dt} = \left\{\begin{array}{l} \left(k_{tc} + k_{td}\right)Y_0Y_1 + \left(k_{fm}[M] + k_{fCTA}[CTA] + k_{fS}[S] + k_{fZ}[Z]\right)Y_1 + k_{fp}\left(Y_1Q_1 - Y_0Q_2\right) \\ -\left(k_p^{*}Y_0Q_1 + k_p^{**}Y_0Q_2\right) \end{array}\right\}V \quad \text{(B-7)}$$

$$\frac{d(VQ_2)}{dt} = \left\{\begin{array}{l} k_{tc}\left(Y_0Y_2 + Y_1^2\right) + k_{td}Y_0Y_2 + \left(k_{fm}[M] + k_{fCTA}[CTA] + k_{fS}[S] + k_{fZ}[Z]\right)Y_2 \\ + k_{fp}\left(Y_2Q_1 - Y_0Q_3\right) - \left(k_p^{*}Y_0Q_2 + k_p^{**}Y_0Q_3\right) \end{array}\right\}V \quad \text{(B-8)}$$

$$\overline{M_n} = Mw_{eff}\frac{Q_1}{Q_0} \quad \text{(B-9)}$$

$$\overline{M_w} = Mw_{eff}\frac{Q_2}{Q_1} \quad \text{(B-10)}$$

where $Mw_{eff} = Mw_1F_1 + Mw_2F_2$

B.2 Hamielec *et al*. (1987b)

Using the parameters τ and β, Hamielec *et al*. (1987b) derived the following moment equations.

$$\frac{d(VQ_0)}{dt} = k_p[M]Y_0V\left(\tau + \frac{\beta}{2} - \frac{\left(k_p^* + k_p^{**}\right)Q_1}{k_p[M]}\right) \tag{B-11}$$

$$\frac{d(VQ_1)}{dt} = k_p[M]Y_0V \tag{B-12}$$

$$\frac{d(VQ_2)}{dt} = k_p[M]Y_0V\left\{\begin{array}{l} 2\left(1+\dfrac{\left(k_p^* + k_p^{**}\right)Q_2}{k_p[M]}\right)\left(\dfrac{1+\dfrac{k_{fp}Q_2 + \left(k_p^* + k_p^{**}\right)Q_2}{k_p[M]}}{\tau+\beta+\dfrac{k_{fp}Q_1}{k_p[M]}}\right) \\ +\beta\left(\dfrac{1+\dfrac{k_{fp}Q_2 + \left(k_p^* + k_p^{**}\right)Q_2}{k_p[M]}}{\tau+\beta+\dfrac{k_{fp}Q_1}{k_p[M]}}\right)^2 \end{array}\right\} \tag{B-13}$$

$$\overline{M_n} = Mw_{eff}\frac{Q_1}{Q_0} \tag{B-14}$$

$$\overline{M_w} = Mw_{eff}\frac{Q_2}{Q_1} \tag{B-15}$$

B.3 Dubé *et al*. (1991)

The final equations for the moments of polymer molecule distribution are slightly different from the ones of Hamielec *et al*. (1987b), due to certain approximations and/or assumptions.

$$\frac{d(VQ_0)}{dt} = k_p[M]Y_0V\left(\tau + \frac{\beta}{2} - \frac{k_p^{**}Q_1 + k_p^*Q_0}{k_p[M]}\right) \tag{B-16}$$

$$\frac{d(VQ_1)}{dt} = k_p[M]Y_0V\left(1+\tau-\frac{k_{td}Y_0}{k_p[M]}\right)$$
$$= k_p[M]Y_0V\left(1+\frac{k_{fm}}{k_p}+\frac{k_{fS}[S]}{k_p[M]}+\frac{k_{fCTA}[CTA]}{k_p[M]}+\frac{k_{fZ}[Z]}{k_p[M]}\right) \quad \text{(B-17)}$$

$$\frac{d(VQ_2)}{dt} = k_p[M]Y_0V\left\{\begin{array}{l}(1+\tau+\beta)+2\left(1+\dfrac{k_p^*Q_1+k_p^{**}Q_2}{k_p[M]}\right)\left(\dfrac{1+\tau+\beta+\dfrac{\left(k_p^{**}+k_{fp}\right)Q_2+k_p^*Q_1}{k_p[M]}}{\tau+\beta+\dfrac{k_{fp}Q_1}{k_p[M]}}\right)\\ +\beta\left(\dfrac{1+\tau+\beta+\dfrac{\left(k_p^{**}+k_{fp}\right)Q_2+k_p^*Q_1}{k_p[M]}}{\tau+\beta+\dfrac{k_{fp}Q_1}{k_p[M]}}\right)^2\end{array}\right\} \quad \text{(B-18)}$$

$$\overline{M_n} = Mw_{eff}\frac{Q_1}{Q_0} \quad \text{(B-19)}$$

$$\overline{M_w} = Mw_{eff}\frac{Q_2}{Q_1} \quad \text{(B-20)}$$

B.4 Xie and Hamielec (1993)

Unlike in Hamielec *et al*. (1987b) and Dubé *et al*. (1991), terminal and internal double bond polymerization rate constants are not considered in equations (B-21) to (B-23).

$$\frac{dQ_0}{dt} = k_p[M]Y_0\left(\tau+\frac{\beta}{2}\right) \quad \text{(B-21)}$$

$$\frac{dQ_1}{dt} = Mw_{eff}R_p = Mw_{eff}k_p[M]Y_0 \quad \text{(B-22)}$$

$$\frac{dQ_2}{dt} = \left(Mw_{eff}\right)^2 k_p[M]Y_0 \times$$
$$\times\left\{\frac{\left(\tau+\beta+\dfrac{k_{fp}[M]_0X}{k_p[M]}\right)\left[\tau+\beta+\dfrac{k_{fp}[M]_0X}{k_p[M]}+2\left(1+\dfrac{k_{fp}Q_2}{k_p[M]\overline{Mw}_{eff}^{\,2}}\right)\right]+\beta\left(1+\dfrac{k_{fp}Q_2}{k_p[M]\overline{Mw}_{eff}^{\,2}}\right)^2}{\left(\tau+\beta+\dfrac{k_{fp}[M]_0X}{k_p[M]}\right)^2}\right\} \quad \text{(B-23)}$$

$$\overline{M_n} = \frac{Q_1}{Q_0} \tag{B-24}$$

$$\overline{M_w} = \frac{Q_2}{Q_1} \tag{B-25}$$

In this derivation, $\overline{Mw_{eff}} = Mw_1 \overline{F_1} + Mw_2 \overline{F_2}$

B.5 Simulation results and discussion

In order to compare the differences among the accumulated number/weight molecular weights calculated by integration of instantaneous ones and the four methods of moments models, hypothetical bulk *co*-polymerization simulations were performed. In addition, hypothetical kinetic parameters were assumed for comparing model predictions in linear, branched and network polymer cases, such as,

Case 1. $k_{fp} = 0$, $k_p^* = 0$, and $k_p^{**} = 0$ (linear *co*-polymer)

Case 2. $k_{fp} \neq 0$, $k_p^* = 0$, and $k_p^{**} = 0$ (branched *co*-polymer)

Case 3. $k_{fp} \neq 0$, $k_p^* \neq 0$, and $k_p^{**} = 0$ (branched *co*-polymer)

Case 4. $k_{fp} \neq 0$, $k_p^* \neq 0$, and $k_p^{**} \neq 0$ (network *co*-polymer)

Therefore, the profiles in Figures B.1 to B.8 are for comparative calculations only and by no means represent expected profiles in a polymerization scenario.

Figures B.1 and B.2 represent simulation results for the number and weight average molecular weights in case 1, respectively. The trends are almost identical, with only very slight differences. The results by Dubé *et al*. (1991) and Hamielec *et al*. (1987b) almost overlap each other. Dubé and Penlidis (1996) reported that typical experimental errors for number and weight average molecular weights are in the range ±15,000 - 25,000 (g/mol). Therefore, the differences between the linear and the method of moments model simulation results are insignificant because all differences are within ±5,000 (g/mol).

Figures B.3 and B.4 show results for case 2, where only transfer to polymer is active. Again, model differences are well within typical experimental errors. It is observed that there

is little difference between Dubé *et al*. (1991) and Hamielec *et al*. (1987b) over the entire conversion range.

When terminal/internal double bond polymerization rate constants are also active in cases 3 and 4, the models differ from one another more distinctively than in case 2. The number average molecular weight trends (Figures B.5 and B.7) predicted by Kuindersma (1992) and Gao (1992) decrease above 70% conversion, which is unusual. Note that the Hamielec *et al*. (1987b) calculations show very high weight average molecular weights (10^6 g/mol) compared with the other models (10^5 g/mol) at high conversion levels in Figures B.6 and B.8. Moreover, the weight average values in case 4 ($k_p^{**} \neq 0$, crosslinking) are much greater than the ones in case 3 ($k_p^{**} = 0$, branching), as expected. When performing weight average calculations by Hamielec *et al*. (1987b), we sometimes experienced unexpected numerical errors at high conversion levels due to the steepness of the profile curves. Of course, these are model predictions largely unverified in practice, since it is very difficult to even determine molecular weight averages experimentally in many situations under cases 3 and 4.

Our model uses the moment equations of Dubé *et al*. (1991) as default for average molecular weight calculations for branched polymers. Of course, the other options are also available in the package.

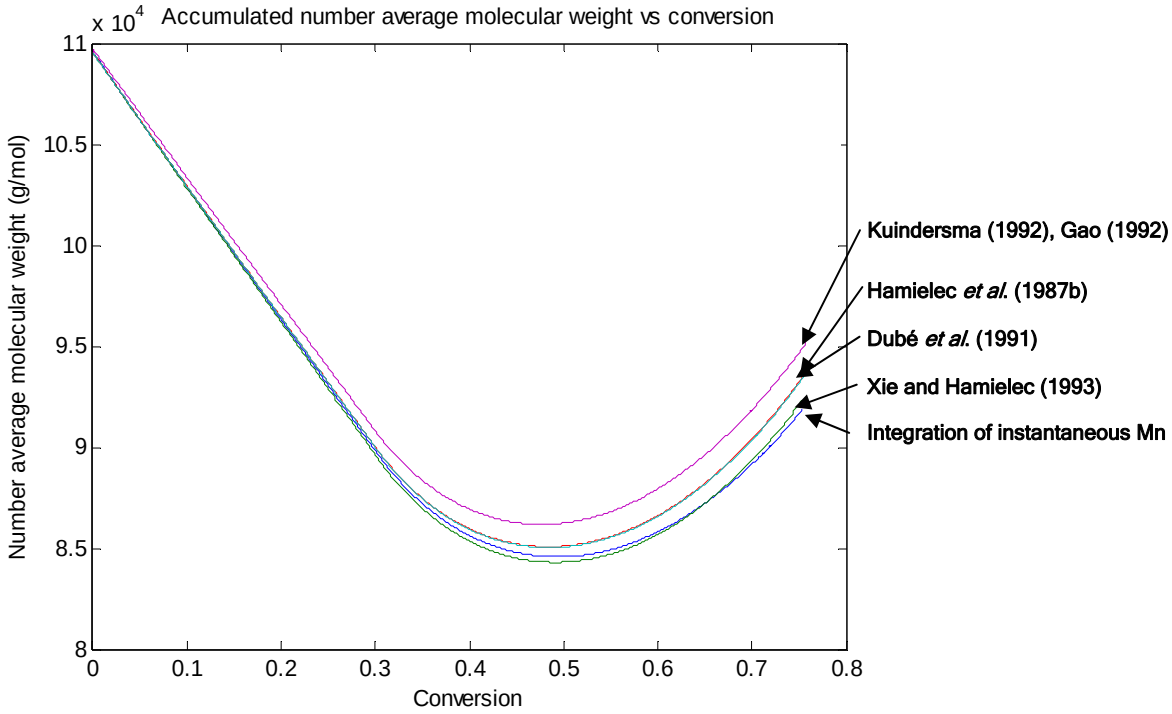

Figure B.1. Accumulated number average molecular weights in case 1

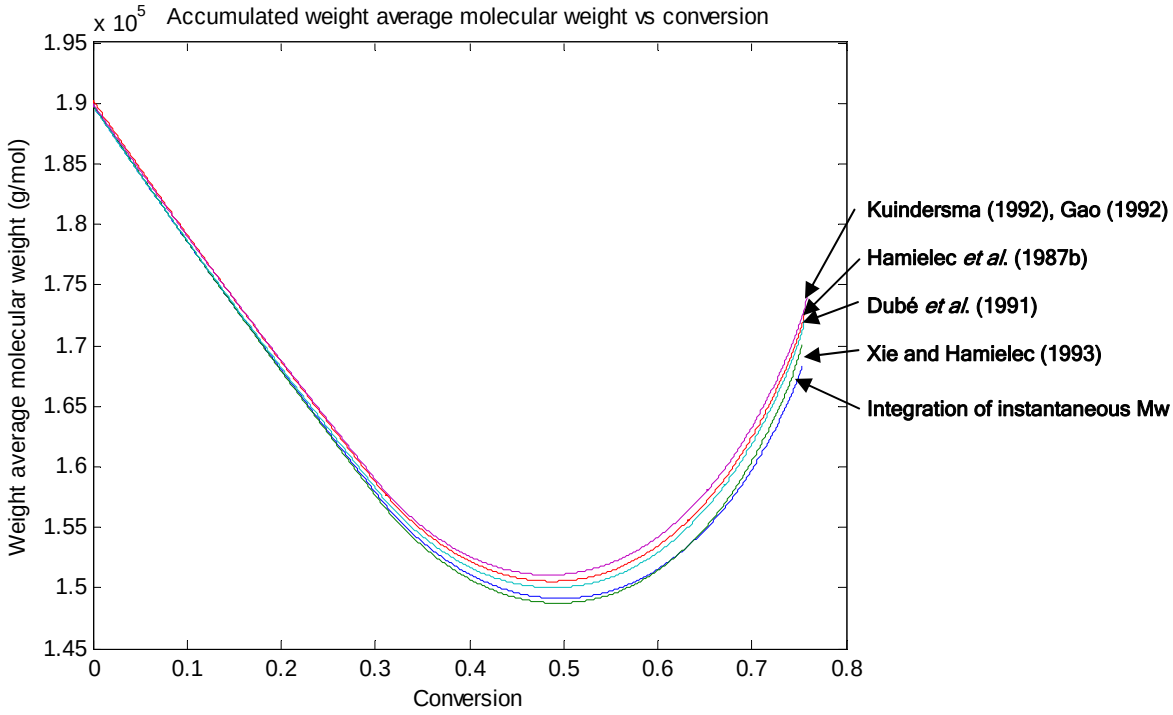

Figure B.2. Accumulated weight average molecular weights in case 1

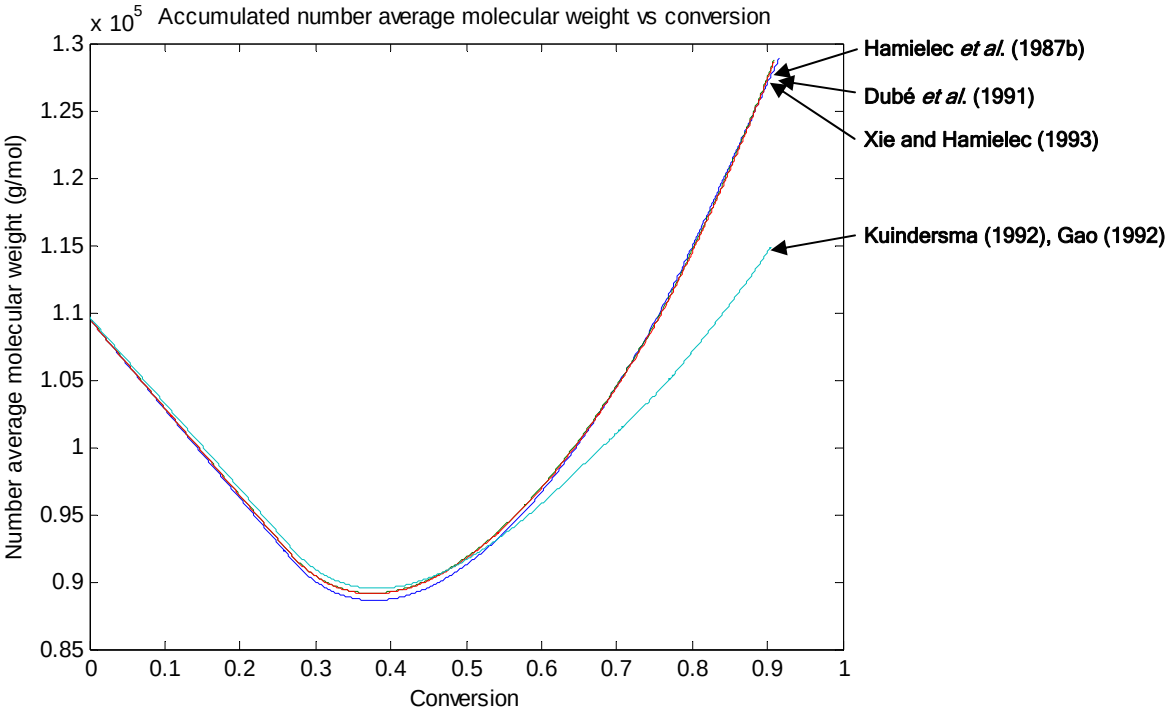

Figure B.3. Accumulated number average molecular weights in case 2

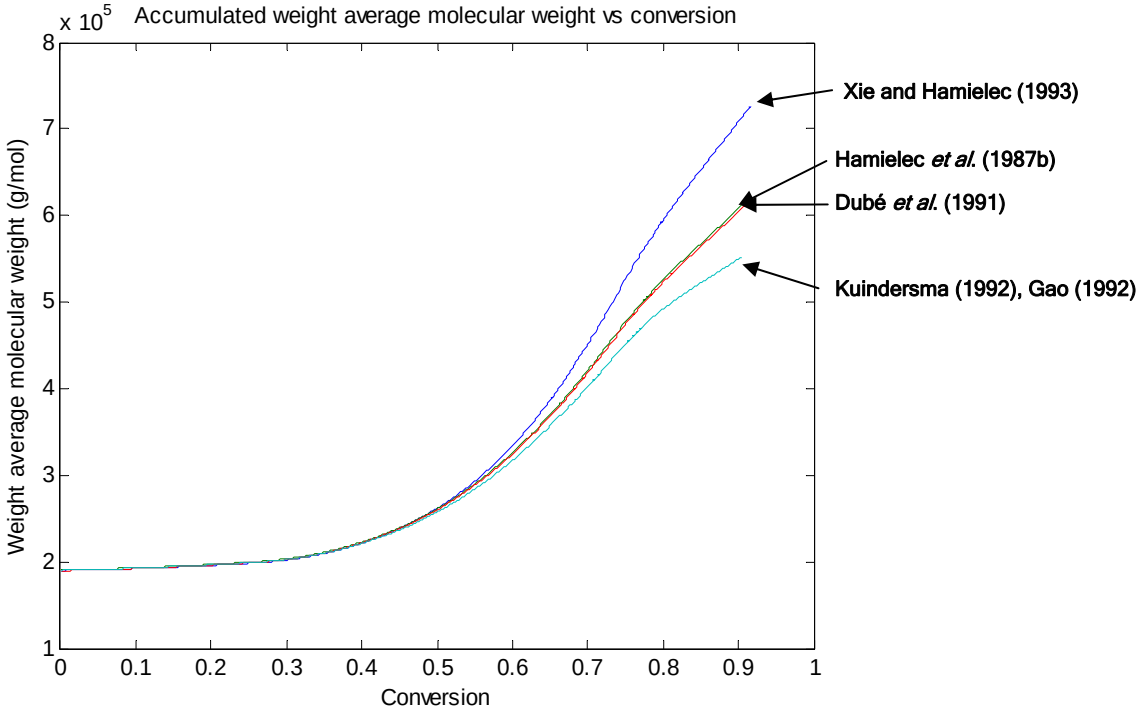

Figure B.4. Accumulated weight average molecular weights in case 2

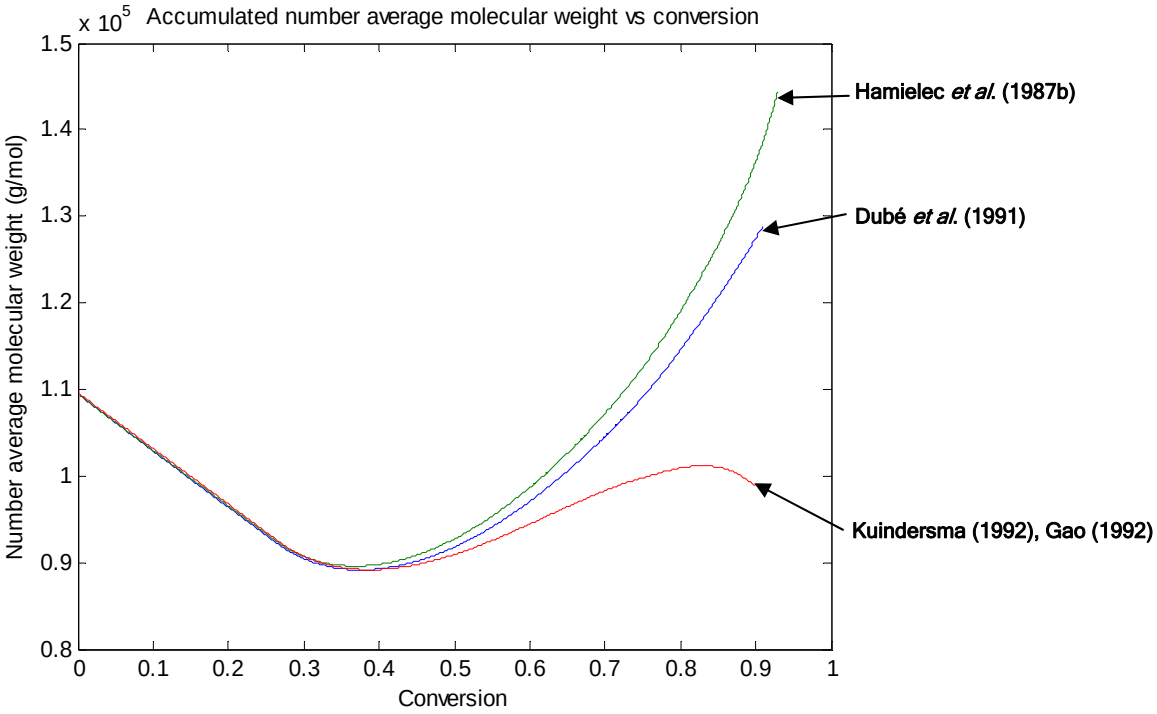

Figure B.5. Accumulated number average molecular weights in case 3

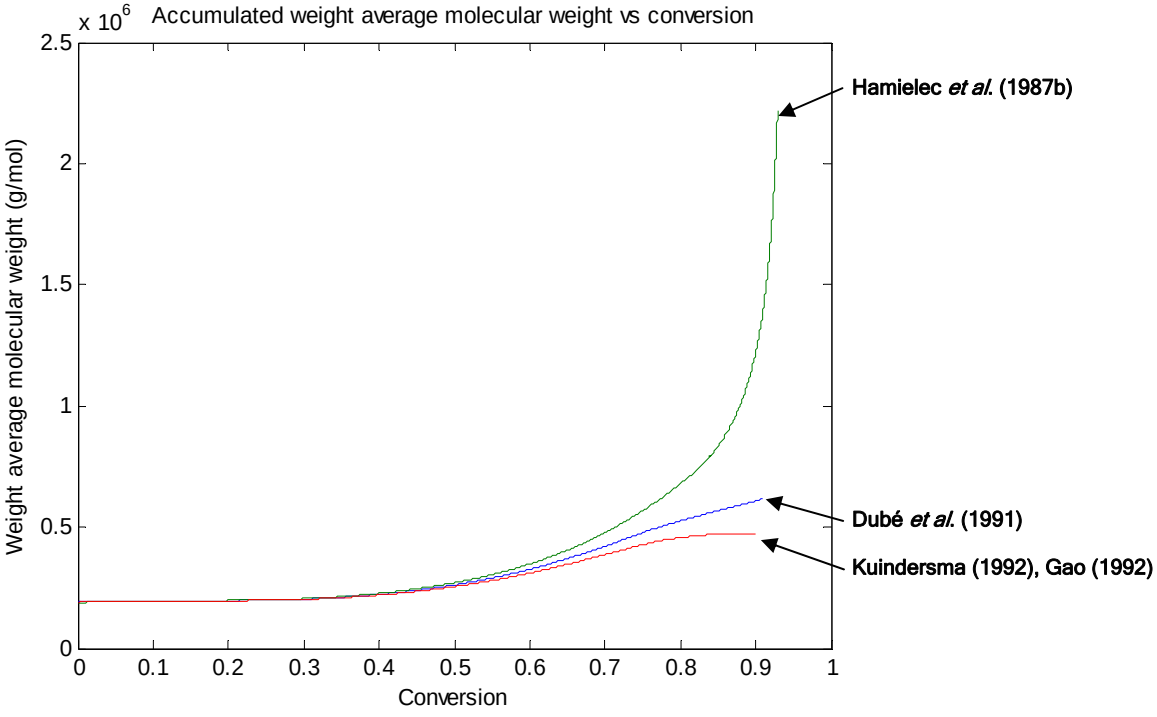

Figure B.6. Accumulated weight average molecular weights in case 3

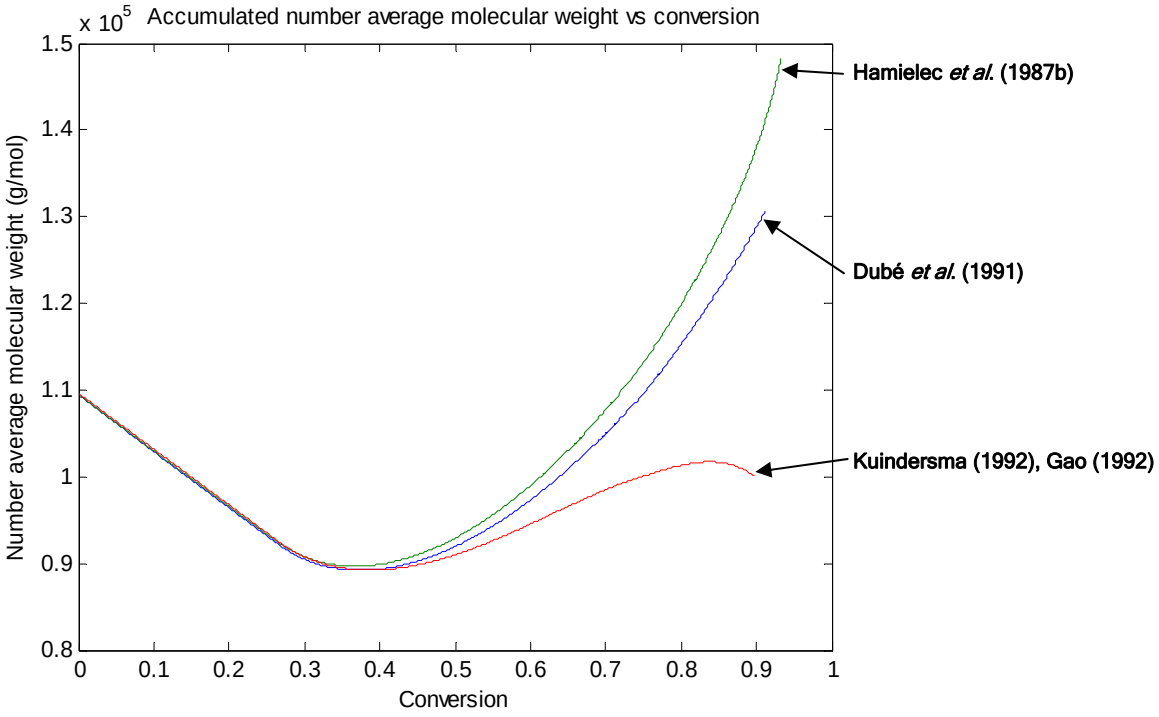

Figure B.7. Accumulated number average molecular weights in case 4

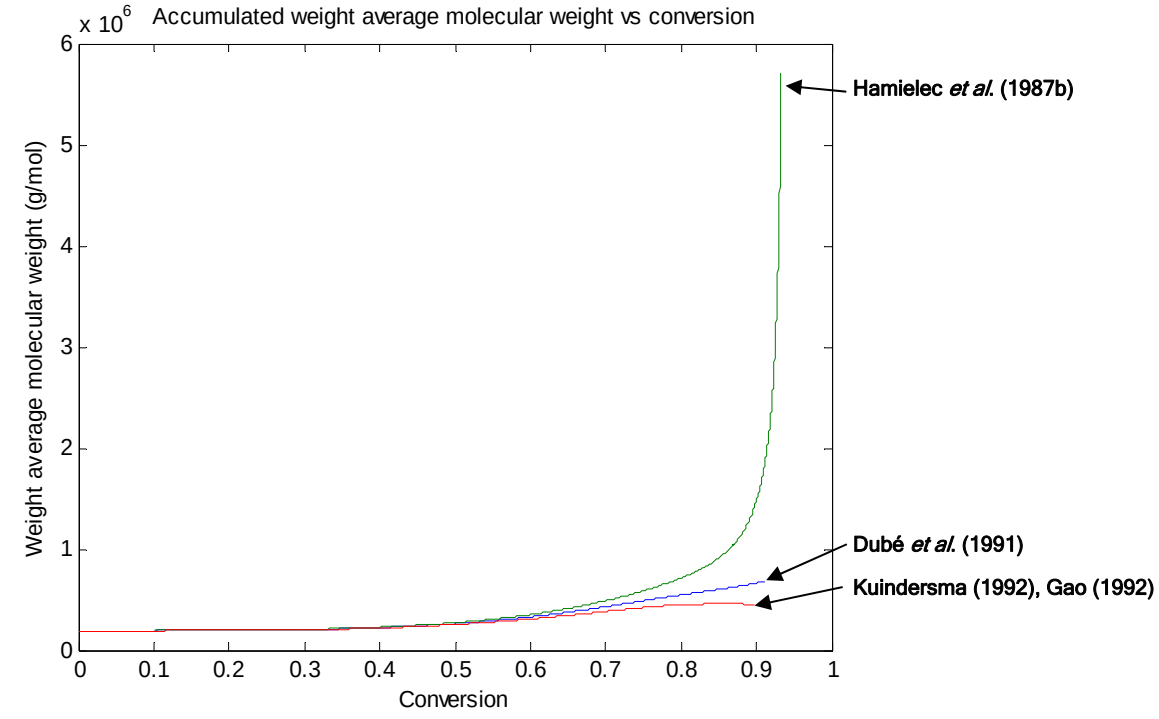

Figure B.8. Accumulated weight average molecular weights in case 4

Appendix C

Monomer Kinetic Database

The following tables cite information on physico-chemical/kinetic characteristics of the monomers (Sty, BA, BMA, HEA, and AA) used in our simulation model. These tables essentially form the database of the simulation model/package. The database, which is an extremely important and integral part of any model/simulator, was developed in a way similar to the database of the WATPOLY simulator (Gao and Penlidis, 1996, 1998, and 2000). Its reliability had already been verified over a wide range of recipes, operating conditions and modes of reactor operation. The current database was once more verified with additional experimental data in this thesis.

We also have tried to test our model as thoroughly as possible with other available kinetic parameters found in different literature sources. These literature sources have either been discussed in the thesis in more detail or simply cited in the various thesis tables as sources of information. In the following tables (Tables C.1 to C.5), in some entries, several values are shown, but only one is indicated in bold font. The bold fond thus indicates the value chosen as the final one for "best" prediction results. Some of these "best" values were arrived at via simulation trials, others via extensive sensitivity analyses, and finally some via parameter estimation based on experimental data. **Model prediction plots throughout this thesis were generated relying solely on the individual monomer database tables shown in the following pages and no parameters were adjusted further or selectively in order to obtain agreement with experimental data.** In other words, the database entries in Tables C.1 to C.5 have generated all model prediction curves throughout the thesis. That is the only way to build confidence in one's database and hence, model. The database can be constantly

updated in the future, every time that new experimental observations become available (and also in parallel to any model modifications/extensions).

Notes: (1) In the following tables, the entry "k_{td} ratio" refers to $\frac{k_{td}}{k_t}$.

(2) If sources of information are not indicated, then the values were based on the well tested WATPOLY database (see Gao and Penlidis, 1996, 1998, 2000)

(3) There is no database for HBA, since no data/information were located in the literature (see section 8.2.2).

Parameter	Value	Unit	Description
Mw	104.12	g/mol	Monomer molecular weight
$T_{g,m}$	185	K	Monomer glass transition temperature
$T_{g,p}$	378	K	Polymer glass transition temperature
Cp_m	430	K	Monomer heat capacity
Cp_p	400	K	Polymer heat capacity
ΔH	-1.7E4	cal/kg/K	Heat of polymerization
ρ_m	0.924 – 9.18E-4(T – 273.15)	kg/L	Monomer density
ρ_p	1.084 – 6.05E-4(T – 273.15)	kg/L	Polymer density
k_p	**1.302E9 exp(-7759.23/RT)** [1] 2.559E9 exp(-7740/RT) [2]	L/mol/min	Propagation rate constant
k_t	**4.92E11 exp(-3471.29/RT)** [3] 1.908E11 exp(-1903.54/RT) [4]	L/mol/min	Termination rate constant
k_{td} ratio	0		Ratio of disproportionation termination
k_{fm}	6.579E8 exp(-13426.8/RT) [5] **1.386E8 exp(-12671/RT)** [6]	L/mol/min	Monomer transfer rate constant
k_{fp}	0	L/mol/min	Polymer transfer rate constant
k_p^*	0	L/mol/min	Terminal double-bond polymerization
k_p^{**}	0	L/mol/min	Internal double-bond polymerization
δ	0.001	L/g	Reaction radius for segmental diffusion
n_s	174		Average number of monomer units in a polymer chain
l_0	7.4	Å	RMS length of monomer unit in a chain
$V_{f,crit}$	3.11052E-1 exp(-1671.76/RT)	volume	Critical free volume of diffusion-control of propagation
$V_{f,m}^0$	0.025	volume	Monomer free volume at T_g
$V_{f,p}^0$	0.025	volume	Polymer free volume at T_g
α_m	0.001	volume/K	Monomer thermal expansion coeff. above and below T_g
α_p	0.00048	volume/K	Polymer thermal expansion coeff. above and below T_g
B	1		Rate of decrease of k_p
m	0.5		Gel-effect model parameter
n	1.75		Gel-effect model parameter
A	0.348 [7]		Rate of decrease of k_t
K_3	9.44 exp(3832.9/RT) [8]		Onset point of translational diffusion-control
k_{th}	1.35E7 exp(-27448.8/RT) [9]	$L^2/mol^2/min$	Thermal initiation rate constant

Table A.1. Kinetic database of Sty

[1] Mahabadi *et al*. (1977) [2] Buback (1995) [3] Mahabadi *et al*. (1977) [4] Buback (1995) [5] Marten and Hamielec (1982)

[6] Hui and Hamielec (1972) [7] Marten and Hamielec (1982) [8] Marten and Hamielec (1982) [9] Hui and Hamielec (1972)

Parameter	Value	Unit	Description
Mw	128.17	g/mol	Monomer molecular weight
$T_{g,m}$	185.15	K	Monomer glass transition temperature
$T_{g,p}$	218	K	Polymer glass transition temperature
Cp_m	430	K	Monomer heat capacity
Cp_p	400	K	Polymer heat capacity
ΔH	-1.84E4	cal/kg/K	Heat of polymerization
ρ_m	0.919 – 0.001012(T-273.15) [1]	kg/L	Monomer density
ρ_p	1.212 – 0.0008(T-273.15)	kg/L	Polymer density
k_p	1.02E10 exp(-7128.46/RT) [2] **1.6646E11 exp(-9630/RT) [3]** 1.344E9 exp(-4278/RT) [4] 1.08E9 exp(-4121/RT) [5]	L/mol/min	Propagation rate constant
k_t	6.937E13 exp(-7312.25/RT) [6] **4.67532E8 exp(-873/RT) [7]** 1.54E10 exp(-575.2/RT) [8]	L/mol/min	Termination rate constant
k_{td} ratio	0.7		Ratio of disproportionation termination
k_{fm}	5.51E5 exp(-7128.46/RT) [9] **9.34E5 exp(-7475.06/RT) [10]** 1.728E7 exp(-7793/RT) [11]	L/mol/min	Monomer transfer rate constant
k_{fp}	35 [12]	L/mol/min	Polymer transfer rate constant
k_p^*	0	L/mol/min	Terminal double-bond polymerization
k_p^{**}	0	L/mol/min	Internal double-bond polymerization
δ	0.001	L/g	Reaction radius for segmental diffusion
n_s	200		Average number of monomer units in a polymer chain
l_0	6.54	Å	RMS length of monomer unit in a chain
$V_{f,crit}$	0.01 exp(-1443.61/RT)	volume	Critical free volume of diffusion-control of propagation
$V_{f,m}^0$	0.025	volume	Monomer free volume at T_g
$V_{f,p}^0$	0.025	volume	Polymer free volume at T_g
α_m	0.001	volume/K	Monomer thermal expansion coeff. above and below T_g
α_p	0.00048	volume/K	Polymer thermal expansion coeff. above and below T_g
B	0.5		Rate of decrease of k_p
m	0.5		Gel-effect model parameter
n	1.75		Gel-effect model parameter
A	1.31		Rate of decrease of k_t
K_3	0.02 exp(12108.5/RT)		Onset point of translational diffusion-control
k_{th}	2e-11	$L^2/mol^2/min$	Thermal initiation rate constant

Table A.2. Kinetic database of BA

[1] Dubé (1989) [2] Dubé (1989) [3] WATPOLY [4] Asua *et al*. (2004) [5] Li *et al*. (2005) [6] Dubé (1989)

[7] WATPOLY [8] Li *et al*. (2005) [9] Kuindersma (1992)/Mallya and Plamthottam (1989)

[10] WATPOLY [11] Li *et al*. (2005) [12] Assumed by Dubé (1989)

Parameter	Value	Unit	Description
Mw	142.191	g/mol	Monomer molecular weight
$T_{g,m}$	224.2	K	Monomer glass transition temperature
$T_{g,p}$	293	K	Polymer glass transition temperature
Cp_m	420	K	Monomer heat capacity
Cp_p	401.914	K	Polymer heat capacity
ΔH	-1.83732E1	cal/kg/K	Heat of polymerization
ρ_m	0.91096 – 0.00089(T-273.15)	kg/L	Monomer density
ρ_p	1.041	kg/L	Polymer density
k_p	**2.064E8 exp(-5574.16/RT)** [1] 2.281E8 exp(-5472.6/RT) [2] 2.064E8 exp(-5568.6/RT) [3] 1.087E8 exp(-4911.9/RT) [4]	L/mol/min	Propagation rate constant
k_t	**2.352E9 exp(-701/RT)** [5] 4.26E9 exp(-1649.2/RT) [6]	L/mol/min	Termination rate constant
k_{td} ratio	0.255		Ratio of disproportionation termination
k_{fm}	**3.08E5 exp(-8322.47/RT)** [7] 9.36E3 exp(-5207.9/RT) [8]	L/mol/min	Monomer transfer rate constant
k_{fp}	0	L/mol/min	Polymer transfer rate constant
k_p^*	0	L/mol/min	Terminal double-bond polymerization
k_p^{**}	0	L/mol/min	Internal double-bond polymerization
δ	0.001	L/g	Reaction radius for segmental diffusion
n_s	126		Average number of monomer units in a polymer chain
l_0	6.2	Å	RMS length of monomer unit in a chain
$V_{f,crit}$	0.06	volume	Critical free volume of diffusion-control of propagation
$V_{f,m}^0$	0.025	volume	Monomer free volume at T_g
$V_{f,p}^0$	0.025	volume	Polymer free volume at T_g
α_m	0.001	volume/K	Monomer thermal expansion coeff. above and below T_g
α_p	0.00048	volume/K	Polymer thermal expansion coeff. above and below T_g
B	1		Rate of decrease of k_p
m	0.5		Gel-effect model parameter
n	1.75		Gel-effect model parameter
A	1.02		Rate of decrease of k_t
K_3	5.8E6		Onset point of translational diffusion-control
k_{th}	0	$L^2/mol^2/min$	Thermal initiation rate constant

Table A.3. Kinetic database of BMA

[1] WATPOLY [2] Li *et al*. (2005) [3] Davis *et al*. (1990) [4] Hutchinson *et al*. (1995)

[5] WATPOLY [6] Li *et al*. (2005) [7] WATPOLY [8] Li *et al*. (2005)

Parameter	Value	Unit	Description
Mw	116.116	g/mol	Monomer molecular weight
$T_{g,m}$	185.15	K	Monomer glass transition temperature
$T_{g,p}$	258	K	Polymer glass transition temperature
Cp_m	429.397	K	Monomer heat capacity
Cp_p	437.5	K	Polymer heat capacity
ΔH	-1.84E4	cal/kg/K	Heat of polymerization
ρ_m	1.011 – 0.001012(T-273.15)	kg/L	Monomer density
ρ_p	1.041 – 0.000845(T-273.15)	kg/L	Polymer density
k_p	6.49E8 exp(-6706.22/RT) [1]	L/mol/min	Propagation rate constant
k_t	2.63E11 exp(-6639.48/RT) [2]	L/mol/min	Termination rate constant
k_{td} ratio	1.91607E2 exp(-3.81775/RT)		Ratio of disproportionation termination
k_{fm}	9.34359E5 exp(-7475.06/RT)	L/mol/min	Monomer transfer rate constant
k_{fp}	0	L/mol/min	Polymer transfer rate constant
k_p^*	0	L/mol/min	Terminal double-bond polymerization
k_p^{**}	0	L/mol/min	Internal double-bond polymerization
δ	0.001	L/g	Reaction radius for segmental diffusion
n_s	126		Average number of monomer units in a polymer chain
l_0	6.2	Å	RMS length of monomer unit in a chain
$V_{f,crit}$	1 exp(-2100/RT) [3]	volume	Critical free volume of diffusion-control of propagation
$V_{f,m}^0$	0.0275	volume	Monomer free volume at T_g
$V_{f,p}^0$	0.0275	volume	Polymer free volume at T_g
α_m	0.0011	volume/K	Monomer thermal expansion coeff. above and below T_g
α_p	0.000528	volume/K	Polymer thermal expansion coeff. above and below T_g
B	1		Rate of decrease of k_p
m	0.5		Gel-effect model parameter
n	1.75		Gel-effect model parameter
A	3.5		Rate of decrease of k_t
K_3	4.0E-5 exp(14470.6/RT) [4]		Onset point of translational diffusion-control
k_{th}	0	$L^2/mol^2/min$	Thermal initiation rate constant

Table A.4. Kinetic database of HEA

[1, 2, 3, 4] These parameters have been modified via sensitivity analysis based on the work by Kim (1994).

Parameter	Value	Unit	Description
Mw	72.06	g/mol	Monomer molecular weight
$T_{g,m}$	189.65	K	Monomer glass transition temperature
$T_{g,p}$	379	K	Polymer glass transition temperature
Cp_m	502	K	Monomer heat capacity
Cp_p	432.69	K	Polymer heat capacity
ΔH	-1.85E4	cal/kg/K	Heat of polymerization
ρ_m	1.07764 – 0.00133(T-273.15)	kg/L	Monomer density
ρ_p	1.442	kg/L	Polymer density
k_p	3.72E9 exp(-5600/RT)	L/mol/min	Propagation rate constant
k_t	6.0E9	L/mol/min	Termination rate constant
k_{td} ratio	0.2		Ratio of disproportionation termination
k_{fm}	1.7172E9 exp(-11116.5/RT)	L/mol/min	Monomer transfer rate constant
k_{fp}	0	L/mol/min	Polymer transfer rate constant
k_p^*	0	L/mol/min	Terminal double-bond polymerization
k_p^{**}	0	L/mol/min	Internal double-bond polymerization
δ	0.001	L/g	Reaction radius for segmental diffusion
n_s	120		Average number of monomer units in a polymer chain
l_0	6.2	Å	RMS length of monomer unit in a chain
$V_{f,crit}$	3.09563 exp(-1683.2/RT)	volume	Critical free volume of diffusion-control of propagation
$V_{f,m}^0$	0.025	volume	Monomer free volume at T_g
$V_{f,p}^0$	0.025	volume	Polymer free volume at T_g
α_m	0.001	volume/K	Monomer thermal expansion coeff. above and below T_g
α_p	0.00048	volume/K	Polymer thermal expansion coeff. above and below T_g
B	1		Rate of decrease of k_p
m	0.5		Gel-effect model parameter
n	1.75		Gel-effect model parameter
A	1.75		Rate of decrease of k_t
K_3	5.0E6		Onset point of translational diffusion-control
k_{th}	0	$L^2/mol^2/min$	Thermal initiation rate constant

Table A.5. Kinetic database of AA

Appendix D

Sty Thermal Polymerization

Sty monomer can polymerize thermally without an initiator. Hui and Hamielec (1972) investigated the kinetics and modeling of Sty thermal polymerization up to high conversion in the industrial temperature range of 100~200℃. They proposed second and third-order initiation models based on a Diels-Alder mechanism. The third-order model could fit conversion and number/weight average molecular weight data in a satisfactory way. Husain and Hamielec (1978) extended the temperature range of kinetic studies up to 230℃ using this model, which accepts that the rate of Sty thermal initiation is of order three in monomer concentration.

$$R_{th} = 2k_{th}[M]^3 \tag{D-1}$$

where k_{th} is a thermal initiation rate constant.

The model by Hui and Hamielec (1972) uses empirical gel effect corrections for transfer to monomer and termination by combination for Sty bulk thermal polymerization, as follows:

$$k_{fm} = k_{fm0} - 0.001013k_p\left(\frac{S}{100}\right)\log\left(\frac{473.12 - T}{202.5}\right) \tag{D-2}$$

$$k_{tc} = k_{tc0}\exp\left[-2g_{T1}\left(\frac{S}{100}\right) - 2g_{T2}\left(\frac{S}{100}\right)^2 - 2g_{T3}\left(\frac{S}{100}\right)^2\right] \tag{D-3}$$

where:

k_{fm0} is the rate constant of chain transfer to monomer at zero conversion.

k_p is the propagation rate constant.

S is the solids level and T is reaction temperature (K).

k_{tc0} is the rate constant of termination by combination at zero conversion.

$g_{T1} = 2.57 - 0.00505T$

$g_{T2} = 9.56 - 0.01760T$

$g_{T3} = -3.03 + 0.00785T$

Matthews *et al.* (2007) presented a new data set with an estimated experimental error of 2% for number/weight/z average molecular weights. They conducted ten bulk and solution experiments over the temperature range from 100 to 180℃ using ethylbenzene as a solvent. First, Matthews *et al.* (2007) compared molecular weight experimental data in bulk polymerization with the original model predictions by Hui and Hamielec (1972) and observed some discrepancies, especially at temperature levels below 130℃. In order to obtain better predictions and to include the solvent chain transfer effect, they kept equation (D-3) and modified the gel effect corrections for chain transfer rate constants to monomer and solvent, as follows.

$$k_{fm} = k_{fm0} + 0.00009k_p\left(\frac{S}{S + \Phi_m(100 - S)}\right)\exp\left[-\frac{12000}{R}\left(\frac{1}{T} - \frac{1}{373.15}\right)\right] \qquad \text{(D-4)}$$

$$k_{fS} = k_{fS0} - 0.0012k_p\left(\frac{S}{S + \Phi_S(100 - S)}\right) \qquad \text{(D-5)}$$

where:

k_{fS0} is the rate constant of chain transfer to solvent at zero conversion.

R is the universal gas constant.

$$\Phi_m = 0.25 + \frac{0.75}{1 + \exp(398.15 - T)}$$

$$\Phi_S = 9 - \frac{8}{1 + \exp(398.15 - T)}$$

Using the modified model and based on the empirical gel correction factors shown above, Matthews *et al.* (2007) could obtain better prediction results. This case study was conducted

in order to check the reliability of our multi-component model by comparing our number/weight average molecular weight predictions with predictions by Hui and Hamielec (1972) and Matthews *et al*. (2007). The difference between our multi-component model and the other approaches is that ours uses the free volume theory for diffusion-controlled kinetics instead of the empirical correction functions (see the diffusion kinetics part in Chapter 3), and hence our model is more general.

The measured final number and weight average molecular weights were compared with the three model predictions through parity plots. Predictions by Hui and Hamielec (1972) and our model are presented in Figures D.1 and D.2, while the ones by Matthews *et al*. (2007) and ours are depicted in Figures D.3 and D.4. No experimental data on molecular weight averages over the entire conversion range but only the final values were available in Mattews *et al*. (2007). Therefore, our final number/weight average molecular weight predictions were compared with their measurements at the end of the polymerization.

Figures D.1 and D.2 represent parity plots for number and weight average molecular weights, respectively. The results show more variability as temperature becomes lower. At 100℃, discrepancies between x and y values increases up to about 100,000 g/mol. Our multi-component model predictions are marked with 'x' symbols in both plots and show better agreement with the measurements over the temperature range.

Figures D.3 and D.4 are parity plots comparing the measured values of the number and weight average molecular weights with predictions using the modified model by Matthews *et al*. (2007) and our model. More predicted values lie on the diagonal line than the ones calculated by the original model (contrast with Figures D.1 and D.2), especially at low temperatures, which means that the modified model predictions have been improved. Our multi-component model predictions are also added in the figures (see 'x' symbols) and show satisfactory results as well over the temperature range. If Matthews *et al*. (2007) had provided full conversion range experimental data (molecular weight averages vs conversion), the model evaluation would have been clearer. This is the reason why all of our model predictions represented only the final number/weight average molecular weights at each temperature level in the parity plots.

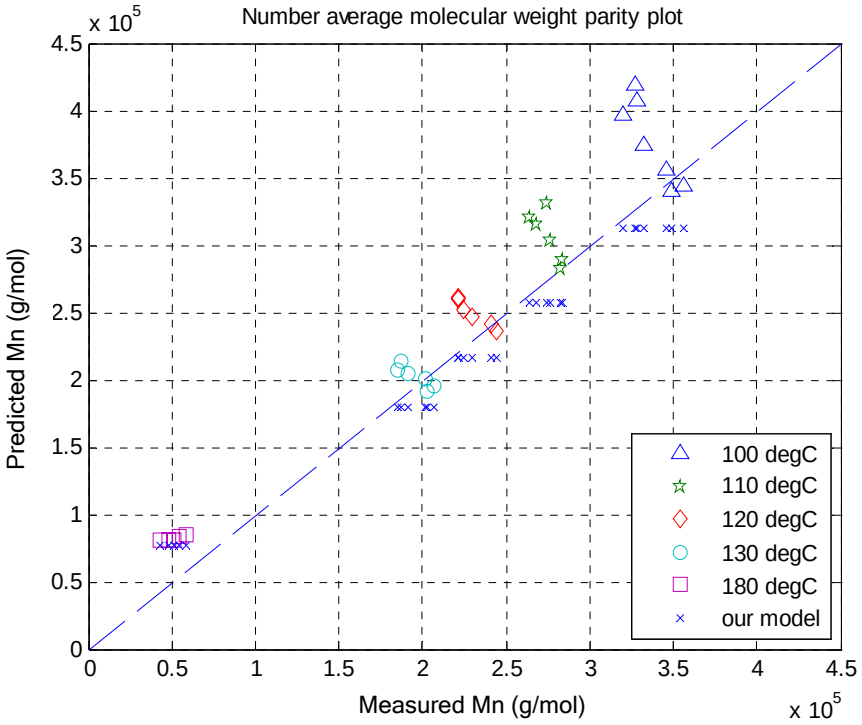

Figure D.1. Number average molecular weight parity plot (predicted by Hui and Hamielec (1972) and our model (denoted as 'x'))

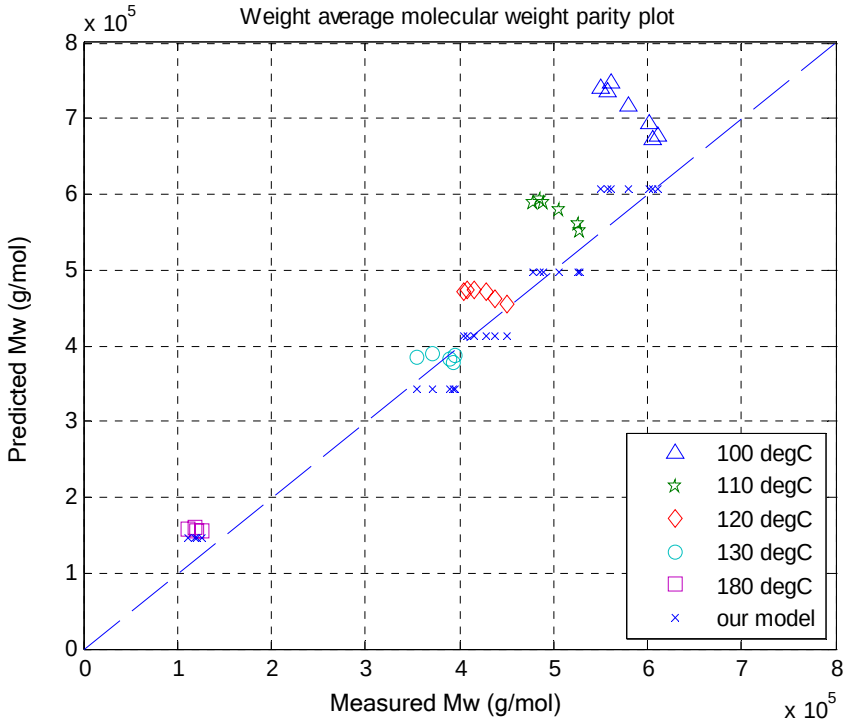

Figure D.2. Weight average molecular weight parity plot (predicted by Hui and Hamielec (1972) and our model (denoted as 'x'))

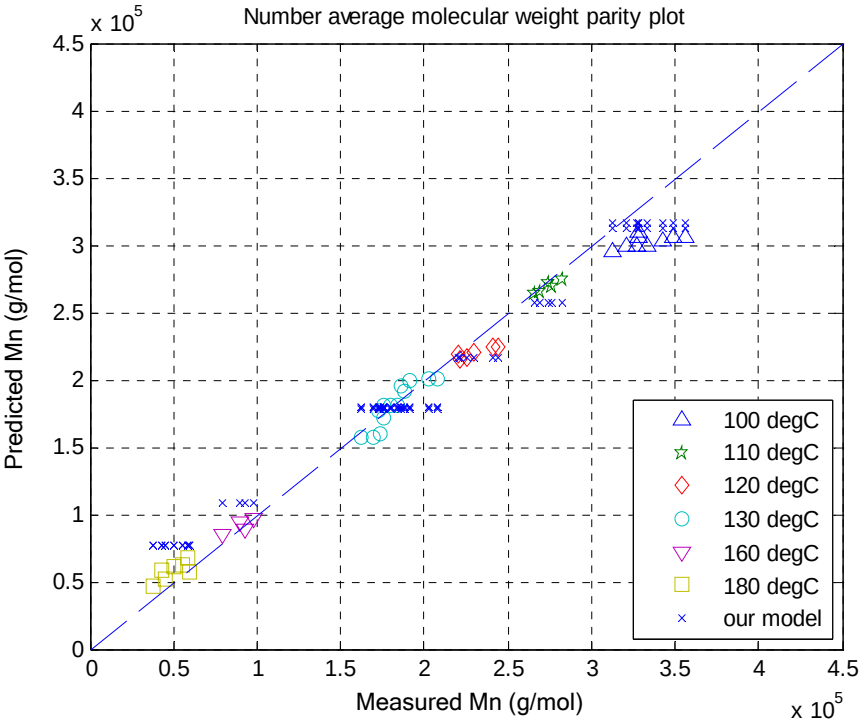

Figure D.3. Number average molecular weight parity plot (predicted by Matthews *et al.* (2007) and our model (denoted as 'x'))

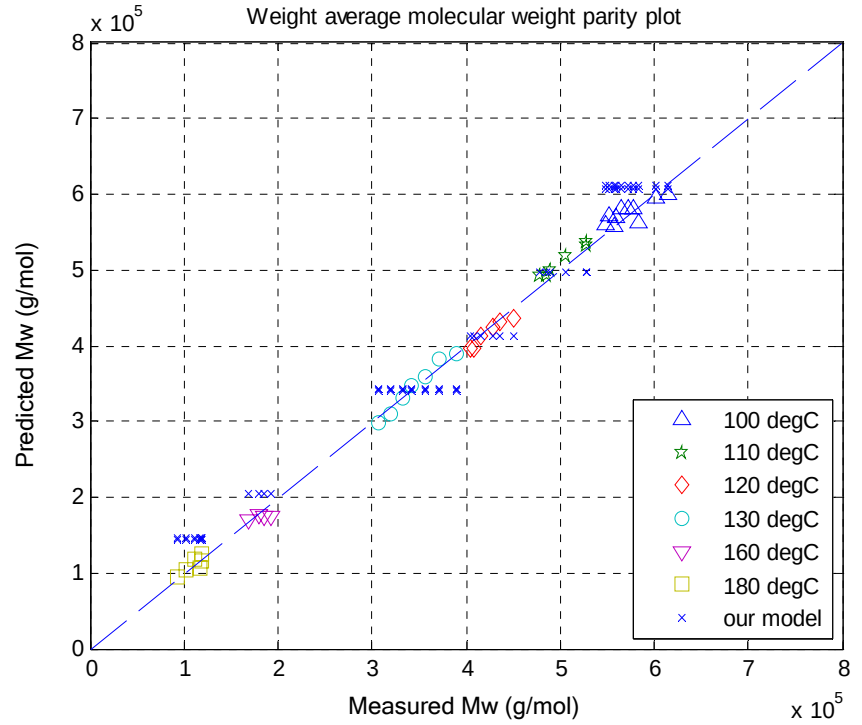

Figure D.4. Weight average molecular weight parity plot (predicted by Matthews *et al.* (2007) and our model (denoted as 'x'))

General Nomenclature

A	rate of decrease of termination rate constant in the free volume model
A_i	rate of decrease of termination rate constant of species i in the free volume model
A_{ijk}	probability of forming triad monomer sequence ijk
$A_{K,i}$	pre-exponential factor of gel effect model parameter for translational diffusion-controlled termination
B	glass-transition effect model parameter
$\overline{B_{N3}}$	average number of *tri*-functional branches
$\overline{B_{N4}}$	average number of *tetra*-functional branches
C	model parameter for diffusion-controlled initiator efficiency
c	mass concentration of accumulated polymer (g/L)
$[CTA]$	chain transfer agent concentration (mol/L)
D	reaction diffusion coefficient (Å^2/min)
$E_{K,i}$	activation energy for gel point parameter for translational diffusion-controlled termination (cal/mol)
F_i	instantaneous polymer composition of species i
$\overline{F_i}$	accumulated polymer composition of species i
$F_{CTA,in}$	molar inflow rate of chain transfer agent (mol/min)
$F_{I,in}$	molar inflow rate of initiator (mol/min)
$F_{i,in}$	molar inflow rate of monomer species i (mol/min)
$F_{pi,in}$	molar inflow rate of monomer species i bound as polymer (mol/min)
$F_{S,in}$	molar inflow rate of solvent (mol/min)
$F_{Z,in}$	molar inflow rate of impurity (mol/min)
f	initiator efficiency
f_0	initiator efficiency at zero conversion
f_i	residual mole fraction (feed ratio) of monomer species i
f_{i0}	initial residual mole fraction (feed ratio) of monomer species i
f_{eff}	initiator efficiency

$f_{eff,i}$ initiator efficiency related with monomer *i*

$f_{eff,\ pseudo}$ pseudo initiator efficiency

ΔG_p Gibbs free energy (cal/mol)

g_{T1}~g_{T3} gel effect parameters for termination by combination of Sty (Appendix D)

ΔH_p enthalpy change upon propagation (cal/mol)

$[I]$ initiator concentration (mol/L)

i, j monomer species

K_{eq} equilibrium constant between propagation and depropagation (L/mol)

$K_{eq,i}$ equilibrium constant between propagation and depropagation of species *i* (L/mol)

K_3 gel point parameter for translational diffusion-controlled termination

$K_{3,i}$ gel point parameter of species *i* for translational diffusion-controlled termination

$K_{3,pseudo}$ pseudo gel point parameter for translational diffusion-controlled termination

$K_{3,test}$ gel point test parameter for translational diffusion-controlled termination

k_d rate constant of initiator decomposition (L/mol/min)

$k_{d,i}$ rate constant of initiator decomposition related with monomer *i* (L/mol/min)

$k_{d,\ pseudo}$ pseudo initiator decomposition rate constant (L/mol/min)

k_{fCTA} overall transfer rate constant to chain transfer agent (L/mol/min)

k_{fCTA0} overall initial transfer rate constant to chain transfer agent (L/mol/min)

k_{fCTAi} transfer rate constant from radical species *i* to chain transfer agent (L/mol/min)

k_{fm} overall transfer rate constant to monomer species *j* (L/mol/min)

k_{fm0} transfer rate constant to monomer at zero conversion (L/mol/min)

k_{fmij} transfer rate constant from radical species *i* to monomer species *j* (L/mol/min)

$k_{fm,\ pseudo}$ pseudo transfer rate constant to monomer (L/mol/min)

k_{fp} overall transfer rate constant (L/mol/min)

k_{fpij} transfer rate constant from radical species *i* to monomer species *j* (L/mol/min)

k_{fS0} transfer rate constant to solvent at zero conversion (L/mol/min)

k_{fSi} transfer rate constant from radical species *i* to solvent (L/mol/min)

$k_{fS,\ pseudo}$ pseudo transfer rate constant to solvent (L/mol/min)

k_{fZ} overall transfer rate constant of to inhibitor (L/mol/min)

k_{fZi}	transfer rate constant from radical species *i* to impurity (L/mol/min)
$k_{fZ,\ pseudo}$	pseudo transfer rate constant to impurity (L/mol/min)
k_p	overall propagation rate constant (L/mol/min)
k_p^{eff}	net propagation rate constant considering depropagation (L/mol/min)
k_p^{*}	overall terminal double bond polymerization rate constant (L/mol/min)
k_p^{**}	overall internal double bond polymerization rate constant (L/mol/min)
$\overline{k_p}$	overall depropagation rate constant (1/min)
$\overline{k_{pij}}$	depropagation rate constant of penultimate species i and terminal species j (1/min)
k_{p0}	chemically controlled initial propagation rate constant (L/mol/min)
k_{pij}	propagation rate constant between radical species *i* and monomer species *j*
$k_{p,\ pseudo}$	pseudo propagation rate constant (L/mol/min)
k_t	overall termination rate constant (L/mol/min)
$k_{t,\ pseudo}$	pseudo termination rate constant (L/mol/min)
k_{tc}	termination rate constant by combination (L/mol/min)
k_{tc0}	termination rate constant by combination at zero conversion (L/mol/min)
$k_{t,cr}$	overall termination rate constant at the onset point of translational diffusion-control (L/mol/min)
k_{td}	termination rate constant by disproportionation (L/mol/min)
k_{th}	thermal initiation rate constant ($L^2/mol^2/min$)
k_{tij}	termination rate constant between radical *i* and radical *j*
$k_{t,seg}$	segmental diffusion-controlled termination rate constant (L/mol/min)
$k_{t,trans}$	translational diffusion-controlled termination rate constant (L/mol/min)
$k_{t,rd}$	reaction diffusion-controlled termination rate constant (L/mol/min)
k_{t0}	chemically controlled initial termination rate constant
l_0	length of monomer unit in the chain (Å)
$[M]$	total monomer concentration (mol/L)
$[M_i]$	concentration of monomer species *i* (mol/L)
$[M]_{eq}$	equilibrium monomer concentration (mol/L)

$[M]_0$	initial monomer concentration (mol/L)
M_n	instantaneous number average molecular weight (g/mol)
$\overline{M_n}$	cumulative number average molecular weight (g/mol)
M_w	instantaneous weight average molecular weight (g/mol)
$\overline{M_w}$	cumulative weight average molecular weight (g/mol)
Mw_i	molecular weight of monomer species *i* (g/mol)
Mw_{eff}	instantaneously effective pseudo molecular weight of monomers (g/mol)
$\overline{Mw}_{eff}$	cumulatively effective pseudo molecular weight of monomers (g/mol)
$\overline{M_{w\,cr}}$	critical accumulated weight-average molecular weight of polymer (g/mol)
m	gel effect model parameter
n	gel effect model parameter
N	number of moles (mol)
N_A	Avogadro's number ($6.023 \cdot 10^{23}$ mol^{-1})
N_I	number of moles of initiator
N_{CTA}	number of moles of chain transfer agent
N_S	number of moles of solvent
n_s	average number of monomer units in one polymer chain
N_Z	number of moles of impurity
N_{in}	sequence probability of monomer *i* with length *n*
$\overline{N_{in,Ray}}$	accumulated sequence probability of monomer *i* with length *n* (Ray)
$\overline{N_{in,HMP}}$	accumulated sequence probability of monomer *i* with length *n* (HMP)
$\overline{N_{i,Ray}}$	accumulated number average sequence length of monomer *i* (Ray)
$\overline{N_{i,HMP}}$	accumulated number average sequence length of monomer *i* (HMP)
$\overline{n_i}$	instantaneous number average sequence length of monomer *i*
P_i	number of moles of monomer species *i* bound as polymer

P_{ij}	probability of finding a primary radical species *j* attached to a penultimate unit *i*
p_{ij}	probability of forming a dyad of monomers *i* and *j*
Q_i	*i*-th moment of dead polymer distribution
R	universal gas constant (1.987 cal/mol/K)
R_{ij}	rate of reaction between radical species *i* and monomer species *j*
R_I	rate of initiation (mol/L/min)
$R_{I,total}$	total rate of initiation (mol/L/min)
r_{ij}	reactivity ratio
R_{ij}	propagation rate between radical species *i* and monomer species *j* (mol/L/min)
R_p	total rate of polymerization (consumption rate) (mol/L/min)
R_{pi}	rate of polymerization (consumption rate) of monomer species *i* (mol/L/min)
R_{th}	rate of thermal initiation (mol/L/min)
$R_i^{'}$	*cross*-depropagation ratio
$[R^{\bullet}]$	total radical concentration (mol/L)
$[R_i^{\bullet}]$	radical concentration of species *i* (mol/L)
$[R_{ij}^{\bullet}]$	radical concentration of penultimate species *i* and terminal species *j* (mol/L)
r	chain length of polymer
r_{ij}	monomer reactivity ratio (monomer species *i* and *j*)
S	solids content level
$[S]$	solvent concentration (mol/L)
ΔS_p	entropy change upon propagation (cal/mol/K)
s	chain length of polymer
T	reaction temperature (K)
T_c	ceiling temperature (K)
T_{gi}	glass transition temperature of *homo*-polymer species *i* (K)
T_{gpij}	glass transition temperature of alternating *co*-polymer from monomers *i* and *j*
T_{gpoly}	glass transition temperature of polymer
t	reaction time (min.)
V	total volume of reaction mixtures (L)

V_i volume for component *i* (L)

V_f free volume of reaction mixtures

$V^0_{f,i}$ free volume of component *i* at glass transition temperature

$V_{f,cr1}$ critical free-volume for translational diffusion-controlled termination

$V_{f,cr2}$ critical free-volume for diffusion-controlled propagation/transfer

$V_{f,cr3}$ critical free-volume for diffusion-controlled initiator efficiency

V_m molar volume of monomer (L/mol)

w_i weight fraction of monomer specis $_i$ bound in the polymer

$w(r, X)$ instantaneous weight fraction of polymer of chain length *r* at conversion X

$\overline{w(r, X)}$ cumulative weight fraction of polymer of chain length *r* at conversion X

$\overline{w_i}$ instantaneous weight average sequence length of monomer *i*

$\overline{W_{i,Ray}}$ accumulated weight average sequence length of monomer *i* (Ray)

$\overline{W_{i,HMP}}$ accumulated weight average sequence length of monomer *i* (HMP)

X overall molar conversion

X_i partial molar conversion of species *i*

Y_i *i*-th moment of radical distribution

$[Z]$ impurity concentration (mol/L)

Greek letters

α_i thermal expansion coefficient above and below glass transition temperature

β parameter used for average molecular weight calculation

δ reaction radius in reaction diffusion termination (Å)

δ_c segmental diffusion parameter

$\rho_{i,monomer}$ density of monomer species *i* (kg/L)

$\rho_{polymer}$ density of polymer (kg/L)

τ parameter used for average molecular weight calculation

$\Phi^{\bullet}_j$ fraction of radical species *j*

Φ_m gel effect parameter for transfer to monomer (in Appendix D)

Φ_S gel effect parameter for transfer to solvent (in Appendix D)

φ *cross*-termination factor, or Walling's φ factor

Bibliography

1. A. M. Alb, P. Enohnyaket, M. F. Drenski, A. Head, A. W. Reed, W. F. Reed, **Online monitoring of *co*-polymerization involving *co*-monomers of similar spectral characteristics**, *Macromolecules*, **39**, 5705-5713 (2006)
2. T. Alfrey, G. Goldfinger, ***Co*-polymerization of systems of three and more components**, *Journal of Chemical Physics*, **12**, 205-209, 322 (1944)
3. T. Alfrey, G. Goldfinger, ***Co*-polymerization of systems containing three components**, *Journal of Chemical Physics*, **14**, 115-116 (1946)
4. K. Arai, S. Saito, **Simulation model for the rate of bulk polymerization over the complete course of reaction**, *Journal of Chemical Engineering of Japan*, **9(4)**, 302-313 (1976)
5. J. M. Asua, S. Beuermann, M. Buback, P. Castignolles, B. Charleux, R. G. Gilbert, R. A. Hutchinson, J. R. Leiza, A. N. Nikitin, JP Vairon. A. M. van Herk, **Critically evaluated rate coefficients for free-radical polymerization, 5 Propagation rate coefficient for BA**, *Macromolecular Chemistry and Physics*, **205**, 2151-2160 (2004)
6. K. S. Balaraman, V. M. Nadkarni, R. A. Mashelkar, **SAN bulk *co*-polymerization: some new insights in kinetics and microstructure**, *Chemical Engineering Science*, **41(5)**, 1357-1368 (1986)
7. S. Beuermann, D. A. Paquet, J. H. McMinn, R. A. Hutchinson, **Propagation kinetics of methacrylic acid studied by pulsed-laser polymerization**, *Macromolecules*, **30**, 194-197 (1997)
8. J. K. Borchardt, **Steric and electronic effects of alkyl substituents on reactivity ratios in *co*-polymerization reactions of acrylates and methacrylates**, *Polymer Preprients*, **23(2)**, 209-211 (1982)
9. J. K. Borchardt, **Calculation of reactivity ratios and sequence distributions in *co*-polymers from monomers ^{13}C-NMR data**, *Journal of Macromolecular Science. Chemistry*, **A22(12)**, 1711-1733 (1985)

10. H. Branson, R. Simha, **On the kinetics of *co*-polymerization**, *Journal of Chemical Physics*, **11(6)**, 297-298 (1943)
11. M. Buback, B. Degener, B. Huckestein, **Conversion dependence of free-radical polymerization rate coefficients from laser-induced experiments. 1. BA**, *Die Makromolekulare Chemie, Rapid Communications*, **10**, 311-316 (1989)
12. M. Buback, **Free-radical polymerization up to high conversion. A general kinetic treatment**, *Makromoleculare Chemie*, **191**, 1575-1587 (1990)
13. M. Buback, R. G. Gilbert, R. A. Hutchinson, B. Klumperman, FD Kuchta, B. G. Manders, K. F. O'Driscoll, G. T. Russell, J. Schweer, **Critically evaluated rate coefficients for free-radical polymerization, 1. Propagation rate coefficient for Sty**, *Macromolecular Chemistry and Physics*, **196**, 3267-3280 (1995)
14. M. Buback, T. Junkers, **Termination kinetics of tert-BMA and of n-BMA free-radical bulk *homo*-polymerizations**, *Macromolecular Chemistry and Physics*, **207**, 1640-1650 (2006)
15. S. Bywater, **Photosensitized polymerization of MMA in dilute solution above 100℃**, *Transactions of the Faraday Society*, **51**, 1267-1273 (1955)
16. G. G. Cameron, G. P. Kerr, **The *co*-polymerization behaviour of alpha-substituted methyl acrylates**, *European Polymer Journal*, **3**, 1-4 (1967)
17. J. M. Catala, A. Nonn, J. M. Pujol, J. Brossas, **Radical *co*-polymerization of HEA with Alkylacrylate – Determination of the reactivity ratios**, *Polymer Bulletin*, **15**, 311-315 (1986)
18. G. Chambard, B. Klumperman, A. L. German, **Dependence of chemical composition of Sty/BA *co*-polymers on temperature and molecular weight**, *Polymer*, **40**, 4459-4463 (1999)
19. R. K. S. Chan, V. E. Meyer, **Computer calculations of binary and ternary *co*-polymerization behaviour**, *Journal of Polymer Science, Polymer Symposia*, **25**, 11-21 (1968)

20. S. Chen, T. Hu, Y. Tian, L. Chen, J. A. Pojman, **Facile synthesis of PHEA by frontal free-radical polymerization**, *Journal of Polymer Science: Part A: Polymer Chemistry*, **45**, 873-881 (2007)

21. S. I. Cheong, A. Penlidis, **Modeling of the *co*-polymerization, with depropagation, of AMS/MMA at an elevated temperature**, *Journal of Applied Polymer Science*, **93**, 261-270 (2004)

22. C. D. Chow, **Monomer reactivity ratio and *Q*-*e* Values for *co*-polymerization of hydroxyalkyl acrylates and 2-(1-aziridinyl)ethyl methacrylate with Sty**, *Journal of Polymer Science: Polymer Chemistry Edition*, **13**, 309-313 (1975)

23. T. P. Davis, K. F. O'Driscoll, M. C. Piton, M. A. Winnik, ***Co*-polymerization propagation kinetics of Sty with alkyl methacrylates**, *Macromolecules*, **23**, 2113-2119 (1990)

24. R. Dhib, J. Gao, A. Penlidis, **Simulation of free-radical bulk/solution *homo*-polymerization using mono- and bi-functional initiators**, *Polymer Reaction Engineering*, **8(4)**, 299-464 (2000)

25. J. M. Dionisio, K. F. O'Driscoll, **High-conversion *co*-polymerization of Sty and MMA**, *Journal of Polymer Science: Polymer Letters Edition*, **17**, 701-707 (1979)

26. M. A. Dubé, ***Co*-polymerization of Sty and BA experimental kinetics and mathematical modeling**, *PhD thesis*, *Department of Chemical Engineering, Univ. of Waterloo* (1989)

27. M. A. Dubé, A. Penlidis, K. F. O'Driscoll, **Mathematical modelling of Sty/BA *co*-polymerization**, *Chemical Engineering Science*, **45(8)**, 2785-2792 (1990)

28. M. A. Dubé, A. Penlidis, K. F. O'Driscoll, **A kinetic investigation of Sty/BA *co*-polymerization**, *Canadian Journal of Chemical Engineering*, **68**, 974-987 (1990)

29. M. A. Dubé, K. Rilling, A. Penlidis, **A kinetic investigation of BA polymerization**, *Journal of Applied Polymer Science*, **43**, 2137-2145 (1991)

30. M. A. Dubé, R. A. Sanayei, A. Penlidis, K. F. O'Driscoll, P. M. Reilly, **A microcomputer program for estimation of *co*-polymerization reactivity ratios**, *Journal of Polymer Science: Part A: Polymer Chemistry*, **29**, 703-708 (1991)

31. M. A. Dubé, A. Penlidis, **A systematic approach to the study of multi-component polymerization kinetics: BA/MMA/VAc example, 1. Bulk *co*-polymerization**, *Polymer*, **36(3)**, 587-598 (1995a)
32. M. A. Dubé, A. Penlidis, **A systematic approach to the study of multi-component polymerization kinetics: BA/MMA/VAc example, 2. Bulk (and solution) *ter*-polymerization**, *Macromolecular Chemistry and Physics*, **196**, 1102-1112 (1995b)
33. M. A. Dubé, A. Penlidis, **Hierarchical data analysis of a replicate experiment in emulsion *ter*-polymerization**, *AIChE Journal*, **42(7)**, 1985-1994 (1996)
34. M. A. Dubé, J. B. P. Soares, A. Penlidis, A. E. Hamielec, **Mathematical modeling of multi-component chain-growth polymerizations in batch, semi-batch, and continuous reactors: A review**, *Industrial & Engineering Chemistry Research*, **36(4)**, 966-1015 (1997)
35. T. A. Duever, K. F. O'Driscoll, P. M. Reilly, **The use of the Error-in-Variables Method in *ter*-polymerization,** *Journal of Polymer Science: Polymer Chemistry Edition*, **21**, 2003-2010 (1983)
36. U. Engelmann, G. Schmidt-Naake, **Free-radical multi-component polymerization reactors and chemical composition distribution**, *Makromolekulare Chemie, Theory and Simulations*, **2**, 275-297 (1993)
37. M. Fernandez-Garcia, M. Fernandez-Sanz, E. L. Madruga, **Free-radical *co*-polymerization of Sty with BA. II. Elemental kinetic *co*-polymerization step predictions from *homo*-polymerization data**, *Journal of Polymer Science: Part A*, **42**, 130-136 (2003)
38. M. Fineman, S. D. Ross, **Linear method for determining monomer reactivity ratios in *co*-polymerization**, *Journal of Polymer Science*, **5(2)**, 259-265 (1950)
39. N. Friis, L. Nyhagen, **A kinetic study of the emulsion polymerization of VAc**, *Journal of Applied Polymer Science*, **17**, 2311-2327 (1973)
40. T. Fujisawa, A. Penlidis, ***Co*-polymer composition control policies: Characteristics and applications**, *Journal of Macromolecular Science, Part A: Pure and Applied Chemistry*, **45**, 115-132 (2008)

41. M. N. Galbraith, G. Moad, D. H. Solomon, T. H. Spurling, **Influences on the initiation and termination reactions on the MWD and compositional heterogeneity of functional *co*-polymers: An application of Monte Carlo Simulation**, *Macromolecules*, **20**, 675-679 (1987)

42. J. Gao, **Mathematical modeling of *homo*-polymerizations: Simulation package and database extensions,** *MASc thesis*, *Department of Chemical Engineering, Univ. of Waterloo* (1992)

43. J. Gao, A. Penlidis, **A comprehensive simulator/database package for reviewing free-radical *homo*-polymerizations**, *Journal of Macromolecular Sciences - REV. Macromolecular Chemistry and Physics*, **C36(2)**, 199-404 (1996)

44. J. Gao, N. T. MaManus, A. Penlidis, **Experimental and simulation studies on EA polymerization**, *Macromolecular Chemistry and Physics*, **198**, 843-859 (1997)

45. J. Gao, A. Penlidis, **A comprehensive simulator/database package for bulk/solution free-radical *co*-polymerizations**, *Journal of Macromolecular Sciences - REV. Macromolecular Chemistry and Physics*, **C38(4)**, 651-780 (1998)

46. J. Gao, A. Penlidis, **A comprehensive simulator/database package for bulk/solution free-radical *ter*-polymerizations**, *Macromolecular Chemistry Physics*, **201**, 1176-1184 (2000)

47. J. Gao, K. D. Hungenberg, A. Penlidis, **Process modeling and optimization of Sty polymerization**, *Macromolecular Symposia*, **206**, 509-522 (2004)

48. L. H. Garcia-Rubio, A. E. Hamielec, J. F. MacGregor, **Bulk polymerization of AN. II. Model development**, *Journal of Applied Polymer Science*, **23**, 1413-1429 (1979)

49. L. H. Garcia-Rubio, M. G. Lord, J. F. MacGregor, A. E. Hamielec, **Bulk *co*-polymerization of Sty and AN: Experimental kinetics and mathematical modeling**, *Polymer*, **26**, 2001-2013 (1985)

50. M. C. Grady, W. J. Simonsick, R. A. Hutchinson, **Studies of higher temperature polymerization of BMA/BA**, *Macromolecular Symposia*, **182**, 149-168 (2002)

51. A. E. Hamielec, J. F. MacGregor, A. Penlidis, **Comprehensive Polymer Science Encyclopedia, Chap. 2**, *Pergamon Press*, **3**, 17-31 (1987a)

52. A. E. Hamielec, J. F. MacGregor, A. Penlidis, **Multi-component free-radical polymerization in batch, semi-batch and continuous reactors - modelling and control of chain composition, microstructure, molecular weight distribution, long chain branching and crosslinking in solution and emulsion polymerization**, *Makromolekulare Chemie, Macromolecular Symposia*, **10-11**, 521-570 (1987b)

53. H. J. Harwood, W. M. Ritchey, **The characterization of sequence distribution in *co*-polymers**, *Polymer letters*, **2**, 601-607 (1964)

54. H. J. Harwood, **A FORTRAN II program for conducting sequence distribution calculations**, *Journal of Polymer Science. Part C*, **25**, 37-45 (1968)

55. D. J. T. Hill, J. H. O'Donnel, P. W. O'Sullivan, **Analysis of the mechanism of *co*-polymerization of Sty and AN**, *Macromolecules*, **15**, 960-966 (1982)

56. M. B. Hocking, K. A. Klimchuk, **A refinement of the *ter*-polymer equation and its simple extension to two- and four-component systems**, *Journal of Polymer Science: Part A: Polymer Chemistry*, **34**, 2481-2497 (1996)

57. J. A. Howell, M. Izu, K. F. O'Driscoll, ***Co*-polymerization with depropagation III. Composition and sequence distribution from probability considerations**, *Journal of Polymer Science: Part A-1*, **8**, 699-710 (1970)

58. A. W. Hui, A. E. Hamielec, **Thermal polymerization of Sty at high conversions and temperatures: An experimental study**, *Journal of Applied Polymer Science*, **16**, 749-769 (1972)

59. A. Husain, A. E. Hamielec, **Thermal polymerization of Sty**, *Journal of Applied Polymer science*, **22**, 1207-1223 (1978)

60. R. A. Hutchinson, D. A. Paquet, Jr., J. H. McMinn, R. E. Fuller, **Measurement of free-radical propagation rate coefficients for EMA, *n*-BMA, and *iso*-BMA by pulsed-laser Polymerization**, *Macromolecules*, **28**, 4023-4028 (1995)

61. R. A. Hutchinson, S. Beuermann, D. A. Paquet, J. H. McMinn, **Determination of free-radical propagation rate coefficients for alkyl methacrylates by pulsed-laser polymerization**, *Macromolecules*, **30**, 3490-3493 (1997)

62. M. Izu, K. F. O'Driscoll, ***Co*-polymerization with depropagation IV. Computer simulation of *co*-polymerization with reversibility**, *Journal of Polymer Science: Part A-1*, **8**, 1675-1685 (1970)

63. H. Jianying, C. Jiayan, Z. Jiaming, C. Yihong, D. Lizong, Z. Yousi, **Some Monomer reactivity ratios of Sty and (meth)acrylates in the presence of TEMPO**, *Journal of Applied Polymer Science*, **100**, 3531-3535 (2006)

64. M. Johnson, T. S. Karmo, R. R. Smith, **High conversion *co*-polymerization of Sty with MMA**, *European Polymer Journal*, **14**, 409-414 (1978)

65. N. W. Johnston, **Sequence distribution – Glass transition effects III. AMS-AN *co*-polymers**, *Macromolecules*, **6(3)**, 453-456 (1973)

66. A. Keramopoulos, C. Kiparissides, **Mathematical modeling of diffusion-controlled free-radical *ter*-polymerization reactions**, *Journal of Applied Polymer Science*, **88**, 161-176 (2003)

67. Y. Kim, H. J. Harwood, **Analysis of sequence distribution in MMA/MA *co*-polymers by ^{13}C NMR spectroscopy**, *Polymer*, **43**, 3229-3237 (2002)

68. J. D. Kim, **A kinetic study of Sty/HEA *co*-polymerization**, *MASc thesis*, *Department of Chemical Engineering, Univ. of Waterloo* (1994)

69. J. L. Koenig, **Chemical Microstructure of Polymer Chains, Chap. 3**, *John Wiley & Sons* (1980)

70. H. Krüger, J. Bauer, J. Rübner, **Ein Modell zur Beschreibung reversibler *Co*-polymerisationen**, *Makromolekulare Chemie*, **188**, 2163-2175 (1987)

71. M. E. Kuindersma, **On the modeling of free-radical polymerization reactions: *Homo*-polymerization**, *MASc thesis*, *Department of Chemical Engineering, Univ. of Waterloo* (1992)

72. V. R. Kumar, S. K. Gupta, **Optimal parameter estimation for MMA polymerization**, *Polymer*, **32(17)**, 3233-3243 (1991)

73. M. J. Leamen, **Kinetic investigation and modeling of multi-component polymer systems with depropagation**, *PhD thesis*, *Department of Chemical Engineering, Univ. of Waterloo* (2005a)

74. M. J. Leamen, N. T. McManus, A. Penlidis, **Binary *co*-polymerization with full depropagation: A study of MMA/AMS *co*-polymerization**, *Journal of Polymer Science: Part A: Polymer Chemistry*, **43**, 3868-3877 (2005b)

75. M. J. Leamen, N. T. McManus, A. Penlidis, ***Ter*-polymerization with depropagation: Modeling the *co*-polymer composition of the MMA/AMS/BA system**, *Chemical Engineering Science*, **61**, 7774-7785 (2006)

76. D. Li, M. C. Grady, R. A. Hutchinson, **High-temperature semi-batch free-radical *co*-polymerization of BMA/BA**, *Industrial and Engineering Chemistry Research*, **44(8)**, 2506-2517 (2005)

77. D. Li, N. Li, R. A. Hutchinson, **High temperature free-radical *co*-polymerization of Sty and BMA with depropagation and penultimate kinetic effects**, *Macromolecules*, **39**, 4366-4373 (2006)

78. D. Li, A. Hutchinson, **Penultimate propagation kinetics of BMA/BA/Sty *ter*-polymerization**, *Macromolucular Rapid Communications*, **28**, 1213-1218 (2007)

79. M. G. Lord, **Computer modelling of Sty and AN bulk *co*-polymerization at high conversion**, *MEng. thesis*, *McMaster Univ.* (1984)

80. G. G. Lowry, **The effect of depropagation on *co*-polymer composition, I. General theory for one depropagating monomer**, *Journal of Polymer Science*, **42**, 463-477 (1960)

81. R. A. Lyons, J. Hutovic, M. C. Piton, D. I. Christie, P. A. Clay, B. G. Manders, S. H. Kable, R. G. Gilbert, **Pulsed-laser polymerization measurements of the propagation rate coefficients for BA**, *Macromolecules*, **29**, 1918-1927 (1996)

82. P. Mallya, S. S. Plamthottam, **Termination rate constant in BA emulsion polymerization**, *Polymer Bulletin*, **21**, 497-504 (1989)

83. F. L. Marten, A. E. Hamielec, **High-conversion diffusion-controlled polymerization of Sty I**, *Journal of Applied Polymer Science*, **27**, 489-505 (1982)

84. F. Martinet, J. Guillot, ***Co*-polymerization with depropagation: Prediction of kinetics and properties of AMS-MMA *co*-polymers. II. Bulk *co*-polymerization**, *Journal of Applied Polymer Science*, **72**, 1611-1625 (1999)

85. B. Matthews, C. Villa, P. Pierini, **Model development in thermal Sty polymerization**, *Macromolecular Symposia*, **259**, 94-101 (2007)

86. F. R. Mayo, F. M. Lewis, **A basis for comparing the behaviour of monomers in *co*-polymerization; The *co*-polymerization of Sty and MMA**, *Journal of American Chemical Society*, **66**, 1594-1601 (1944)

87. F. R. Mayo, C. Walling, ***Co*-polymerization**, *Chemical Reviews (Washington, DC, USA)*, **46**, 191-287 (1950)

88. H. W. McCormick, **Ceiling temperature of AMS**, *Journal of Polymer Science*, **25(111)**, 488-490 (1957)

89. S. McIssac, *MASc thesis*, *Department of Chemical Engineering, U of Waterloo* (1994)

90. T. F. McKenna, A. Villanueva, A. M. Santos, **Effect of solvent on the rate constants in solution polymerization. Part I. BA**, *Journal of Polymer Science: Part A: Polymer Chemistry*, **37**, 571-588 (1999)

91. N. T. McManus, A. Penlidis, **A kinetic investigation of Sty/EA *co*-polymerization**, *Journal of Polymer Science: Part A*, **34**, 237-248 (1996)

92. N. T. McManus, J. D. Kim, A. Penlidis, **Observations on Sty/HEA and Sty/HEA/EA polymerizations**, *Polymer Bulletin*, 41, 661-668 (1998)

93. N. T. McManus, M. A. Dubé, A. Penlidis, **High temperature bulk *co*-polymerization of BA/MMA reactivity ratio estimation**, *Polymer Reaction Engineering*, **7(1)**, 131-145 (1999)

94. N. T. McManus, G. Hsieh, A. Penlidis, **Free-radical *ter*-polymerization of BA/MMA/AMS at high temperature**, *Polymer*, **45**, 5837-5845 (2004)

95. E. Merz, T. Alfrey, G. Goldfinger, **Intramolecular reactions in vinyl polymers as a means of investigation of the propagation step**, *Journal of Polymer Science*, **1(2)**, 75-82 (1946)

96. V. E. Meyer, G. G. Lowry, **Integral and differential binary *co*-polymerization equations**, *Journal of Polymer Science: Part A: General Papers*, **3(8)**, 2843-2851 (1965)

97. G. A. Mun, Z. S. Nurkeeva, A. B. Beissegul, A. V. Dubalazov, P. I. Urkimbaeva, K. Park, V. V. Khutoryanskiy, **Temperature-responsive water-soluble *co*-polymers based on HEA and BA**, *Macromolecular Chemistry and Physics*, **208**, 979-987 (2007)

98. A. S. Nair, M. S. Muthana, **Studies on the polymerization of methacrylic esters Part I. Polymerization of *n*-BMA and *iso*-BMA**, *Makromolekulare Chemie*, **47**, 114-127 (1961)

99. G. Odian, **Principles of polymerization**, *McGraw-Hill*, New York (1970)

100. K. F. O'Driscoll, J. Huang, **The rate of *co*-polymerization of Sty and MMA I. Low conversion kinetics**, *European Polymer Journal*, **25(7/8)**, 629-633 (1989)

101. K. F. O'Driscoll, J. Huang, **The rate of *co*-polymerization of Sty and MMA II. The gel effect in *co*-polymerization**, *European Polymer Journal*, **26(6)**, 643-647 (1990)

102. T. Otsu, T. Ito, M. Imoto, **The reactivities of alkyl methacrylates in their radical polymerizations**, *Polymer Letters*, **3**, 113-117 (1965)

103. D. E. Palmer, N. T. McManus, A. Penlidis, ***Co*-polymerization with depropagation: A study of AMS/MMA in bulk at elevated temperatures**, *Journal of Polymer Science: Part A: Polymer Chemistry*, **38**, 1981-1990 (2000)

104. D. E. Palmer, N. T. McManus, A. Penlidis, ***Co*-polymerization with depropagation: A study of AMS/MMA in solution at elevated temperatures**, *Journal of Polymer Science: Part A: Polymer Chemistry*, **39**, 1753-1763 (2001)

105. H. Patino-Leal, P. M. Reilly, K. F. O'Driscoll, **On the estimation of reactivity ratios**, *Journal of Polymer Science: Polymer Letters Edition*, **18**, 219-227 (1980)

106. A. N. F. Peck, R. A. Hutchinson, **Secondary reactions in the high temperature free-radical polymerization of BA**, *Macromolecules*, **37**, 5944-5951 (2004)

107. A. L. Polic, T. A. Duever, A. Penlidis, **Case studies and Literature review on the estimation of *co*-polymerization reactivity ratios**, *Journal of Polymer Science: Part A: Polymer Chemistry*, **36**, 813-822 (1998)

108. C. Quan, M. Soroush, M. C. Grady, J. E. Hansen, W. J. Simonsick, **High temperature *homo*-polymerization of EA and BA: Polymer characterization**, *Macromolecules*, **38**, 7619-7628 (2005)

109. P. V. T. Raghuram, U. S. Nandi, **Studies on the polymerization of EA. I. Kinetic studies**, *Journal of Polymer Science: Part A-1*, **5**, 2005-2012 (1967)

110. P. V. T. Raghuram, U. S. Nandi, **Studies on the polymerization of EA. III. Effect of temperature on the solvent-transfer reaction**, *Journal of Polymer Science: Part A-1*, **8**, 3079-3088 (1970)

111. F. S. Rantow, M. Soroush, M. C. Grady, G. A. Kalfas, **Spontaneous polymerization and chain microstructure evolution in high-temperature solution polymerization of BA**, *Polymer*, 47, 1423-1435 (2006)

112. H. Ray, R. Laurence, **Chemical Reactor Theory; A review, Chap. 9**, *Prentice-Hall* (1977)

113. P. M. Reilly, H. Patino-Leal, **A Bayesian study of the Error-in-Variables Model**, *Technometrics*, **23(3)**, 221-231 (1981)

114. P. M. Reilly, H. V. Reilly, S. E. Keeler, **Algorithm AS286: Parameter estimation in the Error-in-Variables Model**, *Applied Statistics*, **42(4)**, 693-701 (1993)

115. P. J. Rossignoli, T. A. Duever, **The estimation of *co*-polymer reactivity ratios: A review and case studies using the Error-in-Variables Model and nonlinear least squares**, *Polymer Reaction Engineering*, **3(4)**, 361-395 (1995)

116. N. A. Sahloul, **A Study of multi-component polymerization of Sty/EA/HEA/MAA**, *PhD thesis*, *Department of Chemical Engineering, U of Waterloo* (2004)

117. N. A. Sahloul, A. Penlidis, **High temperature *co*-polymerization of Sty/EA: Reactivity ratio estimation in bulk and solution**, *Advances in Polymer Technology*, **23(3)**, 186-195 (2004)

118. N. A. Sahloul, A. Penlidis, **Sty/MAA monomer reactivity ratio estimation in bulk and solution at high temperatures**, *Polymer-Plastics Technology and Engineering*, **44**, 771-782 (2005)

119. N. A. Sahloul, N. A. Emwas, W. Power, A. Penlidis, **EA/HEA and HEA/MAA: Reactivity ratio estimation from crosslinked polymer using high resolution magnetic angle spinning spectroscopy**, *Journal of Macromolecular Science, Part A: Pure and Applied Chemistry*, **42**, 1369-1385 (2005)

120. C. A. Scholtens, J. Meuldijk, A. A. H. Drinkenburg, **Production of *co*-polymers with a predefined intermolecular chemical composition distribution by emulsion polymerization in a continuously operated reactor**, *Chemical Engineering Science*, **56**, 955-962 (2001)

121. R. Simha, H. Branson, **Theory of chain *co*-polymerization reactions**, *Journal of Chemical Physics*, **12(6)**, 253-267 (1944)

122. I. Skeist, ***Co*-polymerization: the composition distribution curve**, *Journal of American Chemical Society*, **68**, 1781-1784 (1946)

123. M. Stickler, **Free-radical polymerization kinetics of MMA at very high conversions**, *Makromolekulare Chemie*, **184**, 2563-2579 (1983)

124. M. Stickler, D. Panke, A. E. Hamielec, **Polymerization of MMA up to high degrees of conversion: Experimental investigation of the diffusion-controlled polymerization**, *Journal of Polymer Science: Polymer Chemistry Edition*, **22**, 2243-2253 (1984)

125. W. H. Stockmayer, **Distribution of chain lengths and compositions in *co*-polymers**, *Journal of Chemical Physics*, **13(6)**, 199-207 (1945)

126. M. Switata-Zeliazkow, **Microstructure of Sty-MAA and Sty-AA *co*-polymers, 6. Relation of the glass transition temperature to the microstructure of MAA-Sty *co*-polymers**, *Makromolekulare Chemie*, **194(5)**, 1505-1511 (1993)

127. J. C. J. F. Tacx, J. L. Ammerdorffer, A. L. German, **Chemical composition distribution of Sty/EMA *co*-polymers studied by means of t.l.c./f.i.d.: effect of high conversion in various polymerization processes**, *Polymer*, **29**, 2087-2094 (1988)

128. S. Teramachi, A. Hasegawa, N. Uchiyama, **The chemical composition distribution of a high conversion sample of *co*-poly(Sty-stat-MMA) prepared in bulk**, *Journal of Polymer Science: Polymer Letters Edition*, **22**, 71-76 (1984)

129. A. Valvassori, G. Sartori, **Present status of multi-component *co*-polymerization theory**, *Advances in Polymer Science*, **5(1)**, 28-58 (1967)

130. E. Vargün, A. Usanmaz, **Polymerization of HEA in bulk and solution by chemical initiator and by ATRP method**, *Journal of Polymer Science: Part A: Polymer Chemistry*, **43**, 3957-3965 (2005)

131. E. Vivaldo-Lima, A. E. Hamielec, P. E. Wood, **Batch reactor modelling of the free-radical *co*-polymerization kinetics of Sty/divinylbenzene up to high conversions**, *Polymer Reaction Engineering*, **2(1&2)**, 87-162 (1994)

132. F. T. Wall, **The structure of *co*-polymers II**, *Journal of American Chemical Society*, **66**, 2050-2057 (1944)

133. C. Walling, E. R. Briggs, ***Co*-polymerization. III Systems containing more than two monomers**, *Journal of the American Chemical Society*, **67**, 1774-1778 (1945)

134. C. Walling, ***Co*-polymerization XIII. Overall rates in *co*-polymerization. Polar effects in chain initiation and termination**, *Journal of American Chemical Society*, **71**, 1930-1935 (1949)

135. W. Wang, R. A. Hutchinson, **High temperature semi-batch free-radical *co*-polymerization of Sty/DMA**, *Macromolecular Symposia*, **261**, 64-73 (2008)

136. P. Wittmer, ***Co*-polymerization in the presence of depolymerization reactions**, *Advances in Chemistry Series*, **99**, 140-174 (1971)

137. T. Y. Xie, A. E. Hamielec, **Modeling free-radical *co*-polymerization kinetics – evaluation of the pseudo-kinetic rate constant method, 2 Molecular weight calculations for *co*-polymers with long chain branching**, *Makromolekulare Chemie, Theory and Simulations*, **2(3)**, 455-483 (1993)